Freshwater Carbon Across Arctic Lowland Tundra Ecosystems



Melanie Martyn Rosco

Freshwater Carbon Across Arctic Lowland Tundra Ecosystems

Melanie Martyn Rosco

Martyn Rosco, M (2026). Freshwater Carbon Across Arctic Lowland Tundra Ecosystems. PhD Thesis, Faculty of Science, Earth and Climate, Vrije Universiteit Amsterdam, Amsterdam, The Netherlands

Thesis design and layout: Melanie Martyn Rosco
Cover art: Betty Buckmann
Photographs: Melanie Martyn Rosco

This study was funded through the Netherlands Earth System Science Centre (NESSC; Grant No. 024.002.001), supported by the Dutch Ministry of Education, Culture and Science (OCW). Additional funding was provided by the European Union's Horizon 2020 INTERACT project (Grant Agreement No. 730938).

© 2026 Melanie Martyn Rosco.
All rights reserved. No part of this book may be reproduced in any form or by any electronic or mechanical means, without written permission from the author, except in the case of scientific or educational use, for which brief passages can be embodied in articles, a review, or teaching materials.

VRIJE UNIVERSITEIT AMSTERDAM

Freshwater Carbon Across Arctic Lowland Tundra Ecosystems

ACADEMISCH PROEFSCHRIFT

ter verkrijging van de graad Doctor aan
de Vrije Universiteit Amsterdam,
op gezag van de rector magnifcus
prof.dr. J.J.G. Geurts,
volgens besluit van de decaan
van de Faculteit der Betawetenschappen
in het openbaar te verdedigen
op woensdag 30 september 2026 om 15.45 uur
in de universiteit

door
Melanie Martyn Rosco
geboren te München, Duitsland

promotor:	prof.dr. J.E. Vonk
copromotoren:	dr. J.F. Dean
	dr. J.T. Weedon
promotiecommissie:	prof.dr. I. Laurion
	prof.dr. E.H. Stanley
	dr. J.A. Hawkes
	dr. L. Heffernan
	dr. M. Peacock
	dr.ir Y. van der Velde

The nature of things is resistance to change, while the nature of process is resistance to stasis, yet things and process are one, and the line from inorganic to organic and back again is uninterrupted and unbroken. — William Least Heat-Moon, *Blue Highways*

SUMMARY

Arctic lowland tundra landscapes are low-relief regions located in the high latitudes of the Northern Hemisphere and are underlain by permafrost, a defining feature that regulates their hydrological, ecological, and biogeochemical processes. Within these landscapes, freshwater ecosystems, including lakes, ponds, streams, and seasonally flooded areas, are widespread and form important connections between terrestrial environments, downstream aquatic systems, and the atmosphere. These systems receive carbon from surrounding soils and vegetation while also generating and transforming carbon through aquatic primary production and biogeochemical processes, resulting in strong spatial heterogeneity in carbon concentrations and composition. Permafrost underlies approximately 14 % of the Northern Hemisphere land surface and stores an estimated 1056.8 ± 167.2 Pg of carbon in the upper three meters, while freshwater ecosystems can cover up to 40 % of Arctic lowland landscapes. Despite their extensive coverage and connectivity, freshwater ecosystems remain underrepresented in Arctic carbon assessments, particularly with respect to dissolved carbon pools (DOC and DIC), greenhouse gas emissions, and their variability across ecosystem types and spatial scales.

This thesis investigates freshwater carbon across Arctic lowland tundra ecosystems using field observations from two regions: the northeast Siberian Arctic tundra and the Hudson Bay Lowlands (Canada). Measurements were conducted during the ice-free season and focus on dissolved organic carbon (DOC), dissolved inorganic carbon (DIC), dissolved organic matter (DOM) characteristics, and greenhouse gas (CO_2, CH_4, N_2O) concentrations. The thesis addresses three main questions: (1) how freshwater greenhouse gas emissions compare to the terrestrial carbon sink, (2) how DOM composition relates to greenhouse gas concentrations, and (3) how lateral carbon transport varies along hydrological connections. Overall, this thesis evaluates how carbon in freshwater ecosystems varies among ecosystem types and along hydrological gradients in Arctic lowland landscapes.

In the Indigirka River tundra lowlands of northeastern Siberia, a landscape characterized by a mosaic of peat-forming polygonal wetlands, Yedoma uplands, and river floodplains, all freshwater systems were supersaturated in CO_2 (27–1333 µmol L^{-1}) and CH_4 (0.04–251 µmol L^{-1}), with ponds consistently showing the highest concentrations. Upscaled inland water emissions to an area of approximately 18 km^2 (7.03 ± 1.30 to 9.63 ± 1.24 Mg C d^{-1}) offset approximately 9 % to 13 % of the terrestrial carbon sink. Relationships between DOM characteristics and dissolved greenhouse gas concentrations differed among Arctic freshwater ecosystem types, with distinct associations observed in ponds, lakes, and fluvial systems. In a small coastal catchment in the Hudson Bay Lowlands, dissolved carbon transport varied along the terrestrial–freshwater continuum, with headwater peatland and coastal sandy heathland landscapes exhibiting contrasting relationships between soil pore water and surface water carbon. In surface waters, DOC concentrations remained within a relatively narrow range across the catchment, whereas

DIC concentrations increased downstream, accompanied by changes in $\delta^{13}\mathrm{C}$-DIC and DOM characteristics. Differences between soil pore and surface waters were greater in the headwater peatland than in the coastal sandy heathland, highlighting the influence of landscape characteristics and hydrological connectivity on terrestrial–freshwater carbon transport. Late-summer rainfall further altered dissolved carbon transport by increasing DOC concentrations and aromaticity while reducing DIC concentrations in surface waters, demonstrating the sensitivity of carbon export to episodic hydrological events.

Overall, this thesis demonstrates that freshwater carbon cycling in Arctic lowland tundra ecosystems is shaped by interactions among hydrological connectivity, carbon composition, and ecosystem-specific processes. Freshwater greenhouse gas emissions, DOM–greenhouse gas relationships, and lateral carbon transport varied across freshwater ecosystem types highlighting the importance of landscape and ecosystem characteristics in regulating carbon transfer and transformation across the terrestrial–freshwater continuum. Episodic hydrological events, including flooding and rainfall, further altered carbon fluxes by changing water extent, connectivity, and carbon transport. Together, these findings demonstrate that Arctic freshwater ecosystems play an important role in regulating the transfer, transformation, and loss of carbon across the terrestrial–aquatic–atmospheric continuum.

CONTENTS

1 General introduction **15**

High-latitude tundra lowlands 15

Sensitivity to climate change 17

Greenhouse gas emissions from high-latitude lowlands freshwaters 20

Relationships between DOM composition and greenhouse gas concentrations in freshwater ecosystems 20

Terrestrial-aquatic connectivity in arctic lowland tundra catchments 21

Research objectives 22

Thesis outline 24

2 Inland water GHG exchange with the atmosphere **28**

Plain Language Summary 29

Introduction 29

Materials and Methods 31

Results 38

Discussion 44

Conclusions 49

Statments and Declarations 49

Appendix 51

3 Freshwater GHGs relationships with DOM **56**

Introduction 57

Methods 59

Results 67

Discussion 74

Conclusions 84

Statments and Declarations 84

Appendix 86

4 Lateral carbon flow in an Arctic coastal catchment in late summer **98**

Introduction 99

Methods 100

Results 106

Discussion 118

Conclusion 123
Statments and Declarations 124

5 Integration and outlook **128**
Summer greenhouse gas emissions from freshwaters in the Indigirka Lowlands 129
Relationships between DOM and greenhouse gas supersaturation 130
Late-summer lateral carbon flux in a costal Hudson Bay Lowlands catchment . 131
Comparison of the two Arctic lowland study regions 132
Emergent insights from integrating vertical, lateral, and biogeochemical perspectives 132
Future considerations in Arctic freshwater carbon and nitrogen research 134

References **139**

Acknowledgements **160**

Chapter 1

General introduction



High-latitude tundra lowlands

Low-relief landscapes located in the high latitudes of the Northern Hemisphere, in Arctic and Sub-Arctic regions, are composed of vast peatlands, numerous lakes, ponds, streams and rivers. These regions, referred to as 'high-latitude lowlands' in this thesis, are underlain by permafrost, a defining characteristic that governs their hydrological, ecological, and biogeochemical processes. Permafrost, a layer of frozen soil that remains at or below 0°C for at least two consecutive years, often persists for centuries or even millennia (van Everdingen, 1998). It plays a crucial role in shaping hydrological and biogeochemical processes in these landscapes by regulating water flow, nutrient transport, and carbon storage (Prowse et al., 2015).

Permafrost underlies approximately 14 % of the land surface in the Northern Hemisphere (Obu et al., 2019) and contains an estimated 1056.8 ± 167.2 Pg of carbon and 67 Pg of nitrogen in the upper three meters alone, making it a globally significant carbon reservoir (Figure 1.1) (Harden et al., 2012; Wu et al., 2022). These permafrost-rich, low-relief landscapes are primarily found within the Arctic tundra biome, which extends over approximately 5 million km^2 and is characterized by low temperatures, a short growing season, and low-lying vegetation adapted to permafrost conditions (Bjorkman et al., 2018; Loidi et al., 2022; Walker et al., 2005).

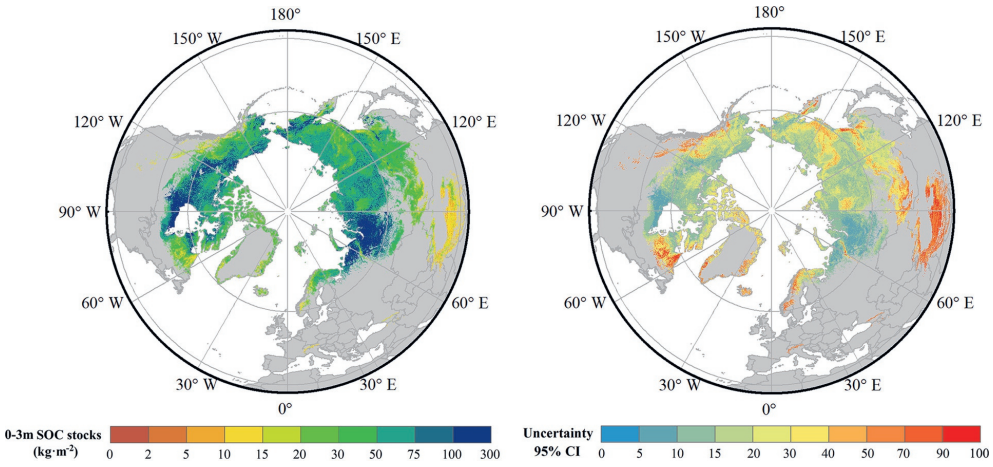

Figure 1.1: Map showing the estimated soil organic carbon content in the top 3 meters of soil in the Arctic and its associated uncertainty. Reproduced from Wu et al. (2022), © Elsevier, used with permission.

Within the Arctic tundra, lowlands are particularly important due to their extensive freshwater ecosystems coverage, including lakes, ponds, and fluvial systems, which can account for up to 40 % of the land surface in some high-latitude lowlands (Barrett, 2000; Grosse et al., 2013). Arctic rivers, which drain into the Arctic Ocean, Bering Strait as well as the Hudson, James, and Ungava Bays, collectively drain an area estimated to be around 15 % of the global land surface (22.1 million km^2) (Feng et al., 2021).

Carbon fluxes between the atmosphere and terrestrial as well as freshwater ecosystems occur along multiple pathways, including gas exchange (CO_2 and CH_4 emissions), lateral transport of dissolved and particulate organic and inorganic carbon (DOC, POC, DIC, PIC), sediment burial and biogeochemical transformations within soils and freshwater systems (Figure 1.2) (McGuire et al., 2009; Aufdenkampe et al., 2011). These processes shape the high-latitude carbon cycle, influencing regional and global climate feedback. The vast carbon reservoir, along with the unique hydrology and carbon cycling of tundra lowlands, makes these landscapes critical for understanding the Earth's response to climate change. Freshwater ecosystems, in particular, play a key role in processing, transporting, and emitting carbon (Williamson et al., 2008), yet their contributions to the Arctic carbon budget remain poorly constrained.

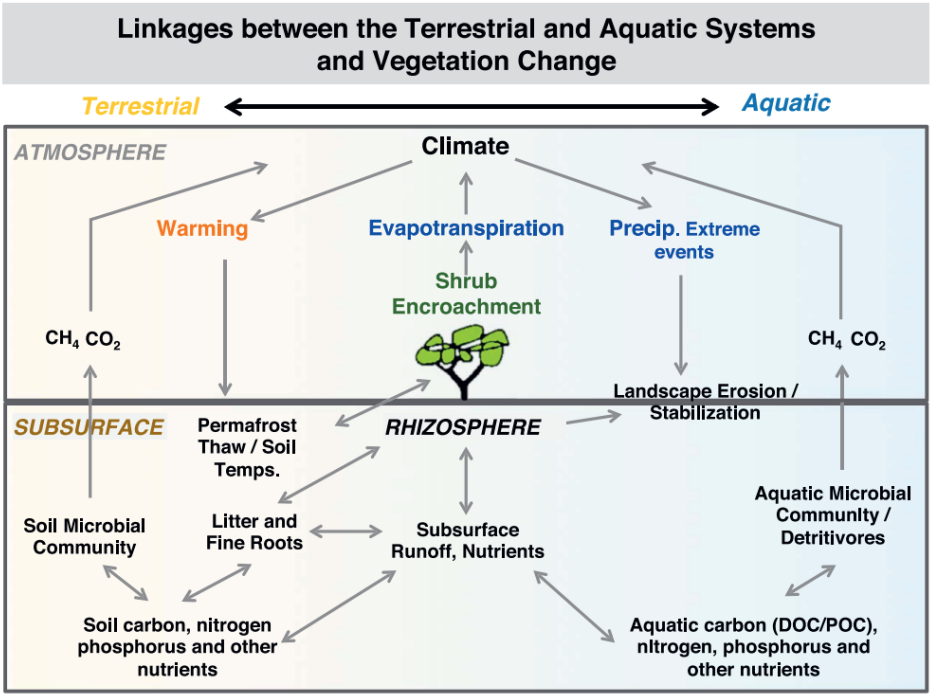

Figure 1.2: Vegetation change can influence carbon and nutrient cycling by altering litter input, nitrogen fixation, runoff, and permafrost stability. Shrub expansion or loss may shift ecosystem function and connectivity, with cascading effects on terrestrial and freshwater carbon fluxes. Adapted from Myers-Smith et al. (2011), summarized in Wrona et al. (2016), © American Geophysical Union, used with permission.

In high-latitude tundra lowlands regions with continuous permafrost (90 % to 100 % of land is underlain by permafrost), surface soils typically consist of organic-rich soils that have accumulated over thousands of years overlying a layer of mineral soils or marine silt deposits (Dredge and Nixon, 1992; Tarnocai, 2009). Between approximately June and

September, seasonal thawing creates a shallow yet widespread soil layer that ranges from centimeters to meters in thickness; this layer is often water-saturated and is known as the active layer (Hinkel and Nelson, 2003). Unlike permafrost, the active layer undergoes annual freezing and thawing cycles; its depth is influenced by surface temperatures, insulation from snow cover and vegetation, and local hydrological conditions (Hinkel and Nelson, 2003). Due to its shallow nature and the impermeability of underlying permafrost, the active layer restricts subsurface flow, forcing water to move laterally near the surface, which enhances organic matter transport laterally. The active layer is of considerable importance in tundra lowlands because most terrestrial hydrological (e.g., runoff, shallow subsurface flow) and biogeochemical activity takes place within it (Figure 1.3). Additionally, this layer is closely connected to freshwater ecosystems, regulating water, carbon, and nutrient transport to them (Frey and McClelland, 2009; Kane et al., 1991).

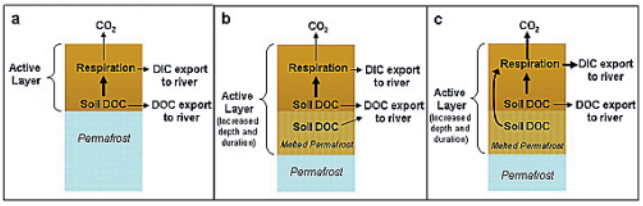

Figure 1.3: Carbon cycling in permafrost soils. (a) Initial condition – Biogeochemical processes in the soil active layer contribute DOC and DIC to streams and rivers and CO2 to the atmosphere; (b) Warming I - DOC in melting permafrost is mostly recalcitrant, DOC transport to rivers increases; (c) Warming II - DOC in melting permafrost is mostly labile, increased respiration leads to decreased DOC and increased DIC transport to rivers. Reproduced from Striegl et al. (2005), © American Geophysical Union, used with permission.

Sensitivity to climate change

The Arctic is warming at rates up to two to four times faster than the global average (Meredith et al., 2019; Rantanen et al., 2022), primarily due to Arctic amplification, which involves complex feedbacks related to temperature, water vapor, albedo, and sea ice loss (Chapin III et al., 2006; Hinzman et al., 2013; Serreze and Barry, 2011). The warming leads to profound transformations in these ecosystems that affect not only local habitats but also the global climate system (McGuire et al., 2018; Schuur et al., 2008; Wrona et al., 2016). One of the most significant consequences of this warming is the thawing of permafrost, which raises concerns due to its potential to release previously stored carbon (Figure 1.3) (Biskaborn et al., 2019; Schuur et al., 2009; Turetsky et al., 2020). This carbon may be emitted directly to the atmosphere as CO_2 and CH_4 or transported as dissolved organic matter (DOM) and DIC into freshwater systems, where it can either be buried in sediments, transformed, or emitted as greenhouse gases (Figure 1.4) (Dasari et al., 2024; Kelley et al., 2026). Whether this mobilized carbon contributes to the permafrost–climate feedback depends on its age. Carbon entering freshwater ecosystems may be contemporary, originating from recently fixed plant and soil carbon,

or older, derived from permafrost or deep peat where it has been stored for centuries to millennia. While the cycling of contemporary carbon largely reflects the turnover of recently fixed carbon, the mobilization and release of older stored carbon represents a net transfer of previously sequestered carbon to the atmosphere, thereby strengthening the permafrost–climate feedback. Consequently, freshwater ecosystems represent an important pathway through which permafrost-derived carbon can influence regional greenhouse gas fluxes and potentially reinforce the permafrost–climate feedback (Abbott, 2022; Schaefer et al., 2014; Schuur et al., 2015).

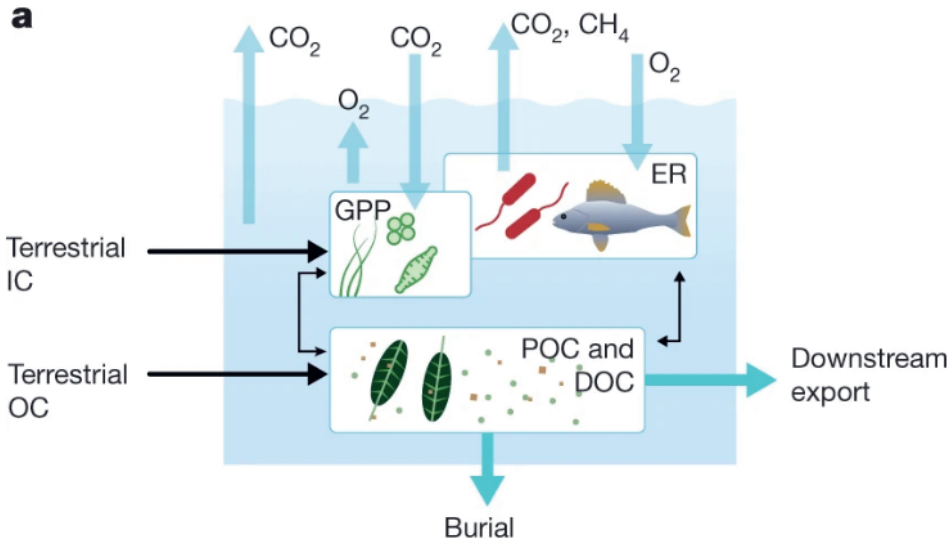

Figure 1.4: Conceptual diagram of carbon inputs and metabolism in river ecosystems. Gross primary production (GPP) and ecosystem respiration (ER) interact with terrestrial inputs of inorganic carbon (IC) and organic carbon (OC), leading to carbon burial, downstream export, and atmospheric gas exchange (CO_2 and CH_4, O_2). Reproduced from Battin et al. (2023), © Springer Nature, used with permission.

Permafrost thaw is reshaping hydrological dynamics, geomorphological processes, and nutrient cycling (Bring et al., 2016; Rawlins et al., 2010; Wrona et al., 2016). Concurrently, climate change is intensifying the Arctic hydrological cycle, with one manifestation being increasing late-summer rainfall in the Arctic, a trend projected to continue (Arp et al., 2020; Bintanja, 2018; Bintanja and Andry, 2017). These changes are altering hydrological connectivity and carbon fluxes between terrestrial and freshwater systems, further affecting high-latitude lowlands biogeochemical cycles and carbon budgets (Beel et al., 2021). The complexity of these interactions, combined with limited understanding of how carbon is processed along these pathways, underscores the importance of studying tundra lowland ecosystems. Beyond its ecological consequences, permafrost thaw is also disrupting Arctic communities and economies. Close to five million people live in permafrost regions (Ramage et al., 2021), relying on the stability of the frozen ground for

livelihood activities, infrastructure, and daily life (Ramage et al., 2022). This aspect highlights that permafrost degradation is not only an environmental issue but also a social and economic concern, reinforcing the need to understand the changes it is undergoing to be able to address these changes for both ecosystem health and community resilience.

In high-latitude lowlands, the active layer, the seasonally thawed layer of soil above permafrost, plays a critical role in mediating ecological and hydrological responses to warming. Rising temperatures and increased precipitation are thickening the active layer, an increase of up to 0.4 m between 1999 and 2019 has been observed in the Russian Arctic, and are projected to continue doing so (Meredith et al., 2019; Smith et al., 2022; Lawrence et al., 2012; Liu et al., 2023). This thickening exposes previously frozen soil, increasing the availability of organic matter for mobilization and decomposition, which releases carbon and other nutrients into soil water (Prokushkin et al., 2009). The thickening of the active layer also has significant hydrological consequences, which are highly dependent on local topography and soil stratigraphy (Woo, 2011). In lowland regions, subsurface flows remain relatively stable due to thick organic layers and high water tables (Figure 1.3), whereas in steeper landscapes, flows decrease as the season progresses due to a drop in the water table and reduced permeability at depth (O'Connor et al., 2019; Neilson et al., 2018). These hydrological changes cascade through the ecosystem, affecting vegetation, soil stability, and nutrient dynamics (Figure 1.2). At the same time, the Arctic growing season is becoming longer, having already lengthened by 2–4 days per decade since 1960 due to earlier snowmelt, with projections indicating a total increase of 37–60 days by the end of the century compared to pre-industrial levels (~100 days) (Euskirchen et al., 2006; Høye et al., 2007). This extended growing season and the thickening active layer are two of several factors driving change in tundra vegetation. For instance, increasing tundra plant growth and productivity ("greening") has been linked to increased summer air and soil temperatures, as well as soil moisture (Berner et al., 2020). While much of the tundra is experiencing greening, some areas are exhibiting the opposite trend which is termed "browning", that is a decrease in plant cover and productivity, such as the Indigirka Lowlands, Siberia (Berner et al., 2020; Magnússon et al., 2023; Myers-Smith et al., 2020).These changes in vegetation and hydrology also influence the composition and age of carbon exported to freshwater ecosystems.

Flooding events in high-latitude lowlands are becoming more frequent and intense due to warming and associated climate driven changes. For example, the Indigirka Lowlands experienced widespread flooding following high snowfall in 2016–2017 (Tei et al., 2020). These floods, driven by rising precipitation, snowmelt runoff, and shifting precipitation patterns, are expected to become more frequent and severe as climate warming leads to deeper snow cover, longer snowmelt seasons, increased rain-on-snow occurrences and a transition toward a rain-dominated precipitation regime (Bintanja and Andry, 2017; Callaghan et al., 2011; Rennert et al., 2009; McCrystall et al., 2021). Considering that an 11 % increase in total inland water carbon emissions was observed during a 'normal' spring flood over a 30-day period in Western Siberia (Karlsson et al., 2021), more extreme and frequent flooding events could further amplify carbon release from these ecosystems.

Greenhouse gas emissions from high-latitude lowlands freshwaters

Lakes, ponds, and fluvial networks receive terrestrial organic material and inorganic carbon via surface and subsurface hydrological pathways, while carbon within these freshwater ecosystems is continuously transformed through microbial and photochemical degradation, gas exchange, sedimentation, and autochthonous primary production (Drake et al., 2018; Kling et al., 1991). These freshwater ecosystems are often net emitters of CO_2 and CH_4, with additional but relatively minor emissions of N_2O (Hu et al., 2016; Raymond et al., 2013; Rosentreter et al., 2021). Despite their small surface area relative to terrestrial ecosystems, studies suggest that greenhouse gas emissions from freshwater ecosystems can reduce the net carbon uptake of tundra ecosystems (Dean et al., 2020; Karlsson et al., 2021). However, scaling freshwater emissions to landscape-level estimates remains challenging due to their high spatial and temporal variability (Denfeld et al., 2015; Lundin et al., 2013; Prėskienis et al., 2021). The extent of freshwater ecosystems in Arctic lowlands also varies widely (Grosse et al., 2008), shifting with the drainage of water bodies (Jones and Arp, 2015) and ground subsidence driven by permafrost thaw and topographical changes (Liljedahl et al., 2016; Vonk et al., 2015). Episodic events such as flooding can further enhance emissions, as observed in Siberian rivers (Krickov et al., 2021; Vorobyev et al., 2021). To accurately quantify their role in the Arctic carbon cycle, we need to be able distinguish and quantify emissions from lakes, ponds, fluvial systems, and floodwaters, as well as their contribution to offsetting the landscape carbon sink.

Relationships between DOM composition and greenhouse gas concentrations in freshwater ecosystems

During the summer, DOM in freshwater ecosystems originates from both allochthonous and autochthonous sources. Allochthonous DOM is derived from surrounding terrestrial ecosystems and enters freshwater systems through surface and subsurface pathways, including leaching from vegetation and soils, overland runoff, and lateral flow through thawed active layer soils (Figure 1.2; Bring et al., 2016), whereas autochthonous DOM is produced within freshwater ecosystems by primary producers such as algae and freshwater macrophytes. The relative contribution of these sources influences DOM composition, which in turn affects its susceptibility to biological and photochemical degradation (Grunert et al., 2021). These degradation pathways transform DOM and regulate its role in freshwater carbon cycling and greenhouse gas production. The balance between biological and photochemical degradation varies with environmental conditions, including light availability, residence time, dissolved ion concentrations, and the chemical characteristics of the DOM (Obernosterer and Benner, 2004; Cory and Kling, 2018; Guillemette and del Giorgio, 2011; Lapierre and del Giorgio, 2014). Photochemical degradation is constrained by light penetration into the water column. Consequently, factors such as water depth, water colour, and vertical mixing or stratification play an important role in determining the extent of photochemical DOM processing (Cory and Kling, 2018; Cory

et al., 2014). Generally, low molecular weight DOM (e.g., carbohydrates, fatty acids, amino acids) degrades rapidly, whereas high molecular weight DOM, including tannins, lignin derivatives, and other humic substances, tends to be more resistant to biological degradation while remaining susceptible to photochemical degradation (Kellerman et al., 2018; Raymond and Spencer, 2015; Cory and Kling, 2018).

Understanding how DOM characteristics relate to greenhouse concentrations across freshwater ecosystems would offer necessary insights into Arctic carbon and nitrogen cycling (Breton et al., 2009; Rasilo et al., 2017; Tank et al., 2011). Freshwater ecosystems in tundra lowlands are dynamic interfaces where terrestrial carbon and nutrients are processed, stored, or emitted, yet the extent to which DOM and its characteristics regulate dissolved CO_2, CH_4, and N_2O concentrations remains uncertain (Figure 1.4). Consistent linking of specific DOM components to greenhouse gas supersaturation could be indicative of fundamental controls on biogeochemical processes across freshwater ecosystems. Alternatively, the variation of these relationships by ecosystem type may reflect that hydrological, biological, and photochemical processes shape carbon and nitrogen transformations differently in lakes, ponds, and fluvial systems (Cory and Kling, 2018; Knutson et al., 2025). As permafrost thaw, shifting precipitation regimes and increasing temperatures alter DOM supply and processing pathways, clarifying these connections would aid the prediction of future changes in Arctic greenhouse gas dynamics and their implications for climate (Beel et al., 2021; Johnston et al., 2020; Liljedahl et al., 2016; Liu et al., 2022; Neilson et al., 2018).

Terrestrial-aquatic connectivity in arctic lowland tundra catchments

The lateral transport of carbon between terrestrial and freshwater ecosystems is a significant component of Arctic carbon cycling, connecting terrestrial, atmosphere, and marine carbon reservoirs. This transport includes both organic and inorganic carbon, primarily in the forms of DOC, POC, DIC, and dissolved CH_4 (Tank et al., 2018). It is thought that this lateral carbon export is closely linked to the supersaturation of these gases in streams, fueling their high emissions (Lundin et al., 2013; Raymond et al., 2013; McClain et al., 2003). However, greenhouse gas emissions represent only one possible fate of laterally transported carbon, which may also be transported downstream or retained through sediment burial within freshwater ecosystems (Aufdenkampe et al., 2011; Lundin et al., 2015). Uncertainties remain regarding how lateral carbon fluxes influence the fate of carbon within freshwater ecosystems, including their contribution to greenhouse gas emissions (Gómez-Gener et al., 2021; Hotchkiss et al., 2015). A key question is whether carbon enters freshwater ecosystems primarily as soil-produced CO_2 (as part of the DIC pool) or CH_4 or as DOC, which may be degraded either at the terrestrial-aquatic interface or within the fluvial systems themselves (Tank et al., 2018).

As the Arctic hydrological cycle intensifies with increasing late-summer rainfall, studies suggest that DOC export in lowland tundra responds more immediately to precipitation events than to active layer thickening (Beel et al., 2021). The transition from snowmelt-dominated to more rainfall-driven hydrology could modify the timing and mag-

nitude of DOC and DIC export, influencing downstream carbon budgets (Leith et al., 2015; Shogren et al., 2020a). Additionally, Arctic vegetation shifts, such as increased plant productivity and seasonal CO_2 uptake, may further complicate terrestrial-aquatic carbon interactions (Myers-Smith et al., 2020; Pearson et al., 2013). Given our limited understanding of lateral carbon fluxes and terrestrial-aquatic connectivity, especially in the context of ongoing environmental changes, gaining clearer insights into these processes is necessary to understand their role in the Arctic carbon cycle.

Research objectives

Arctic freshwater systems are an important component in high-latitude tundra lowland carbon cycles, particularly in the context of a changing climate. These systems act as conduits, processors, and emitters of carbon, influencing greenhouse gas fluxes and lateral carbon export (Figures 1.1–1.4). Figure 1.5 provides a conceptual overview of the terrestrial–freshwater–atmospheric carbon continuum components considered in this thesis: carbon transport from terrestrial ecosystems into freshwater systems, greenhouse gas emissions to the atmosphere, downstream carbon export, and ecosystem-specific relationships between DOM and dissolved greenhouse gas concentrations.

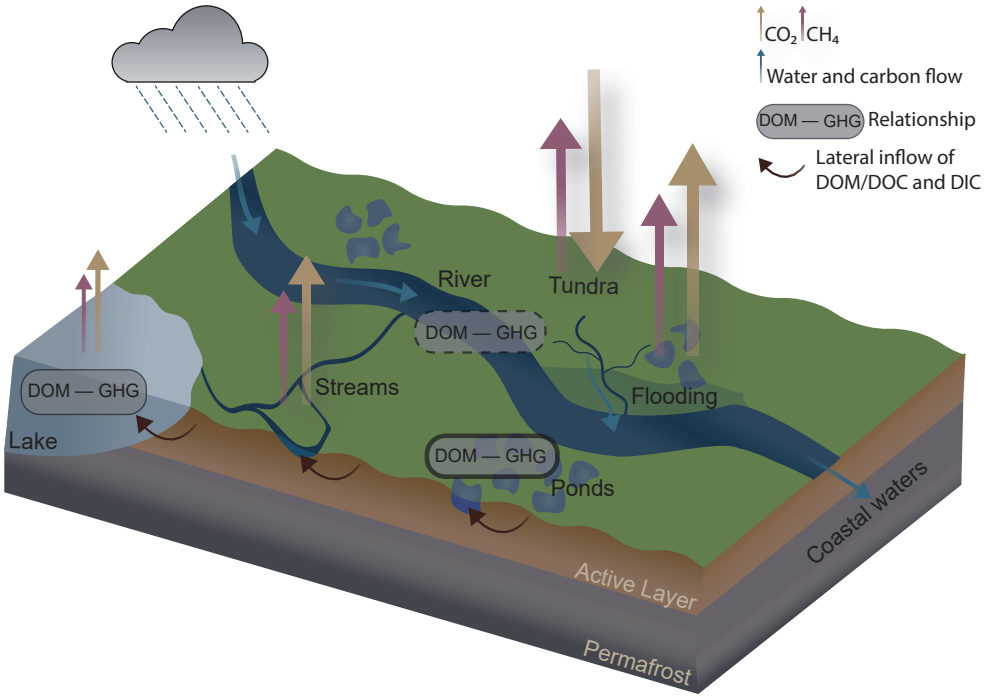

Figure 1.5: Conceptual overview of the terrestrial–freshwater–atmospheric carbon continuum in Arctic lowland tundra ecosystems. Carbon enters freshwater systems via lateral transport from the active layer and surrounding soils in the form of dissolved inorganic carbon (DIC), and dissolved organic matter (DOM) which also quantified as dissolved organic carbon (DOC). Within freshwater systems (lakes, ponds, and fluvial networks), carbon is processed through a combination of photochemical and microbial pathways and can be emitted to the atmosphere as CO_2 and CH_4, or transported downstream to coastal waters. Grey boxes indicate relationships between DOM composition and dissolved greenhouse gas concentrations, with differences in outline stroke representing system-specific DOM–GHG relationships across lakes, ponds, and fluvial systems.

Following geopolitical developments associated with Russia's invasion of Ukraine, fieldwork opportunities in northeast Siberia became unavailable, necessitating a shift in field activities to the Hudson Bay Lowlands, Canada. This thesis therefore combines observations from two different Arctic lowland regions: the Indigirka River Lowlands in northeast Siberia and the Hudson Bay Lowlands in Canada. Although differing in geology, hydrology, vegetation, and landscape characteristics, both regions are organic-rich, permafrost-affected Arctic lowlands where freshwater ecosystems play a role in carbon processing and transport. Together, these study systems broaden the geographical perspective of this thesis and provide context for considering freshwater carbon cycling across Arctic lowland landscapes.

This thesis aims to explore the role of Arctic freshwaters in regional carbon cycling by investigating (1) freshwater greenhouse gas emissions and their contribution relative to the terrestrial sink, (2) the relationship between DOM composition and dissolved greenhouse gas concentrations, as well as (3) lateral carbon export, including terrestrial-aquatic connectivity and longitudinal carbon transport through a catchment. To achieve this goal, observational data are combined with advanced statistical methods, remote sensing information, and machine learning approaches to assess patterns, relationships and broader implications of Arctic freshwater carbon fluxes.

The research objectives for each chapter are as follows:

- **Chapter 2**: Quantify freshwater CO_2, CH_4, and N_2O emissions from lakes, ponds, and low-order fluvial systems in the Indigirka River Lowlands in the context of the terrestrial sink. Assess how seasonal flooding influences the magnitude and variability of these emissions.
- **Chapter 3**: Investigate DOM composition and its relationship to dissolved CO_2, CH_4, and N_2O concentrations in Arctic freshwater ecosystems in the Indigirka River Lowlands. Determine whether these relationships differ between lakes, ponds, and fluvial systems, and if so investigate how they differ qualitatively.
- **Chapter 4**: Assess lateral carbon export in a coastal Arctic catchment in the Hudson Bay Lowlands by analyzing the ratio of organic to inorganic carbon concentrations, carbon composition and isotopic signatures. Examine how late-summer precipitation events influence the mobilization of terrestrial DOM to freshwater systems and the export of DOM to coastal waters.

Thesis outline

This thesis has five chapters, beginning with an introduction to the research topics in this first chapter and concluding with a final chapter that summarizes key findings and discusses future perspectives.

Chapter 2: This chapter up-scales greenhouse gas emissions (CO_2, CH_4, and N_2O) from Arctic inland waters and integrates them with the landscape sink over the study area (18 km^2) in the Indigirka River tundra Lowlands. Dissolved gas samples were collected from lakes, ponds, and fluvial systems over two summers (2016-2017), capturing the impact of large-scale flooding in 2017. These measurements were used to calculate fluxes through bootstrapping combined with satellite-derived water surface area to estimate daily, daytime carbon emissions during the summer.

Chapter 3: This chapter investigates relationships between DOM characteristics and dissolved CO_2, CH_4, and N_2O concentrations in Arctic freshwater ecosystems during the summer in the Indigirka Lowlands. DOM composition was analyzed using optical

properties (absorbance and fluorescence spectroscopy) and high-resolution mass spectrometry (PTR-MS). Statistical analyses, including principal component analysis (PCA), partial least squares regression (PLSR), and Spearman rank correlations were applied to determine whether DOM-greenhouse gas relationships exist across all freshwater systems or if they exist for each ecosystem type (ponds, lakes, fluvial systems).

Chapter 4: This chapter examines lateral carbon transport and the effects of rainfall on this transport in a small Arctic coastal catchment within the Hudson Bay Lowlands during late summer and early fall. Surface water and soil pore water samples were analyzed for DOC, DIC, $\delta^{13}\mathrm{C}$-DOC, $\delta^{13}\mathrm{C}$-DIC, POC; CO_2, CH_4, and water stable isotopes ($\delta^{2}\mathrm{H}$, $\delta^{18}\mathrm{O}$) as well as optical indices $SUVA_{254}$ and S_R to assess terrestrial-aquatic connectivity. Statistical analyses, including spatial autocorrelation (Moran's I) and Spearman rank correlations, were applied to investigate spatial patterns. We also assessed the impact of late-season rainfall on the lateral carbon export by considering carbon in the subsurface and along the surface water in the catchment.

Chapter 2

Inland water GHG exchange with the atmosphere

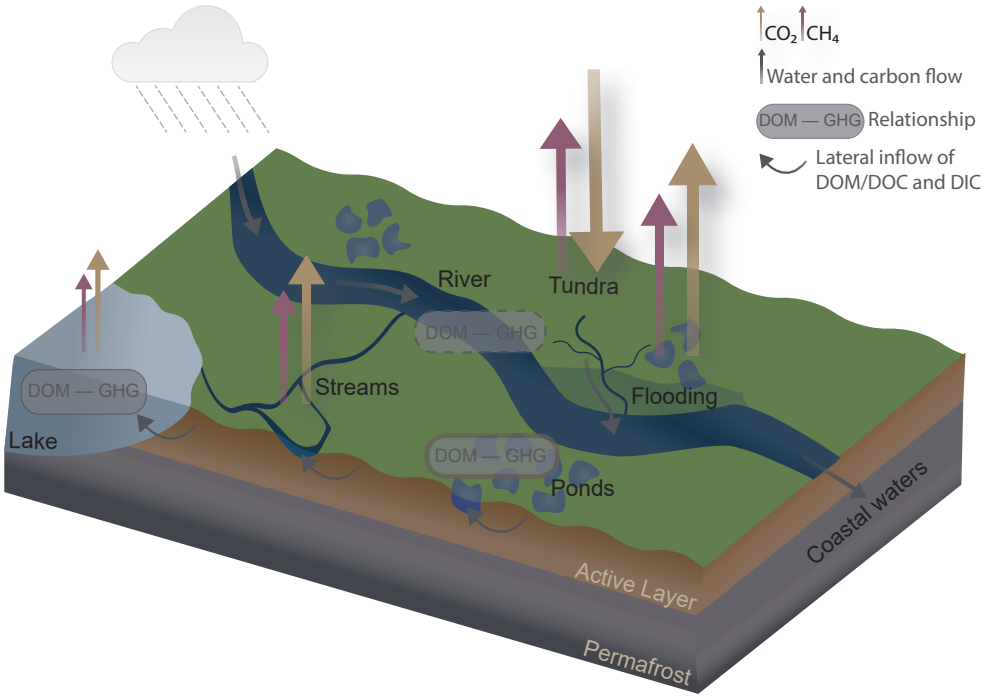

Published in Journal of Geophysical Research: Biogeosciences, 2025 as:

The Importance of Inland Water CO_2, CH_4, and N_2O for Summertime Greenhouse Gas Exchange With the Atmosphere in Arctic Tundra Lowlands

Melanie Martyn Rosco, Joshua F. Dean, Alberto V. Borges, Ove H. Meisel, Richard van Logtestijn, Geert Hensgens, Sergei Karsanaev, Trofim Maximov, James T. Weedon, Rien Aerts, Jorien E. Vonk, and A. Johannes Dolman

Inland waters in Arctic landscapes act as conduits of terrestrial organic material, transporting and processing organic material into the greenhouse gases (GHGs) carbon dioxide (CO_2), methane (CH_4) and nitrous oxide (N_2O), and subsequently exchanging these gases with the atmosphere. To assess the role of inland water emissions in the Arctic GHG budget, it is necessary to quantify their emissions in relation to the terrestrial sink capacity. We present measurements of dissolved CO_2, CH_4 and N_2O from lake, pond and low order fluvial systems across two summers (2016–2017) in the Arctic Siberian Indigirka River tundra lowlands. During May-July 2017, the region experienced large-scale flooding of which we captured the tail end. Using remote sensing images to up-scale inland water emissions to an area of approximately 18 km^2 we calculated combined carbon (C) emissions, CO_2-C and diffusive CH_4-C, under non-flood and flooded scenarios. These ranged from 7.03 ± 1.30 Mg C d^{-1} (non-flood; mean ± SD) to 9.63 ± 1.24 Mg C d^{-1} (flooded). Integrating these values into the total C landscape exchange offset the terrestrial C sink by ~9 to ~13 %. When N_2O emissions were calculated as CO_2 equivalents, these emissions were negligible relative to CO_2 and CH_4. Our study shows that in the northeast Siberian Arctic tundra, summertime CO_2 and CH_4 emissions from inland waters are a potentially important component of landscape C exchange with the atmosphere, offsetting the terrestrial sink capacity, and this may be an important consideration for constraining future Arctic responses to climate warming.

Plain Language Summary

In the Arctic, lakes, ponds, and rivers release greenhouse gases into the atmosphere as a result of biological, chemical and physical processes. Understanding how large these emissions are is important for predicting climate change impacts. To investigate this, we measured the levels of the three most important greenhouse gases in ponds, lakes and streams in an area of Arctic Siberia over two summers (2016–2017). The second year of measurements coincided with a major flooding event, allowing us to learn about the system under different conditions. We combined our measurements with satellite images that allowed us to determine the total surface area of different types of waterbodies and calculate an estimate of greenhouse gas emissions from the larger study area. When we compared these emissions to the amount of carbon absorbed by the plants on land, we found that the inland water emissions offset the carbon uptake capacity of the plants by 9 to 13%. This effect was mainly driven by emissions of methane and carbon dioxide – nitrous oxide emissions played a minor role. Our study shows that greenhouse gas emissions from Arctic lakes, ponds, and streams are an important part of the carbon exchange between the land and atmosphere.

Introduction

Inland waters, such as ponds, lakes and fluvial systems, are common features of Arctic tundra landscapes, with carbon and nutrient cycles that are closely coupled to terrestrial processes (Kling et al., 1991). Terrestrial organic material that enters inland waters can be transported, sequestered in sediments, and subjected to biogeochemical transformation processes (Drake et al., 2018). Riparian wetlands also provide inorganic and organic carbon to inland waters. As a result of both terrestrial and wetland subsidies, inland waters are important emitters of the greenhouse gases (GHGs) carbon dioxide (CO_2) and methane (CH_4), and to a lesser extent nitrous oxide (N_2O), to the atmosphere (Hu et al., 2016; Raymond et al., 2013; Rosentreter et al., 2021). In the Arctic, the terrestrial organic matter transformed in inland waters is comprised of primarily contemporary carbon fixed from the atmosphere within the last century (Dean et al., 2020; Elder et al., 2018; Raymond et al., 2007). However, older and previously sequestered soil organic matter is increasingly vulnerable to remobilization and degradation due to permafrost thaw (Biskaborn et al., 2019), driven by amplified warming in the northern high latitudes (Hensgens et al., 2021; Meredith et al., 2019; Schwab et al., 2020). Approximately, half of the global soil organic matter is stored in the upper 3 m of Arctic permafrost soils, containing an estimated 1300 Pg of carbon (Hugelius et al., 2014) and 67 Pg of nitrogen (N) (Harden et al., 2012). Therefore, permafrost thaw could result in a potentially large, yet poorly constrained, feedback to ongoing climate change (Dean et al., 2018; Schuur et al., 2015; Voigt et al., 2017).

While high-latitude inland waters are generally net carbon emitters, the contribution of CO_2 and CH_4 emissions from inland water to landscape carbon exchange with the atmosphere is poorly quantified (Denfeld et al., 2013; Karlsson et al., 2021; Lundin et al., 2013). GHG emissions from Arctic inland waters typically show high degrees of spatial

and temporal variability, driven by local environmental and climatic factors. Relatively few direct observations of these emissions exist, especially in the remote northeast lowlands of the Siberian Arctic (ca. 493,000 km^2) where ponds, lakes and fluvial systems are widespread features and soils are estimated to contain 100 Pg of carbon (Grosse et al., 2013; Muster et al., 2017; Nitzbon et al., 2020). Inland water coverage in Arctic lowland landscapes is highly variable (Grosse et al., 2008) and can change due to drainage of water bodies (Jones and Arp, 2015) or ground subsidence driven by permafrost thaw and shifts in local topography (Liljedahl et al., 2016; Vonk et al., 2015). Understanding the distinct contributions of ponds, lakes, and fluvial systems is crucial because these water bodies exhibit different hydrological, biogeochemical, and emission dynamics. By differentiating between these systems, we can more accurately assess their individual roles which will allow for a better balancing of regional carbon budgets (Webb et al., 2019), in addition to improving estimates of future emissions.

The Arctic has generally low availability of nitrogen (N), partially due to low atmospheric deposition (Dentener, 2006) and partially due to high competition between microbes and vegetation for the available N (Jonasson et al., 1999). Thus, N_2O emissions from Arctic landscapes and their inland waters have received less attention than those of CO_2 and CH_4 (Martikainen et al., 1993; Rodionow et al., 2006). High N_2O emissions have been recorded from subarctic bare peat surfaces after permafrost thaw (2.81 ± 0.60mg N_2O m^{-2} d^{-1}, (Voigt et al., 2017)). However, inland waters tend to be either minor N_2O sinks or sources (Harms et al., 2020; Kortelainen et al., 2020; Soued et al., 2015). This was also observed in other low N inland water environments such as the Congo River (Borges et al., 2019). The uncertain role of inland waters in the Arctic N_2O budget makes it difficult to constrain how N_2O emissions might impact permafrost climate feedbacks.

One possible consequence of a warming Arctic is the risk of increased flooding of lowland tundra landscapes. Deeper snow depth and longer snow cover duration have already been observed in Siberia (Bulygina et al., 2011), while climate models predict continued increases in snow depth during this century (Callaghan et al., 2011; Thackeray et al., 2019). This means greater meltwater runoff in the spring, resulting in increased magnitude and/or duration of flood events. Flooding can increase inland water emissions as observed in other Siberian rivers (Krickov et al., 2021; Vorobyev et al., 2021). In northeast Siberia, an additional ~250 % of precipitation fell in autumn 2016 (as snow) compared to the average of the previous 11 years. This increased snowfall resulted in the Indigirka River spring melt runoff lasting from May until mid-July 2017 compared to its usual abatement in June (Iwahana et al., 2014; Tei et al., 2020). The high runoff caused extreme flooding which increased the inundated area of the Indigirka River lowlands from 10,789 km^2 in July of 2015 to 16,016 km^2 in July of 2017, a ~50 % increase (Tei et al., 2020).

Quantifying GHGs (CO_2, CH_4 and N_2O) emissions from different types of inland waters in a range of hydrological condition in the context of the terrestrial sink demonstrates the potential importance of inland waters to regional GHGs budgets. Here we present simultaneous concentration measurements of dissolved CO_2, CH_4 and N_2O from ponds, lakes and low order fluvial systems in the Indigirka River lowlands in northeast Siberia

across two summers (2016 and 2017). Our field campaigns included the tail end of the May-July 2017 flood event. The measured concentrations were used to calculate diffusive CO_2, CH_4 and N_2O emissions to the atmosphere and their relative magnitude to terrestrial emissions during a flood (2017) and non-flood year (2016). The objectives of this study were to quantify: (a) the importance of daily CO_2-C and diffusive CH_4-C emissions from all inland water types present in comparison to the combined terrestrial CO_2-C and diffusive CH_4-C exchange of the study area; (b) the importance of inland water N_2O emissions relative to CO_2 and CH_4 emissions; and (c) the impact of flooding on the landscape GHG exchange with the atmosphere.

Materials and Methods

Study area

The 'Kytalyk' National Park is located in the Indigirka lowlands, Sakha Republic, north-east Siberia (70°49′N, 147°29′E). The study area occupies ~18 km^2 on the north bank of the Berelekh River, a western tributary to the Indigirka River, 30 km northwest of the town Chokurdakh (Figure 2.1). The broader Indigirka River basin encompasses approximately 120,610 km^2 (Tei et al., 2020). Our study area lies within the lower Indigirka floodplain, where hydrological boundaries are often diffuse and not well-defined, particularly in thermokarst-affected landscapes with none to minimal gauging infrastructure. The region is underlain by continuous permafrost over 300 m thick (Shahgedanova, 2003) with an overlying active layer that thaws ~20-30 cm deep every summer during July/August (Dean et al., 2020). The local climate is continental, with a mean annual air temperature of -13.4°C and an average July temperature of 10.3°C (1981–2010) (Trouet and Van Oldenborgh, 2013). The mean annual precipitation is ~230 mm, of which roughly half falls as rain during the growing season (May – September) and the other half as snow (Dean et al., 2020). Snowmelt usually begins at the end of May to early June (Iwahana et al., 2014). The landscape is dominated by three topographical levels, from lowest to highest: river floodplain areas, drained thermokarst lake basins of Holocene age (alases), and ridges of Pleistocene-aged sediments termed yedoma. The local vegetation, is classified as graminoid tundra: tussock-sedge, dwarf-shrub, moss-tundra (Walker et al., 2005).

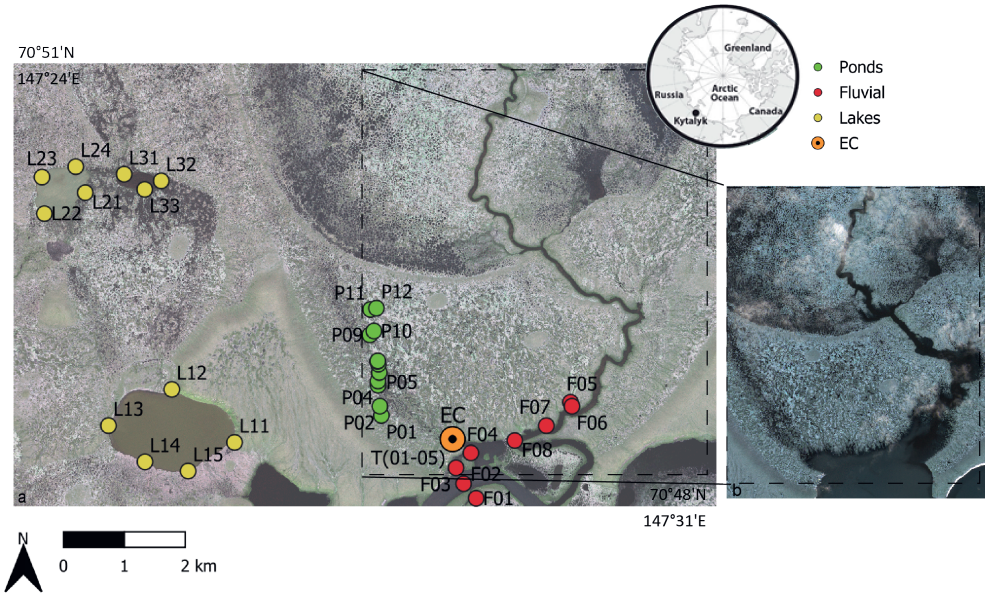

Figure 2.1: (a) Kytalyk research area shown in a WorldView-2 image from July 2015. The image shows the study area over which the landscape greenhouse gas exchange was determined (17.81 km^2). (b) Flooding extent shown in a WorldView-2 image from July 2017. The left half of the image was obscured by cloud cover and was therefore excluded from the analysis. The dashed black box in panel (a) indicates the area covered by panel (b). Flood samples were taken by the EC tower and are indicated by T01–T05. EC marks the location of the eddy covariance tower.

Study approach

In the interest of clarity throughout this study we briefly define the terminology used here. In this study we define 'C emissions' as the combined daily CO_2-C and diffusive CH_4-C while GHG emissions are defined as the combined CO_2, and CH_4 and N_2O emissions in CO_2-equivalents:

$$\text{C emissions} = CO_2\text{-C} + \text{diffusive } CH_4\text{-C per day}$$

$$\text{GHG emissions} = CO_2 + CH_4 + N_2O \text{ per day}$$

When discussing the dissolved gas concentrations we refer to 2016 as a 'normal' year and 2017 as a 'wet' year:

$$\text{Normal year} = 2016 \text{ dissolved gas concentrations}$$

$$\text{Wet year} = 2017 \text{ dissolved gas concentrations}$$

The flooding that occurred in 2017, mainly along the extended riparian zone of the

Berelekh River, did not reach the northernmost two lakes (L21-L24, L31-L33) and ponds (Figure 2.1). Nonetheless, the influence of the higher snow fall from the previous autumn (2016) is reflected in the observed measurements (see section 3 and section 4). In the up-scaling results and discussion, we refer to a non-flood and a flooded scenario. In the flooded scenario we include floodwaters (Figure 2.1 b) as a separate inland water system to discern their effects on up-scaled emissions (see also Section Landscape GHG exchange calculations).

$$\text{Non-flood scenario} = \text{all inland water systems included in up-scaling}$$

$$\text{Flooded scenario} = \text{all inland water systems + floodwater as conceptual}$$

Sampling

Inland water sites were sampled in summer (late July to early September) of 2016 and 2017. In total, two small lakes (<3 m deep, 0.04 and 0.14 km^2 in area), one thermokarst lake (L11-L15, up to 7 m deep, 0.51 km^2, actively eroding into a yedoma ridge), 12 pond sites (<0.5 m deep, 3-240 m^2), and 8 fluvial sites along a ~5 m wide stream and the Berelekh River bank were sampled (Figure 2.1). Due to the logistical challenges of site access in the far east Siberian Arctic tundra at the Kytalyk Nature Reserve, water bodies could only be accessed by foot. Therefore, sampling of dissolved concentrations could only be obtained by syringe headspace equilibrations, and direct flux measurements were not possible. Further, water bodies could only be sampled from the edge (Dean et al., 2020). Lake areas were derived from a geomorphological map of the study area (van Huissteden et al., 2021) while pond surface areas and stream width were measured in the field with tape measures and are indicative. Additionally, five locations of flooded tundra area were sampled in 2017. For an overview of the sampling locations and frequency please see Table 2.S1. Ponds are defined in this study as lentic water bodies with a surface area smaller than 0.01 km^2. Each flooded tundra location was sampled four times in 2017. In-situ measurements of water temperature, pH, electrical conductivity (EC), water depth and surface area were performed during sample collection. Temperature and EC were measured with a Greisinger GMH 3431 meter (accuracy of ± 2 µs/cm and ± 0.2 K), pH was measured using a Sensorex SAM-1^{TM} meter (accuracy of ± 0.01). EC values were converted to freshwater salinity values using a factor of 0.55 (Rusydi, 2018). Dissolved gas samples from the surface water and ambient air samples were collected using the headspace technique following Borges et al. (2015) and Dean et al. (2020). Surface water was collected directly using a 60 ml polypropylene syringe, which was pre-rinsed three times with sample water before collection. Water was drawn gently from 5–10 cm below the surface to minimize turbulence and bubble formation. Samples were equilibrated in 60 ml syringes by shaking 30 ml water with 30 ml ambient air for 1 minute, away from direct sunlight. After equilibration, the headspace was transferred to a pre-evacuated 12 ml Exetainer® vial (Labco, UK).

Greenhouse gas analyses

Headspace GHG concentrations were determined using an SRI 8610C Gas Chromatograph (GC) at the University of Liège. CO_2 and CH_4 concentrations were measured by a flame ionization detector fitted with a methanizer, N_2O concentrations were measured by an electron capture detector equipped in the GC. The GC was calibrated with CH_4:CO_2:N_2O mixtures (Air Liquide Belgium) of 1, 10, 30 ppm CH_4, 400, 1000, 4000 ppm CO_2 and 0.2, 2.0 and 6.0 ppm N_2O. The concentrations of CO_2, CH_4 and N_2O were calculated according to Henry's Law using solubility coefficients from Weiss (1974), Yamamoto et al. (1976) and Weiss and Price (1980), respectively.

GHG flux calculations

The GHG fluxes (F) between the water surface and atmosphere were calculated according to Fick's first law:

$$F = k\,(c_{\mathrm{surf}} - c_{\mathrm{eq}}) \tag{2.1}$$

where k is the gas exchange constant (cm h^{-1}), c_{surf} is the gas concentration in surface water (µmol L^{-1}) and c_{eq} is the gas concentration in surface water in equilibrium with the atmosphere (µmol L^{-1}). Daily average atmospheric gas concentrations were determined from ambient samples taken throughout the sampling campaign. In 2016 no N_2O ambient air samples were available, and in 2017 no CO_2 ambient air samples were available. In these instances, monthly averages were used from discrete flask measurements taken at the NOAA Hydrometeorological Observatory of Tiksi, Russia (~300 km away from the field site) (Conway, 2007).

The gas exchange constant k was computed by normalizing the gas transfer velocity to the Schmidt number of 600, which corresponds to the Schmidt number of CO_2 at 20°C in freshwater.

$$k = k_{600} \left(\frac{Sc}{600} \right)^{-b} \tag{2.2}$$

Here b is the Schmidt exponent; b = 0.67 for wind speeds < 3 m s^{-1} and b = 0.5 for wind speeds $\geq$ 3 m s^{-1} (Jähne et al., 1987). Sc is the Schmidt number of the gas calculated from empirical fourth-order polynomial fits of Schmidt number versus water temperature (Wanninkhof, 2014). K_{600} was calculated using a power relationship between wind speed at a height of 10 m and gas exchange determined for low wind environments (Cole and Caraco, 1998):

$$k_{600} = 2.07 + 0.215\,U_{10}^{1.7} \tag{2.3}$$

where wind speed per day was the average of all measurements taken by the local meteorological tower, gapfilled with ERA5 data (Hersbach et al., 2020), every 30 minutes between 9:00 and 17:00 (Dean et al., 2020). The power law was used to convert the measurements taken at a height of 5 m (U_r) to corresponding wind speeds at a 10 m

height (U_{10}):

$$U_{10} = U_r \left(\frac{10}{z_r} \right)^a \tag{2.4}$$

where the exponent *a* quantifies wind shear and for near-neutral stability conditions, over land *a* is approximately $\frac{1}{7}$ and z_r is the reference height at 5 m. Finally, values are averaged to provide daily wind speed values.

Equation 2.3 was used to derive k_{600} values for lake fluxes and floodwater fluxes as the floodwater was characterized by standing water with large surface areas equivalent to a lake (Figure 2.1 b). The power relationship does not always apply consistently for ponds and fluvial systems. For ponds, five k_{600} values were found in the literature (Holgerson et al., 2017; Kuhn et al., 2018). For fluvial systems, two values were found in the literature (Aufdenkampe et al., 2011; Denfeld et al., 2013) and two values were derived from a parameterization as a function of stream slope and velocity (Raymond et al., 2012) with stream slope values taken from RiverATLAS (Linke et al., 2019) and stream velocity computed from discharge (Liu et al., 2022). For a list of the aforementioned k_{600} values please see Table 2.S2. To account for the possible range in k_{600} values in pond and fluvial sites a uniform distribution containing 1,000 values, to represent the equal likelihood of each value, was generated from the literature values. Values from the corresponding distribution were randomly assigned to each sample to estimate a non-biased k_{600} value.

Inland water surface areal coverage calculations

In order to estimate inland water emissions the surface areal coverage is needed in addition to the fluxes of each inland water system. The relative areal coverage of ponds, fluvial systems and the tundra was derived by classifying an available WorldView-2 satellite image with a 2 m spatial resolution and four spectral bands (blue, green, red and near infrared) from the 10th of July 2015. We estimated from visual corroboration during field work that water surface area coverage in 2016 was similar to 2015. Polygons of the lake areas from a geomorphological map of the study area (van Huissteden et al., 2021) were used to mask out the lakes in the satellite image. Digital numbers in the remote sensing products were converted to radiance values and subsequently to top of atmosphere reflectance values. A random forest (RF) classification model (Breiman, 2001) was used (*scikit-learn* package (Pedregosa et al., 2011)) in *Python 3* (Rossum, 2009) to classify pixels either as pond, fluvial or tundra classes. Training data was generated by visual inspection, 1,000 points were selected for each class. The out-of-bag error (OOB) is derived in a bootstrapping procedure using about one third of the data and provides an unbiased estimate of the model performance (Breiman, 2001). The OOB prediction of accuracy for the 2015 image classification was 99.4 %. Single pixels were sieved to remove noise. We set a limit of each water body consisting of at least two pixels, which equates to a surface area of 16 m^2: only one sampled pond (P06) had a surface area smaller than this, which is discussed further in the Section Results and Discussion Sub-Section Concentrations.

To analyze the effect of tundra flooding on the landscape's GHG exchange, the cal-

culation of inland water areal coverage assumed that the flooded tundra area was the difference in water surface area coverage between the cloud-free segment of a Worldview image from the 9th of July 2017 and the image from 2015 (Figure 2.1 b). The 2015 image represents a 'normal' year with no extreme flooding, and it serves as the baseline for comparison with the 2017 flood event. The fluvial surface area coverage was assumed to be the same in 2017 as in 2015, and is considered separately from flooded tundra in the flooded-scenario up-scaling calculations described below (Section Landscape GHG exchange calculations) in order to isolate the effect of the additional flooded area separate from the usual fluvial surface area coverage (i.e., the floodwaters are considered their own inland water "type" in addition to the ponds, lakes and existing fluvial system). RF classification on the Worldview image from the 9th of July 2017 was carried out with its own 1,000 points per class training dataset and yielded an OOB prediction accuracy of 86.5 %.

Landscape GHG exchange calculations

The CO_2 and CH_4 flux of the tundra land cover class is derived from measurements recorded by an eddy covariance tower during the 2016 sampling period (31 July 2016 – 09 August 2016) (Dean et al., 2020). Eddy covariance measurements were only available for 2016. The tower site was flooded during summer 2017, which disrupted instrumentation and prevented data collection that year. The eddy covariance (EC) tower was installed in 2003 and is outfitted with an ultrasonic anemometer (Gill Instruments, Lymington, Uk, R3-50) for measuring wind speed and temperature, and two open-path infra-red gas analyzers for the measurements of CO_2 (LI-COR LI-7500) and CH_4 (LI-COR LI-7700). The methane analyzer was initially installed in 2008 and has been upgraded to the model mentioned above in 2014. All measurements are collected at 10 Hz at a height of 4.7 m. The footprint of the tower has a diameter of approximately 300 m. Method validation of the eddy covariance methods was demonstrated at the site previously (Dean et al., 2020).

Data was processed using EddyPro (version 6.2.2) software and transformed to 30 min flux averages. The configuration was set to include 2D rotation of anemometer coordinates, WPL correction (compensation of air density variations), spectroscopic corrections for the LI-7700 and spectral corrections. Data quality was ensured by removing values that did not pass the EddyPro quality control and implausibly high fluxes. Subsequent filtering was done by removing fluxes with too low air friction ($u^* < 0.163$). Spikes were removed only for CO_2 fluxes following a standardized method, using a threshold z of 4 over a period of 13 days (Papale et al., 2006).

Only fluxes measured during the day, between 09:00 and 17:00 were selected to match that the dissolved gas concentrations were only sampled during the day. Additionally, only fluxes captured from a wind direction covering a dry or mixed area that did not contain the river are used, as open water covers less than 1 % of these areas in the study site (Abbott, 2022). Tundra N_2O fluxes (48 in total) are selected from aggregated data published by Voigt et al. (2020) if they matched the following criteria: measured in-situ in Arctic and Subarctic regions, either on upland or peatland ecosystems, on vegetated or partly vegetated surfaces, without disturbance or experimental manipulation.

To evaluate the contribution of CH_4 and N_2O emissions to the daily inland water GHG emissions and daily landscape GHG exchange with the atmosphere, CH_4 and N_2O were converted to CO_2-equivalent using sustained global warming (SGWP) and cooling potentials (SGCP) over a 100-year timeframe (Neubauer and Megonigal, 2015) (CH_4: SGWP = 45, SGCP = 203; N_2O: SGWP = 270, SGCP = 349).

To calculate the daily GHG and C fluxes for each inland water system and to estimate associated uncertainties, we followed a non-parametric bootstrapping procedure (Efron, 1987). First outliers in c_{surf}, identified following the 1.5 interquartile range rule, were excluded from the flux calculations. For each water system we generated 1000 k, c_{surf} and c_{eq}, by values by sampling with replacement from the data observed or computed (as detailed above), and calculated the median of each bootstrap sample. This resulted in 1000 values of each parameter which were then used to compute a corresponding distribution of flux estimates by Equation 2.1. The same method was applied to tundra GHG and C fluxes, also 1,000 times. The median GHG and C flux was multiplied by the corresponding water surface area coverage to calculate day-time summer GHG and C diffusive emissions per day. In 2017, when the floodwater fluxes were included, fluvial and floodwaters were considered separate classes. Daily landscape GHG or C exchange, the sum of tundra emissions and inland water GHG or C diffusive emissions, was calculated for the study area (17.81 km^2; Figure 2.1).

We used the standard rules of error propagation to quantify uncertainty in resulting emissions (Karlsson et al., 2021; Serikova et al., 2019). We assumed 15 % uncertainty in the water areas, 15 % being a conservative estimate based on the OOB values from the RF classifications:

$$\delta R_i = R \times \sqrt{(\delta x)^2 + (\delta y)^2}$$

Here, δR_i is the uncertainty of GHG/C emissions for each inland water system or the tundra, δR is the mean calculated emission, δx is the coefficient of variation of the emission, and δy is the 15 % uncertainty estimate of surface areas. Then the uncertainties for the total inland water GHG/C emissions and landscape GHG/C exchange are estimated as:

$$\delta R_{total} = \sqrt{\sum (\delta R_i)^2}$$

Here R_{total} is the uncertainty of the total inland water GHG/C emissions or landscape GHG/C exchange, and δR_i are GHG/C emissions uncertainties for each inland water system or the tundra. The up-scaled emissions and the corresponding uncertainties are reported as a mean $\pm$ 1 SD.

Statistical analysis

To investigate the spatiotemporal variability and autocorrelation of the dissolved gas concentrations from lake and pond samples we used linear mixed model (LMM) with random effects in *R* (Team et al., 2016) using the *lme4* package (Bates et al., 2015). Sampling

years and sampling sites are set as random effects. Model assumptions were verified by plotting residuals versus fitted values to check homogeneity, and plotting residuals vs. theoretical values from a normal distribution on a q-q plot to check normality (Zuur et al., 2009). No fixed-effects were set because the model is used only to analyze spatiotemporal variance by implementing random effects, therefore the assumption of multicollinearity was not checked. There was insufficient fluvial data to run an insightful LMM analysis due to inconsistencies in the locations of sample sites caused by the flooding in 2017.

Note that in the text we report measured values including outliers. When reporting measured variables and uncertainty we used median [interquartile range] due to the non-normal distribution of the data.

Results

All sampled inland waters were supersaturated with CO_2 and CH_4 with respect to atmospheric concentrations (Figures 2.2-2.3). Dissolved CO_2 concentrations ranged from 27 to 1333 µmol L^{-1} and dissolved CH_4 from 0.04 to 251 µmol L^{-1} (Table 2.1). Ponds generally had the highest concentrations, followed by fluvial and then lake sites (Figures 2.2-2.3). CO_2 concentrations at ponds sites were ~9 and ~3-fold greater than at lake and fluvial sites, respectively. The difference between pond CH_4 concentrations and lake and fluvial sites was even higher (~25-fold and ~4-fold, respectively; Figure 2.3).

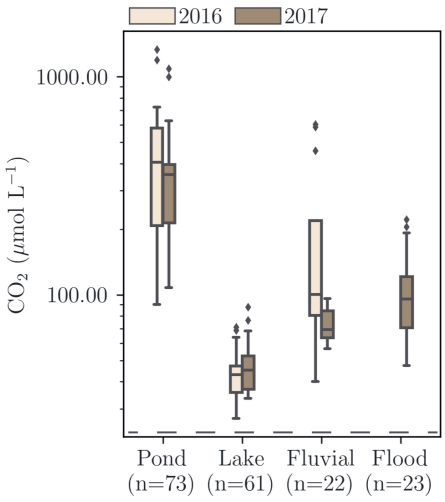

Figure 2.2: CO_2 surface water dissolved concentrations from ponds, lakes, fluvial, and flood sites in Kytalyk, Siberia, in 2016 and 2017. The dashed line at the bottom of the panel indicates the mean atmospheric concentration in equilibrium with the atmosphere (CO_2 = 19 µmol L^{-1}). Boxes indicate the interquartile range, whiskers indicate 1.5 × the interquartile range, and dots indicate values lying outside the 1.5 × interquartile range. Note that the y-axis is shown on a logarithmic scale. Values in parentheses indicate sample size (n).

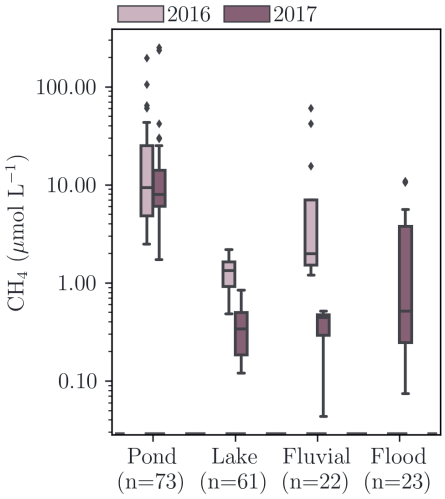

Figure 2.3: CH_4 surface water dissolved concentrations from ponds, lakes, fluvial, and flood sites in Kytalyk, Siberia, in 2016 and 2017. The dashed line at the bottom of the panel indicates the mean atmospheric concentration in equilibrium with the atmosphere (CH_4 = 0.004 µmol L^{-1}). Boxes indicate the interquartile range, whiskers indicate 1.5 $\times$ the interquartile range, and dots indicate values lying outside the 1.5 $\times$ interquartile range. Note that the y-axis is shown on a logarithmic scale. Values in parentheses indicate sample size (n).

Table 2.1: Summary of measured physical and biogeochemical characteristics per inland water system.

	Unit	Lake	Ponds	Fluvial	Flood
Individual area	m^2	511,200; 140,600; 41,720	3–240	–	–
Surface area coverage of study area	km^2	0.95	1.84	0.33	1.7
	%	5	10	2	7
Surface temperature	°C	9–17	9–22.4	9–15	8–17
		13 [10–14]	14 [11–16]	14 [10–15]	14 [10–15]
pH		4.8–9.1	4.4–7.6	4.9–7.8	4.9–6.3
		7.0 [6.3–7.8]	5.8 [5.4–6.0]	6.4 [5.7–7.2]	5.8 [5.5–6.2]
Conductivity	µS cm^{-1}	10–209	13–52	14–77	16–32
		29 [16–176]	21 [16–27]	46 [17–49]	19 [18–22]
Dissolved CO_2	µmol L^{-1}	27–87	90–1,333	40–603	47–220
		43 [36–49]	358 [208–496]	84 [66–106]	121 [71–121]
Dissolved CH_4	µmol L^{-1}	0.12–2.2	2–251	0.04–60	0.07–11
		0.8 [0.4–1.4]	9 [5–15]	1.2 [0.5–2.0]	0.5 [0.3–4]
Dissolved N_2O	nmol L^{-1}	5–16	0.1–13	3–15	9–14
		8 [7–13]	6 [4–8]	8 [6–13]	11 [11–12]

Note. Values are ranges (min–max) and median [interquartile range].

The variance of pond CO_2 and CH_4 concentrations were, according to the linear mixed model (LMM; see Sub-Section Landscape GHG exchange calculations in Section Materials and Methods), as much explained by the spatial variance between ponds (42 % and 58 % of total variance respectively) as by variance within a pond and year (49 % and 59 %

respectively). The highest pond CO_2 and CH_4 concentrations were found in P06 (median 1041 [IQR 793 - 1163] µmol L^{-1} and 151 [73 - 225] µmol L^{-1}), which is the smallest sampled pond with a sub-pixel surface area of 3 m^2. As a result of these high values, site P06 was excluded from the LMM analysis. This pond appears to have formed within a melting ice wedge (Figure 2.S1 A).

For lake concentrations, the variance of CO_2 and CH_4 concentrations between sampling sites within a lake was higher (35 % and 4 % respectively) than the variance between lakes (3 % for CO_2 and 5 % for CH_4). These results indicate no significant variance between dissolved gas concentrations from different lakes. In the LMM with the spatial random effect set as the sampling sites within a lake a much lower proportion of the total variance in lake dissolved gas concentrations was explained by variation between the sampling years for CO_2 concentrations (13 %) in comparison to CH_4 concentrations (79 %).

Dissolved CO_2 and CH_4 concentrations had the largest variation at fluvial sites (Figures 2.2-2.3) in part due to the highest CO_2 and CH_4 concentrations found at the site F05 (588 [522 - 596] µmol L^{-1}, 42 [29 - 51] µmol L^{-1}, respectively); these values were an order of magnitude for CO_2 and two orders of magnitude for CH_4 higher than those of all other fluvial sites (75 [65 - 90] µmol L^{-1}, 0.5 [0.4 – 1.7] µmol L^{-1}). Site F05 was categorized as a fluvial site as it appears on satellite images to be a small channel joining the stream. The field campaign revealed that F05 was largely disconnected from the main channel that joins the stream (Figure S1B). It is unclear if F05 was a pond that connects to the stream when overland flow occurs or if it had become disconnected overtime. A quantitative analysis of fluvial CO_2 and CH_4 concentrations variance was not possible due to the logistical disruption caused by the flooding in 2017 making the sites sampled in 2016 inaccessible. As a result, none of the same fluvial sites were sampled in both years. Nonetheless, visual inspection of Figures 2.2-2.3 indicates that CO_2 and CH_4 concentrations were lower in 2017 than in 2016, especially for CH_4 concentrations.

Given the lack of consistent spatial patterns in lake CO_2 and CH_4 concentrations, and the approximately equal within- and between-pond variability, we combined data from each inland water type within a sampling year for the upscaling analysis. Temporal differences were clearer for CH_4 than for CO_2 (Figures 2.2-2.3), but this variation did not warrant treating sites separately within an inland water type. As a result, we defined one representative land cover class per inland water type (lake, pond, fluvial) for each year. This resulted in a single lake, pond and fluvial land cover class for 2016 and 2017. The impact of flooding on fluvial CO_2 and CH_4 concentrations is taken into consideration through the up-scaling exercise by accounting for a non-flood summer scenario using concentration values from 2016 only, and a separate up-scaling for a flooded summer scenario using concentration values from 2017 (see Sub-Section Study approach in Section Materials and Methods).

CO_2 and CH_4 emissions and up-scaling

The estimated C emissions (defined as the combined daily CO_2-C and diffusive CH_4-C in sub-section 2.2) from all inland waters across the study area in the non-flood summer

scenario were 7.03 ± 1.30 Mg C d^{-1} (mean ± SD). Ponds had the largest surface area coverage (10 %) of the different inland water systems (Table 2.1) and the largest contribution to inland water C emissions with 5.13 ± 1.24 Mg C d^{-1} (73 %), fluvial systems were the second largest contributors with 1.40 ± 0.38 Mg C d^{-1} (20 %), and lakes contributed 0.50 ± 0.09 Mg C d^{-1} (7 %). CO_2-C accounted for the majority of inland water C emissions (97 %) in contrast to CH_4-C (3 %). Tundra emissions were –83.35 ± 13.30 Mg C d^{-1} for CO_2 and 0.54 ± 0.11 Mg C d^{-1} for CH_4-C resulting in a landscape C exchange with the atmosphere of –75.78 ± 13.29 Mg C d^{-1}. Lakes account for less than 1 % of total landscape C exchange, fluvial systems for 2 % and ponds for 7 %. Including C emissions from the inland waters offset the landscape C sink by around 9 %.

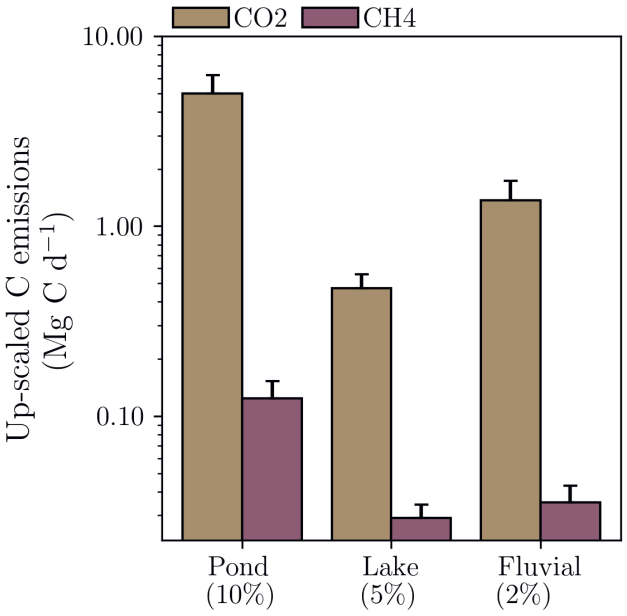

Figure 2.4: Estimated daily C emissions (CO_2-C and diffusive CH_4-C) per inland water system (pond, lake, and fluvial), integrated over their corresponding surface area coverage of the study area in Kytalyk, Siberia, for the non-flood summer scenario. Relative surface area coverage (%) is given in parentheses. Bars represent the mean, and error bars represent the standard deviation (SD).

N_2O emissions and up-scaling

In 2016, the pond, lake and fluvial sites were undersaturated with N_2O with respect to the atmosphere. Whereas in 2017, the wet year, lake and fluvial sites became oversaturated while pond and flood N_2O concentrations ranged from under- to oversaturation (Figure 2.5). Pond N_2O concentrations were on average the lowest of the four inland water systems. The LMM analysis showed that the variance between sampling years

explained much of the variance observed in N_2O concentrations in ponds (68 % of total variance) and lakes (95 %).

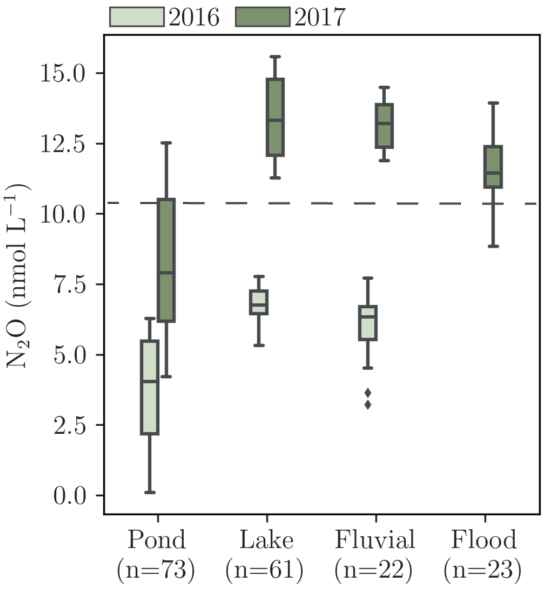

Figure 2.5: N_2O surface water dissolved concentrations from ponds, lakes, fluvial, and flood sites in Kytalyk, Siberia, in 2016 and 2017. The dashed line indicates the mean atmospheric N_2O concentration in equilibrium with the atmosphere (10.77 nmol L^{-1}). Boxes indicate the interquartile range, whiskers indicate 1.5 × the interquartile range, and dots indicate values lying outside the 1.5 × interquartile range. Values in parentheses indicate sample size (n).

In the non-flood summer scenario, CO_2 emissions accounted for 70 %, and diffusive CH_4 emissions for 31 %, of the inland water GHG emissions in CO_2-equivalents; N_2O emissions acted as a net weak sink, reducing the net radiative forcing of inland water emissions by the equivalent of < 1 %. Integrating inland water N_2O emissions with the tundra, which acted as a N_2O source, resulted in N_2O emissions offsetting the net radiative forcing of the landscape GHG sink by the equivalent of ~0.1 %.

The tundra was a CH_4 source (3 ± 1 × 10^4 kg $CO_{2\text{-eq}}$ d^{-1}) which due to its large warming potential offset the tundra GHG sink by 10 %. However, since the tundra was a large CO_2 sink (-30 ± 5 × 10^4 kg $CO_{2\text{-eq}}$ d^{-1}), this part of the landscape continued to act as a net GHG sink (-28 ± 5 × 10^4 kg $CO_{2\text{-eq}}$ d^{-1}). The additional net radiative forcing of inland water GHG emissions (4 ± 1 × 10^4 kg $CO_{2\text{-eq}}$ d^{-1}) does offset the tundra GHG sink, but the landscape GHG exchange in $CO_{2\text{-eq}}$ remains overall a GHG sink relative to the atmosphere (Figure 2.6).

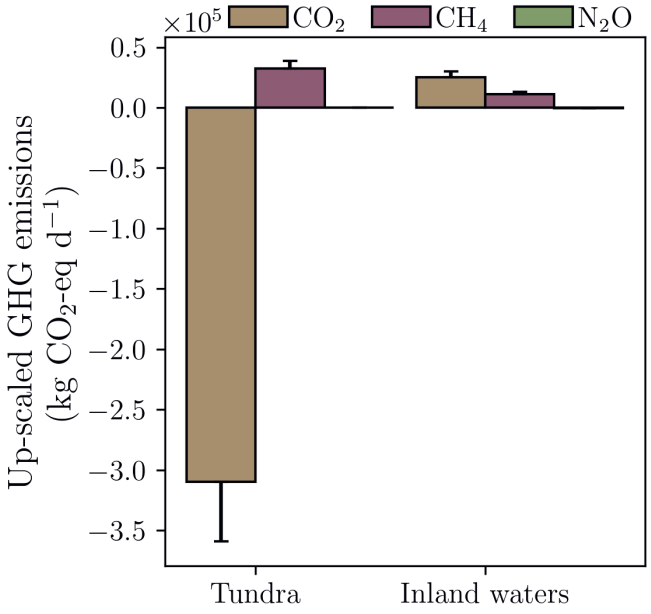

Figure 2.6: Estimated daily GHG (CO_2, CH_4, and N_2O) emissions of inland waters and the tundra, integrated over their corresponding surface area coverage of the study area in Kytalyk, Siberia, for the non-flood summer scenario. Bars represent the mean, and error bars represent the standard deviation (SD). Note .that the y-axis is shown in scientific notation ($\times 10^5$).

Floodwater

In 2017, an estimated 10 % of our study area, previously classified as tundra, was flooded and reclassified as such. As a result the tundra was reduced from a land area coverage of 83 % down to 73 % (Figure 2.1b). Floodwater CO_2 and CH_4 concentrations (median 96 [IQR 71 - 121] µmol L^{-1} and median 0.5 [IQR 0.3 – 3.8] µmol L^{-1}, respectively) were slightly lower than pond and fluvial concentrations but higher than in the lakes (Figures 2.2- 2.3). We include floodwater C emissions in a flooded summertime up-scaling scenario, resulting in a combined CO_2-C and diffusive CH_4-C emissions from all inland waters across the study area of 9.63 ± 1.24 Mg C d^{-1} (mean ± SD), of which flood emissions accounted for 32 % (Figure 2.7). The landscape C exchange with the atmosphere in this scenario was –63.52 ± 11.71 Mg C d^{-1}. Lake and fluvial systems, and floodwaters were small N_2O emission sources in this scenario, while ponds remained small N_2O sinks, resulting in inland water N_2O emissions in CO_2-equivalents being overall a small source to the atmosphere.

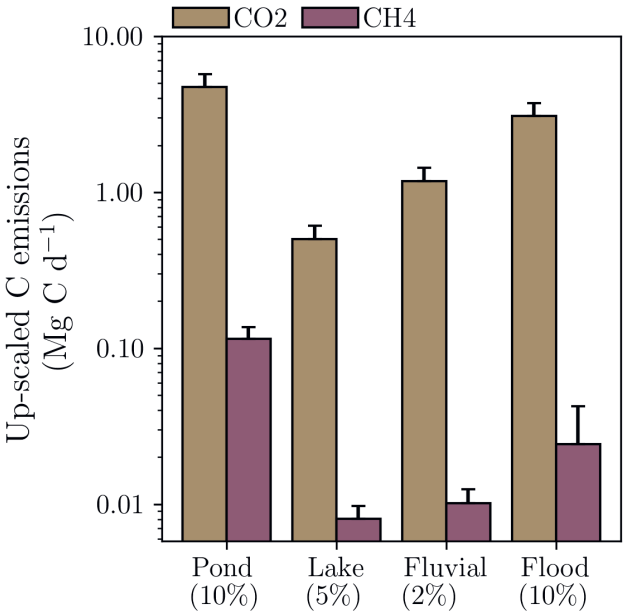

Figure 2.7: Estimated daily C emissions (CO_2-C and diffusive CH_4-C) per inland water system (pond, lake, fluvial, and flooded tundra), integrated over their corresponding surface area coverage of the study area in Kytalyk, Siberia, for the flooded summer scenario. Bars represent the mean, and error bars represent the standard deviation (SD).

Discussion

CO_2 and CH_4

Concentrations

The inland water dissolved CO_2 and CH_4 concentrations observed in this study show that ponds, lakes and fluvial systems have markedly different carbon dynamics. The median concentrations in ponds, lakes and fluvial systems are all significantly different to each other in both sampling years (Figures 2.2- 2.3). Our lake sites on average had lower CO_2 and CH_4 concentrations than lakes in Western Siberia (Repo et al., 2007) and Western Canada (Dean et al., 2016), but were comparable to lakes in Northern Sweden (Lundin et al., 2013) (Table 2.S4). Our pond CO_2 and CH_4 concentrations were similar to concentrations measured in Western Canada (Dean et al., 2016), lower than in Northern Sweden (Kuhn et al., 2018) and considerably higher than an average of 'temperate & boreal' ponds (Holgerson and Raymond, 2016) (Table 2.S5). Fluvial CO_2 concentrations in our study area were lower than measured concentrations in Northern Sweden (Lundin

et al., 2013), comparable to Western Canada (Dean et al., 2016) and to streams in the Kolyma watershed (Denfeld et al., 2013). However, CH_4 concentrations at our fluvial sites were on average an order of magnitude higher than in Northern Sweden (Lundin et al., 2013) and Western Canada (Dean et al., 2016) (Table 2.S6). The range of flood CH_4 concentrations in this study were two orders of magnitude higher than observations in tributaries located further south to our study site, close to Chokurdakh, upstream of the Indigirka under the same flood conditions in 2017 (Morozumi et al., 2019).

We observed lower surface water CH_4 concentrations in the wet year of 2017 compared to 2016 at fluvial and lake sites. However, we did not observe this in ponds or for CO_2 concentrations. While it is likely that the deeper and longer snow cover in 2017 had an effect on CO_2 and CH_4 concentrations during the ice-cover period, it has been observed that higher precipitation in winter as snow does not have an effect on ice-free season lake CO_2 concentrations (Rantakari and Kortelainen, 2005). Ice and snow cover dynamics can affect inland water concentrations by limiting gas exchange and solar radiation, affecting the transformation processes of organic carbon into CO_2 or CH_4. It is likely that if the deeper and longer snow cover had an effect on dissolved gases this would have been visible for a short period at ice-off (Denfeld et al., 2015). It is more likely that lower lake and fluvial site CH_4 concentrations in the wet year are related to other environmental drivers such as temperature (Yvon-Durocher et al., 2014). We observed that lake and fluvial surface water temperatures were on average 4°C lower in 2017 compared to 2016, whereas pond temperatures were similar in both years. The lower surface water temperatures in the wet year could have been driven by the late snowmelt, and snow was still present on part of the landscape during the 2017 field campaign. Whereas in ponds, the cooling effect of late snowmelt could be negated by rapid warming through solar radiation of their shallow water columns.

The high CO_2 and CH_4 concentrations measured at the smallest pond P06 could be driven by local geomorphological features, such as its close connection to local organic carbon-rich soils due to the melting ice wedge (Holgerson, 2015; Kortelainen et al., 2006). A high degree of local connectivity with soils is also likely the reason fluvial site F05 has much higher CO_2 and CH_4 concentrations than the other fluvial site (Harms et al., 2020). For up-scaling exercises, these high emission sites pose an interesting challenge: on the one hand, including them in the present method used for up-scaling skews the values and results in high emissions that are not representative of the median emission rates. On the other hand, if several of these high emission rate sites are present in a landscape it would appear necessary for them to be included in up-scaling calculations to avoid underestimating total emissions. Thus, first a spatially extensive study into how widespread high-GHG-emitting ponds are in different landscapes is needed followed by determining a suitable method to integrate them in up-scaling exercises.

Up-scaled emissions

Inland water C emission contributions to C budgets and to climate forcings remain uncertain but our results characterize inland waters in Arctic tundra lowlands as potentially important components of the landscape C exchange. In this section, we discuss the in-

land water C emissions (combined daily CO_2-C and diffusive CH_4-C emissions) during the studied summer months of July and August in the non-flood scenario (e.g., 2016) when inland waters covered around 3 km^2 (17 %) of the study area.

Ponds dominated the inland water C emissions contributing 73 % or 5.13 ± 1.24 Mg C d^{-1} in our study area (Figure 2.4). This is due to a combination of a high surface area coverage of 10 % (1.8 km^2) and high CO_2 and CH_4 concentrations relative to other inland water systems both at the study site (Figures 2.2-2.3) and across the Arctic (Tables 2.S3-2.S5). While our estimate of 10% pond coverage is relatively high for this part of the Arctic (Muster et al., 2017), it is not abnormally high with similar pond coverage (12 %) also observed on Samoylov Island in the Lena Delta (Abnizova et al., 2012). Determining the surface area coverage of ponds within a landscape is one of the biggest challenges in accurately quantifying their emissions. This is mainly due to their small surface areas, requiring high-resolution satellite imagery (Muster et al., 2012), and this difficulty is exacerbated by vegetation coverage. However, because ponds in Arctic lowlands contribute up to 30 % of total inland water coverage (Muster et al., 2012, 2017), the potential contribution of ponds to total landscape C exchange is substantial. At the scale of our study site (~18 km^2), our estimated pond C emissions dominate inland water C emissions. It is possible that at larger scales their contribution to the C budget is constrained by their small spatial extent (Emmerton et al., 2016), especially in comparison to that of lakes (Rocher-Ros et al., 2017; Wik et al., 2016). It should be noted that pond emissions could become considerable contributors to the Arctic C budget once additional CH_4 evasion pathways are considered. One of these pathways is CH_4 emission through vegetation (Knoblauch et al., 2015), another is ebullition (bubbles). For example, a study in Sweden which included CH_4 ebullition resulted in a ~39 % reduction of a wetland C sink even though pond surface area coverage was only 4 % (Kuhn et al., 2018). Thus, while our estimates can be considered conservative, the combined daily CO_2-C and diffusive CH_4-C emissions from ponds (calculated as pond C contribution = pond C emissions / landscape C exchange) still accounted for an estimated 7 % of the landscape C exchange (Figure 2.4).

Lakes were the second largest inland water system by area, covering 5 % of the study area but only accounting for 7 % of inland water C emissions. This is in agreement with observations at a similar scale (15 km^2) in northern Sweden where lake (CO_2 and diffusive CH_4) emissions accounted for only 5 % of inland water C emissions, compared to 95 % by streams (Lundin et al., 2013). Again, we consider our estimates to be conservative because ebullitive CH_4 emissions were not included. Ebullition emissions have been found to range from being equivalent to diffusive CH_4 emissions in boreal peatland lakes (Kuhn et al., 2021) to accounting for the majority of lake CH_4 emissions (Sepulveda-Jauregui et al., 2015; Walter et al., 2006).

Additionally, lakes are likely higher emitters during other times of the year. Some northern lakes have been observed to emit up to half of their annual C emissions during spring melt when CO_2 and CH_4 that was trapped in the lake ice over the winter is released (Karlsson et al., 2013; Lundin et al., 2013). This means that the relative contribution of C emissions from ponds, lakes and fluvial systems to regional C budgets is likely to be different in other seasons. For example, C emissions from lakes in western Siberia were observed to be 2-fold greater in spring, although this seasonal effect was not seen in

fluvial emission rates (Serikova et al., 2018, 2019).

In our study area, small fluvial systems accounted for 20 % of inland water C emissions (97 % of which was CO_2-C) despite only covering 2 % of the study area. This is in line with estimates on a global scale, indicating that fluvial systems account for more than 85 % of inland water CO_2 emissions despite only covering 17 % of total inland water surface area (Raymond et al., 2013). It is also in agreement with estimates on regional scales where small streams contributed 86 % of the total fluvial CO_2 emissions in a 1871 km^2 sub-watershed in north-east Siberia (Denfeld et al., 2013) and water tracks accounted for 53 % to 85 % of total CH_4 emissions in a high Arctic catchment in Alaska (Harms et al., 2020). Additionally, we did not measure diurnal fluctuations which have been shown to be significant in temperate regions, 27 % higher than those estimates solely from diurnal concentrations (Gómez-Gener et al., 2021), but it is unknown whether inland water diurnal fluctuations are important in Arctic lowland tundra fluvial systems.

Certain relationships in inland water emission observations are present in several studies indicating patterns that hold true at multiple scales throughout different northern high-latitude regions. One of these is the dominance of CO_2-C to total inland water C emissions compared to CH_4-C. CO_2-C contributed 97 % of C emissions in our study compared to 3 % CH_4-C. Similarly, in western Siberia 90 % of C emissions from small lakes were in the form of CO_2-C (Repo et al., 2007), as were 98 % of C emissions from fluvial systems in Western Siberia (Serikova et al., 2018), and in northern Sweden, CO_2-C emissions accounted for 98 % of C emissions from streams and lakes (Lundin et al., 2013).

We estimate that inland waters offset the landscape C sink by 9 % with an associated estimated uncertainty of ± 18 %. When considering the conservative nature of our estimates we do propose that inland waters are significant components of the carbon cycle in Arctic tundra lowlands. Specifically, our study indicates that small inland waters (ponds and low-order fluvial systems) are high CO_2 and CH_4 emitters in these landscapes. Despite being small in surface area, ponds can be highly abundant (Downing, 2010) and low-order fluvial systems account for the majority of stream length in many landscapes (Downing et al., 2012), and both systems are closely tied to the soil and riparian-wetland C release. Multi-year, spatially extensive sampling campaigns combined with higher resolution surface area data (Muster et al., 2017) will allow for more certain quantification of inland water contributions to regional C budgets.

Do N_2O emissions matter in this Arctic tundra landscape?

Our observed N_2O concentrations are comparable to values of inland waters in Québec, Canada; to our knowledge the only other study with N_2O emission rates from inland waters in permafrost regions (Soued et al., 2015). Our sampled inland water systems were undersaturated in N_2O relative to the atmosphere during the 'normal' year. However, in the 'wet' year N_2O concentrations were higher resulting in all inland water systems, besides ponds, being oversaturated with respect to the atmosphere. Interestingly, the 'wet' year had a higher effect on N_2O concentrations compared to CO_2 and CH_4. Higher N_2O concentrations in 2017 were potentially due to the deeper snow cover and delayed

snowmelt allowing for increased N mineralization in winter, resulting in higher N availability in summer. Increased N_2O fluxes in the Arctic soils due to deeper snow cover have been observed in snow fence experiments (Mörsdorf et al., 2020; Xu et al., 2023) and along a natural snowmelt gradient (Kolstad et al., 2021). The delayed snowmelt resulting in a wet landscape could explain the higher N_2O concentrations as soil moisture (and oxygen availability) exhibit a large control on tundra N_2O production (Voigt et al., 2020). While we acknowledge that nitrogen availability and transformations (e.g., nitrification, denitrification) are important controls on N_2O production, this study does not include process-level measurements of inorganic nitrogen species (NO_3^- or NH_4^+). To our knowledge, such data are not available for this specific region. Our interpretations are therefore constrained to observed patterns in N_2O concentrations and hydrological context, rather than specific nitrogen cycling pathways. Contrary to our findings, N_2O undersaturation was observed in a year with higher than average summer rainfall in comparison to oversaturation during an average precipitation year in water tracks in Alaska (Harms et al., 2020). While this could indicate different effects on biogeochemical cycles due to different types of precipitation intensification, it could also be due to temperature effects or regional differences in topography, soil and vegetation and the type of inland water sampled. The generally low N_2O emissions relative to CO_2 and CH_4 mean that variability in N_2O estimates is unlikely to significantly alter the overall contribution of N_2O emissions both in terms of inland water emissions, and inland water emissions integrated with the landscape GHG exchange.

The impact of flooding

The floodwaters in the study area were estimated to cover 10 % of the landscape and resulted in a 37 % increase of inland water C emissions compared to the non-flood summer scenario. Floodwater contributions to total inland water C emissions was second only to ponds (40 %) (Figure 2.7). We defined the floodwater separately from fluvial systems to isolate the effect of the flooding although in reality they are a single connected system. Our results show that when tundra becomes flooded, the landscape C sink is further offset because tundra that was previously acting as a C sink became a C source (i.e., behaves as an inland water system rather than primarily taking up carbon into plant biomass). Arctic tundra lowlands can readily be flooded, for example during the spring snowmelt (Zakharova et al., 2009). In Western Siberia, an estimated 30 days of flooding increased total inland water C emissions by ~11 %, supporting our findings (Karlsson et al., 2021). Climate change could further increase the magnitude and duration of flooding in tundra lowlands by changing precipitation patterns and altering local geomorphology as a result of permafrost thaw (Callaghan et al., 2011; Liljedahl et al., 2016). Precipitation, dominated by winter snowfall, has been predicted to increase for at least the next 40 years (Wang et al., 2022). In 2017, summer water levels in the Indigirka River, of which the Berelekh is a tributary, were the highest in 48 years of records, corresponding to an approximate 49-year return period (Tei et al., 2020). How long a landscape remains flooded will be crucial in determining to what degree flooding offsets landscape C sink. The considerable influence of flooding on landscape C exchange with the atmosphere, offsetting the landscape C sink by an additional 4 % as observed in this study, indicates

that the effects of flooding on regional Arctic C budgets could be considerable.

Conclusions

Emissions from small inland water systems such as ponds and low-order fluvial systems contributed disproportionately to landscape C exchange, relative to their small surface areas. Thus, our results indicate that such small inland water systems should be further investigated and included in up-scaling exercises to accurately determine inland water C emissions in Arctic lowland tundra landscapes. Reliable data on surface area coverages of all inland water systems, coupled with direct measurements of dissolved CO_2 and CH_4 gas concentrations and emission rates in different Arctic regions, would allow for a better assessment of the overall importance of inland water C emissions to landscape C exchange across a range of scales. These improvements would facilitate more accurate estimation of Arctic C budgets and quantification of the permafrost carbon feedback.

Inclusion of N_2O emissions in the total radiative forcing estimates of inland water GHG emissions showed that despite the high warming potential of N_2O, its contribution to the net warming effect of total landscape GHG exchange is negligible in our study area. This is in line with a general downward re-evaluation of N_2O emissions from inland waters compared to the earlier studies (Hu et al., 2016; Lauerwald et al., 2019). However, very few direct observations of inland water N_2O emissions exist in the Arctic, and a better understanding of inland water N_2O concentration dynamics in high latitude landscapes could enable predictions of not only how N_2O dynamics but also terrestrial and aquatic biogeochemical cycles could change under a warming climate.

Flooding caused a substantial additional offset to the landscape C sink capacity in our study area. This highlights the need for long-term and simultaneous monitoring of CO_2 and CH_4 emissions during flood events in the Arctic lowland tundra landscapes to gain a better understanding of their dynamics and possible feedback effects on future climate.

With continued Arctic warming, permafrost will continue to thaw and as a result alter tundra hydrology and carbon supply to inland water systems. It is therefore increasingly important to understand inland water carbon dynamics and to accurately determine their GHG emissions in the context of lowland tundra landscapes. Especially, since the amount of carbon that is cycled through inland waters shows that they are a potentially important component of regional carbon cycles.

Statments and Declarations

Code and data availability

The data used in the study are available at PANGEAE

via *https://doi.pangaea.de/10.1594/PANGAEA.939906*. The code written for this study is available on Zenodo: Melanie Martyn Rosco. (2024). up-scaling [Code]. Zenodo. DOI:10.5281/zenodo.14512643

Acknowledgments

This work was carried out under the program of the Netherlands Earth System Science

Centre (NESSC), financially supported by the Ministry of Education, Culture and Science (OCW). JFD received additional support from a UKRI Future Leaders Fellowship MR/V025082/1.

Appendix

This supplementary information contains one figure and six tables. The figure provides additional visual information on one pond and two fluvial sampling sites. The tables provide detailed information on the sampling campaigns, data from literature used in the methodology of the study, a comprehensive overview of the results, and previously published data to which results are compared.

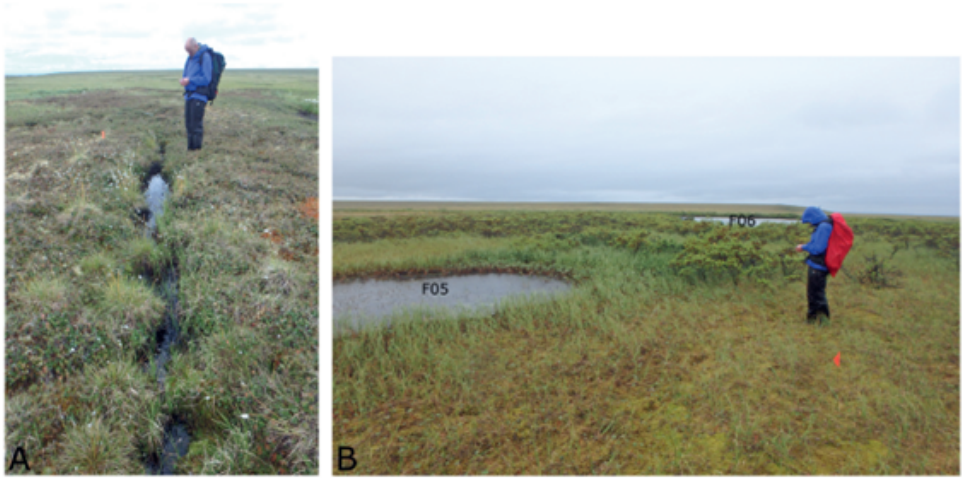

Figure 2.S1: (A) Pond site P06. (B) Fluvial site F05 and F06 in the background.

Table 2.S1: Sampling locations, number of samples and dates of sample collection. Repeated dates indicate duplicate samples. There is no location data available for the flood water samples (T).

Site	Latitude	Longitude	# Samples	Sampling dates
P01	70.83082	147.47493	5	03/08/2016, 07/08/2016, 10/07/2017, 13/07/2017, 17/07/2017
P02	70.83150	147.47461	6	31/07/2016, 03/08/2016, 07/08/2016, 10/07/2017, 13/07/2017, 17/07/2017
P03	70.83304	147.47424	6	31/07/2016, 03/08/2016, 07/08/2016, 10/07/2017, 13/07/2017, 17/07/2017
P04	70.83335	147.47423	7	31/07/2016, 03/08/2016, 07/08/2016, 10/07/2017, 10/07/2017, 13/07/2017, 17/07/2017
P05	70.83398	147.47453	6	31/07/2016, 03/08/2016, 07/08/2016, 10/07/2017, 13/07/2017, 17/07/2017
P06	70.83459	147.47435	6	31/07/2016, 03/08/2016, 07/08/2016, 10/07/2017, 13/07/2017, 17/07/2017
P07	70.83479	147.47415	6	31/07/2016, 03/08/2016, 07/08/2016, 10/07/2017, 13/07/2017, 17/07/2017
P08	70.83483	147.47423	6	31/07/2016, 03/08/2016, 07/08/2016, 10/07/2017, 13/07/2017, 17/07/2017
P09	70.83675	147.47250	6	31/07/2016, 03/08/2016, 07/08/2016, 10/07/2017, 13/07/2017, 17/07/2017
P10	70.83703	147.47340	6	31/07/2016, 03/08/2016, 07/08/2016, 10/07/2017, 13/07/2017, 17/07/2017
P11	70.83862	147.47270	6	31/07/2016, 03/08/2016, 07/08/2016, 10/07/2017, 13/07/2017, 17/07/2017
P12	70.83871	147.47400	6	31/07/2016, 03/08/2016, 07/08/2016, 10/07/2017, 13/07/2017, 17/07/2017
L11	70.82892	147.44202	5	01/08/2016, 05/08/2016, 08/08/2016, 11/07/2017, 16/07/2017
L12	70.83285	147.42805	5	01/08/2016, 05/08/2016, 08/08/2016, 11/07/2017, 16/07/2017
L13	70.83022	147.41382	5	01/08/2016, 05/08/2016, 08/08/2016, 11/07/2017, 16/07/2017
L14	70.82754	147.42194	6	01/08/2016, 05/08/2016, 08/08/2016, 11/07/2017, 16/07/2017, 16/07/2017
L15	70.82684	147.43158	5	01/08/2016, 05/08/2016, 08/08/2016, 11/07/2017, 16/07/2017
L21	70.84735	147.40897	6	02/08/2016, 07/08/2016, 09/08/2016, 08/07/2017, 08/07/2017, 14/07/2017
L22	70.84583	147.39978	5	02/08/2016, 07/08/2016, 09/08/2016, 08/07/2017, 14/07/2017
L23	70.84852	147.39929	5	02/08/2016, 07/08/2016, 09/08/2016, 08/07/2017, 14/07/2017
L24	70.84927	147.40688	5	02/08/2016, 07/08/2016, 09/08/2016, 08/07/2017, 14/07/2017
L31	70.84869	147.41772	5	02/08/2016, 06/08/2016, 09/08/2016, 08/07/2017, 14/07/2017
L32	70.84803	147.42638	5	02/08/2016, 07/08/2016, 09/08/2016, 08/07/2017, 14/07/2017
L33	70.84756	147.42230	5	02/08/2016, 07/08/2016, 09/08/2016, 14/07/2017
F01	70.493982	147.293631	2	09/07/2017, 15/07/2017
F02	70.493542	147.293989	3	09/07/2017, 09/07/2017, 15/07/2017
F03	70.493348	147.294136	3	12/07/2017, 12/07/2017, 15/07/2017
F04	70.494005	147.294637	1	12/07/2017
F05	70.831670	147.517290	3	01/08/2016, 05/08/2016, 08/08/2016
F06	70.831380	147.517610	3	01/08/2016, 05/08/2016, 08/08/2016
F07	70.829970	147.511840	3	01/08/2016, 05/08/2016, 08/08/2016
F08	70.828900	147.504750	3	01/08/2016, 05/08/2016, 08/08/2016
T01	–	–	5	09/07/2017, 09/07/2017, 12/07/2017, 15/07/2017, 17/07/2017
T02	–	–	4	09/07/2017, 12/07/2017, 15/07/2017, 17/07/2017
T03	–	–	5	09/07/2017, 12/07/2017, 12/07/2017, 15/07/2017, 17/07/2017
T04	–	–	4	09/07/2017, 12/07/2017, 15/07/2017, 17/07/2017
T05	–	–	5	09/07/2017, 12/07/2017, 15/07/2017, 17/07/2017, 17/07/2017

Table 2.S2: k_{600} ($cm\,h^{-1}$) values from literature.

Inland water system	k_{600} ($cm\,h^{-1}$)	Reference
Fluvial	18.70	Linke et al. (2019); Liu et al. (2022); Raymond et al. (2012)
Fluvial	23.40	Linke et al. (2019); Liu et al. (2022); Raymond et al. (2012)
Fluvial	13.10	Aufdenkampe et al. (2011)
Fluvial	21.00	Denfeld et al. (2015)
Pond	3.00	Holgerson et al. (2017)
Pond	2.88	Holgerson et al. (2017)
Pond	1.67	Holgerson et al. (2017)
Pond	0.92	Holgerson et al. (2017)
Pond	3.29	Kuhn et al. (2018)

Table 2.S3: Results of up-scaled emissions for each inland water system for the non-flood and flood scenario. Results are presented as mean ± SD. Note that CH_4-C is diffusive fluxes only.

Inland water system	Scenario	CO_2-C (Mg C d^{-1})	CH_4-C (Mg C d^{-1})	CO_2-C + CH_4-C (Mg C d^{-1})
Pond	Non-flood	5.00 ± 1.23	0.12 ± 0.03	5.13 ± 1.24
	Flood	4.83 ± 1.00	0.11 ± 0.02	4.83 ± 1.01
Lake	Non-flood	0.47 ± 0.09	0.03 ± 0.01	0.50 ± 0.09
	Flood	0.50 ± 0.11	0.01 ± 0.00	0.51 ± 0.11
Fluvial	Non-flood	1.37 ± 0.37	0.04 ± 0.01	1.40 ± 0.38
	Flood	1.17 ± 0.26	0.01 ± 0.00	1.18 ± 0.27
Flood	n/a	3.08 ± 0.66	0.02 ± 0.02	3.10 ± 0.66

Table 2.S4: Lake CO_2 and CH_4 concentrations published in other studies. a indicates mean ± SE; b indicates mean ± SD.

Study	Location	Study site	CO_2 (µmol L^{-1})	CH_4 (µmol L^{-1})
This study	NE Siberia	Lakes	42 ± 2	0.9 ± 0.1
Repo et al. (2007)[b]	Western Siberia, Russia	Lakes	68 ± 22	1.1 ± 1.3
Lundin et al. (2013)[b]	Northern Sweden	Lakes	36 ± 26	0.9 ± 1.1
Dean et al. (2016)[a]	Western Canada	Lakes	99 ± 8	1.6 ± 0.28

Table 2.S5: Pond CO_2 and CH_4 concentrations published in other studies. a indicates mean ± SE; b indicates mean ± SD; c indicates range (min–max); d indicates mean; e indicates mean ± IQR.

Study	Location	Study site	CO_2 (µmol L^{-1})	CH_4 (µmol L^{-1})
This study[a]	North-eastern Siberia, Russia	Ponds	377 ± 27	22 ± 5
Laurion et al. (2010)[d]	Northern Canada	Ponds	30 ± 2	1.4 ± 1.3
Kuhn et al. (2018)[a]	Northern Sweden	Ponds	467 ± 21	24 ± 3
Holgerson and Raymond (2016)[a]	Temperate & Boreal	Ponds (<0.001 km^2)	134 ± 17	–
Dean et al. (2016)[a]	Western Canadian Arctic	Ponds	343 ± 35	11 ± 0.45

Table 2.S6: Fluvial CO_2 and CH_4 concentrations published in other studies. a indicates mean ± SE; b indicates mean ± SD; c indicates range (min–max); d indicates mean; e indicates mean ± IQR.

Study	Location	Study site	CO_2 (µmol L^{-1})	CH_4 (µmol L^{-1})
This study[a]	North-eastern Siberia, Russia	Fluvial	139 ± 30	5 ± 3
Lundin et al. (2013)[b]	Northern Sweden	Fluvial	200 ± 144	1.4 ± 1.1
Morozumi et al. (2019)[c]	North-eastern Siberia, Russia	Non-flood (2016) fluvial	–	0.1–0.2
Morozumi et al. (2019)[c]	North-eastern Siberia, Russia	Flood-year tributaries (2017) fluvial	–	0.7–1.1
Morozumi et al. (2019)[c]	North-eastern Siberia, Russia	Flood-year main channel Indigirka (2017) fluvial	–	0.2–0.4
Denfeld et al. (2013)[c,b]	North-eastern Siberia, Russia	Kolyma streams	167 ± 137	–
Denfeld et al. (2013)[c,b]	North-eastern Siberia, Russia	Kolyma tributaries	21 ± 13	–
Denfeld et al. (2013)[c,b]	North-eastern Siberia, Russia	Kolyma river	31 ± 16	–
Serikova et al. (2018)[e]	Western Siberia	Fluvial	109 ± 3	–
Dean et al. (2016)[a]	Western Canadian Arctic	Fluvial	167 ± 8	0.4 ± 0.14

Chapter 3

Freshwater GHGs relationships with DOM

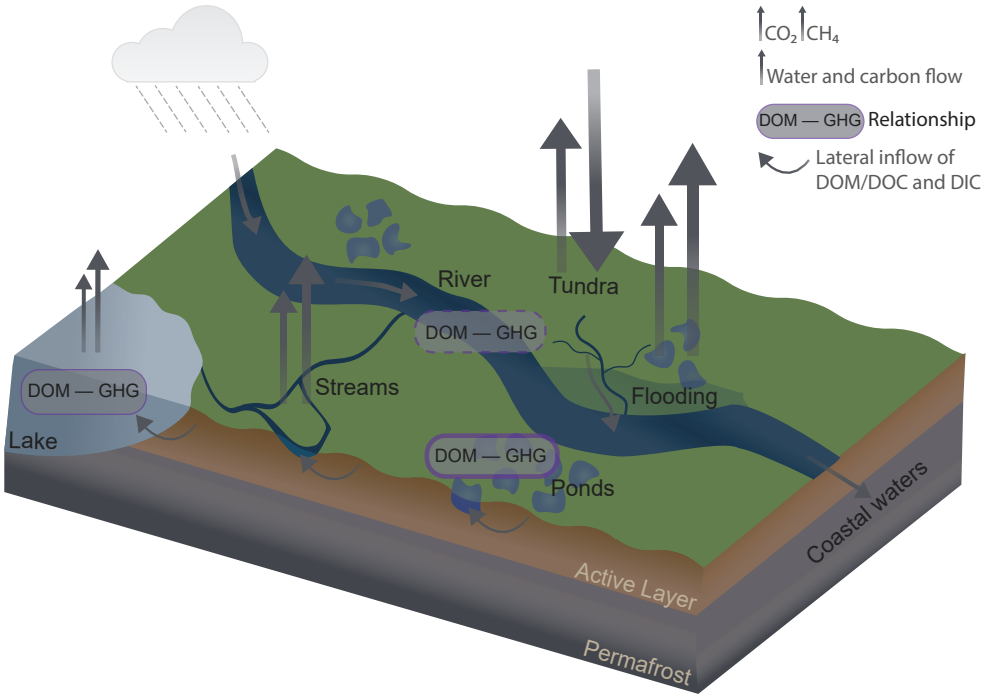

Submitted to Biogeosciences (EGU), 2026 as:

Distinctive DOM patterns coupled to CO_2, CH_4 and N_2O concentrations across freshwater ecosystems in the NE Siberian Arctic tundra

Melanie Martyn Rosco, Joshua F. Dean, Ove H. Meisel, Richard van Logtestijn, Thibault Lambert, Dušan Materić, Sergei Karsanaev, Trofim Maximov, Jorien E. Vonk, and James T. Weedon

The supply and composition of dissolved organic matter (DOM) are important factors associated with greenhouse gas (GHG) concentrations in Arctic freshwater ecosystems. This study investigated relationships between DOM characteristics and dissolved carbon dioxide (CO_2), methane (CH_4), and nitrous oxide (N_2O) concentrations across ponds, lakes, and fluvial ecosystems within an 18 km^2 area in the Berelekh River floodplain, northeastern Siberia. DOM was characterised using optical measurements, with a subset of samples additionally analysed using Thermal Desorption Proton Transfer Reaction–Mass Spectrometry (TD-PTR-MS) to provide complementary information on broad molecular groups.

Ponds exhibited the highest DOC, chromophoric DOM, dissolved CO_2, and dissolved CH_4 concentrations, whereas lakes exhibited lower DOC and greenhouse gas concentrations together with optical characteristics consistent with a relatively greater contribution of recently produced and microbially processed DOM. Fluvial systems displayed intermediate DOM characteristics but the greatest departure in DOM–greenhouse gas relationships from the overall freshwater pattern. Partial Least Squares Regression revealed that relationships between DOM characteristics and dissolved greenhouse gases differed among ecosystem types. In ponds, dissolved CO_2 and CH_4 were most strongly associated with DOM quantity, while additional analyses indicated relationships with dissolved Fe and pond morphology. In lakes, the DOM fractions associated with dissolved greenhouse gases differed from those in ponds, indicating that differences in DOM composition altered which components of the DOM pool were most closely associated with dissolved greenhouse gas concentrations. In fluvial systems, dissolved CO_2, CH_4, and several optical DOM characteristics exhibited contrasting relationships to those observed in standing waters, while dissolved N_2O retained a consistent negative relationship with DOC across all ecosystem types.

These findings demonstrate that DOM–greenhouse gas relationships are ecosystem dependent and cannot be transferred directly between Arctic freshwater ecosystem types. They further indicate that both the quantity and composition of DOM, together with ecosystem-specific environmental characteristics, should be considered when investigating greenhouse gas dynamics in northern freshwaters.

Introduction

Freshwater ecosystems, including lakes, ponds, and rivers, play a crucial role in the global carbon cycle by facilitating carbon flux to the atmosphere, sequestration in sediments, or transfer to the ocean (Cole et al., 2007; Ward et al., 2017). In regions such as Arctic permafrost tundra lowlands, terrestrial and freshwater systems form an interconnected continuum. Freshwater ecosystems are integral to biogeochemical processes, especially since lakes cover an estimated 30 % of the land and ponds an estimated 6 % (lentic waterbodies with surface area ($< 1.0 \times 10^6$ m^2) (Grosse et al., 2013). We specify this threshold to distinguish ponds from larger lakes, as these systems differ in hydrology, connectivity, and DOM–GHG dynamics (Arsenault et al., 2022). Arctic fluvial systems contribute significantly to carbon fluxes, delivering roughly 25 Tg of dissolved organic carbon (DOC) to the Arctic Ocean annually, while emitting an estimated 0.22 ± 0.25 Pg C yr^{-1} of CO_2 and 0.0008 ± 0.0002 Pg C yr^{-1} of CH_4 to the atmosphere (Battin et al., 2023; Raymond et al., 2007).

Dissolved organic matter (DOM) constitutes a major portion of organic carbon in freshwaters and originates from terrestrial sources (allochthonous, e.g., soil, terrestrial vegetation), or aquatic sources (autochthonous, e.g., benthic and pelagic algae, aquatic macrophytes) (Kellerman et al., 2014). Both allochthonous and autochthonous processes continuously add DOM to waters, commonly quantified by concentrations of DOC. A subset of the DOM pool also contains nitrogen, and permafrost soils can be net emitters of N_2O (Voigt et al., 2020). Permafrost soils, excluding the active layer, store an estimated 67 Pg N within the upper 3 m (Harden et al., 2012). Terrestrial DOM enters freshwaters via leaching and runoff from land, and offers valuable insights into terrestrial processes such as soil, vegetation and organic matter decomposition. Arctic permafrost regions store an estimated 1330 to 1580 Pg C, including surface and deep carbon, which exceeds the current atmospheric carbon levels by about 45 % (approx. 875 Pg C) (Friedlingstein et al., 2022; Hugelius et al., 2014; Schuur et al., 2015; Treat et al., 2024).

The supply of DOM to lakes, ponds, and rivers can vary widely by freshwater ecosystem. Here, we use “DOM supply” to refer broadly to both the quantity (e.g., DOC concentration) and origin (e.g., terrestrial or autochthonous inputs) of DOM. Arctic surface air temperatures are increasing at nearly double the global average rate, leading to accelerating permafrost thaw and changes in hydrological regimes (Beel et al., 2021; Overland et al., 2019; Walvoord and Kurylyk, 2016). Such alterations change hydrological connectivity and cause heterogeneous effects on tundra vegetation (Liljedahl et al., 2016). Some regions experience 'greening', characterized by increased vegetation productivity and biomass, as first observed in global satellite data during the late 1990s (Frost et al., 2023). In contrast, other areas undergo 'browning', which refers to a decline in vegetation health or productivity. Such shifts are expected to alter the lateral export of terrestrial DOM into freshwater ecosystems, impacting biogeochemical processes that regulate greenhouse gas emissions (Vonk et al., 2015). Lakes metabolize carbon from both allochthonous and autochthonous sources (Tank et al., 2011), whereas Arctic ponds, owing to their shallow depths and relatively small water volumes, have a higher sediment-to-water volume ratio, resulting in stronger interactions with sediments, surrounding terrestrial ecosystems, and the atmosphere (Breton et al., 2009). In contrast, Arctic river

systems, influenced by landscape type and seasonal changes, play dynamic roles in carbon and nitrogen cycling, particularly in hyporheic zones (Rasilo et al., 2017; Shogren et al., 2020b; Soued et al., 2015). Variations in water residence times, flow velocities, and hydrological connectivity between flowing and still waters further contribute to differences in biogeochemical cycles and greenhouse gas emissions (Johnston et al., 2020; Liljedahl et al., 2016; Liu et al., 2022; Neilson et al., 2018).

DOM is composed of a highly complex variety of organic molecules. Its composition varies in time and space and is generally determined by the environmental processes it has gone through and its distance from its source (Hansen et al., 2016). The composition of DOM changes as it travels through freshwater systems, influenced by processes like biological or photochemical degradation and flocculation (Obernosterer and Benner, 2004). DOM composition in turn influences its biogeochemical role which dictates its transport, storage and/or degradation in freshwater environments, potentially resulting in the production of CO_2, CH_4 or N_2O (Hansen et al., 2016). Terrestrial DOM influences aquatic metabolism and greenhouse gas dynamics primarily through photochemical and biological (microbial) degradation, both of which can occur concurrently in freshwater environments (Obernosterer and Benner, 2004). The extent of their relative contribution is determined by factors like light availability, water color, residence time, dissolved ion concentrations, and the inherent characteristics of the DOM (Cory and Kling, 2018; Guillemette and del Giorgio, 2011; Lapierre and del Giorgio, 2014). The rates of DOM degradation are influenced by abiotic factors, including pH and temperature (Quick et al., 2019). N_2O production and consumption are primarily driven by microbial processes, involving reactive nitrogen species such as ammonia, nitrate, and nitrite in oxidation and reduction processes (Vitousek et al., 1997).

A combined analytical approach is required to better understand links between DOM composition and dissolved greenhouse gases in freshwater ecosystems. DOM composition can be characterised using stable carbon isotopes ($\delta^{13}C$), optical properties derived from absorbance and fluorescence spectroscopy, and mass spectrometry. Optical techniques characterize the light-absorbing (chromophoric DOM; cDOM) and fluorescent (fDOM) fractions of DOM, providing information on bulk compositional characteristics but only representing part of the overall DOM pool. High-resolution mass spectrometry can provide complementary molecular-level information on DOM composition and has been widely used to investigate how DOM responds to environmental drivers such as temperature, hydrological connectivity, and microbial processing (Kellerman et al., 2018; Pan et al., 2020).

In this study, we additionally applied thermal desorption proton transfer reaction mass spectrometry (TD-PTR-MS), which has previously been used to investigate DOM composition in peatlands, snowpacks, and freshwater systems and to assess DOM bioavailability (Materić et al., 2017, 2018; Peacock et al., 2018). During analysis, compounds are thermally desorbed from DOM samples and ionized via proton transfer before mass spectrometric detection, enabling characterization of the volatile and semi-volatile fraction of the DOM mixture. We included TD-PTR-MS to determine whether this fraction of DOM provided additional insight into relationships between DOM composition and dissolved greenhouse gas concentrations.

Although considerable progress has been made in characterizing DOM composition in Arctic freshwater systems, it remains unclear whether and how DOM–GHG relationships vary among freshwater ecosystem types. Here, we examine these relationships across lakes, ponds, and fluvial systems in the Indigirka tundra lowlands, an understudied region where such data are limited. We hypothesized that differences in hydrology, DOM sources, and biogeochemical processing among ecosystem types would result in distinct DOM–GHG relationships. To test this hypothesis, we applied Partial Least Squares Regression (PLSR) to evaluate associations between DOM characteristics and concentrations of dissolved CO_2, CH_4, and N_2O. Our primary analyses used ecosystem-specific models, with a global model included for comparison. Principal component analysis (PCA) of DOM and environmental variables supported this stratified approach by revealing strong clustering among ecosystem types.

Methods

Study area

Field campaigns were carried out during the summers of 2016 and 2017 within the Kytalyk Nature Reserve (70°49′N, 147°29′E) located in the Indigirka River lowlands of northeastern Siberia, Russia. A full list of sampling locations and timings are provided in Suppl. 2. The research site sits atop continuous permafrost with an active layer that thaws to a depth of up to 30 cm deep every summer (July/August) (Dean et al., 2020). The tundra landscape has three main landscape units: thaw-induced drained lake basins or ”alases”, a 25 m high Yedoma ridge and the floodplain of the Berelekh River, an Indigirka River tributary (Dean et al., 2020). The late Pleistocene-aged Yedoma deposits contain high ground ice content, comprising as much as 80% of their total volume (Schirrmeister et al., 2011). Annual precipitation averages 232 mm, with approximately half occurring as rainfall during the growing season (May–September) and the remainder as snowfall (Dean et al., 2020). During autumn 2016, precipitation exceeded the 2009–2017 average by 75–100 mm (Tei et al., 2020), which led to flooding in the area during the summer of 2017. At the Chokurdakh airport weather station (WMO station 21946, 01 April 2005 to 01 May 2024), located 30 km northwest of the study area, the daily average temperature over the year is -11.8°C, with July temperatures averaging 10.5°C. According to the Circumpolar Arctic Vegetation Map (Raynolds et al., 2019) the vegetation is described as erect dwarf-shrub tundra (S1 type) and tussock-sedge, dwarf shrub, moss tundra (G4).

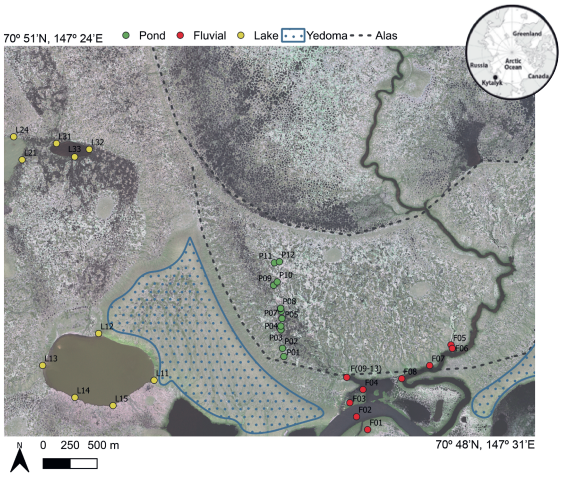

Figure 3.1: Kytalyk research area, roughly 18 km^2, showing the sampling locations and landscape units on a WorldView-2 image taken in July 2015.

Field data collection

Samples were collected to analyze concentrations of dissolved gas concentrations, DOC and optical properties of DOM across a freshwater gradient, including ponds, lakes, and fluvial surface waters, during July-August 2016 and July 2017.The sampling included two small lakes (less than 3 m deep, with surface areas of 0.04 and 0.14 km^2), one thermokarst lake (L11-L15; up to 7 m deep, covering 0.51 km^2, actively eroding into a Yedoma ridge), 12 pond sites (less than 0.5 m deep, with surface areas between 3 and 240 m^2), and 8 fluvial locations along a ~5 m wide stream and the Berelekh River bank (Figure 3.1). In 2017, five additional fluvial sites (n = 5) were sampled, consisting of flooded tundra channels (sites F09–F13; see Suppl. 2) Given the remote location in the far eastern Siberian Arctic tundra, sampling was limited to accessible edges of water bodies (Dean et al., 2020). Pond surface areas were measured on-site using tape measures and should be regarded as approximate. Supplementary Table 2 provides detailed sampling information, including site frequency. In this study, ponds are defined as lentic systems covering less than 0.01 km^2 in surface area. Within thaw lake basins, two distinct types of thaw ponds are identified based on their formation and surrounding vegetation:

1. Through Ponds: These ponds are formed by the collapse of waterlogged permafrost and are typically surrounded by vegetation such as *Eriophorum vaginatum*,

Ledum palustre, the moss *Dicranum and Betula nana*. Occasionally, submerged *Betula nana* can be found within these ponds (Magnússon et al., 2020). Examples of through ponds in this study include P01, P06, P10 which are characterized by dwarf-shrub vegetation.

2. Polygonal Ponds: These ponds occur in areas where ice wedge degradation has reached a stable state, resulting in the development of polygonal ground features, including both low-centered and high-centered polygons (van Huissteden et al., 2021)(van Huissteden et al., 2021). The vegetation surrounding these polygonal ponds predominantly consists of *Sphagnum fuscum* and *Carex aquatilis* (Magnússon et al., 2020). Ponds such as P02-P05, P07, P08 and P11 are characterized by sedge wetland vegetation, while P09 and P12 are associated with *Sphagnum* wetland vegetation.

The classification of vegetation types for each pond was performed using a high-resolution vegetation map of the area (Siewert et al., 2015). For each pond, the predominant vegetation type was identified by analyzing the vegetation at the pond's coordinates and within a surrounding neighborhood scaled to the pond's area. The most frequently occurring vegetation type within this neighborhood was considered representative of the pond's predominant vegetation. See Table S3.1 for an overview of the dominant vegetation in each sampled pond.

The three studied lakes are located in drained lake basins. At one of the lake edges, where the site of sample L11 is located, the Yedoma ridge is actively eroding into the lake (L1x), mostly via thaw slumps. In 2017, additional samples were collected for TD-PTR-MS analysis from ponds, lakes and fluvial surface waters. For an overview of sampling locations, see Figure 3.1, and for a detailed overview of the sampling campaign, see Suppl. 2. Coordinates for fluvial sampling locations F09-13 were not available but the approximate area is shown in Figure 3.1. Lake samples were collected along the shorelines due to logistical constraints. Samples were taken from multiple locations around the edges of each lake, capturing the range of conditions in these relatively small lakes (< 1 km^2) and providing useful representative data from smaller lakes in the study region.

Dissolved Gases

Dissolved greenhouse gas concentrations were measured using a headspace equilibration technique. At each site, surface water was sampled from 5–10 cm depth and mixed with ambient air (1:1 ratio, 30 mL each) in 60 mL syringes. The mixture was shaken vigorously for one minute to allow equilibration between the phases. The resulting headspace gas was then transferred into pre-evacuated 12 mL Exetainer® vials (Labco, UK) for analysis. This method follows established protocols (adapted from Borges et al. (2015); Dean et al. (2020)). Headspace gas samples were analyzed at the University of Liège using an SRI 8610C gas chromatograph (GC). Carbon dioxide (CO_2) and methane (CH_4) concentrations were quantified using a flame ionization detector with a methanizer, while nitrous oxide (N_2O) concentrations were measured with an electron capture detector integrated into the GC system. Calibration was performed using certified gas standards (Air Liquide Belgium), including mixtures containing 1, 10, and 30 ppm CH_4; 400, 1000, and

4000 ppm CO_2; and 0.2, 2.0, and 6.0 ppm N_2O.

DOC

At each sampling location 100 mL of water was collected. The water samples were filtered through a pre-combusted 0.7 µm pore size Whatman GF/F glass fiber filter with a diameter of 47 mm, using a Millipore vacuum filter tower. Filtration was performed at the end of the sampling day. The filtrate was acidified with nitric acid (60 % HNO_3) before transport. All samples were kept in dark, cool conditions until analysis was carried out. All analyses were conducted within two months of sample collection to minimize potential changes in sample composition. The DOC samples from 2016 and all the δ^{13}C-DOC were analyzed by wet oxidation with an Aurora1030 total organic carbon analyzer (OI Analytical) coupled to a Delta V Advantage isotope ratio mass spectrometer at the Department of Earth and Environmental Sciences, KU Leuven, Belgium The DOC samples from 2017 were analysed with an Aurora 1030W analyser using the wet oxidation (heated persulfate) method at the Vrije Universiteit Amsterdam. DOC concentrations were determined from the calibration curve generated by measuring 4 standards in each run (5 ppm, 10 ppm, 20 ppm, 60 ppm) (Dean et al., 2020).

Absorbance and Fluorescence Spectroscopy

DOM samples for chromophoric DOM (cDOM) and fluorescent DOM (fDOM) were syringe filtered to 0.2 µm in the field and stored in 20 mL glass vials with polytetrafluoethylene-coated septa. DOM samples underwent absorbance and fluorescence analysis at the Chemical Oceanography laboratory of the Université de Liège, Belgium. The absorbance spectra measurements were conducted using a Perkin-Elmer UV/Vis 650S spectrophotometer.

Spectral parameters included for each sample were: absorbance at 350 nm (a_{350}), a proxy for chromophoric dissolved organic matter concentration (cDOM) (Spencer et al., 2009); the ratio of absorption at 250 to 365 nm (E2:E3), an indicator of molecular weight due to its inverse relationship with it (Helms et al., 2008); the spectral slopes of wavelengths 275-295 nm and 350-400 nm, along with the spectral ratio between these slopes (S_R; S275-295 : S350-400), these properties are linked to the molecular weight and aromaticity of DOM, where lower values suggest greater molecular weight and higher aromatic content (Helms et al., 2008); specific ultraviolet absorbance at 254 nm obtained by normalizing the UV absorbance at α = 254 nm (a_{254}) to the corresponding DOC concentration (Weishaar et al., 2003). To account for the natural UV absorbance of Dissolved iron (Fe) at α = 254 nm, it was approximated using measured Fe concentrations and subtracted, providing $SUVA_{245}$ as an indicator of aromaticity (Weishaar et al., 2003). Fe concentrations were measured at the Department of Earth and Environmental Sciences, KU Leuven, Belgium, using inductively coupled plasma mass spectrometry (ICP-MS; Agilent 7700x) at the ^{56}Fe isotope in helium collision mode, with ^{72}Ge used as the internal standard. Quantification was calibrated using certified standards (e.g., NIST SRM1643f), and the limit of quantification (LOQ) for Fe was 0.370 µL.

The fluorescent properties of dissolved organic matter (fDOM) were characterized us-

ing excitation-emission matrices (EEMs) measured with a Perkin-Elmer LS45 fluorescence spectrophotometer. Fluorescence intensity was recorded across excitation wavelengths from 220 to 450 nm (5 nm (increments) and emission wavelengths from 230 to 600 nm (0.5 nm increments). The EEMs were preprocessed to remove Raman scattering and standardized to Raman units using a Milli-Q water analyzed on the same day. A five-component PARAFAC model was developed with the drEEM 0.3.0 Toolbox (Murphy et al., 2013) for MATLAB (MathWorks, Natick, MA, USA) (Figure S3.1). The model underwent validation through split-half analysis, random initialization, and inspection of residual EEMs to ensure accurate component identification (Dupas et al., 2024). To assess the positions of the maximum fluorescence peaks of the PARAFAC components, comparisons were made using the OpenFluor spectral database (Murphy et al., 2014). Matches were selected based on excitation and emission maxima overlap and the relevance of the comparison studies to freshwater biogeochemical contexts. These comparisons were used to support interpretation of DOM source and composition. Maximum fluorescence intensities (F_{Max}) for each component were used to determine the contributions of individual fluorophores, with the total fluorescence (F_{Tot}) determined by summing all F_{Max} values for each sample. Each PARAFAC component's relative abundance was calculated as $\%CX = F_{Max}(X)/F_{Tot}$, where %CX denotes the percentage contribution of component X to the total fluorescence signal. This technique made it possible to identify DOM structural properties connected to varying sources and processing histories.

Other indices derived from fluorescence data were the freshness index ($\beta{:}\alpha$), fluorescence index (FI) and the humification index (HIX). The fluorescence index (FI) was determined as the ratio of emission intensities between 470–520 nm and an excitation wavelength of 370 nm, providing insight into the DOM aromaticity and source (Cory et al., 2010; McKnight et al., 2001). The humidification index (HIX), as described by Ohno (2002), is calculated as the ratio of the area under the emission spectra from 435 to 480 nm to the combined areas between 300–345 nm and 435–480 nm. It serves as an indicator of DOM source and its humification degree (Hansen et al., 2016; Ohno, 2002). The freshness index ($\beta{:}\alpha$) is defined as the ratio of emission intensity at 380 nm divided by the emission intensity of the peak between 420 and 435 nm at excitation of 310 nm (Parlanti et al., 2000). The biological index (BIX), described by Huguet et al. (2009), is an adapted version of the $\beta{:}\alpha$ ratio. Both parameters indicate the relative contribution of fresher, recent production to DOM (Parlanti et al., 2000). The Pearson's correlation r value between both parameters is r = 0.99 (Figure S3.2), therefore only the freshness index ($\beta{:}\alpha$) is considered.

TD-PTR-MS

TD-PTR-MS analysis was carried out on 11 samples from the dataset using a TD-PTR-OF 8000 instrument (IONICON Analytik, Innsbruck, Austria). Additional information is available in (Materić et al., 2017), where a comprehensive description of the sample preparation and analysis methodology is presented. The analysis result is referred to as "PTR-DOC". For each sample, we computed the PTR-DOC metrics including H/C, O/C, average oxidative state of carbon (OSC), and average number of carbon (nC) atoms per molecule (Materić et al., 2017; Peacock et al., 2018). The percentage of PTR-DOC

was calculated by first summing the concentrations of individual ions, adjusting for their carbon mass fractions derived from the chemical formulas, and then expressing this value as a proportion of the DOC concentration measured with the Aurora instrument (see above). Ions with m/z values below 100 were excluded from the elemental composition analysis because they predominantly represent thermal dissociation fragments of non-volatile compounds with high molecular weights (Materić et al., 2018). The individual compounds were the species, and the relative sum-normalized peak intensities were used as species abundance. Chemical formulas were identified and categorized into structural groups using slightly modified parameters for FT-ICR MS (Peacock et al., 2018) and the adjusted aromaticity index but (AI_{mod}) (Stubbins et al., 2014). Compound classes include condensed aromatics ($AI_{mod} > 0.67$), aromatics ($0.5 \leq AI_{mod} \leq 0.67$), highly unsaturated compounds with high oxygen content ($AI_{mod} < 0.5$, H/C < 0.5, O/C between 0.5 and 0.9), highly unsaturated compounds with low oxygen content ($AI_{mod} < 0.5$, H/C < 0.5, O/C < 0.5), peptides (H/C > 1.5, O/C < 0.9, N > 0), aliphatics (H/C > 1.5, O/C < 0.9, N $= 0$), and sugars (O/C > 0.9). Chemodiversity for each sample was computed using Shannon's diversity index.

Statistical analysis

We conducted several statistical analyses to investigate the relationships between vegetation, DOM, dissolved gas concentrations, and environmental variables across different freshwater ecosystems (ponds, lakes, and fluvial systems). This study was not originally designed for time-based analysis, as samples were not collected at regular intervals or on identical dates annually. The absence of a uniform time sampling protocol leads to data variability, and any differences noted across years could be caused by various reasons, including shifts in meteorological conditions. Consequently, our analysis does not explore the impact of inter-annual variability. The structure and sampling method in this analysis are specifically aimed at spatial variability and the potential co-variance of DOM and dissolved gas concentrations.

Since the three lakes in our dataset included multiple sampling sites, we evaluated whether repeated sampling within individual lakes influenced our key response variables: dissolved concentrations of CO_2, CH_4 and N_2O. Specifically, we used linear mixed-effects models (LMMs) with nested random effects for site identity within lake to partition variance into components attributable to differences between lakes, sampling sites, and residual error. These models showed that variance attributable to lake identity was negligible (0 %), with nearly all variation in dissolved gas concentrations explained by site-level and residual effects (Table S3.2). This supports our treatment of sampling sites as independent observational units in the main analysis.

To test for differences among ecosystem types (ponds, lakes, and fluvial systems), we used LMMs with site_name included as a random effect to account for repeated sampling within sites and avoid violating independence assumptions. Group-level differences among ecosystem types were then assessed using Tukey-adjusted pairwise comparisons of estimated marginal means.

We examined differences in pond water chemistry and dissolved gas concentrations

among ponds with varying dominant vegetation types (response variables: CO_2, CH_4, N_2O, DOC, a_{350}, Fe, specific conductivity, %C2, %C4, $S_{350\text{-}400}$, FI, and $SUVA_{254}$). To address the non-independence of samples within the same pond, we used LLMs with a random intercept for site_name, accounting for repeated sampling within ponds.

Significant differences among vegetation categories were assessed using pairwise comparisons of estimated marginal means with Tukey adjustment for multiple comparisons. This approach allowed us to identify significant contrasts while accounting for repeated sampling at same sites and potential non-normality in response variables. Only significant pairwise differences ($\mathrm{p} < 0.05$) are reported in Supplementary Figure S3 and the accompanying summary table (Table S3.3).

To assess the potential influence of dissolved Fe on DOM characteristics and dissolved gas concentrations in ponds, we employed again LMMs. Each model included dissolved Fe concentration as a fixed effect predictor and pond site as a random effect to account for repeated measurements within sites. Models were constructed for each response variable: CO_2, CH_4, N_2O, DOC, a_{350}, specific conductivity, %C2, %C4, $S_{350\text{-}400}$, FI and $SUVA_{254}$ Statistical significance of the Fe effect was evaluated at $\mathrm{p} < 0.05$, and only significant results are reported in Table S3.4. For each analysis, only samples with complete data for the relevant response variable were included. In all of the above-described LMMs, models were fit using both the original and log-transformed scales of each response variable. The best-fitting transformation was selected based on residual diagnostics, including skewness and standard deviation. To assess whether freshwater ecosystem types differ in DOM composition and environmental characteristics, we performed Principal Component Analysis (PCA) on all optical DOM properties, DOC concentrations, environmental variables and dissolved gas concentrations. All variables were standardized to have a mean of zero and a variance of one before analysis. The PCA included 37 observations with complete data. This analysis revealed clear clustering by ecosystem type, suggesting distinct biogeochemical profiles among ponds, lakes, and fluvial systems.

We hypothesized that relationships between DOM properties and dissolved GHG concentrations was unique for each ecosystem type. To test this, we used Partial Least Squares Regression (PLSR, (Guebel and Torres, 2013)). We constructed four PLSR models: one for each ecosystem type (ponds, lakes, and fluvial systems), and a fourth "global" model that included all ecosystems combined. The data used in the analysis were standardized to a mean of zero and a variance of one. PLSR was chosen for its effectiveness in handling multicollinearity within the dataset. The target variables were the concentrations of dissolved gases (CO_2, CH_4, N_2O), and the predictor variables included spectrophotometric and fluorescence-based indices, DOC, surface water temperature, specific conductivity, pH, and dissolved Fe. Predictor variables were selected based on their ecological relevance to DOM–GHG relationships and their availability across the majority of samples to ensure consistent comparison across models. The subsets of data with complete observations for the PLSR analyses were as follows: Pond (n = 18), Lake (n = 12), Fluvial (n = 5), and Combined freshwater ecosystems (n = 35).

Each PLSR model was fitted using two components. The analysis involved calculating the scores for the first two latent variables (LV1 and LV2) for both predictor and response

variables. These scores, along with the loadings, were used to create biplots, where black arrows represent predictor variable loadings and blue arrows represent response variable loadings. The positions of the samples (ponds, lakes, or fluvial sites) in latent variable space were indicated by scatter points. To facilitate comparison of the PLSR results, we normalized the absolute PLSR coefficients by dividing each coefficient by the maximum absolute value found within each variable's set of coefficients. This max-scaling was performed separately for CO_2, CH_4, and N_2O across all ecosystem types (ponds, lakes, fluvial systems, and all combined). This scaling ensured consistent comparison of the relative influence of each predictor variable across different ecosystems. Finally, heatmaps were generated to visually compare the scaled PLSR coefficients, with each heatmap displaying the sorted coefficients to highlight the most influential predictor variables.

All analyses were performed using Python version 3.11.6 and R version 4.1.3. The PCA was conducted with the scikit-learn library (Pedregosa et al., 2011) and the PLSR was conducted using the statsmodel library (Seabold et al., 2010). Shannon's diversity index was computed using the R software package vegan (Oksanen et al., 2013). Linear mixed-effects models were fitted using the R package lme4 (Bates et al., 2015), with p-values calculated using the lmerTest package (Kuznetsova et al., 2017), and estimated marginal means (EMMs) and pairwise comparisons were computed using the emmeans package (Lenth, 2023).

Results

Greenhouse gas concentrations

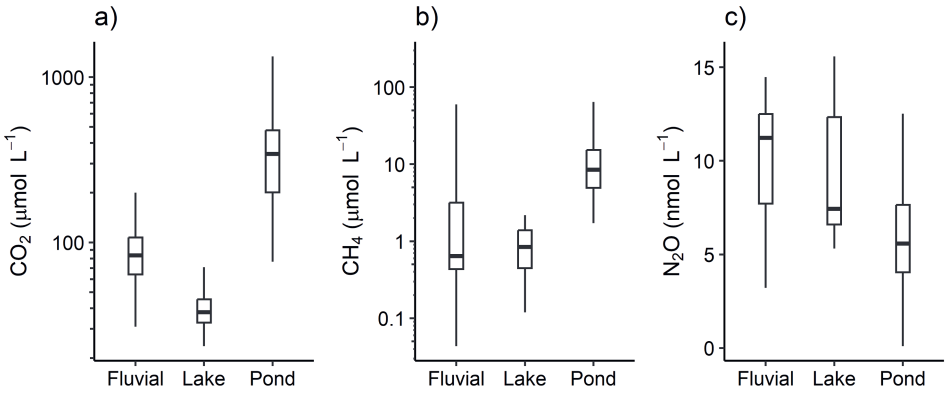

Figure 3.2: Dissolved gas concentrations from fluvial, lake, and pond sites in Kytalyk, Siberia, in 2016 and 2017. The boxes indicate the interquartile range and the whiskers the 1.5 $\times$ interquartile range. The line in the middle of the boxes indicates the median. (a) Dissolved CO_2 concentrations; (b) dissolved CH_4 concentrations; (c) dissolved N_2O concentrations. Note that the y-axis in (a) and (b) is on a log scale. This data is published and diescribed in detail in (Martyn Rosco et al., 2025)

Ponds exhibited the highest mean concentrations of CO_2 (378 µmol L^{-1}) and CH_4 (24.1 µmol L^{-1}), with particularly large variability in CH_4 concentrations (ranging from 2.2 µmol L^{-1} to 251.1 µmol L^{-1}). In contrast, ponds exhibited the lowest N_2O concentrations (mean: 6.4 nmol L^{-1}). Lakes showed substantially lower concentrations of CO_2 (41.5 µmol L^{-1}) and CH_4 (0.88 µmol L^{-1}), but had the highest N_2O concentrations (10.0 nmol L^{-1}). Fluvial sites fell between ponds and lakes for all three gases, both in terms of mean concentration and variability.

DOC and $\delta^{13}C$ of DOC

The DOC concentrations in ponds exhibited the largest range, from 9.3 mg L^{-1} to 46.7 mg L^{-1}, and were significantly higher than DOC concentrations in lakes (1.2 mg L^{-1} to 8.8 mg L^{-1}) and fluvial sites (2.4 mg L^{-1} to 14.1 mg L^{-1}) (pairwise comparison, $p < 0.05$; Figure 3.3). Similar high DOC values have also been observed in other thaw ponds (Abbott et al., 2014; Breton et al., 2009; Wauthy et al., 2018).

The $\delta^{13}C$ of DOC varied from –27.7 ‰ to –22.9 ‰ in lake samples, which was significantly higher (less negative) than the ranges observed in pond samples (–29.9 ‰ to –27.4 ‰) and fluvial samples (–29.5 ‰ to –29.0 ‰), as confirmed by post hoc pairwise comparisons (Figure 3.3). These values were similar to those previously reported in sub-Arctic ponds and fluvial systems (Wang et al., 2018).

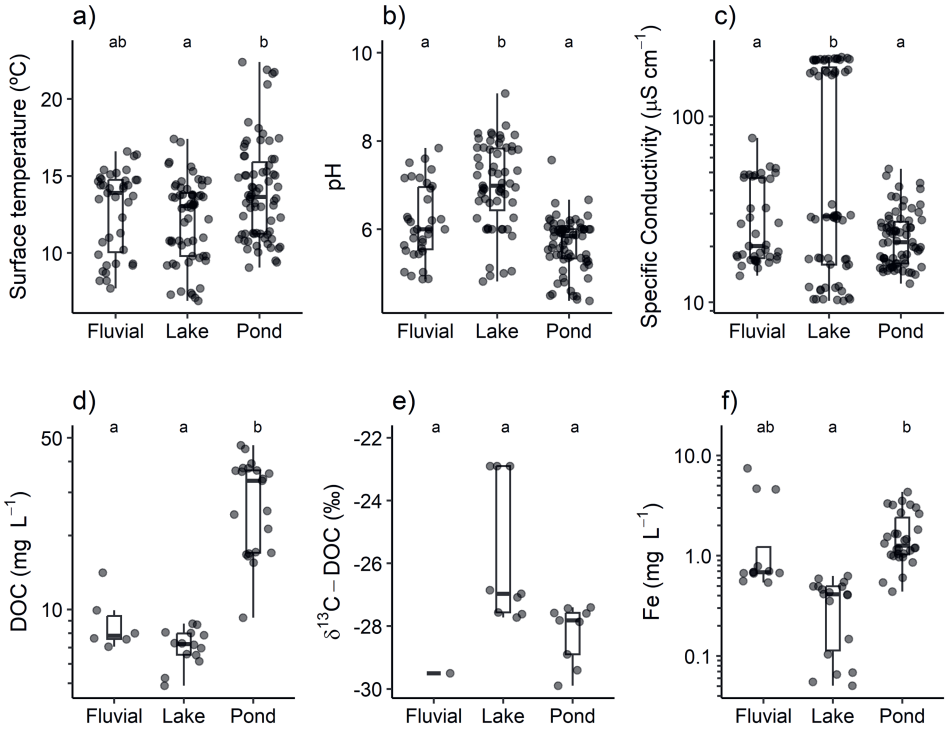

Figure 3.3: Boxplots of measurements from lakes, ponds, and fluvial systems in the Kytalyk region, Siberia (2016–2017). Each point represents a sample-level measurement of surface temperature (a), pH (b), specific conductivity (c), DOC (d), δ^{13}C-DOC (e), or dissolved Fe (f). Boxes show the interquartile range (IQR; 25th–75th percentiles), with the median as a horizontal line; whiskers extend to 1.5 × IQR. Statistical differences among ecosystem types were assessed using linear mixed-effects models with site as a random effect. Letters indicate significant pairwise differences (Tukey-adjusted, $p < 0.05$) based on estimated marginal means. Fe was log-transformed in the model to meet assumptions. Specific conductivity and DOC were modeled on the original scale but are plotted on $\log_{10}$ axes for visual clarity. All other variables were both modeled and displayed on the original scale.

Optical indicators of DOM source and processing

Pond a_{350} values (a proxy for cDOM) were significantly higher (median = 62.1 m^{-1}) than lake values (median = 9.0 m^{-1}) and fluvial system values (median = 18.4 m^{-1}) (Pairwise comparison $p < 0.05$, Figure 3.4). Comparably high cDOM values have been observed in other thaw ponds (Abbott et al., 2014; Breton et al., 2009; Wauthy et al., 2018), mirroring DOC concentrations. Pond HIX values (median = 0.96) were slightly higher than lake-site HIX values (median = 0.93), but these differences were not statistically significant in the

mixed-effects model analysis (Figure 3.5).

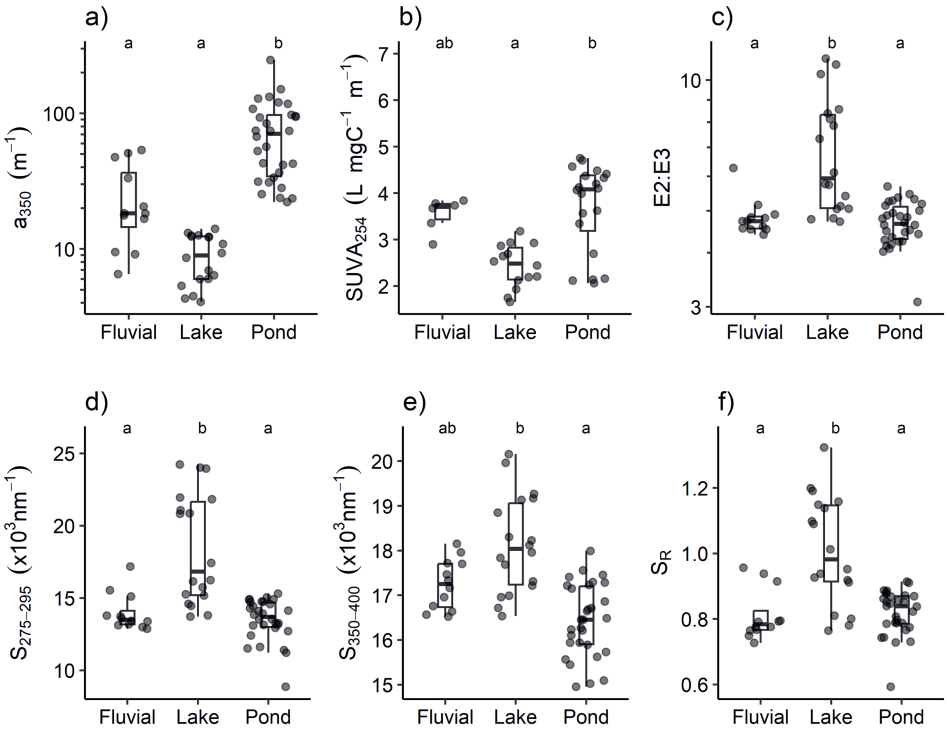

Figure 3.4: Boxplots of measurements from lakes, ponds, and fluvial systems in the Kytalyk region, Siberia (2016–2017). Each point represents a sample-level measurement of a_{350} (a), $SUVA_{254}$ (b), E2:E3 (c), $S_{275\text{-}295}$ (d), $S_{350\text{-}400}$ (e), or the slope ratio S_R(f). Boxes represent the interquartile range (IQR; 25th–75th percentiles), with the median shown as a horizontal line; whiskers extend to 1.5 $\times$ IQR. Statistical differences among ecosystem types were assessed using linear mixed-effects models with site as a random effect. Letters indicate significant pairwise differences (Tukey-adjusted, $\mathrm{p} < 0.05$) based on estimated marginal means. a_{350} and E2:E3 were log-transformed in the model and are shown on $\log_{10}$-scaled axes. $S_{350\text{-}400}$ was log-transformed in the model but is plotted on the original axis. All other variables were both modeled and displayed on the original scale.

Lake $SUVA_{254}$ values (median = 2.5 L mg^{-1} C m^{-1}) were significantly lower than pond values (median = 4.0 L mg^{-1} C m^{-1}) (Pairwise comparison $\mathrm{p} < 0.05$, Figure 3.4). Comparable $SUVA_{254}$ values were measured in lakes in the Mackenzie Delta (2.0 ± 4.0 L mg^{-1} C m^{-1}; (Tank et al., 2011)) and the Western North American Arctic (0.3 ± 0.9 L mg^{-1} C m^{-1}; Kurek et al., 2022). Lake sites had overall the highest $S_{350\text{-}400}$ values (median = 0.018), which were significantly higher than pond values but not significantly different from fluvial system values (Figure 3.4). Lake β:α values were significantly higher (median = 0.59) than

fluvial system values (median = 0.46) and pond values (median = 0.43) (Figure 3.5). Lake FI values (median = 1.61) were slightly higher than pond values (median = 1.53), but these differences were not statistically significant in the mixed-effects model analysis (Figure 3.5) and were similar to values measured in Western North American Arctic lakes (1.33 ± 1.70; Kurek et al., 2022).

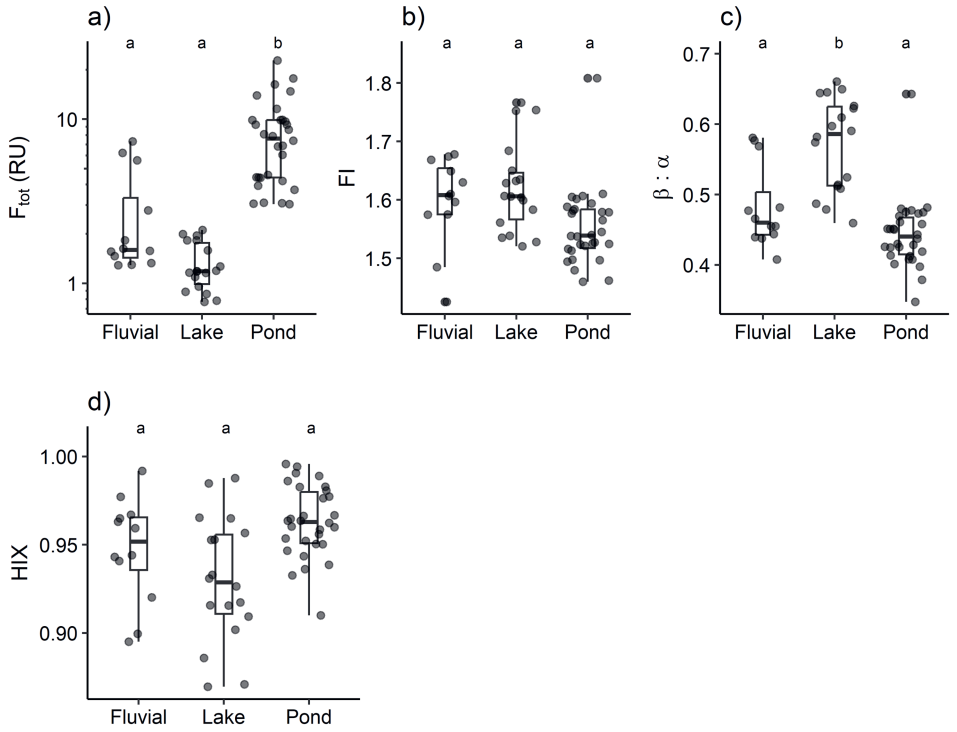

Figure 3.5: Boxplots of measurements from lakes, ponds, and fluvial systems in the Kytalyk region, Siberia (2016–2017). Each point represents a measurement of F_{tot} (a), FI (b), $\beta{:}\alpha$ (c), or HIX (d). Boxes represent the interquartile range (IQR; 25th–75th percentiles), with the median shown as a horizontal line; whiskers extend to 1.5 × IQR. Statistical differences among ecosystem types were assessed using linear mixed-effects models with site as a random effect. Letters indicate significant pairwise differences (Tukey-adjusted, $\mathrm{p} < 0.05$) based on estimated marginal means. All variables were log-transformed in the model to meet assumptions. F_{tot} is also shown on a $\log_{10}$-scaled y-axis for visual clarity, while FI, $\beta{:}\alpha$, and HIX are plotted on their original axes.

The only optical index of cDOM that was significantly different between fluvial and pond waters was a_{350}, which was significantly higher in pond waters compared to both fluvial and lake waters (Pairwise comparison $\mathrm{p} < 0.05$, Figure 3.4). The fluvial values were similar to a_{350} values measured in streams of the Kolyma watershed (Frey et al., 2016) and the Yukon River (Spencer et al., 2009). It also corresponded to the range of

values observed in tundra streams on Herschel Island, Canada, which receive terrestrial-derived material from vegetation (Coch et al., 2019b). The fluvial system $SUVA_{254}$ values (median = 3.4 L mg^{-1} C m^{-1}) lie between those of ponds and lakes measured in this study (Figure 3.4) and were similar to values measured in soil pore waters and streams in the Kolyma watershed (3.52 and 2.94 L mg^{-1} C m^{-1}, respectively) (Frey et al., 2016). The $S_{350\text{-}400}$ values we measured in fluvial waters (median = 0.017 nm^{-1}) were between those of ponds and lakes and not significantly different from either group Figure 3.4). The fluvial $S_{275\text{-}295}$ values in this study (median = 0.014 nm^{-1}) were similar to pond values (median = 0.014 nm^{-1}) and significantly lower than lake values (median = 0.017 nm^{-1}) (Pairwise comparison $\mathrm{p} < 0.05$, Figure 3.4). The $S_{275\text{-}295}$ values we measured were in the same range as previously reported values for wetlands (0.014 nm^{-1} to 0.018 nm^{-1}; Helms et al. (2008)) and terrestrial systems (0.012 nm^{-1} to 0.023 nm^{-1}; Spencer et al. (2012)).

The PARAFAC model identified 5 components (Figure S3.1), of which the first four presented humic-like fluorescent characteristics from terrestrial (C1, C2, C4) and from microbial (C3) sources. The components were analyzed in relation to previously published studies using the OpenFluor online database (Murphy et al., 2014). In general, the terrestrial humic-like component C2 accounted for the highest proportion of fDOM (around 40 %) in all sampled freshwater ecosystems. Component C2 shares fluorescent characteristics with humic material derived from terrestrial material (Table S3.5) but is associated with lower aromaticity and molecular weight than components C1 and C4 (Kellerman et al., 2015). C2 matched highly with components identified in the Congo River (Lambert et al., 2016) and moderately with published data from Arctic rivers (Walker et al., 2013), lakes (Berggren et al., 2019) and ponds (Wauthy et al., 2018). C1 is commonly linked to aromatic molecules and higher molecular weight (HMW) and (Table S3.5) and did not have many matches in the OpenFluor database. But it matched well with terrestrially derived humic-like components found in freshwaters in a variety of ecosystems (Lambert et al., 2016; Lapierre and del Giorgio, 2014; Wheeler et al., 2017) and was comparable to components identified in sub-arctic lakes (Berggren et al., 2019). The component C3 is linked to the degradation of both aquatic and terrestrial derived DOM (Wauthy et al., 2018) (Table S3.5) and was found to be positively related to DOM biological degradation in samples from Arctic and sub-arctic ponds (Berggren et al., 2019). In OpenFluor it also matched well with microbe-derived humic-like components found in sub-arctic lakes (Berggren et al., 2019). Component C5 displays an emission peak in the UV-A region that coincides with the acid-like peak of tryptophan (Fellman et al., 2010) (Table S3.5). The tryptophan-like component is associated with low molecular weight DOM fractions a higher proportion of aliphatic molecules (Stedmon et al., 2003). These molecules can originate from decomposition of terrestrial DOM by microbes (Stedmon et al., 2003), autochthonous primary production in freshwater environments (Guillemette and del Giorgio, 2011; Kellerman et al., 2015), or a combination of both processes. The identified component C5 matched well with components identified in rivers (Lambert et al., 2016; Walker et al., 2013) and moderately with a component in peatland pools DOM (Hassan et al., 2023).

Optical indices of DOM coupled to dissolved gas concentrations

The first two principal components of the PCA accounted for 66 % of the overall variance, with PC1 contributing 50 % and PC2 contributing 16 % (Figure 3.6). PC1 implied that a large amount of variability in the data can be described by the type of freshwater ecosystem sampled. Fluorescent components C1 and C4, along with HIX, exhibited negative loadings on the first principal component (PC1), corresponding with pond sample scores. Conversely, specific conductivity $\beta{:}\alpha$, pH, $S_{275\text{-}295}$, and the proportion of fluorescent components C3 and C5 showed positive loadings on this axis, with lakes having the highest scores on PC1. Although the distinction between ponds and lakes was clear along the axis of PC1, fluvial samples clustered within the negative segment of PC2 at approximately 0 or the midpoint of PC1, an indication of fluvial characteristics being a mixture of those from pond and lake samples.

The PLSR analysis shows that there were distinct relationships in each freshwater ecosystem type between specific DOM parameters and all three GHGs analysed here (Figure 3.8). In ponds, CO_2 and CH_4 were positively related with each other and with DOC, dissolved Fe, a_{350}, specific conductivity and FI (Figure 3.8). Similarly, in lakes, dissolved concentrations of CO_2 and CH_4 showed a positive relationship with each other, with CO_2 exhibiting associations with variables such as water surface temperature, DOC and %C5 (Figure 3.8). In lakes, dissolved concentrations of CO_2 and CH_4 increased as HIX and %C4 decreased (Figure 3.8). In fluvial systems there was a negative relationship between CO_2 and pH, $\beta{:}\alpha$, $S_{275\text{-}295}$, and %C5 (Figure 3.8). We observed in the fluvial systems in our study area that dissolved CO_2 concentrations positively related with %C1, %C4, DOC, and a_{350} thus, as the amount of terrestrial HMW DOM rises, so does CO_2. Dissolved CO_2 concentrations showed a positive relationship with reduced S_R values (Figure 3.8), indicating higher HMW organic material (Helms et al., 2008).

Influence of dissolved iron on DOM and dissolved gas concentrations in ponds

The linear mixed-effects models (LMMs) revealed several significant relationships between dissolved Fe concentrations and environmental variables in the pond samples (Table S3.4). Higher Fe concentrations were significantly associated with increased concentrations of CO_2 (Estimate = 0.28, SE = 0.12, p = 0.031; log-transformed) and DOC (Estimate = 4.38, SE = 1.73, p = 0.021; original scale), as well as elevated levels of a_{350} (cDOM) (Estimate = 0.35, SE = 0.12, p = 0.009; log-transformed). In contrast, Fe concentration showed a significant negative relationship with $S_{350\text{-}400}$ (Estimate = -0.48, SE = 0.13, p = 0.008; original scale), suggesting changes in the spectral slope of cDOM with increasing Fe. Additionally, significant positive relationships were observed between Fe concentration and both the proportion of the C2 DOM component (%C2) (Estimate = 0.018, SE = 0.007, p = 0.018; log-transformed) and HIX (Estimate = 0.011, SE = 0.005, p = 0.031; original scale), indicating shifts in DOM composition and humic character associated with higher Fe levels.

Influence of vegetation type on DOM and dissolved gas concentrations in ponds

The analysis investigated, using LMMs, how the identified vegetation types (dwarf-shrub, sedge wetland, and *Sphagnum* wetland) influenced DOM and dissolved gas concentrations in the study area's ponds. Ponds dominated by dwarf-shrub vegetation consistently exhibited higher concentrations of several variables compared to those dominated by sedge or *Sphagnum*. Specifically, dwarf-shrub ponds had significantly higher CO_2 concentrations than those with sedge vegetation ($t(9.1) = 2.997$, $p = 0.036$; estimate = 0.79 ± 0.26 on the log scale, equivalent to ~$1.20\,mg\,L^{-1}$ higher). These ponds also showed significantly higher specific conductivity compared to sedge ponds ($t(9.1) = 4.53$, $p = 0.0036$; estimate = 0.58 ± 0.13 on the log scale, ~$0.79\,\mu S\,cm^{-1}$ higher). Moreover, dissolved Fe concentrations were substantially higher in dwarf-shrub ponds compared to both sedge ($t(4.1) = 8.15$, $p = 0.0026$; estimate = $1.99 \pm 0.24\,\mu g\,L^{-1}$) and *Sphagnum* ponds ($t(8.4) = 4.72$, $p = 0.0033$; estimate = $1.97 \pm 0.42\,\mu g\,L^{-1}$). In contrast, no significant differences in a_{350}, %C2, $S_{350\text{-}400}$, $SUVA_{254}$, CH_4, or DOC were detected in the mixed-effects model comparisons. *Sphagnum* ponds generally showed intermediate values between dwarf-shrub and sedge ponds, with fewer significant differences noted. However, it is important to note that only two *Sphagnum*-dominated pond samples were available, which limits the robustness of comparisons involving this vegetation type ((Table S3.1); (Figure S3.3)).

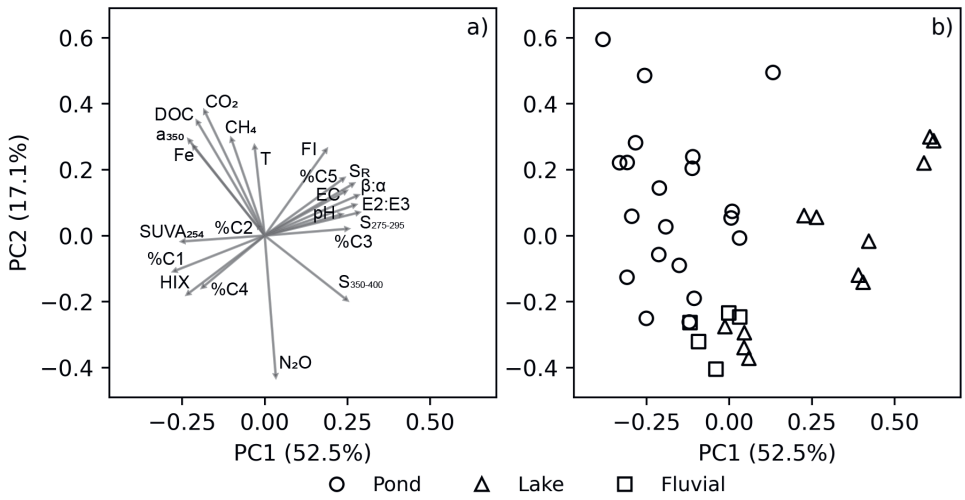

Figure 3.6: Loadings of properties on principal components 1 and 2 (PC1 vs. PC2) and the scores of lake, pond, and fluvial system samples from Kytalyk, Siberia (2016–2017). EC = specific conductivity; DOC = dissolved organic carbon; a_{350} = absorption coefficient at a wavelength of 350 nm; $SUVA_{254}$ = specific ultraviolet absorbance at 254 nm; HIX = humification index; FI = fluorescence index; C1–C5 = five fluorescent dissolved organic matter components.

TD-PTR-MS

TD-PTR-MS identified 515 unique ions in all analysed samples, ranging from *m/z* 14.002 to 479.472. On average, this represented 1.56 % of the quantified DOC pool (PTR-DOC; Table 3.1). When only ions with *m/z* > 100 were considered, TD-PTR-MS detected 428 unique ions, to which 399 molecular formulae could be assigned. The assigned molecular formulae were primarily aliphatics (mean = 38 ± 20 %, *n* = 11; Table 3.1). This compound class is typically associated with fresh, recently produced DOM sources; however, the observed values were lower than those reported for lakes in Alaska (Johnston et al., 2020). The second largest contribution was from condensed aromatic and aromatic compounds, with respective ranges of 10 % to 40 % (mean = 21 ± 9 %; Table 3.1) and 6 % to 21 % (mean = 13 ± 6 %; Table 3.1). These values are, on average, an order of magnitude higher than the proportional contribution to the DOM pool measured in Alaskan lakes (Johnston et al., 2020). Condensed aromatic and aromatic compound classes are linked to terrestrial DOM and are associated with allochthonous sources, such as DOM derived from lignin and tannins. Condensed aromatics are typically considered to originate from incomplete terrestrial DOM combustion, but have also been suggested to result from hydroxyl radical-initiated oxidation of lignin during photochemical reactions (Waggoner et al., 2015).

Table 3.1: TD-PTR-MS results for analysed samples. Compound group percentages represent relative contributions to the total measured PTR-DOC.

Site	%PTR	H/C	O/C	n_C	OSC	Aliph	Arom	Cond. arom	Sugars	Chemodiv
P01	1.69	0.30	7.9	–1.0	4173	10	14	0	4.20	
P02	1.40	0.35	5.6	–0.4	7141	15	40	0	4.09	
P03	1.39	0.26	7.7	–0.7	303	21	28	0	5.16	
P08	1.73	0.33	8.0	–0.9	536	10	18	0	4.18	
P11	1.37	0.35	5.4	–0.4	7450	13	47	0	4.04	
L23	1.50	0.28	7.8	–0.8	228	19	29	0	5.03	
L31	1.55	0.28	7.9	–0.8	253	18	24	0	4.90	
L11	1.78	0.33	8.1	–1.0	847	7	13	0	3.88	
L12	1.86	0.34	8.2	–1.1	717	6	11	0	3.65	
L14	1.89	0.35	8.3	–1.1	731	6	10	0	3.44	
F13	1.60	0.30	8.4	–0.9	859	13	19	1	4.55	

Discussion

Our results show that DOM and dissolved gas concentrations vary across the different freshwater ecosystems we sampled, indicating that each system is biogeochemically distinct. This distinctiveness is supported by the PCA performed on the combined dataset of DOM optical properties, general water quality parameters, and concentrations of DOC, CO_2, CH_4, and N_2O (Figure 3.6). To further explore these differences, we examined specific indicators of the source and processing of DOM within each ecosystem, revealing their association with the observed dissolved gas concentrations.

Variable sources of DOM across freshwater ecosystems

In the studied freshwater ecosystems, ponds and fluvial systems exhibited a stronger terrestrial DOM signature than lakes, whereas lakes showed evidence of a greater contribution from autochthonous and/or microbially processed DOM.

Although PARAFAC components associated with terrestrial DOM dominated across all sampled ecosystems, lakes contained lower proportions of these components (C1 and C4) and higher proportions of components commonly associated with autochthonous production or microbial processing (C3 and C5) than ponds and fluvial systems (Figure 3.7). This pattern suggests that, while lakes in our study area receive terrestrial DOM inputs, they exhibit a stronger signature of autochthonous production and/or microbial processing than ponds and fluvial systems. FI values were also consistent with a greater contribution of microbially derived DOM in lakes than in ponds (Figure 3.5). Similarly, the elevated $\beta{:}\alpha$ values observed in lakes (Figure 3.5) are consistent with a greater relative contribution of recently produced DOM, whereas the lower $\beta{:}\alpha$ values in ponds and fluvial systems are consistent with a lower relative contribution of recently produced DOM and a relatively stronger terrestrial influence (Fellman et al., 2010; Fouché et al., 2017). Although individual fluorescence-derived metrics can be influenced by biological and photochemical processing, the consistent patterns observed across PARAFAC components, FI, and $\beta{:}\alpha$ strengthen the interpretation of DOM source differences among ecosystem types (D'Andrilli et al., 2022; Hansen et al., 2016).

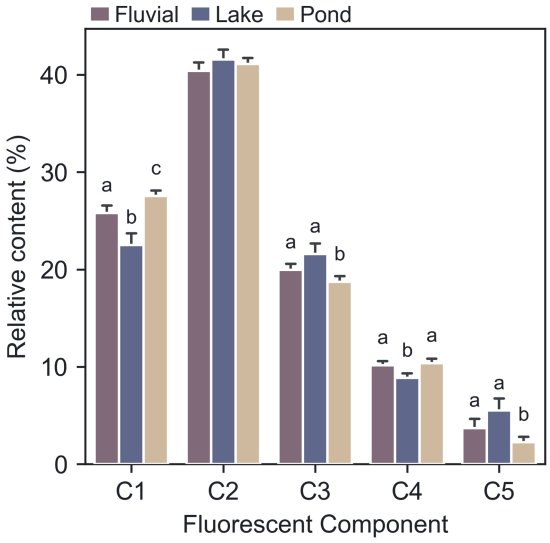

Figure 3.7: Median relative content of each PARAFAC component in each freshwater ecosystem. The error bars indicate the 95 % confidence interval. See Table S3.5 for an overview of the components.

One possible explanation for the stronger autochthonous and/or microbially processed

DOM signature observed in lakes is differences in seasonal hydrological connectivity. Lakes in Arctic permafrost landscapes can be most strongly connected to surrounding terrestrial environments during spring snowmelt, with hydrological connectivity often decreasing as the growing season progresses (Ala-Aho et al., 2018). Reduced hydrological connectivity later in the growing season can increase water residence times, potentially allowing greater in-lake processing of DOM relative to systems receiving more continuous terrestrial inputs.

The stronger terrestrial DOM signature observed in ponds compared to lakes is likely related to their high perimeter-to-water surface area ratio, which increases interactions with surrounding soils and sediments, together with their shallow morphology and small water volume, which enhance the relative influence of catchment-derived inputs (Wauthy et al., 2018). This interpretation is supported by the $SUVA_{254}$, a_{350}, $S_{350\text{-}400}$, $S_{275\text{-}295}$, S_R, and FI values, which collectively indicate a strong terrestrial DOM signature in the sampled ponds, consistent with previous observations from Arctic thaw ponds (Roiha et al., 2015).

Further supporting the interpretation of contrasting DOM sources among ecosystem types, a linear mixed-effects model revealed a significant positive relationship between DOC and cDOM in lakes (Estimate = 0.70 ± 0.26, p = 0.027), whereas no significant relationship was observed in ponds (Estimate = 1.96 ± 1.28, p = 0.18). This indicates that changes in DOC concentration were accompanied by proportional changes in the coloured fraction of DOM in lakes, whereas this relationship was more variable in ponds. One possible explanation is that the stronger terrestrial influence in ponds results in DOM inputs with more heterogeneous optical characteristics, resulting in greater variability in the relationship between DOC concentration and cDOM.

The $SUVA_{254}$ values measured in our lakes exceeded those reported for DOM leached from thawed Yedoma permafrost soils, both before and after 200 hours of laboratory incubation (Drake et al., 2015). However, these values are not directly comparable because Drake et al. measured laboratory incubations of permafrost soil leachates, whereas our measurements were obtained from natural lake surface waters. Future studies incorporating water-column depth profiles and sediment porewater sampling would help determine whether the optical characteristics observed in surface waters are representative of the wider lake system and assess the contribution of benthic DOM to lake DOM composition.

Our observations suggest that permafrost thaw and vegetation influence terrestrial inputs and the composition of DOM in the lakes and ponds within our research area. The presence of allochthonous DOM in the researched ponds is suggested by the differences we observed between DOC, cDOM (a_{350}), specific conductivity, and dissolved Fe concentrations depending on the dominant vegetation of each pond (Figure 3.3). For instance, ponds like P01 and P06, dominated by dwarf-shrub vegetation, exhibited higher levels of dissolved Fe, cDOM (a_{350}), CO_2, specific conductivity, and DOC compared to polygonal ponds dominated by sedge vegetation, although only the differences in dissolved Fe, specific conductivity, and CO_2 concentrations were statistically significant (Figure S3.3). This suggests a greater input of organic matter, likely from surrounding shrubs whereas the stabilization of ice-wedge degradation in polygonal ponds might re-

sult in less organic material entering the pond. However, it is important to note that these vegetation-related differences may be influenced by underlying factors such as soil type, water content, or active layer depth, with vegetation potentially serving as an indicator of these environmental conditions.

Pond P01 contained a greater proportion of aliphatic compounds contributing to its PTR-DOC, as opposed to the more aromatic and condensed compounds found in polygonal ponds such as P02, P03, and P11 (Table 3.1). Previous studies have linked higher proportions of aliphatic compounds to permafrost leachates, suggesting that these ponds may be receiving organic matter from thawing permafrost (MacDonald et al., 2021). Additionally, the thermokarst-affected lake at our study site (Sites L11-L15, Figure 3.1) exhibited higher levels of aliphatic compounds compared to the other two sampled lakes (Table 3.1), providing further support for permafrost inputs to DOM. These findings demonstrate the potential of TD-PTR-MS to identify permafrost-derived DOM contributions in Arctic freshwater ecosystems.

Interestingly, pond P08, a polygonal pond, showed a higher proportion of aliphatics, similar to through pond P01 (Table 3.1). Despite being a polygonal pond, P08 might have local environmental conditions that promote the release of aliphatic compounds. This suggests that local environmental factors, possibly related to permafrost influence or microhabitats, are playing a role in determining its DOM characteristics. This outlier behavior emphasizes the complexity and variability within pond ecosystems and the need to consider both broader classifications and local conditions when analyzing pond DOM chemistry and vegetation interactions. Overall, these findings highlight the role of permafrost thaw and vegetation type in shaping DOM characteristics in Arctic tundra freshwater ecosystems.

We identified variations in terrestrial input and DOM composition across the three sampled freshwater ecosystems, similar to the differences observed in dissolved gas concentrations (Figure 3.2). In our study area, ponds were characterized by a stronger terrestrial DOM signature, lakes exhibited a relatively greater contribution of autochthonous and/or microbially processed DOM alongside substantial terrestrial inputs, and fluvial systems displayed intermediate characteristics.

Distinct relationships between DOM and dissolved gas concentrations by freshwater ecosystem

The PCA revealed clear differences in DOM characteristics and associated environmental variables among the sampled freshwater ecosystems, with ponds, lakes, and fluvial systems clustering separately along the first principal component (PC1), which explained 52.5 % of the total variance (Figure 3.6). In contrast, DOC, cDOM, dissolved CO_2, and dissolved CH_4 exhibited similar directional loadings on the second principal component (PC2; 17.1 % of the total variance), suggesting that these variables co-varied across the sampled surface waters regardless of ecosystem type (Figure 3.6). Together, these patterns indicate that although DOM characteristics and dissolved greenhouse gas concentrations are broadly related across the study area, the nature of these relationships may differ among freshwater ecosystem types. To further investigate these ecosystem-

specific relationships, we examined the associations between individual DOM parameters and dissolved greenhouse gas concentrations separately for ponds, lakes, and fluvial systems using PLSR (Figure 3.8). The ecosystem-specific relationships identified by the PLSR are discussed in the following sections

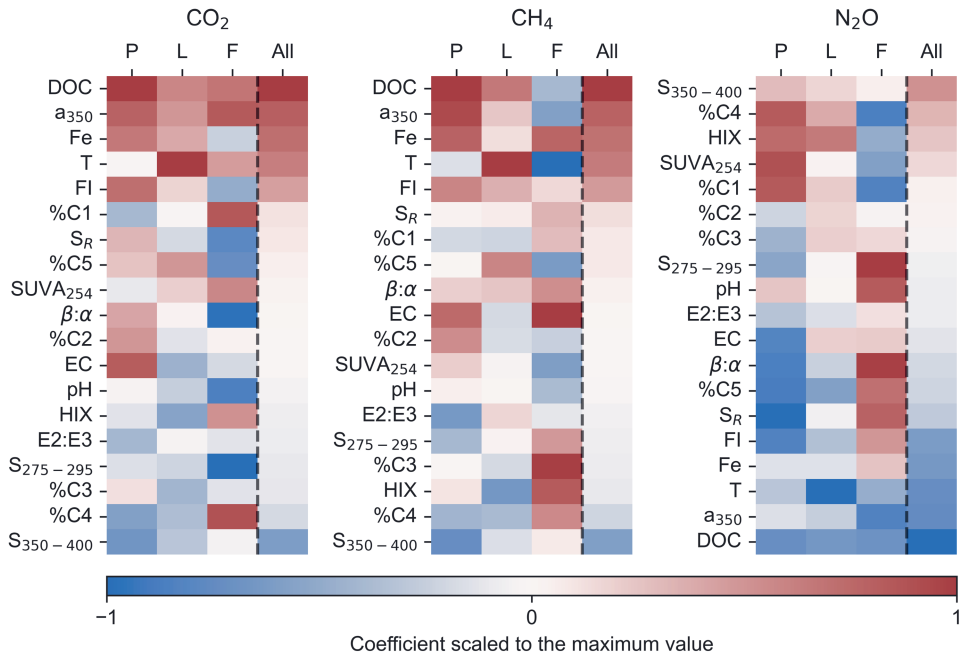

Figure 3.8: Heatmap of Partial Least Squares Regression (PLSR) coefficients for each model, with dissolved CO_2, CH_4, or N_2O concentrations as response variables. The 'All' model includes all freshwater ecosystem samples from this study, while the 'P' model includes only pond samples, the 'L' model only lake samples, and the 'F' model only fluvial samples. Figures showing the results of each PLSR are available in the Supplementary Information (Fig. S3–S6). All samples were collected in Kytalyk, northeastern Siberia, during the summer months of 2016 and 2017. The regression coefficients in each model are scaled to their maximum value. Positive (red) values indicate a positive coefficient for the corresponding GHG response variable, with values closer to 1 and deeper colors signifying a stronger effect. Negative (blue) values indicate a negative coefficient, with deeper colors indicating a stronger negative effect.

Ponds

This section explores how DOM characteristics, dissolved Fe, and pond morphology relate to dissolved CO_2 and CH_4 concentrations in the studied Arctic thaw ponds.

The strongest positive relationships with dissolved CO_2 and CH_4 were observed for DOC and cDOM (a_{350}), whereas the strongest negative relationship was observed for $S_{350\text{-}400}$ (Figure 3.8). Similar relationships between dissolved greenhouse gases and

DOM optical properties have previously been reported for Arctic thaw ponds (Breton et al., 2009). The positive relationships with DOC and cDOM suggest that ponds containing larger quantities of coloured organic matter also contained higher dissolved greenhouse gas concentrations. One possible explanation is that greater organic matter availability provides more substrate for microbial respiration, resulting in greater dissolved CO_2 production. This interpretation is broadly consistent with the TD-PTR-MS analyses, which showed that DOM in ponds P02 and P11 was more oxidised and had lower chemodiversity, characteristics previously associated with DOM that is more susceptible to microbial degradation (Peacock et al., 2018). Greater organic matter inputs may also promote organic matter burial and oxygen depletion, creating conditions favourable for methanogenesis and consequently higher dissolved CH_4 concentrations. In addition, cDOM-rich DOM is particularly susceptible to photochemical processing because it absorbs solar radiation, allowing photochemical oxidation to contribute directly to dissolved CO_2 production or indirectly increase DOM bioavailability for subsequent microbial degradation (Koehler et al., 2014; Cory et al., 2014; Laurion et al., 2021).

The positive relationships between dissolved Fe, cDOM, and dissolved CO_2 suggest several, non-mutually exclusive explanations. Under the mildly acidic conditions observed in the sampled ponds (pH range: 4.4–7.6; Figure 3.3), dissolved Fe may promote photo-Fenton reactions that generate hydroxyl radicals capable of degrading DOM (Molot et al., 2005). Iron complexes may also contribute directly to photochemical CO_2 production (Ward and Cory, 2016). In addition, elevated Fe concentrations have been shown to stimulate the biodegradation of humic-like DOM (Dean et al., 2016), which is consistent with the positive relationships observed between dissolved Fe, HIX, and dissolved CO_2 (Table S3.4). Alternatively, the positive relationships between dissolved Fe, cDOM, and dissolved CO_2 may reflect common terrestrial inputs, whereby runoff transports Fe-rich, terrestrially derived DOM together with elevated dissolved CO_2 into the ponds. This interpretation is also consistent with the positive relationship between specific conductivity and dissolved CO_2 (Figure 3.8).

In addition to DOM composition, pond morphology may also influence greenhouse gas dynamics. Dissolved CO_2 and CH_4 concentrations were positively related to decreasing pond surface area and water depth (Figure S3.5). One possible explanation is that ponds with lower surface area and shallower water receive proportionally greater catchment-derived organic matter inputs relative to their water volume because of their high perimeter-to-water surface area ratio (Wauthy et al., 2018; Wik et al., 2016). Alternatively, shallower ponds may experience stronger coupling between sediments and the overlying water column together with reduced water-column mixing, increasing the accumulation of dissolved greenhouse gases prior to atmospheric exchange (Prėskienis et al., 2021). Another factor that may influence water-column mixing is cDOM concentration. The positive association between a_{350} and dissolved CO_2 and CH_4 concentrations observed in the ponds (Figure 3.8) may therefore also reflect differences in cDOM-mediated thermal structure among ponds. Because cDOM absorbs solar radiation, higher cDOM concentrations can alter light penetration and thermal structure, potentially influencing water-column mixing and microbial degradation in Arctic ponds (Prėskienis et al., 2021, 2024).

Overall, the observed relationships suggest that DOM characteristics, dissolved Fe, and pond morphology all contribute to the dissolved greenhouse gas dynamics of Arctic thaw ponds through interacting microbial, photochemical, and physical processes.

Lakes

This section explores how DOM characteristics relate to dissolved CO_2 and CH_4 concentrations in the studied Arctic lakes, with particular attention to the contrasting relationships observed relative to ponds. We consider how differences in DOM composition, lake morphology, and Yedoma influence may contribute to these ecosystem-specific patterns.

Dissolved CO_2 exhibited similar relationships with several DOM properties in both ponds and lakes, including positive associations with DOC and cDOM, and negative associations with HIX, %C4, and $S_{350–400}$ (Figure 3.8). These consistent relationships suggest that similar controls link DOM characteristics and dissolved CO_2 concentrations across both ponds and lakes. However, the relationships with the relative proportions of the PARAFAC components differed between ecosystem types. Dissolved CO_2 was positively associated with the relative proportion of the humic-like component C2 (%C2) in ponds, whereas in lakes the only positive association was with the relative proportion of the protein-like component C5 (%C5). One possible explanation is that these contrasting relationships reflect the differences in DOM composition between ponds and lakes identified earlier in this discussion (Section 3), with ponds exhibiting a stronger allochthonous DOM signature and lakes containing a greater contribution of autochthonous and/or microbially processed DOM. As shown in Figure 3.5, lakes contained significantly lower relative proportions of the humic-like components C1 and C4, together with higher relative proportions of C3 and C5. These differences in DOM composition may influence which fractions of the DOM pool are preferentially transformed, resulting in different relationships between the relative abundance of PARAFAC components and dissolved CO_2 concentrations (Hansen et al., 2016). Alternatively, the differing relationships with the relative proportions of the PARAFAC components may indicate that DOM in lakes has undergone differing transformation in the water column to in ponds. Previous studies have shown that DOM composition is influenced by both hydrological transport and in-lake processing, with PARAFAC components varying in their reactivity and persistence within lakes (Kothawala et al., 2014, 2012). The same explanations may also account for the contrasting relationships observed between dissolved CO_2 and S_R, with a weak positive association in ponds and a weak negative association in lakes (Figure 3.8). Given that S_R provides information related to DOM molecular weight, these contrasting relationships are also consistent with the differing associations observed between dissolved CO_2 and the proportions of PARAFAC components.

Compared with ponds, lakes exhibited weaker or absent positive relationships between dissolved CH_4 and DOC, cDOM, dissolved Fe, specific conductivity, and the relative proportion of the humic-like PARAFAC component C2 (%C2), while exhibiting a stronger positive relationship with the relative proportion of the protein-like component C5 (%C5) and a stronger negative relationship with HIX (Figure 3.8). One possible explanation for these contrasting relationships is that differences in lake and pond morphology alter

how dissolved surface-water CH_4 relates to DOM characteristics. In shallow ponds, the close physical coupling between the sediments, overlying water column, and atmosphere means that dissolved CH_4 measured in surface waters may more closely reflect conditions throughout the entire water column if ponds are well mixed. In contrast, the greater water depth of lakes increases the physical separation between the sediments, where methane is predominantly produced through microbial methanogenesis under anoxic conditions (Peeters et al., 2019), and the surface waters sampled in this study. Consequently, dissolved surface-water CH_4 concentrations likely integrate methane production in the sediments together with subsequent transport and oxidation within the water column, affected by whether the water column is well mixed or thermally stratified. These processes have been shown to vary with lake morphometry and depth, both of which are important controls on methane dynamics in northern lakes and ponds (Jansen et al., 2020).

Although dissolved CO_2 and CH_4 showed stronger positive associations with temperature in lakes than in ponds, temperature was measured as an instantaneous surface value and therefore likely reflects sampling conditions rather than a primary control on dissolved gas concentrations.

The thermokarst-affected lake (L11-L15) exhibited a neutral to mildly alkaline pH (6.8–9.1; Figure 3.3), similar to pH values reported for thermokarst lakes influenced by Yedoma deposits (Sepulveda-Jauregui et al., 2015). Previous work at this study site has shown that this lake is geochemically distinct from the neighbouring lakes owing to inputs from eroding Yedoma soils and sediments, whereas the other lakes are primarily influenced by contemporary soils and vegetation (Meisel et al., 2023). Older radiocarbon ages of dissolved CO_2 and CH_4 in the same lake also indicate a greater contribution of pre-aged carbon than in the neighbouring lakes (Dean et al., 2020). Our PTR-DOC analysis further distinguished the thermokarst-affected lake (L11, L12, L14) from the other two lakes (L23, L31), with higher %PTR-DOC, a greater proportion of aliphatic compounds relative to aromatic and condensed aromatic compounds, and the lowest chemodiversity among the sampled freshwater ecosystems (Table 3.1).

Overall, the observed relationships suggest that DOM composition and lake morphology contribute to the associations between DOM characteristics and dissolved CO_2 and CH_4 concentrations in the studied Arctic lakes. In addition, the distinct molecular composition of the thermokarst-affected lake is consistent with previous geochemical and radiocarbon evidence indicating that Yedoma degradation contributes to spatial variability in DOM composition within the studied lake systems.

Fluvial

Fluvial systems exhibited the greatest departure from the relationships observed across all freshwater ecosystems in the ecosystem-specific PLSR (Figure 3.8).

Compared with ponds and lakes, fluvial systems exhibited stronger positive relationships between dissolved CO_2 and the proportions terrestrial humic-like PARAFAC components C1 (%C1) and C4 (%C4), while maintaining positive relationships with DOC and cDOM (a_{350}). In contrast, dissolved CO_2 exhibited negative relationships with the

recently produced DOM index $\beta{:}\alpha$, $S_{275–295}$, and, to a lesser extent, S_R (Figure 3.8). Collectively, these relationships indicate that higher dissolved CO_2 concentrations were associated with higher molecular weight, humic DOM that is typically considered characteristic of terrestrial inputs. One possible explanation is that dissolved CO_2 is preferentially produced from terrestrially derived, humic DOM during transport through the fluvial network. Alternatively or in addition, dissolved CO_2 and terrestrially derived DOM may be transported simultaneously from surrounding soils into streams. Previous studies have shown that both direct transport of soil-derived CO_2 and in-stream degradation of terrestrial DOM contribute to dissolved CO_2 dynamics in streams (Rasilo et al., 2017; Hutchins et al., 2017). Another possible explanation is the shorter water residence times of fluvial systems, which could preserve stronger relationships between dissolved CO_2 and terrestrially derived DOM characteristics. In contrast, the longer residence times of ponds and lakes provide greater opportunity for microbial degradation, photochemical processing, sedimentation, and gas exchange to modify both DOM composition and dissolved CO_2 concentrations, potentially resulting in the different relationships observed among ecosystem types (Kling et al., 2000).

Unlike dissolved CO_2, dissolved CH_4 was not associated with a single, coherent set of DOM characteristics. For example, the positive relationship with HIX is generally associated with more humified DOM, whereas the positive relationship with $S_{275–295}$ is commonly interpreted as indicating lower molecular weight DOM. Together with the positive relationship with the relative proportion of C3 (%C3), these relationships do not point to a single, consistent DOM characteristic. These relationships differ markedly from those observed in ponds and lakes, where dissolved CH_4 was more closely associated with DOC and exhibited weak or negative relationships with HIX, $S_{275–295}$, and the relative proportion of C3 (%C3). In fluvial systems, these relationships were reversed, with little relationship to DOC and positive associations with HIX, $S_{275–295}$, and %C3 (Figure 3.8). These contrasting relationships may reflect fundamental differences in how dissolved CH_4 is produced and transported in fluvial systems compared with ponds and lakes. Unlike ponds and lakes, where dissolved methane reflects processes within a single standing water body, dissolved CH_4 in fluvial systems is influenced by methane produced in anoxic streambed sediments and subsequently transported downstream. Street et al. (2016) found that methane concentrations in Arctic streambed sediments were several orders of magnitude higher than those in adjacent hillslope soils, suggesting that stream sediments can represent an important methane source to stream waters. Consequently, dissolved surface-water CH_4 may not be expected to exhibit a single, coherent relationship with surface-water DOM characteristics, because methane production, downstream transport, and methane oxidation can all modify dissolved concentrations independently of the DOM composition measured in the water column.

A similar ecosystem-specific pattern was also evident for dissolved N_2O. Although dissolved N_2O exhibited a consistently negative relationship with DOC across ponds, lakes, and fluvial systems, several optical DOM indices displayed contrasting relationships in the fluvial systems. For example, HIX and $SUVA_{254}$, which were positively associated with dissolved N_2O in ponds and remained weakly positive in lakes, exhibited negative relationships in the fluvial systems. Conversely, FI and S_R, which were negatively as-

sociated with dissolved N_2O in ponds and lakes, exhibited weak positive relationships in the fluvial systems (Figure 3.8). The consistent negative relationship between dissolved N_2O and DOC across all ecosystem types suggests that the quantity of DOM is associated with dissolved N_2O irrespective of ecosystem type. This relationship is consistent with previous observations from boreal freshwater ecosystems, where higher DOC concentrations were associated with lower dissolved N_2O concentrations, although the mechanisms underlying this relationship remain uncertain (Soued et al., 2015). In contrast, the relationships with optical DOM characteristics varied among ecosystem types, indicating that while the relationship with bulk DOC was broadly conserved, associations between dissolved N_2O and DOM composition were ecosystem dependent. In particular, the strongest contrasts occurred between the fluvial systems and the lakes and ponds, with the latter generally exhibiting relationships of similar direction but differing strength.

Overall, these findings demonstrate that the relationships between DOM characteristics and dissolved gases are ecosystem specific. The contrasting patterns observed in fluvial systems indicate that flowing waters are governed by different combinations of hydrological and biogeochemical processes than lake and ponds, resulting in distinct DOM–greenhouse gas relationships.

Limitations

Our findings are based on spatial comparisons of point-in-time samples and therefore do not capture temporal variability or directly resolve the mechanisms underlying the observed DOM–greenhouse gas relationships. Consequently, the reported associations should be interpreted as ecosystem-specific correlations rather than evidence of causal relationships.

While this study incorporates both direct measurements (e.g., absorbance and DOC) and derived optical metrics (e.g., $SUVA_{254}$, FI, HIX, spectral slopes, and PARAFAC components), interpretation of these measurements requires environmental context. Optical properties provide valuable insight into DOM composition and processing but do not uniquely represent molecular composition or environmental reactivity, as similar optical signatures may arise from different mixtures of compounds and distinct processing histories. Moreover, the ecological significance of optical metrics depends on the environmental setting in which they are measured, and bulk optical properties alone cannot fully resolve DOM fate or function (D'Andrilli et al., 2022; Buckley et al., 2024). Likewise, individual optical indices can respond differently to biological and photochemical alteration, reinforcing the importance of interpreting multiple complementary measurements together rather than relying on any single index in isolation (Hansen et al., 2016). This multivariate approach underpins the analyses presented here.

Finally, the subset of samples analysed using PTR-MS was relatively small, limiting our ability to comprehensively investigate relationships between individual dissolved organic compounds and greenhouse gas concentrations. Nevertheless, these molecular measurements provided complementary information to the optical analyses and demonstrate the potential of future studies integrating molecular- and optical-level characterisation across larger datasets.

Conclusions

This study demonstrates that relationships between DOM characteristics and dissolved greenhouse gas concentrations differ among Arctic freshwater ecosystem types. Rather than exhibiting a single, consistent set of DOM–greenhouse gas relationships, ponds, lakes, and fluvial systems each displayed distinct associations between dissolved CO_2, CH_4, and N_2O and DOM quantity and composition. Together, these findings indicate that DOM–greenhouse gas relationships reflect not only the quantity of DOM present, but also differences in the fractions of the DOM pool that dominate individual freshwater ecosystems. In ponds, greenhouse gas concentrations were associated with DOM quantity, dissolved Fe, and pond morphology, indicating that both DOM characteristics and the physical characteristics of these shallow systems contribute to observed DOM–greenhouse gas relationships. In lakes, the dominant DOM fractions associated with dissolved greenhouse gases shifted relative to ponds, indicating that differences in DOM composition alter which fractions of the DOM pool are most closely associated with dissolved greenhouse gas concentrations. In fluvial systems, the greatest departure from the relationships observed in ponds and lakes indicates that associations between DOM characteristics and dissolved greenhouse gases differ fundamentally between standing and flowing waters, emphasizing that DOM–greenhouse gas relationships cannot be transferred directly across freshwater ecosystem types. Unlike dissolved CO_2 and CH_4, dissolved N_2O exhibited one relationship that was conserved across all freshwater ecosystem types: a consistent negative association with DOC. In contrast, relationships between dissolved N_2O and optical DOM characteristics varied among ecosystems, with ponds and lakes exhibiting broadly similar patterns and fluvial systems displaying contrasting relationships. These findings suggest that while the quantity of DOM is consistently associated with dissolved N_2O, the relationship between dissolved N_2O and DOM composition remains ecosystem dependent.

Future research should therefore investigate DOM–greenhouse gas relationships alongside ecosystem-specific limnological and environmental characteristics, including water-column structure, sediment–water interactions, nutrient availability, and hydrological connectivity. Integrating these factors with molecular- and optical-level DOM characterisation will improve understanding of why DOM–greenhouse gas relationships differ among freshwater ecosystem types and determine whether broader predictive relationships can be developed that are transferable across Arctic freshwater ecosystems.

Statments and Declarations

Funding

This work was carried out within the Netherlands Earth System Science Centre (NESSC; Grant No. 024.002.001), financially supported by the Dutch Ministry of Education, Culture and Science (OCW). JFD received additional support from the UKRI Future Leaders Fellowship (MR/V025082/1). This study was also supported in part by the project Study of biogeochemical cycles and adaptive reactions of plants of boreal and arctic ecosystems of northeastern Russia (AAAA-A21-121012190034-2) of the Ministry of Education and

Science of Russia.

Competing Interests

The authors have no relevant financial or non-financial interests to disclose.

Acknowledgments

We thank Steven Bouillon and Zita Kelemen from the Department of Earth and Environmental Sciences, KU Leuven, Belgium, for their valuable contributions in measuring DOC $\delta^{13}C$-DOC and Fe for this study.

Data availability

The datasets generated and analysed during this study, including dissolved organic matter (DOM) properties, dissolved greenhouse gas concentrations (CO_2, CH_4, and N_2O), and associated environmental variables, have been deposited in the PANGAEA data repository (DOI: 10.1594/PANGAEA.993666) and are currently under moratorium until publication of the associated manuscript. Fluorescence excitation–emission matrices (EEMs) and the derived parallel factor analysis (PARAFAC) model have been submitted to OpenFluor and will be made publicly available upon publication of the associated manuscript.

Author contributions

M.M.R.: Conceptualization, data curation, formal analysis, investigation, methodology, software, visualization, writing – original draft.

J.F.D.: Conceptualization, funding acquisition, investigation, project administration, supervision, writing – review and editing.

O.H.M.: Investigation, resources, writing – review and editing.

R.v.L.: Investigation, resources.

T.L.: Investigation, resources, validation.

D.M.: Investigation, resources, validation.

S.K.: Investigation, resources.

T.M.: Investigation, resources, project administration.

J.E.V.: Funding acquisition, project administration.

J.T.W.: Methodology, supervision, validation, writing – review and editing.

Appendix

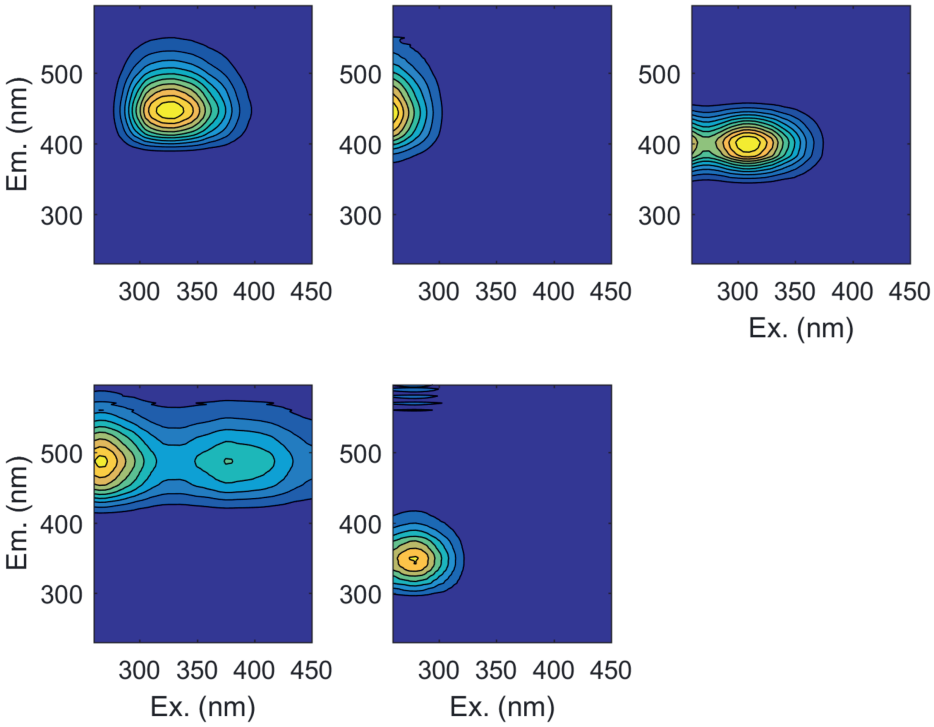

Figure S3.1: EEMs of PARAFAC components 1–5.

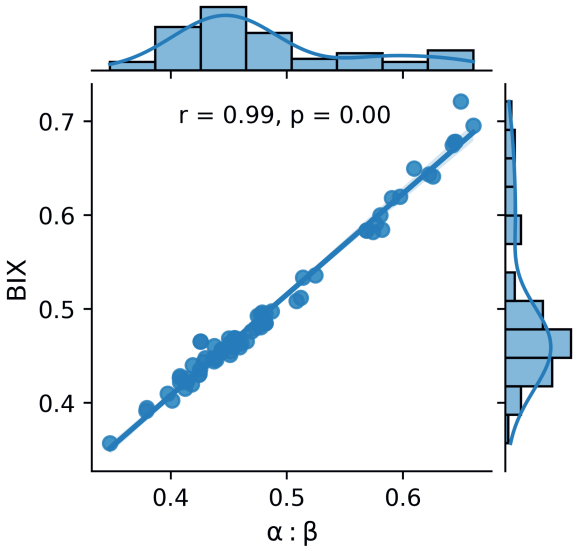

Figure S3.2: Relationship between the Freshness index (β:α) and the Biological index (BIX). r and p show results from Pearson's correlation.

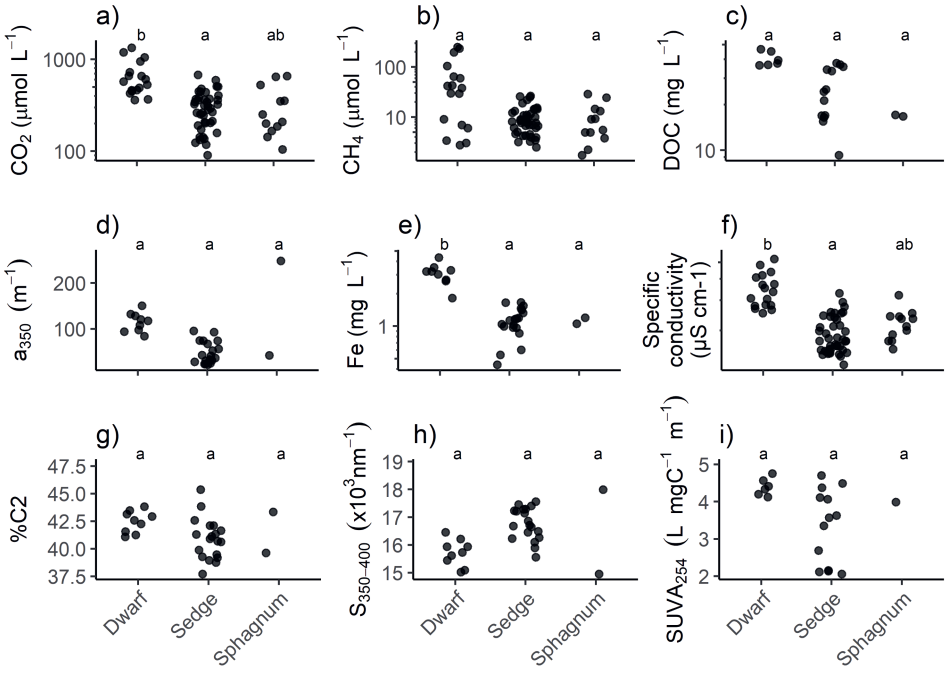

Figure S3.3: Data ponds sampled in Kytalyk, Siberia in 2016 and 2017 plotted sub-divided into their dominant vegetation type. Each data point represents a measurement of either dissolved CO_2 concentrations (a), dissolved CH_4 concentrations (b), DOC (c), a_{350} (d), dissolved Fe (e), EC (f), %C2 (g), $S_{350\text{-}400}$ (h) or $SUVA_{254}$ (i). Statistically significant differences among vegetation types were identified using linear mixed-effects models (LMMs) with site as a random effect, followed by Tukey-adjusted pairwise comparisons of estimated marginal means. Different letters denote significantly different groups $p < 0.05$. The x-axis vegetation labels are consistent across all subplots. Note that panels (a), (b), (c), (d), and (f) are displayed on log-scaled y-axes for visual clarity.

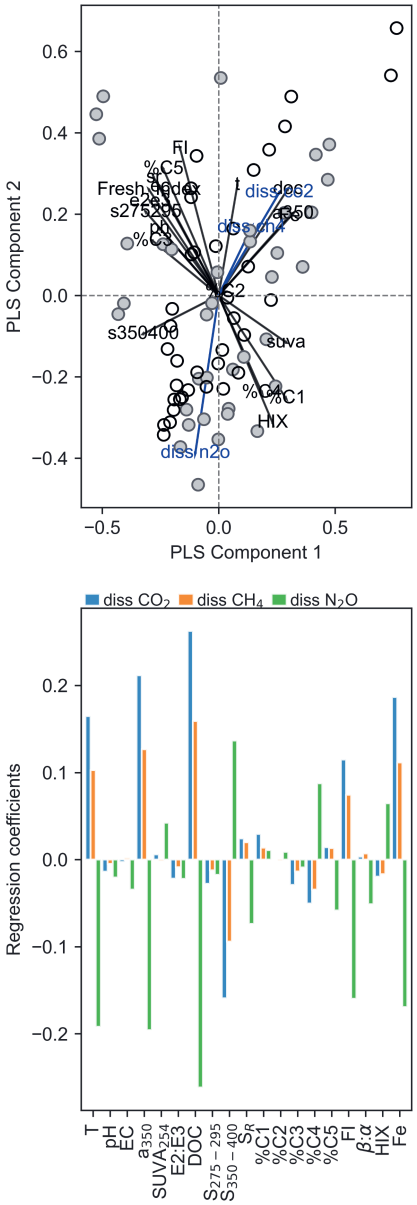

Figure S3.4: Partial least square regression (PLSR) of dissolved CO_2, CH_4 and N_2O concentrations in relation to optical parameters for all samples. a) Variables in blue are the response variables and variables in black the explanatory variables. Dots represent the dissolved gas measurements in ponds. The first two axes which correspond to PLSR components 1 and 2 are shown. b) The regression coefficients from PLSR show the strength and direction of the relation between the explanatory and response variables.

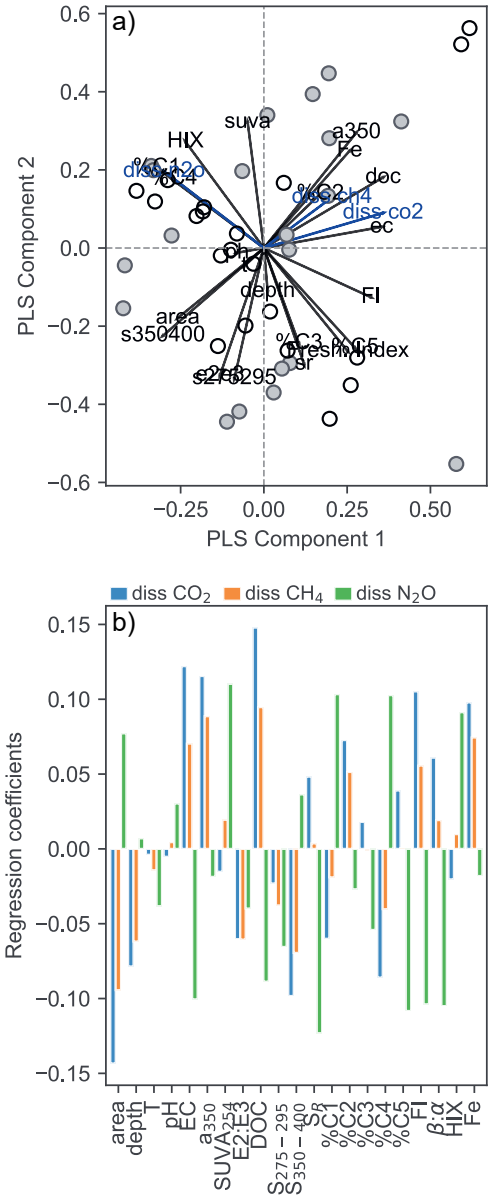

Figure S3.5: Partial least square regression (PLSR) of dissolved CO_2, CH_4 and N_2O concentrations in relation to optical parameters for pond samples. a) Variables in blue are the response variables and variables in black the explanatory variables. Filled dots represent lake samples in the explanatory variable (X) space, and unfilled dots represent the same samples in the response variable (Y) space in ponds. The first two axes which correspond to PLSR components 1 and 2 are shown. b) The regression coefficients from PLSR show the strength and direction of the relation between the explanatory and response variables.

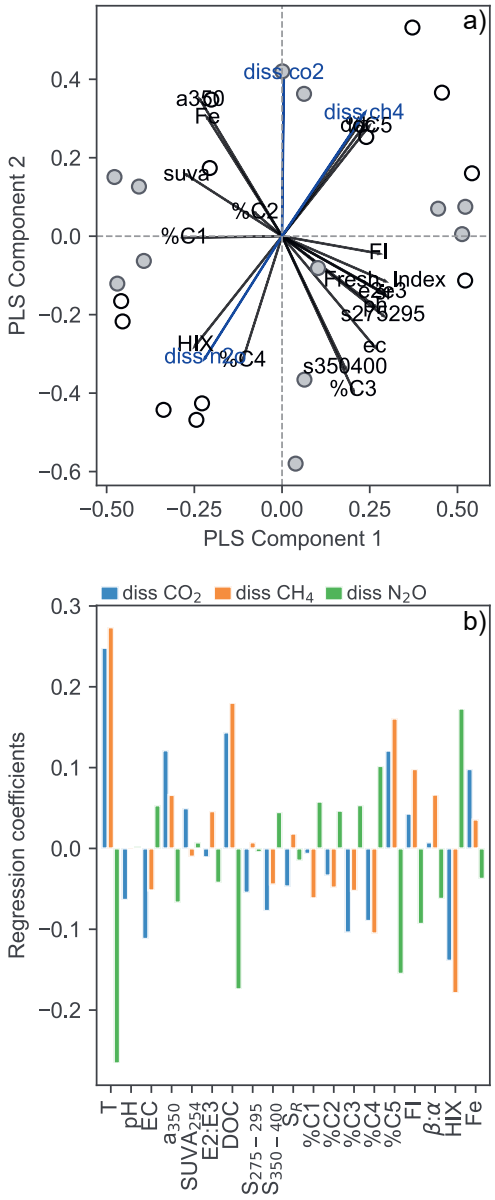

Figure S3.6: Partial least square regression (PLSR) of dissolved CO_2, CH_4 and N_2O concentrations in relation to optical parameters for lake samples. a) Variables in blue are the response variables and variables in black the explanatory variables. Filled dots represent lake samples in the explanatory variable (X) space, and unfilled dots represent the same samples in the response variable (Y) space in lakes. The first two axes which correspond to PLSR components 1 and 2 are shown. b) The regression coefficients from PLSR show the strength and direction of the relation between the explanatory and response variables.

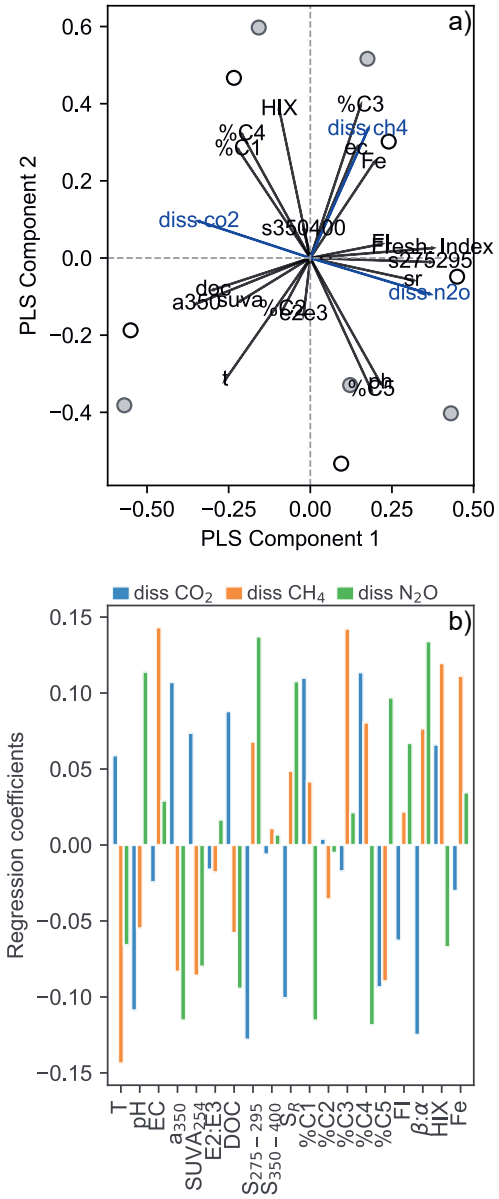

Figure S3.7: Partial least square regression (PLSR) of dissolved CO_2, CH_4 and N_2O concentrations in relation to optical parameters for fluvial samples. a) Variables in blue are the response variables and variables in black the explanatory variables. Filled dots represent lake samples in the explanatory variable (X) space, and unfilled dots represent the same samples in the response variable (Y) space in fluvial samples. The first two axes which correspond to PLSR components 1 and 2 are shown. b) The regression coefficients from PLSR show the strength and direction of the relation between the explanatory and response variables.

Site	Vegetation
P01	Dwarf-shrub wetland
P02	Sedge wetland
P03	Sedge wetland
P04	Sedge wetland
P05	Sedge wetland
P06	Dwarf-shrub wetland
P07	Sedge wetland
P08	Sedge wetland
P09	*Sphagnum* wetland
P10	Dwarf-shrub wetland
P11	Sedge wetland
P12	*Sphagnum* wetland

Table S3.1: Vegetation classes identified in sampled ponds using the vegetation map from Siewert et al. (2015)

Variable	Model Type	Lake (%)	Sampling Site (%)	Residual (%)
CO_2	log	0.0	56.4	43.6
CH_4	log	0.0	69.7	30.3
N_2O	non-log	0.0	5.9	94.1

Table S3.2: Proportion of variance in dissolved gas concentrations explained by lake identity (Lake), site identity within lake (Sampling Site), and residual error, based on linear mixed-effects models fit to lake-only data. All models included a nested random effects structure $(1 \mid \texttt{lake/sampling_site})$.

Contrast	Variable	Estimate	Std Error	p-value
Dwarf-shrub wetland - Sedge wetland	CO_2	0.79	0.265	0.036
Dwarf-shrub wetland - Sedge wetland	EC	0.58	0.129	0.004
Dwarf-shrub wetland - Sedge wetland	Fe	1.99	0.245	0.003
Dwarf-shrub wetland - *Sphagnum* wetland	Fe	1.97	0.417	0.003

Table S3.3: Summary of statistically significant differences in DOM characteristics, dissolved gas concentrations, and environmental variables among pond vegetation types. Results are based on linear mixed-effects models (LMMs) with vegetation category as a fixed effect and pond site as a random intercept to account for repeated sampling within ponds. The table reports estimated contrasts, standard errors, and p-values for pairwise comparisons between vegetation types, using Tukey-adjusted estimated marginal means. A significance threshold of $\mathrm{p} < 0.05$ was applied. Only significant pairwise comparisons are included.

Contrast	Estimate	Std Error	p-value	Transformation
CO_2	0.28	0.120	0.031	log
DOC	4.38	1.730	0.021	original
a_{350}	0.35	0.120	0.009	log
$S_{350\text{-}400}$	-0.48	0.126	0.008	original
%C2	0.018	0.007	0.018	log
HIX	0.011	0.005	0.031	original

Table S3.4: Summary of statistically significant relationships between dissolved iron (Fe) concentrations and measured response variables in pond samples. Results are from linear mixed-effects models (LMMs) with Fe concentration as a fixed effect and pond site as a random effect to account for repeated measurements. The table presents effect estimates, standard errors, and p-values for the Fe effect, with significance determined at $\mathrm{p} < 0.05$. Models were fit with and without log-transformation of response variables, and the best-fitting transformation (as determined by residual diagnostics) is noted. Only results with statistically significant Fe effects are included.

Component	Ex max (nm)	Em max (nm)	Description and likely structure	Source
C1	330	446	UVC humic-like, high molecular weight component	Terrestrial
C2	<260	444	UVA humic-like, resembles fulvic-like material	Terrestrial
C3	(<260) 310	402	UVA humic-like or fulvic-like, low molecular weight component	Terrestrial, Autochthonous, Microbial
C4	265 (375)	488	UVA humic-like with fulvic acid, high molecular weight, aromatic humic	Terrestrial
C5	280	350	Tryptophan-like, amino acids, free or bound in proteins	Terrestrial, Autochthonous, Microbial

Table S3.5: Description of five fluorescent components identified by PARAFAC.

Chapter 4

Lateral carbon flow

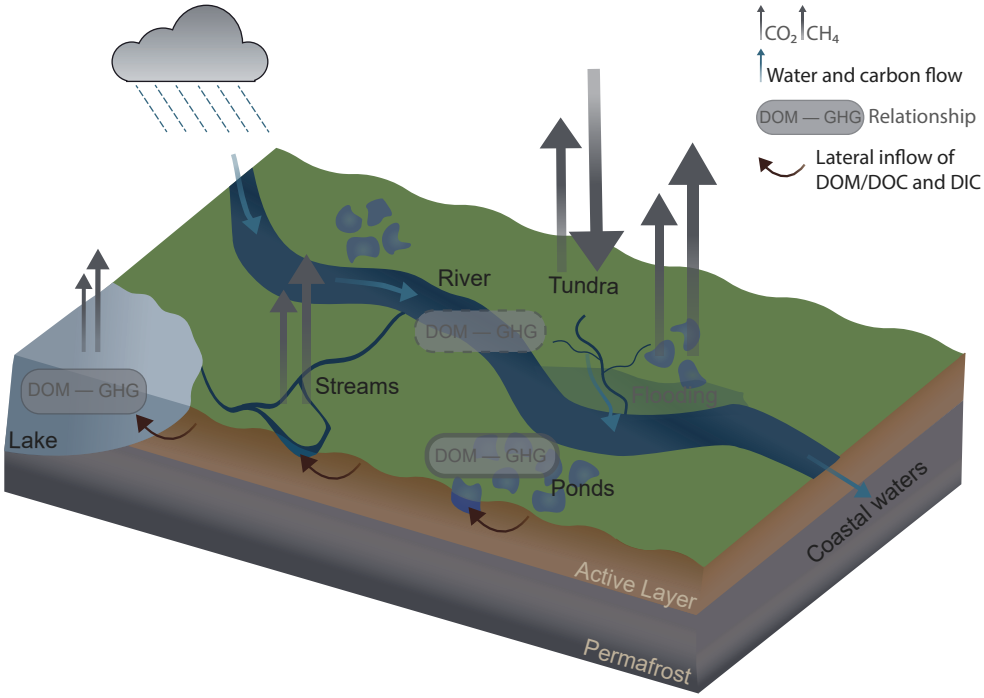

Undergoing changes following reviews from Arctic Sciences in 2025:

Lateral carbon flow in an Arctic coastal catchment in late summer

Melanie Martyn Rosco, Geert Hensgens, Jorien E. Vonk, James T. Weedon, Joshua F. Dean

As the timing, duration, and environmental conditions of Arctic growing seasons shift, and late-summer rainfall increases, it is critical to understand lateral carbon transport in small (<1000 km^2), understudied catchments, which account for 9 % of the Arctic terrestrial area. We investigated lateral carbon transport within a small coastal catchment in the Hudson Bay Lowlands by sampling a stream network with connected ponds, lakes, and adjacent soil pore waters to quantify carbon concentrations, dissolved organic matter (DOM) composition, and stable carbon isotopes. Dissolved inorganic carbon (DIC) concentrations increased downstream, accompanied by changes in $\delta^{13}\mathrm{C}$-DIC and DOM optical properties, suggesting that the dissolved organic pool (DOC) processing contributed to the downstream increase in DIC, while additional DIC inputs from the subsurface likely also contributed. In contrast, DOC concentrations remained within a relatively narrow range, while changes in DOM optical properties indicate that bulk DOC stability did not preclude changes in DOM composition during downstream transport. Differences between soil pore water and surface water varied between the headwater peatland and coastal sandy heathland, with greater differences in several carbon characteristics in the headwater peatland. Late-summer rainfall increased DOC concentrations and aromaticity in surface waters while reducing DIC concentrations, whereas DOM composition in soil pore waters remained relatively stable. These findings emphasize the importance of accounting for landscape heterogeneity and rainfall-driven hydrological variability when assessing lateral carbon export from small Arctic coastal catchments in the Hudson Bay Lowlands.

Introduction

Lateral carbon fluxes between terrestrial and freshwater ecosystems form a key pathway in Arctic terrestrial, atmospheric and marine carbon cycling. Arctic regions, warming at roughly four times the global average (Rantanen et al., 2022), are undergoing significant changes in permafrost depth and distribution, hydrology, and vegetation, all of which alter the quantity and composition of lateral carbon fluxes. The Hudson Bay Lowlands, one of the largest peatland complexes globally, stores approximately 30 Pg of carbon and contributes 23 % of the total organic carbon input to the Arctic Ocean (Hugelius et al., 2020; Mundy et al., 2009). Shallow water bodies, covering 25 % to 40 % of the Hudson Bay Lowlands' surface area (Duguay and Lafleur, 2003), are particularly important in mobilizing and transporting carbon (Guo et al., 2007; Stackpoole et al., 2017). Although no significant long-term changes in pond surface area were detected through 2008 despite regional warming, future increases in surface water extent are considered possible under projected wetter climatic conditions (Macrae et al., 2014). However, the region remains understudied, especially the small coastal catchments contributing to carbon fluxes. The Hudson Bay Lowlands exhibit substantial variability in landscape features, vegetation types, and hydrological processes, including discontinuous permafrost, taiga-tundra transitions, and localized hydrological responses (Wolfe et al., 2011). These factors directly influence lateral carbon transport by controlling soil drainage, organic matter decomposition, and the connectivity between terrestrial and aquatic systems. Given the region's sensitivity to climate change, detailed studies are needed to assess how shifts in permafrost thaw, vegetation composition, and hydrological patterns will alter carbon export from the Hudson Bay Lowlands.

Lateral carbon export in river catchments moves organic carbon primarily as dissolved organic carbon (DOC) and particulate organic carbon (POC), and inorganic carbon as dissolved inorganic carbon (DIC), which includes dissolved CO_2, while methane (CH_4) represents an additional dissolved carbon species (Tank et al., 2018). Streams, though small in surface area, are hotspots for carbon processing and the emission of greenhouse gases (Lundin et al., 2013; McClain et al., 2003; Raymond et al., 2013). The degree to which these emissions are linked to the lateral carbon export of DOC, POC and DIC remains poorly constrained (Gómez-Gener et al., 2021; Hotchkiss et al., 2015). For instance, questions persist about whether terrestrial carbon enters fluvial networks primarily as soil-derived CO_2/DIC and CH_4 or as DOC, which may degrade at the terrestrial-aquatic interface or within streams (Tank et al., 2018). Evidence from low-order boreal streams suggests that degradation of soil-derived DOM in either the stream or hyporheic zone can account for 75 % of stream CO_2 (Rasilo et al., 2017), and in six subarctic streams the annual mass of laterally exported carbon as DIC was on the same order of magnitude as DOC (Giesler et al., 2014). In-stream mineralization of DOC and oxidation of CH_4 have also been found to be important contributors to CO_2 emissions (Lupon et al., 2019). The contribution of terrestrially derived CO_2, in contrast to in-stream produced CO_2, is thought to depend on stream size and terrestrial-aquatic connectivity, and within headwaters, terrestrial CO_2 fluxes to streams can be highly spatially and temporally variable (Duvert et al., 2018; Hotchkiss et al., 2015). The links between lateral carbon export and stream CO_2 and CH_4 emissions are therefore complex, and the extent to

which stream greenhouse gas emissions are supported by direct terrestrial inputs of dissolved gases versus the degradation of laterally exported organic carbon remains poorly understood.

In the Arctic, growing seasons are lengthening and becoming warmer, with deeper active layers and more intense late-season rainfall events (Beel et al., 2021; Tank et al., 2020). These shifts are likely to significantly alter an already poorly understood carbon flux to small-order Arctic fluvial systems. This study focused on a small coastal catchment in the Hudson Bay Lowlands during late summer. Late summer, when the active layer is deepest, presents unique conditions for catchment carbon dynamics, including enhanced microbial activity, high soil carbon availability, and increased potential for hydrological flushing and export (Judd and Kling, 2002). At the end of the growing season (late summer), increased precipitation can result in increased inputs of both organic carbon and soil CO_2 to streams (Leith et al., 2015; Shogren et al., 2020a). Here we aimed to: (1) quantify variations in the concentrations and isotopic composition of organic and inorganic carbon through the study catchment; (2) evaluate the coupling between freshwater carbon and adjacent soil pore water; and (3) assess the impact of a precipitation event on these dynamics. By examining these processes, this study aimed to provide insights into the spatial and temporal variability of lateral carbon flows in small Arctic catchments and their potential responses to climatic and hydrological changes.

Methods

Study area and sampling strategy

This study was conducted in a drainage basin situated within the subarctic peatland of the forest-tundra ecotone near Churchill, Manitoba, Canada, approximately 10 km inland from the western coast of Hudson Bay. The ecotone is characterized by the sandy coastline of Hudson Bay extending inland to small, rolling peat hummocks within coastal wetlands (Peter Kershaw and McCulloch, 2007). The Churchill area is largely flat, with an average gradient of about 1 m km^{-1}, and continues to experience gradual uplift following glacial retreat, at a rate of approximately 11.4 ± 0.7 mm yr^{-1} (Wolf et al., 2006). The surface geology of the region consists of marine silts and glacial till from the Pleistocene epoch, overlain by a peat layer that varies from just a few centimeters near the coast to over 4 m further inland (Dredge and Nixon, 1992). Glacial tills in the Churchill region contain limestone and dolomite clasts transported from Paleozoic carbonate terrains surrounding Hudson Bay, while postglacial marine inundation deposited additional marine sediments across the lowlands (Dredge and McMartin, 2011). Beneath this, continuous permafrost prevails, with the active layer typically extending to less than 1 m depth (Dyke and Sladen, 2010).

Despite being located in the subarctic region, the study area's climate is heavily influenced by Hudson Bay, resulting in weather patterns similar to those found in the High Arctic regions further north. In Churchill, the average temperature in August is 12.5°C, while in January, it drops to -25.3°C, with an average annual precipitation of 447.7 mm,

approximately 40 % of which falls as snow (Environment Canada, 2024). During the study period (12 August to 05 September 2022), the site received a total of 66 mm of rainfall. From 12 August to 23 August 2022, precipitation and air temperature data were obtained from the Government of Canada's monitoring station (Climate ID 5060608, WMO ID 71696). Starting 23 August 2022, data from a tipping bucket rain gauge installed at one of the field sites became available. For the period from 23 August to 30 August 2022, hourly data from the tipping bucket were averaged with data from the same Government of Canada monitoring station to ensure comprehensive coverage. Up until the night of 28 August and throughout the day of 29 August 2022, the weather was relatively dry, with a total of only 9 mm of rainfall recorded. During this period, temperatures were notably warm, with a mean of 17.3°C and a maximum reaching 32.3°C. This was followed by a significant rainfall event, delivering 19 mm of precipitation, and another major rainfall event on 02 September 2022, contributing an additional 33 mm.

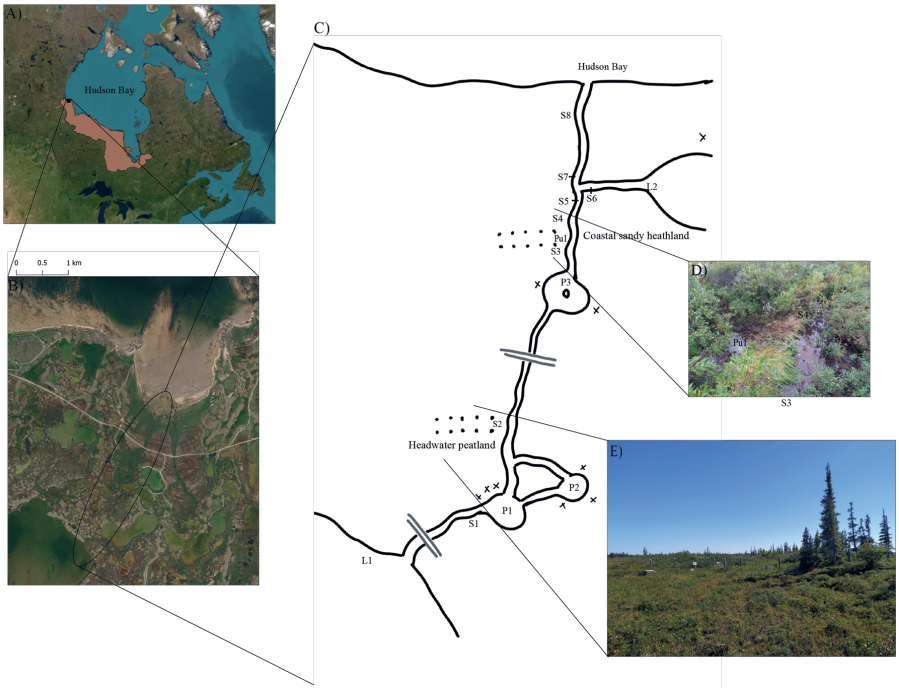

Figure 4.1: Overview of the study area and sampling design in a small coastal catchment near Churchill, Manitoba. (A) Location of Hudson Bay within Canada and the extent of the Hudson Bay Lowlands. Boundary layer for the Hudson and James Bay Lowlands: publicly available dataset from a national geodata repository. (B) Regional view showing the catchment location near Churchill. Satellite imagery from Esri World Imagery (Esri, Maxar, Earthstar Geographics, GIS User Community). (C) Conceptual diagram of the studied catchment (not to scale). Water flows from L1 downstream toward Hudson Bay. X symbols mark soil pore water sampling sites. Dots represent locations where soil pore water samples were collected along two parallel transects perpendicular to the stream. Double grey lines indicate a discontinuity in the diagram, representing a transition to the next section of the catchment. (D) Photograph showing sampling sites S3, S4, and puddle site Pu1. S3 is located upstream from the photographed area, slightly above the visible stream segment. Photo by M.M. Rosco. (E) Photograph of the headwater peatland near site S2, where soil pore water samples were collected. The location is adjacent to the visible pipes protruding from the ground. Photo by M.M. Rosco.

Based on field observations, the inlet of the catchment is a large headwater lake (L1, Figure 4.1). The headwater area is characterized by well-developed peat layers, and possibly gleyed mineral layers beneath. The vegetation is dominated by peatland species such as sweet gale (*Myrica gale*), sedges (*Carex spp.*), bog rosemary (*Andromeda polifolia*), and dwarf birch (*Betula glandulosa*). In higher, drier areas, lichen (*Cladonia* spp.) and black spruce (*Picea mariana*) thrive, while moisture-loving plants like water sedge (*Carex aquatilis*) dominate near freshwater bodies, typical of peatland vegetation. For the purposes of this study, this area is referred to as headwater peatland. In the head-

water peatland, sampling included ponds (P1, P2) and streams (S1, S2). Due to logistical and time constraints, further sampling efforts were focused downstream, closer to Hudson Bay. This second area, which displays characteristics typical of an older, well-drained beach, has sandy soils with less peat development. Many soil profiles, especially deeper ones, had a grey layer of mineral-rich material, suggesting mineral accumulation or periodic waterlogging. The vegetation here includes species such as bog rosemary (*Andromeda polifolia*), Arctic bearberry (*Arctostaphylos rubra*), bilberry (*Vaccinium uliginosum*), dwarf birch (*Betula glandulosa*), and Arctic willow (*Salix arctica*), all typical of a sandy heathland. Therefore, this area is referred to as coastal sandy heathland in this study. In this area sampling focused on streams (S3, S4, S5, S6, S7, S8), a lake (L2), and a puddle (Pu1).

Surface water samples were collected in a pre-rinsed 1 L Nalgene bottle, at a depth of 10 cm to 20 cm below the surface. Surface water samples were taken in the middle of all ponds and L2. The surface area and depth of the headwater lake (L1) did not permit sample collection from its centre, so samples were collected 4 m from the shore at the east side of the lake, the side at which the catchment originates. The surface water samples were kept in dark and cool conditions until decanted, which was done within a day. Specific conductivity, temperature, and pH were measured in surface waters using a Conrad Electronic Benelux BV GMH 3431 meter.

Soil pore water samples were collected using a pushpoint sampler (M.H.E. Products) to minimize disturbance during sample collection. For clarity, 'soil pore water' refers to water residing in the subsurface soil matrix. Throughout this study, we may also refer to this as 'subsurface water' when discussing broader hydrological processes. The sampler consisted of a 6.4 mm diameter stainless-steel tube with a 4 cm slotted screen at the bottom, covered by a fine nylon mesh 'sock' to prevent soil clogging. A syringe (the 'sampling syringe') was attached to a three-way valve connected to a tube at the top of the pushpoint sampler, allowing for the creation of a vacuum to pull pore water into the syringe. The first 10 mL to 20 mL of pore water were discarded to rinse the syringe. Once the sampling syringe was full, a second syringe (the 'storage syringe') was attached to the valve, and the water was transferred while avoiding contact with air. Any remaining air bubbles in the storage syringe were carefully removed before the sample was stored and transported to the laboratory. Two storage syringes were filled at each sampling point. The pushpoint sampler was driven into the ground until it reached resistance from the permafrost, and samples were collected in 20 cm increments from this point up to the top 20 cm of the soil profile. The top 20 cm never contained enough water to collect samples.

At sites S2 and S4, soil pore water samples were collected along two transects perpendicular to the stream. Sampling occurred at 5 m intervals, starting at the stream's edge and extending up to 25 m away. Each transect was sampled twice, once before and once after the rainfall on 28 August 2022 (Figure 4.1), with the parallel transects spaced approximately 5 m apart. Elsewhere in the catchment, surface water and soil pore water were sampled opportunistically to provide a broader spatial perspective. Additional samples were collected at three locations around ponds P1 and P2 and at two locations around P3, all within 10 m of the ponds. These soil pore water samples from the vicinity of S2, S4, and P1–3 are collectively referred to as 'periaquatic' in this study. At P3, an

additional sample was collected from a small vegetated islet located in the middle of the site. In the stream at site S2 soil pore water samples from the hyporheic zone and the stream bank were collected at the same time as the corresponding surface water sample. Additional lake and pond bed samples, also referred to as sediment samples, were collected at sites L2 and P2 at the same time as surface water samples, but other stream hyporheic zones and pond and lake beds could not be sampled due to rocky substrates preventing sampler insertion. At the headwater lake (L1) we attempted to sample the ridge but could not extract any water. But it was possible to get a soil pore water sample on the other side of the ridge, on the north-eastern side of the lake, where we consider the catchment to originate.

Laboratory analyses

Surface water samples were filtered through a pre-combusted 0.7 µm pore size Whatman GF/F glass fiber filter with a diameter of 47 mm, using a Millipore vacuum filter tower. The filters were air dried and all samples were kept in dark, cool conditions until analysis was carried out. The filters were stored and analysed for POC. Acidified DOC samples were analysed with an OI Analytical Aurora model 1030 wet TOC analyzer coupled to a Thermo Finnigan Deltaplus XP isotope ratio mass spectrometer at the Jan Veizer lab from Ottawa University.

Optical measurements to derive $SUVA_{254}$ and S_R indices were made analysing DOM samples with an Aqualog (Horiba Scientific) at Lund University. $SUVA_{254}$ was determined by normalizing the absorbance at 254 nm to the DOC concentrations, and then adjusted for iron concentrations (mg L^{-1}), providing an indicator of aromaticity in DOM (Weishaar et al., 2003). Dissolved iron concentrations were analysed with Agilent 7700x ICP-MS at the Division of Soil and Water Management of KU Leuven. Spectral slope ratio (S_R), the ratio of spectral slopes in the 275 nm to 295 nm and 350 nm to 400 nm ranges, was used as a proxy for DOM molecular weight and photodegradation (Helms et al., 2008).

Water samples for DIC analysis were filtered (Whatman 0.7 µm) into 12 mL borosilicate Exetainer® vials (Labco, UK) pre-treated with 100 µL of saturated KI solution and vacuum-sealed. The vials were filled to minimize headspace and stored at 5°C until analysis. The $\delta^{13}C$ of DIC was analyzed using a Finnigan GasBench II interfaced with a Thermo Finnigan Delta+ IRMS at the Vrije Universiteit Amsterdam. Samples were acidified with phosphoric acid, releasing CO_2 gas, which was analyzed relative to the Vienna Pee Dee Belemnite (V-PDB) scale. Calibration used carbonate standards BCT (2.07 ‰) and LSVEC (–46.6 ‰) against V-PDB. Duplicate analyses showed a standard deviation of <0.15 ‰. DIC concentrations were determined using sodium bicarbonate standards interspersed throughout each run.

Headspace concentrations of CO_2 and CH_4 were measured at the University of Liège using an SRI 8610C gas chromatograph (GC) equipped with a flame ionization detector and methanizer. The instrument was calibrated with certified CO_2:CH_4 gas mixtures (Air Liquide Belgium) containing 400, 1000, and 4000 ppm CO_2 and 1, 10, and 30 ppm CH_4.

The $\delta^{2}H$ and $\delta^{18}O$ of water samples were analyzed using a Thermo Finnigan Delta+ IRMS equipped with a GasBench II at the Vrije Universiteit Amsterdam Earth Sciences

Stable Isotope Laboratory. Samples were equilibrated with CO_2 in helium for 24 h prior to analysis. Calibration was performed using in-house water standards (DNS3 and KEILA) traceable to VSMOW and SLAP, while accuracy and precision were monitored using the KONA control standard. The average measured values for KONA were –0.14 ‰ for $\delta^{18}\mathrm{O}$ (SD = 0.14 ‰) and –1.13 ‰ for $\delta^{2}\mathrm{H}$ (SD = 0.81 ‰).

Hydrological and statistical analyses

The stream velocity was measured using a Gurley Pygmy current meter (625AF2N, analog wading rod suspended pygmy-type current meter; Gurley Precision Instruments, Troy, N.Y). Based on the shallow and narrow stream sections that were measured, where there were no large obstacles or significant channel irregularities, stream cross-sectional uniformity was assumed. Hence, water velocity measurements were taken at around 0.6 of the depth at the midpoint of the measured stream transect. At every 10 cm interval (w) of the transect the water depth (d) was measured. To calculate the cross-sectional area (A) of the stream, the transect was treated as a series of trapezoids between each pair of depth measurements:

$$A_{\mathrm{total}} = \sum_{i=1}^{n-1} \left(\frac{d_i + d_{i+1}}{2} \right) \times w$$

To check the repeatability and accuracy of stream velocity measurements, duplicate readings were taken at the same site on the same date. In total, four duplicate measurements were recorded. The values were averaged to obtain a single representative velocity value for analysis. The average percentage difference between duplicates ranged from 2 % to 15 %, primarily due to the manual nature of the flow velocity measurements, which involved listening through headphones and counting. While a more automated meter would reduce this variability, the current method provides reliable discharge estimates for their intended use in this study. All averaged values were used in the subsequent statistical analyses.

Volumetric water content sensors (Campbell Scientific CS 655) were installed parallel to the soil surface to measure infiltration in both the headwater peatland and the sandy coastal heathland at depths of 15 cm and 35 cm.

To examine the impact of precipitation and the influence of soil pore water on surface water along the catchment longitudinal gradient we calculate deuterium excess. The deuterium excess was calculated following Dansgaard, 1964 and Clark and Fritz, 2013:

$$D\text{-excess} = \delta^{2}\mathrm{H} - 8 \times \delta^{18}\mathrm{O}$$

To determine the distances of each sampling site from the catchment inlet at L1 a distance matrix of linear type (N*k x 3) in QGIS was derived from the coordinates of the sampling sites. The sampling site L1 is set to have distance 0 since it is the inlet of the catchment.

To examine spatial patterns in log-transformed DOC and DIC concentrations, Moran's

I statistic was calculated both for the entire dataset and for the two studied sites (headwater peatland and coastal sandy heathland) separately. Moran's I is a measure of spatial autocorrelation, indicating whether similar values cluster spatially. The significance of Moran's I statistic was tested using permutation methods, with the results indicating whether observed patterns could be attributed to spatial processes. A Local Indicators of Spatial Association (LISA) analysis was also performed to visualize spatial clusters and outliers. The LISA analysis was conducted using the PySAL library in Python (Rey and Anselin, 2009), and the results were visualized using cluster maps to identify areas of high and low concentrations relative to their neighbors. To improve normality and reduce the influence of extreme values, DOC and DIC concentrations were log-transformed prior to spatial analysis. Log transformation is commonly applied in environmental data analysis to correct for skewed distributions, stabilize variance, and meet statistical assumptions required for parametric tests. Model assumptions were verified by testing for spatial stationarity using Moran's I on the residuals, normality with an Omnibus test, and heteroscedasticity using Breusch-Pagan and White tests.

To assess differences in measured parameters between surface water and soil pore water at the same site, we applied the Mann-Whitney U test, which evaluates whether one group tends to have higher or lower values than the other. Although samples were collected from the same general site, they were not paired or taken simultaneously due to fieldwork constraints, and thus were treated as independent groups for the purposes of this analysis. We acknowledge the potential for pseudo-replication and interpret results with caution. To investigate the correlations between d-excess, DOC concentrations, DIC concentrations, $\delta^{13}\mathrm{C}$-DOC, $\delta^{13}\mathrm{C}$-DIC, $SUVA_{254}$ and S_R with sampling depth and distance from the stream, we applied Spearman rank correlation analysis with a significance level set at 0.05. As multiple depth samples were collected at individual sampling points along transects, we acknowledge that some degree of spatial dependence may exist within the data. Therefore, these correlations are interpreted as indicative trends rather than strictly independent statistical relationships. This analysis was conducted specifically for periaquatic samples collected at sites S2 and S4. All analyses were performed in Python version 3.11.6, utilizing the SciPy library (Virtanen et al., 2020). The nonparametric LOWESS model (locally weighted linear regression) shown in the scatterplots with the significant results from Spearman rank correlations were performed using functions in the library statsmodel (Seabold et al., 2010).

Results

Surface water concentrations along the catchment

DIC exhibited the highest concentrations across all sampled surface waters, with a mean concentration of 52.93 ± 10.31 mg C L^{-1} ($n = 48$) and an overall increase in concentration downstream, from 31.56 mg C L^{-1} at L1 ($n = 1$) to 53.53 mg C L^{-1} at S8 ($n = 5$). DOC concentrations were lower with a mean of 8.52 ± 2.17 mg C L^{-1} (mean ± SD, $n = 46$), and the $\delta^{13}\mathrm{C}$ values of DOC averaged –28.2 ± 1.1 ‰ ($n = 46$). An exception was measured at site S2, a stream sampling site in the headwater peatlands, on 13 August 2022

where δ^{13}C-DOC was less depleted (–21.7 ‰) (Figure 4.2). Indicators of DOM composition also varied spatially, with $SUVA_{254}$ (a proxy for aromaticity in the DOM pool) higher and S_R (spectral slope ratio, indicative of molecular weight) lower in the headwater peatland compared to surface waters in the coastal sandy heathland (Figure 4.3). The DOC:DIC ratio decreased in samples collected sequentially downstream, with the highest ratio recorded at the stream's origin (L1) (Figure 4.3), reflecting a general trend of increasing DIC concentrations as water flows downstream (Figure 4.2). The δ^{13}C-DIC values became progressively more depleted downstream, starting at –2.3 ‰ at the catchment origin (L1), averaging –4.7 ± 1.1 ‰ in the headwater peatland, and reaching –8.6 ± 1.2 ‰ in the coastal sandy heathland (Figure 4.2).

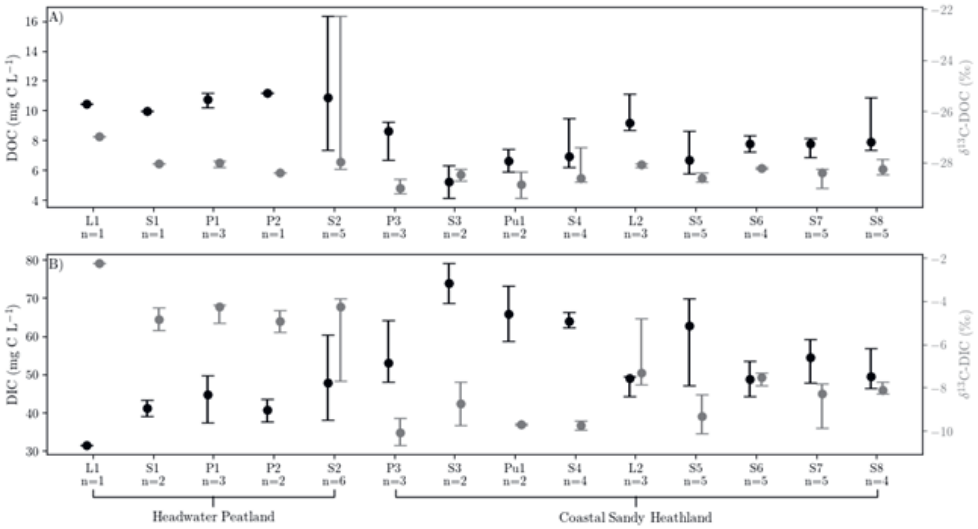

Figure 4.2: Each panel presents median values with whiskers indicating the 95 % confidence intervals of surface water measurements during August and September 2022. Panel A shows median DOC and δ^{13}C-DOC values and Panel B shows median DIC and δ^{13}C-DIC values at each surface water sampling site. Data are ordered from L1 to S8, representing increasing distance downstream from the catchment origin at L1 (distance = 0) to S8, located just before the outflow to Hudson Bay. The n values on the axes indicate the number of samples.

Median dissolved CO_2 concentrations were 2311.6 ppm (IQR: 1596.7 – 2694.5 ppm, $n = 7$), while dissolved CH_4 concentrations had a median of 768.6 nmol L^{-1} (IQR: 327.4 nmol L^{-1} to 1085.5 nmol L^{-1}, $n = 10$). POC concentrations showed a median of 3.08 mg C L^{-1} (IQR: 2.37 mg C L^{-1} to 5.21 mg C L^{-1}, $n = 41$). DOC accounted for a higher proportion of organic carbon compared to POC, with an average DOC/POC ratio of 2. The pH of surface waters was on average 7.8 ± 0.4 and specific conductivity measured 2060 ± 1067 µS cm^{-1}.

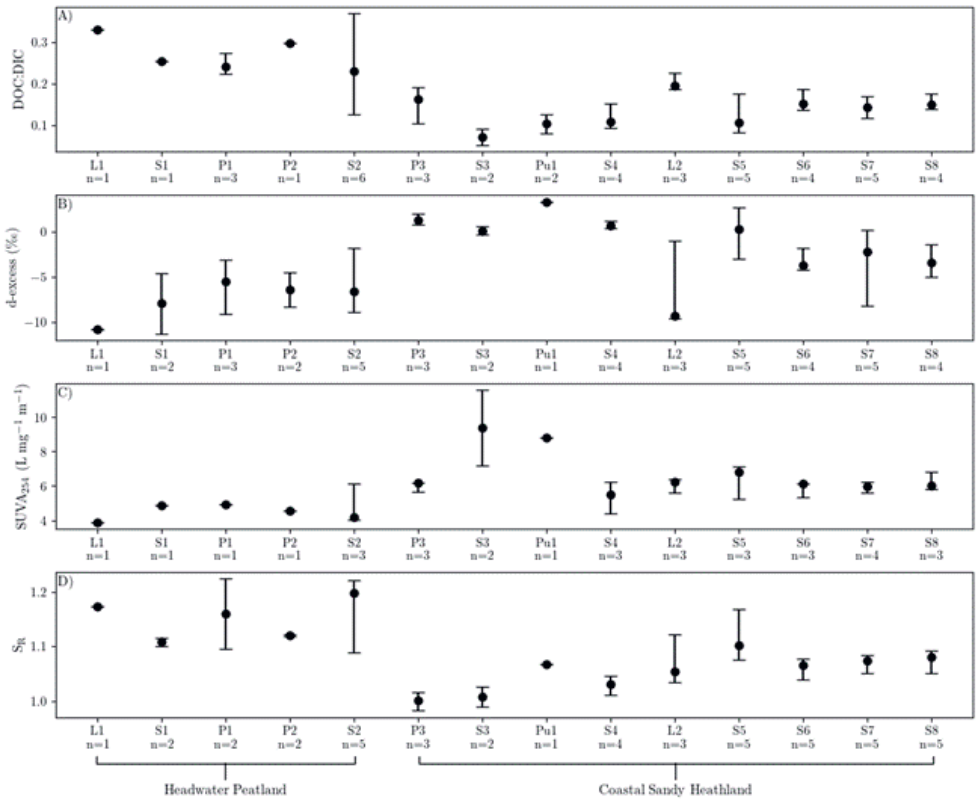

Figure 4.3: Each panel presents median values with whiskers indicating the 95 % confidence intervals of surface water measurements during August and September 2022. Panel A shows median DOC:DIC ratios, panel B shows median d-excess values (an indicator of evaporation), panel C shows median $SUVA_{254}$ values (a proxy for DOM aromaticity), and panel D shows median S_R values (a proxy for DOM molecular weight) at each surface water sampling site. Data are ordered from L1 to S8, representing increasing distance downstream from the catchment origin at L1 (distance = 0) to S8, located just before the outflow to Hudson Bay. The n values on the axes indicate the number of samples.

The results of the Moran's I analysis indicate significant spatial patterns in carbon concentrations across the studied catchment. For log-transformed DOC concentrations, the overall Moran's I value of 0.392 (p = 0.001) suggests significant positive spatial autocorrelation, meaning sites with similar DOC concentrations are more likely to be located near each other than expected under a random distribution. Interestingly, clusters included sites from both catchment areas (headwater peatland and coastal sandy heathland), indicating that similar DOC concentrations are observed at non-adjacent sites as well. However, when examined within individual catchment areas, there was no significant spatial autocorrelation for DOC concentrations (coastal sandy heathland: Moran's I = 0.020, p = 0.093; headwater peatland: Moran's I = -0.087, p = 0.358).

For log-transformed DIC concentrations, the Moran's I analysis yielded an overall value of 0.249 (p = 0.001), also indicating significant positive spatial autocorrelation. Unlike DOC concentrations, DIC clusters were confined within individual catchment areas. In the coastal sandy heathland, Moran's I was positive and significant (Moran's I = 0.139, p = 0.002), suggesting moderate spatial autocorrelation. Conversely, in the headwater peatland, Moran's I was slightly negative and not significant (Moran's I = -0.053, p = 0.278), indicating no meaningful spatial autocorrelation. This suggests that while DIC concentrations in the coastal sandy heathland display moderate spatial clustering, DIC concentrations in the headwater peatland are more randomly distributed, with no clear spatial patterns emerging.

Subsurface waters

The mean $\delta^{13}C$ value of DOC in soil pore waters was –28.0 ± 0.6 ‰ ($n = 94$), while that of DIC was –10.4 ± 2.4 ‰ ($n = 105$). Both DOC and DIC in soil pore waters were more isotopically depleted compared to surface waters, except in the headwater peatland ponds (HP P), where surface water $\delta^{13}C$-DOC values fell within the range of soil pore water $\delta^{13}C$-DOC values (Figure 4.4). Statistically significant depletion of $\delta^{13}C$-DIC in soil pore waters was observed at HP P (U = 127.0, p < 0.001, n = 27 pore vs. 5 surface samples), P3 (U = 42.0, p < 0.01, n = 14 pore vs. 3 surface), S2 (U = 44.0, p < 0.01, n = pore vs. 4 surface), and S3–4 (U = 6.0, p < 0.001, n = 13 pore vs. 5 surface) in comparison to surface waters prior to the rainfall event (Figure 4.5). Median dissolved gas concentrations in soil pore waters were 14 300ppm for CO_2 (IQR: 11 790 to 22 535ppm , $n = 22$) and 2420 nmol L^{-1} for CH_4 (IQR: 171 nmol L^{-1} to 5832 nmol L^{-1}, $n = 22$).

Subsurface DOC concentrations were generally higher, averaging 15.10 ± 6.60 mg C L^{-1} ($n = 94$), than those in surface waters (Figure 4.4). These differences were statistically significant at pond P3 (U = 0.0, p < 0.01, n = 14 pore vs. 3 surface samples), stream sites S3–4 prior to the rainfall event (U = 2.0, p < 0.01, n = 12 pore vs. 5 surface), and lake site L2 (U = 0.0, p < 0.01, n = 9 pore vs. 3 surface). An exception was observed at stream site S2 before the rainfall event, where DOC concentrations in soil pore waters were lower than those in surface waters (Figure 4.4). Similarly, soil pore water DIC concentrations were higher in most subsurface waters, averaging 63.65 ± 18.14 mg C L^{-1} ($n = 105$), compared to surface waters. This was statistically significant at sites S2 (U = 0.0, p < 0.01, n = 11 pore vs. 4 surface samples) and L2 (U = 0.0, p < 0.01, n = 9 pore vs. 3 surface), but not at S3–4, where soil pore water DIC concentrations (59.13 ± 9.79 mg C L^{-1}, $n = 26$) were similar to surface water DIC concentrations (67.00 ± 6.72 mg C L^{-1}, $n = 8$). At the stream site S2 in the headwater peatland, $SUVA_{254}$ values in soil pore waters (6.41 ± 2.95 L mg^{-1} m^{-1}, $n = 8$) were statistically significantly higher than in surface waters (4.09 ± 0.10 L mg^{-1} m^{-1}, $n = 2$) (U = 0.0, p < 0.05, n = 8 pore vs. 2 surface samples) and S_R values were statistically significantly lower in soil pore waters (1.14 ± 0.29, $n = 11$) in comparison to surface waters (1.20 ± 0.02, $n = 4$) (U = 40.0, p < 0.05, n = 11 pore vs. 4 surface samples). Lower S_R values indicate the presence of higher molecular weight (HMW) DOM, while higher S_R values suggest lower molecular weight (LMW) DOM. S_R values were statistically significantly lower in soil pore waters (1.14 ± 0.37, $n = 12$) at the stream site S3–4 in the coastal sandy heathland in

comparison to the surface water (1.04 ± 0.02, $n = 5$) (U = 50.0, p < 0.05, n = 12 pore vs. 5 surface samples).

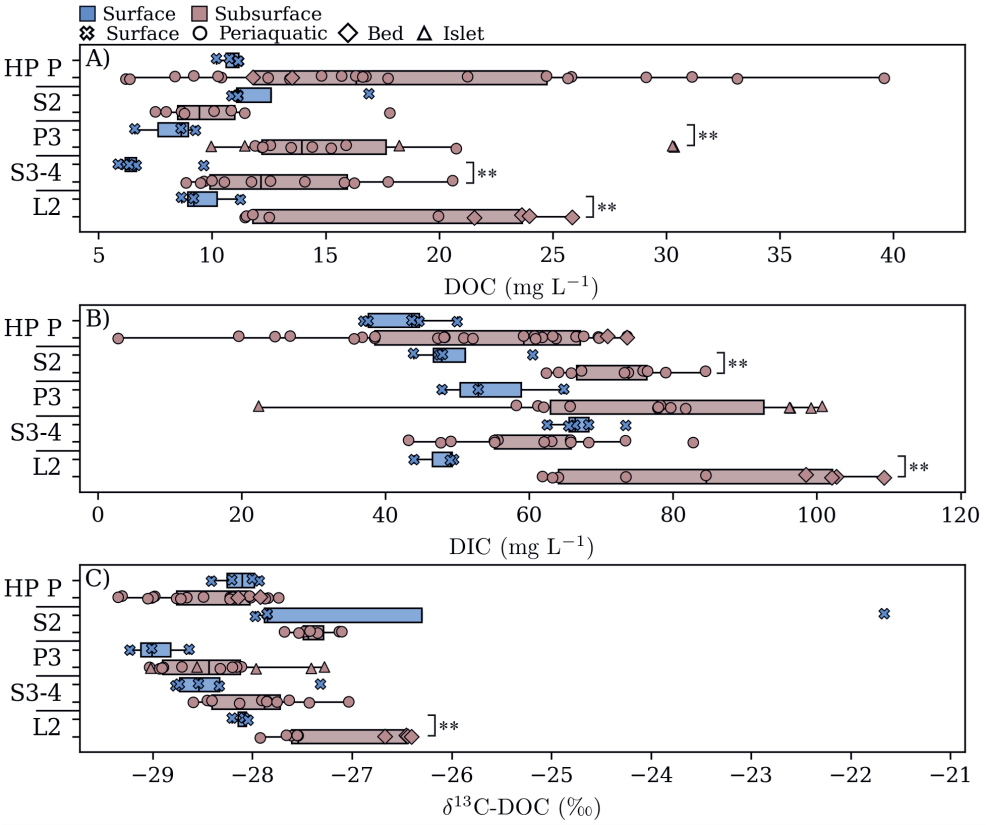

Figure 4.4: Boxplots showing soil pore water and surface water characteristics at the study site during late summer 2022. Data are presented for DOC (Panel A), DIC (Panel B), and δ^{13}C-DOC (Panel C). Sampling locations across the catchment are represented from upstream to downstream, with HP P denoting data from ponds P1 and P2 and their surrounding areas. Surface water data from sites S3, Pu1, and S4 are combined as S3–4 due to proximity. Soil pore water was sampled at S2 and S3–4 locations in 5 m increments perpendicular to the stream. The data from S2 and S3–4 are from before the rainfall event. Different hydrological environments, including surface, periaquatic, hyporheic zone and islet are marked distinctly. In the boxplots, the line represents the median, and whiskers denote the interquartile range. Statistically significant differences were determined using the Mann-Whitney U test (* $\leq$ 0.05, ** $\leq$ 0.01, *** $\leq$ 0.001).

At lake L2 in the coastal sandy heathland, soil pore water DOC concentrations showed a wide range (11.46 mg C L^{-1} to 25.87 mg C L^{-1}, $n = 9$), reflecting differences between samples from the lake sediments and the periaquatic zone. Lake sediment samples (23.76 ± 1.77 mg C L^{-1}, $n = 4$) represented the higher end of soil pore water DOC concentrations, while lake bank samples (13.45 ± 3.67 mg C L^{-1}, $n = 5$) fell at the lower

end (Figure 4.4). Similarly, soil pore water DIC concentrations at L2 were approximately 30 mg C L^{-1} higher in lake sediment samples compared to the lake bank (Figure 4.4). At pond P3 in the coastal sandy heathland, soil pore water DIC concentrations from the pond islet were about 20 mg C L^{-1} higher than the average periaquatic samples (Figure 4.4). $\delta^{13}C$-DOC values at P3 were more depleted in the periaquatic zone (maximum of –28.1 ‰) compared to the islet (maximum of –27.3 ‰) (Figure 4.4). Enrichment of $\delta^{13}C$-DOC and $\delta^{13}C$-DIC was also observed in lake sediment pore waters (–26.7 ‰ to –26.4 ‰, $n = 4$; –5.5 ‰ to –3.4 ‰, $n = 4$, respectively) compared to the lake bank (–27.9 ‰ to –27.5 ‰, $n = 5$; –13.1 ‰ to –9.0 ‰, $n = 5$) (Figure 4.4; Figure 4.5). Statistically significant $\delta^{13}C$-DOC enrichment in soil pore waters compared to surface waters was observed only at lake L2 (U = 0.0, p < 0.01, $n = 9$ pore vs. 3 surface samples) (Figure 4.4). In addition, $SUVA_{254}$ values in L2 soil pore waters (4.58 ± 0.46 L mg^{-1} m^{-1}, $n = 9$) were statistically significantly lower than in surface waters (6.06 ± 0.44 L mg^{-1} m^{-1}, $n = 3$) (U = 27.0, p < 0.01, $n = 9$ pore vs. 3 surface samples) and S_R values were statistically significantly higher in soil pore waters (1.54 ± 0.57, $n = 9$) in comparison to surface waters (1.07 ± 0.05, $n = 3$) (U = 0.0, p < 0.01, $n = 9$ pore vs. 3 surface samples).

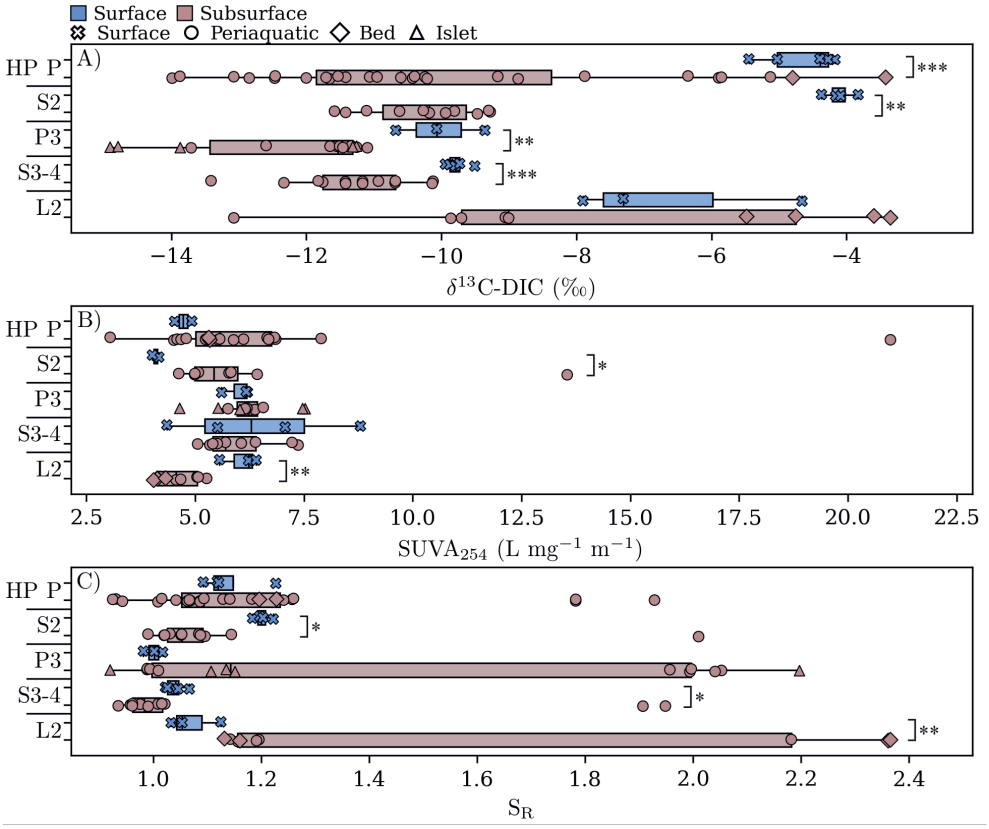

Figure 4.5: Boxplots depicting soil pore water and surface water characteristics sampled in Churchill, Manitoba, during late summer 2022. Data are shown for δ^{13}C-DIC (Panel A), $SUVA_{254}$ (Panel B) and S_R (Panel C). Sampling locations across the catchment are represented from upstream to downstream, with HP P denoting data from ponds P1 and P2 and their surrounding areas. Surface water data from sites S3, Pu1, and S4 are combined as S3–4 due to proximity. Soil pore water was sampled at S2 and S3–4 locations in 5 m increments perpendicular to the stream. The data from S2 and S3–4 are from before the rainfall event. Different hydrological environments, including surface, periaquatic, hyporheic zone and islet are marked distinctly. In the boxplots, the line represents the median, and whiskers denote the interquartile range. Statistically significant differences were determined using the Mann-Whitney U test (* $\leq$ 0.05, ** $\leq$ 0.01, *** $\leq$ 0.001). A δ^{13}C-DOC measurement from a sample collected on 13 August 2022 at site S2 was excluded to maintain clarity in the plot, as it was significantly less depleted than the other samples (–21.7‰).

We found no statistically significant correlations between most of the variables (DOC, DIC, δ^{13}C-DOC, δ^{13}C-DIC, d-excess, DOC:DIC and $SUVA_{254}$) and the distance from the stream at which periaquatic soil pore water samples were collected at site S3–4. The spectral slope (S_R) was the only variable statistically significant correlated with the distance from the stream at site S2. The correlation of S_R was negative with increasing distance from the stream at site S2 before the rainfall ($\rho = -0.62$, p $\leq$ 0.05) and this

negative correlation became even stronger following the rainfall ($\rho = -0.92$, p $\leq$ 0.001).

However, Spearman rank correlations between these variables and the depth of the periaquatic soil pore water samples revealed three significant relationships (detailed results of all correlations are reported in Table S1). Specifically, δ^{13}C-DIC exhibited a positive correlation with depth at S2 before the rainfall event and at site S3–4, with δ^{13}C-DIC values becoming more enriched at greater depths in both cases (Figure 4.6). In contrast, a significant negative correlation was observed between d-excess and depth at site S3–4, indicating that d-excess values were more depleted at deeper depths (Figure 4.6).

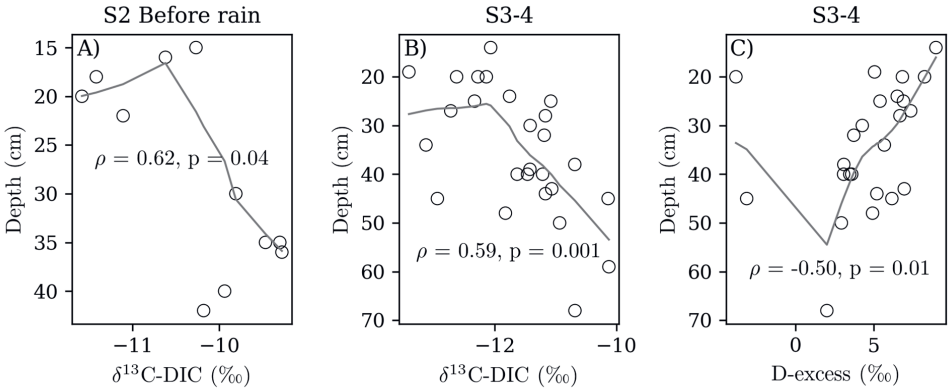

Figure 4.6: Significant Spearman rank correlations between variables (DOC, DIC, δ^{13}C-DOC, δ^{13}C-DIC, d-excess, and DOC:DIC) and soil pore water sampling depth during late summer 2022. At site S2, periaquatic soil pore water data are divided into 'Before Rain' and 'After Rain' subcategories, as Mann-Whitney U tests revealed statistically significant differences for some variables between these periods. In contrast, no significant differences were found at site S3–4, so data from this site are analyzed together. Only significant correlations are plotted; for full test results, refer to Table S1. The grey line represents the estimate from a nonparametric LOWESS model (locally weighted linear regression), with the Spearman rank correlation coefficient (ρ) and p-value provided for each relationship. Panel A shows δ^{13}C-DIC and depth at site S2 before rainfall, Panel B shows δ^{13}C-DIC and depth at site S3–4, and Panel C shows d-excess and depth at site S3–4.

Effects of rainfall event

The hydrograph of the rainfall event was captured using surface water level sensors deployed at stream locations S2 and S4, illustrating that the sampling campaign covered the rising limb of the hydrograph (Figure 4.7). During this period, the rainfall event caused the stream to gain DOC and lose DIC (Figure 4.8). S_R did not exhibit a trend with $\log(Q)$ across most sites, while $SUVA_{254}$ increased with increasing discharge (Figure 4.8). Site S3 was located very close (<0.5 m) to S4, so discharge measurements were only conducted at S4. At site S5, the water velocity was consistently below 0.02 m s^{-1}, which is the lower detection limit of the measuring device (Gurley Pygmy meter, see Methods),

preventing velocity measurements used to calculate discharge at this sampling location.

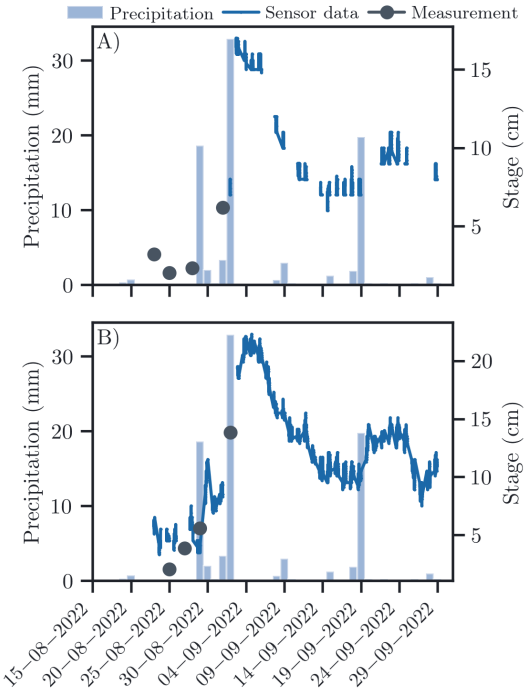

Figure 4.7: Precipitation data (mm) alongside water level measurements. Manual stage measurements ('Measurements' in grey, water depth in cm) were taken at S4 in the coastal sandy heathland (A) and S2 in the headwater peatland (B). Sensor data, recorded using ultrasonic distance meters (accuracy: 5 mm) designed by the Electronics Department of the Faculty of Science at the Vrije Universiteit Amsterdam, captured two measurements per minute and are provided to give context to the manual stage measurements and to illustrate stream level responses to precipitation events.

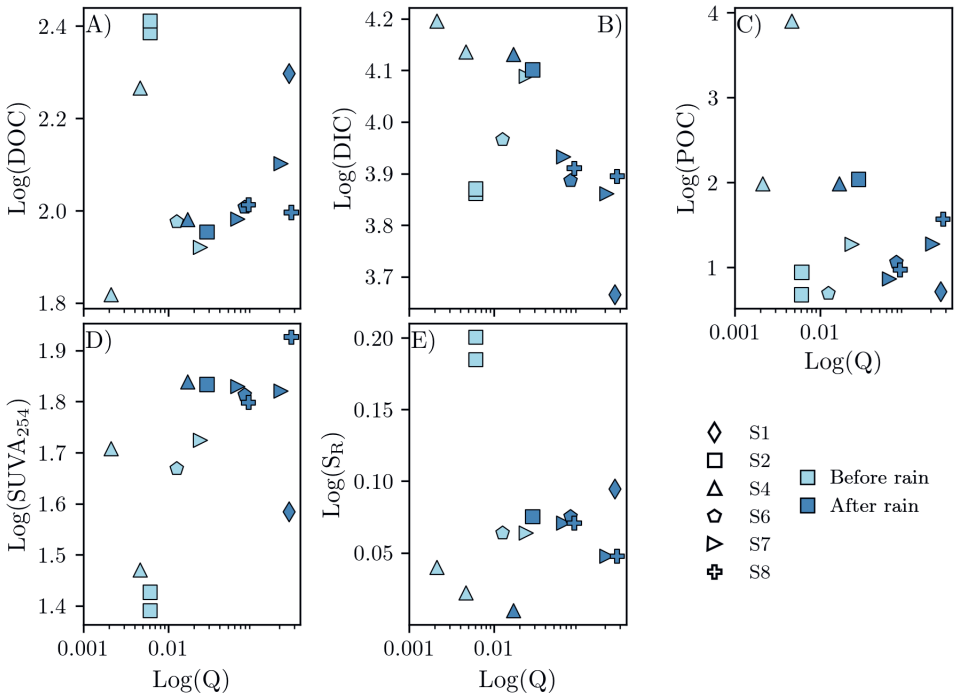

Figure 4.8: Log-log plots illustrating the relationship between discharge and DOC (Panel A), DIC (Panel B), POC (Panel C), $SUVA_{254}$ (Panel D), and S_R (Panel E). Each panel demonstrates how these variables scale with changes in streamflow due to the rainfall event in late summer 2022 at the study site.

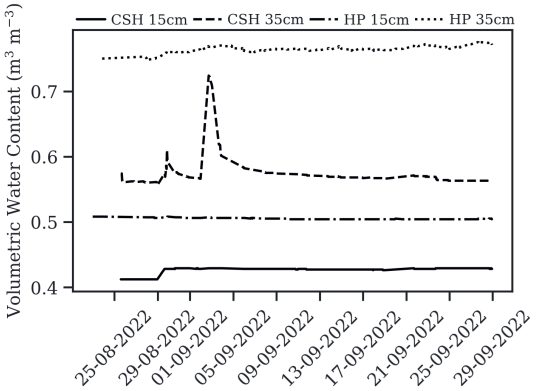

Figure 4.9: Temporal variation in volumetric water content (VWC) at different depths (15 cm and 35 cm) at two locations, headwater peatland (HP) and coastal sandy heathland (CSH), from 25 August to 29 September 2022. Measurements were made with soil moisture sensors inserted parallel to the ground surface.

Figure 4.9 illustrates the temporal changes in VWC observed in the coastal sandy heathland (CSH) and headwater peatland (HP) at depths of 15 cm and 35 cm from 25 August to 29 September 2022. Rainfall began on 28 August 2022, leading to a small increase in VWC in the coastal sandy heathland at 15 cm depth, where levels rose from approximately 0.40 $m^3\,m^{-3}$ to around 0.44 $m^3\,m^{-3}$ before stabilizing. At 35 cm depth, the response was more significant and delayed, with a sharp peak observed around 02 September 2022, following additional rainfall. The subsequent decline, suggests infiltration and redistribution of water within the soil profile. In contrast, VWC in the headwater peatland remained relatively stable at 15 cm depth, hovering around 0.50 $m^3\,m^{-3}$ throughout the observation period, with minimal response to the rainfall events. At 35 cm depth, VWC remained consistently high, exceeding 0.75 $m^3\,m^{-3}$, with only minor variations detected.

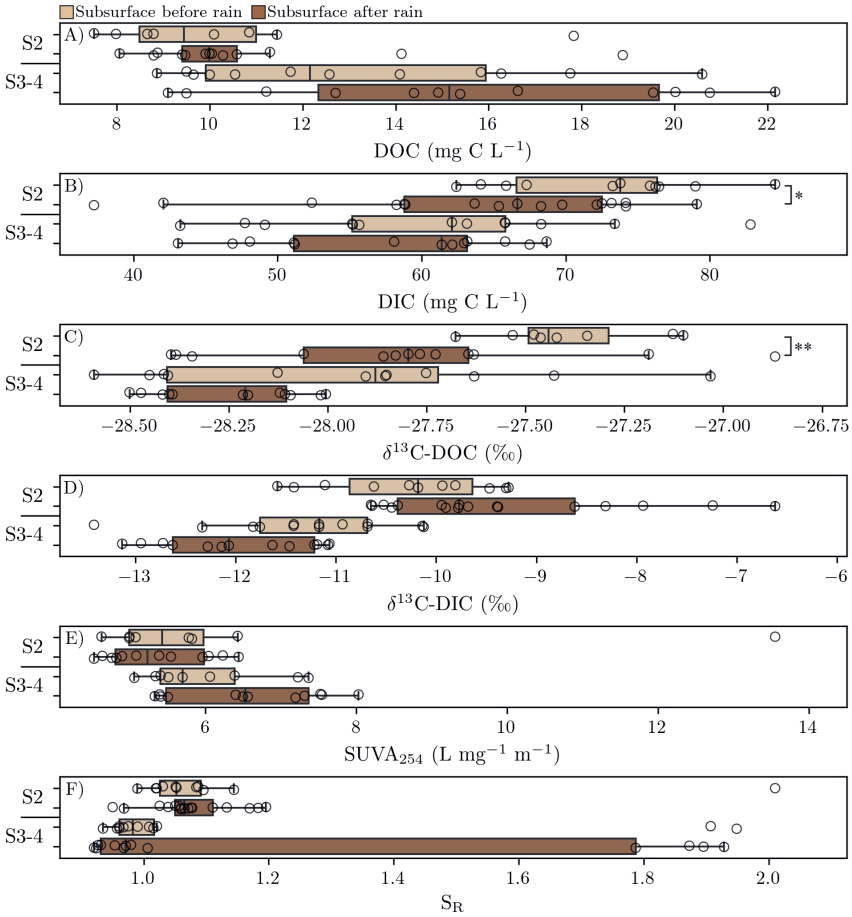

Figure 4.10: Boxplots showing soil pore water characteristics before and after a rainfall event, which started on the evening of 28 August 2022. Data are presented for DOC (Panel A), DIC (Panel B), δ^{13}C-DOC (Panel C), δ^{13}C-DIC (Panel D), $SUVA_{254}$ (Panel E) and S_R (Panel F). Surface water data from sites S3, Pu1, and S4 are combined as S3–4 due to proximity. Soil pore water was sampled at S2 and S3–4 locations in 5 m increments perpendicular to the stream. In the boxplots, the line represents the median, and whiskers denote the interquartile range. Statistically significant differences were determined using the Mann-Whitney U test (* ≤ 0.05, ** ≤ 0.01).

At site S2 soil pore water DOC concentrations were on average similar before the rainfall event (10.39 ± 3.31 mg C L^{-1}, $n = 8$) and after it (10.74 ± 2.86 mg C L^{-1}, $n = 13$). In contrast at site S3–4 soil pore water DOC concentrations had a slightly lower average before the rainfall event (13.12 ± 3.78 mg C L^{-1}, $n = 12$) in comparison to after the event (15.53 ± 4.42 mg C L^{-1}, $n = 12$). Overall, after the rainfall event DOC concentrations increased in soil pore waters at the sites S2 and S3–4, and DIC concentrations decreased, and δ^{13}C-DOC decreases (Figure 4.10). In contrast, δ^{13}C-DIC decreased after the rain-

fall event at S2 but increased at S3–4 (Figure 4.10). The composition of DOM did not appear to change as $SUVA_{254}$ and S_R remain more or less the same (Figure 4.10). The only statistically significant differences observed in soil pore waters before and after the rainfall event were for DIC concentrations (U = 139.0, p < 0.01, $n = 11$ before vs. 17 after) and $\delta^{13}C$-DOC (U = 88.0, p < 0.001, $n = 8$ before vs. 13 after) (Figure 4.10).

Discussion

Downstream carbon export and isotopic trends in surface waters

DOC concentrations remained within a relatively narrow range along the longitudinal gradient from the headwater lake to Hudson Bay. In contrast, DIC concentrations increased downstream, accompanied by declining DOC:DIC ratios and increasingly depleted $\delta^{13}C$-DIC values. Together, these patterns suggest that carbon was actively processed and redistributed during downstream transport, despite the relative stability of bulk DOC concentrations.

DOC concentrations remained within a relatively narrow range along the longitudinal gradient of the catchment. However, DOC concentrations were not spatially random: the significant positive Moran's I value (0.392, p=0.001) and LISA analysis indicate that sites with similar DOC concentrations tended to occur closer together than expected by chance. This spatial organization is consistent with previous studies demonstrating strong landscape controls on DOC transport and distribution in Arctic catchments (Shogren et al., 2020b). In contrast, no significant spatial autocorrelation was detected within either the headwater peatland or coastal sandy heathland individually, suggesting that the overall spatial structure primarily reflects differences between the major landscape units rather than localized variation or a simple longitudinal gradient.

The relatively narrow range in DOC concentrations, despite this spatial structuring, suggests that differences in DOC inputs and processing may have been broadly balanced across the catchment. Hydrological connectivity can redistribute DOC among soils, riparian areas, ponds, lakes, and streams, while microbial and photochemical processing can remove DOC from the dissolved pool and alter its composition (Lynch et al., 2019; Cory and Kling, 2018; Cory et al., 2014). Physical processes such as aggregation and flocculation, followed by particulate settling, may also contribute to the transfer of organic matter from the dissolved to particulate phase (He et al., 2016). Together, these processes occur alongside continued DOC inputs from terrestrial and aquatic sources, such that the relatively stable bulk DOC concentrations likely reflect the net result of ongoing inputs and losses across the connected surface-water network.

We found that DIC concentrations increased downstream (Figure 4.2). In contrast to DOC, the LISA cluster analysis indicated that DIC exhibited stronger spatial autocorrelation within specific sections of the catchment, suggesting that localized hydrological and biogeochemical processes influenced its spatial distribution. Consistent with the downstream increase in DIC concentrations, DOC:DIC ratios declined along the flow path and were lowest in the coastal sandy heathland (Figure 4.3). Throughout the catchment, DIC

concentrations exceeded those of DOC, resulting in DOC:DIC ratios consistently below one. Similar patterns have been reported in northern catchments and have been associated with summer baseflow conditions (Giesler et al., 2014).

A possible explanation for the increasing DIC concentrations downstream is that as water moves downstream, microbial and photochemical degradation of DOC contribute to the DIC pool (Cory and Kling, 2018; Cory et al., 2014). Although we did not directly measure DOC mineralization, the relatively narrow range of bulk DOC concentrations does not preclude continued processing of individual components of the DOC pool, as losses of more labile DOC can occur alongside continued inputs of new DOC (Lapierre and del Giorgio, 2014). The downstream depletion in $\delta^{13}\mathrm{C}$-DIC, together with decreases in S_R and slight increases in $SUVA_{254}$ (Figure 4.2; Figure 4.3), indicates that the composition of the carbon pools changed along the flow path. The increasingly depleted $\delta^{13}\mathrm{C}$-DIC values are consistent with an increasing contribution of isotopically depleted carbon to the DIC pool, which may partly reflect the incorporation of carbon derived from organic matter degradation (Bade et al., 2004). Similarly, the decrease in S_R and increase in $SUVA_{254}$ are consistent with changes in DOM composition during downstream transport, including preferential transformation or removal of lower molecular weight, less aromatic compounds (Cory and Kling, 2018). However, these optical trends may also reflect changing DOM sources and hydrological conditions, as flow pathways and residence time can influence both the composition and processing of DOM (Coch et al., 2019a). Taken together, these observations suggest that processing of the DOC pool likely contributed to the downstream increase in DIC, while the magnitude of the increase also indicates that additional DIC inputs, including inputs from soils, likely contributed to the downstream DIC pool.

DOC concentrations were generally higher in ponds and lakes (e.g., L1 and L2) than in stream segments, whereas DIC concentrations were higher in streams than in ponds and lakes (Figure 4.2). Similar patterns have been reported in Arctic catchments in Alaska and on Herschel Island (Coch et al., 2019b; Kling et al., 2000). The contrasting DOC and DIC patterns between lentic and stream waters suggest that freshwater ecosystem type influences the processing and transport of dissolved carbon. Differences in water residence time, hydrological connectivity, and in-stream biogeochemical processing may contribute to the higher DIC concentrations observed in streams, while lakes and ponds may retain and process a greater proportion of the DOC pool before water continues downstream (Coch et al., 2019b; Cory and Kling, 2018). The influence of lakes on downstream carbon concentrations is also evident in the similarity between L2 and S6, with concentrations at S7 reflecting the convergence of water from S5 and S6 (Figure 4.2).

Comparison of soil pore and surface waters

To evaluate the relationship between freshwater carbon and adjacent soil pore waters, we compared DOC and DIC concentrations, their isotopic signatures, and DOM optical properties across the catchment. Differences between soil pore water and surface water varied among landscape settings, with larger differences in the headwater peatland than in the coastal sandy heathland for several carbon characteristics. These differences suggest that landscape and hydrological conditions influence the relationship between sub-

surface and surface-water carbon (Zolkos et al., 2022). The composition of surface-water carbon may additionally reflect processes occurring within and between terrestrial and aquatic environments, including terrestrial carbon inputs, gas exchange, and in-stream processing (Venkiteswaran et al., 2014).

In the headwater peatland, our results suggest greater differences in DOM characteristics between soil pore water and stream surface water than in the coastal sandy heathland. High and relatively stable VWC at both 15 cm and 35 cm depths indicates slower hydrological flushing (Figure 4.9), which may have provided greater opportunity for DOM processing within the soil profile before carbon was exported to surface waters (Speetjens et al., 2022). This interpretation is supported by significant differences in $SUVA_{254}$ and S_R between soil pore water and surface water at S2 (Figure 4.5), with lower $SUVA_{254}$ and higher S_R in surface water indicating less aromatic, lower molecular weight DOM (Harms et al., 2016). Alternatively, or in addition, soil-derived DOM may have undergone rapid photochemical alteration following export to surface waters, further contributing to the observed differences (Cory et al., 2014). Higher DOC concentrations and lower DIC concentrations in surface water relative to soil pore water may reflect additional processes affecting stream carbon composition, including upstream inputs, vegetation leachates, and evaporation. The influence of evaporation is supported by the mean d-excess value of -8.1 during warm, dry conditions.

In contrast, the coastal sandy heathland exhibited greater similarity between soil pore water and surface water DIC concentrations. Fluctuating VWC at 35 cm, together with consistently low VWC at 15 cm, suggests more rapid hydrological flushing through the sandy soils (Figure 4.9). Similar DIC concentrations in soil pore water and surface water, together with the observed vertical gradients in DIC and d-excess (Figure 4.6), are consistent with greater hydrological connectivity (Harms et al., 2016). The greater permeability of the sandy heathland soils may therefore facilitate more efficient transport of dissolved carbon through the soil profile, potentially reducing opportunities for in-soil processing and contributing to the observed similarity in DIC concentrations between the two water types.

Comparisons between soil pore waters and surface waters revealed differences in dissolved gas and DIC concentrations, as well as in DIC isotopic composition. Median dissolved CO_2 and CH_4 concentrations in surface waters were approximately an order of magnitude lower than in soil pore waters, while DIC concentrations were also generally lower in surface waters, with the exception of site S3–4 (Figure 4.4). The substantially lower dissolved gas concentrations in surface waters are consistent with gas evasion, which can occur rapidly when CO_2-rich subsurface waters enter surface waters (Biehler et al., 2023). Differences in DIC concentrations may reflect multiple processes, including gas exchange, dilution, biogeochemical processing, and differences in carbon sources. Outgassing of CO_2 preferentially removes isotopically lighter ^{12}C, enriching the remaining DIC pool in ^{13}C (Doctor et al., 2007; Venkiteswaran et al., 2014). This process is consistent with the observed increase in mean $\delta^{13}C$-DIC values from –10.4 ‰ in subsurface waters to –7.4 ‰ in surface waters (Figure 4.5). However, additional DIC derived from carbonate weathering of carbonate-bearing glacial and marine sediments underlying the catchment may also have contributed to the observed surface-water values.

Together, these observations show that soil pore water and surface water differed substantially in their dissolved carbon characteristics, while the measurements do not allow the processes responsible for these differences to be uniquely identified.

The lake exhibited dissolved carbon characteristics that differed from those observed at the stream sites. At L2, S_R values were higher and $SUVA_{254}$ values lower in sediment pore water than in the overlying lake water, opposite to the pattern observed at S2 and S3–4 (Figure 4.5). These observations suggest that lake sediment pore waters contained less aromatic, lower molecular weight DOM than the overlying lake water. This difference may reflect differences in DOM sources and processing between the sediment pore water and overlying lake water.

Stable carbon isotopes also revealed differences between sediment pore waters beneath lakes and ponds and the surrounding periaquatic soils. At L2, $\delta^{13}\mathrm{C}$-DOC and $\delta^{13}\mathrm{C}$-DIC values indicate that lake sediment pore waters contained isotopically lighter carbon than the surrounding periaquatic soil pore waters. Similarly, at pond P3, the islet soil pore waters exhibited distinct $\delta^{13}\mathrm{C}$-DOC and $\delta^{13}\mathrm{C}$-DIC values compared with the surrounding periaquatic soil pore waters, which were similar to those measured elsewhere in the coastal sandy heathland (Figure 4.5). These observations indicate that sediment pore waters beneath lakes and ponds can exhibit distinct dissolved carbon isotopic signatures compared with adjacent terrestrial soils.

Together, these results show that the relationship between soil pore water and surface-water carbon varied across the catchment. The greater differences in DOM characteristics between soil pore and surface waters in the headwater peatland, together with the relatively stable soil moisture conditions, are consistent with greater modification of carbon within the peatland soil profile. In contrast, the greater similarity in DIC concentrations in the coastal sandy heathland, together with evidence of more variable water movement through the soil, is consistent with more direct hydrological connectivity. Lakes and ponds showed additional differences from the surrounding terrestrial pore waters, indicating that carbon characteristics within these systems cannot be explained solely by their adjacent soils. Overall, our results suggest that landscape setting and hydrological conditions influence the extent to which subsurface carbon characteristics are reflected in surface waters, while the observed differences likely arise from multiple interacting sources and processes rather than a single controlling mechanism.

Precipitation effects on carbon mobilization and transport

Our study aimed to assess the impact of late-summer rainfall events on lateral carbon transport within a coastal catchment of the Hudson Bay Lowlands by examining changes in DOC and DIC concentrations, isotopic composition, and hydrological conditions. Our results suggest that rainfall altered carbon concentrations and composition in surface waters, while DOM composition in soil pore waters remained relatively stable. Differences in the response of carbon pools between the headwater peatland and coastal sandy heathland further suggest that rainfall effects varied with local hydrological conditions and landscape characteristics.

Rainfall and carbon mobilization

Rainfall events did not cause significant changes in DOM composition in soil pore waters, as shown by stable $SUVA_{254}$ and S_R values, while surface-water DOC concentrations increased with discharge (Figure 4.10; Figure 4.8). This suggests that rainfall increased the delivery of DOM to surface waters without substantially altering the bulk DOM composition of soil pore waters. Similar increases in DOC concentrations with discharge have been observed in other low-gradient Arctic catchments (Shogren et al., 2020b, 2024).

Decreases in DIC concentrations in soil pore waters at S2 and S3–4, as well as in surface waters, with increasing discharge indicate that rainfall also altered DIC dynamics. These changes may reflect increased hydrological transport and connectivity, together with dilution and gas exchange during transport to and within surface waters (Campeau et al., 2018). Rapid evasion of dissolved CO_2 and CH_4 can occur when carbon-rich subsurface waters enter streams and may therefore contribute to lower surface-water DIC concentrations (Duvert et al., 2018; Lupon et al., 2019). The concurrent decrease in soil-pore-water DIC suggests that increased hydrological export may have reduced DIC concentrations within the soil profile, although the measurements do not allow the relative contributions of production, transport, and loss processes to be distinguished. Thus, rainfall appears to have altered the transport and fate of DIC more strongly than the bulk composition of soil-derived DOM.

In surface waters, the concurrent increase in DOC concentration and $SUVA_{254}$ with discharge indicates that the additional DOC transported during rainfall was relatively more aromatic than the background surface-water DOM. This may reflect increased contributions from near-surface organic horizons as hydrological pathways became more connected during rainfall. Similar rainfall-driven shifts toward more aromatic, plant-derived DOM have been observed in Arctic catchments, although the direction and magnitude of DOM responses can depend on rainfall intensity and antecedent hydrological conditions (Coch et al., 2019b).

Spatial differences within the catchment

Differences in soil properties and hydrological connectivity are evident in S_R dynamics, with S2 showing a significant negative correlation between S_R and distance from the stream, while no such trend was observed at S3–4. The significant negative correlation of S_R with increasing distance from the stream at site S2 before rainfall ($\rho = -0.62$, $p \leq 0.05$), which strengthened following rainfall ($\rho = -0.92$, $p \leq 0.001$), indicates a greater contribution of lower-molecular-weight DOM closer to the stream. One possible explanation is the combined influence of microbial processing and selective sorption within the soil matrix. Wetter conditions closer to the stream may promote greater microbial processing of DOM, while sorption of relatively hydrophobic and aromatic compounds to the soil matrix may preferentially retain these components and leave a greater proportion of hydrophilic, lower molecular weight DOM in solution (Karavanova, 2013). The lack of a significant S_R-distance correlation in the coastal sandy heathland (S3–4) periaquatic soil pore waters further suggests that differences in soil properties and hydrological connec-

tivity influence the spatial distribution of DOM characteristics.

Contrasting post-rainfall changes in $\delta^{13}C$-DIC at S2 and S3–4 suggest that different hydrological and biogeochemical processes influenced DIC dynamics at the two sites. At both S2 and S3–4, $\delta^{13}C$-DIC values showed a significant trend from more negative to less negative with increasing depth, indicating systematic variation in the sources and processing of DIC along the soil profile. At S2, $\delta^{13}C$-DIC values became less negative following rainfall. In the saturated peat soils, slower infiltration and greater mixing may have altered the relative contribution of DIC from different soil depths. Alternatively, partial loss of isotopically lighter CO_2 through outgassing could have enriched the remaining DIC in ^{13}C, as CO_2 outgassing has been shown to increase $\delta^{13}C$-DIC in headwater systems (Doctor et al., 2007). In contrast, $\delta^{13}C$-DIC became more negative at S3–4, where the sandy, high-porosity soils may have allowed rainfall to rapidly infiltrate and transport isotopically lighter, surface-derived DIC into deeper soil layers. These contrasting responses highlight how differences in soil properties and hydrological connectivity can influence the transport and processing of DIC following rainfall.

Conclusion

This study investigated lateral carbon transport within a small coastal catchment in the Hudson Bay Lowlands during late summer and early fall. Surface water DIC concentrations exceeded those of DOC throughout the catchment and increased downstream, whereas DOC concentrations remained within a relatively narrow range. Differences between soil pore waters and adjacent surface waters varied between the headwater peatland and coastal sandy heathland, with greater differences in several carbon characteristics in the headwater peatland. Late-summer rainfall increased DOC concentrations and aromaticity while reducing DIC concentrations in surface waters, whereas $SUVA_{254}$ and S_R in soil pore waters showed no significant changes. Together, these findings suggest that local landscape characteristics, freshwater ecosystem type, and hydrological conditions influence dissolved carbon transport and composition within this Arctic coastal catchment during the summer.

The within-catchment variability observed in this study raises the question of whether this variability propagates to larger spatial scales or is averaged out when dissolved carbon transport is integrated across catchments and regions. Whether the variability observed here influences larger-scale estimates depends in part on how representative these late-summer observations are of annual dissolved carbon transport, highlighting the need for observations spanning complete hydrological cycles. In addition, the Hudson Bay Lowlands encompass considerable variation in soils, vegetation, permafrost, and hydrology. Understanding how these differences influence the magnitude and timing of dissolved carbon export from individual small coastal catchments from individual small coastal catchments is necessary before their contribution to regional variability can be assessed. Determining how variability among small coastal catchments compares with the variability observed within this study catchment will require studies across multiple catchments. Such work will help establish whether incorporating small coastal catchment landscape heterogeneity into regional upscaling frameworks improves estimates of

dissolved carbon transport across the Hudson Bay Lowland.

Statments and Declarations

Competing interests statement

Competing interests: The authors declare there are no competing interests.

Author contribution statment

M.M.R.: Conceptualization, Data curation, Formal analysis, Funding acquisition, Investigation, Methodology, Project administration, Resources, Validation, Writing – original draft, Writing – review & editing.

G.H.: Investigation, Formal analysis, Writing – review & editing.

J.E.V.: Funding aquisition, Project administration.

J.T.W.: Supervision, Writing – review & editing.

J.F.D.: Supervision, Funding acquisition, Data curation, Writing – review & editing.

Funding Statment

This work was carried out under the program of the Netherlands Earth System Science Centre (NESSC), financially supported by the Ministry of Education, Culture and Science (OCW). JFD received additional support from a UKRI Future Leaders Fellowship MR/V025082/1. MMR received funding from the European Union's Horizon 2020 project INTERACT, under grant agreement No 73093.

Data availability

The dataset supporting the findings of this study has been deposited in Zenodo and is under embargo pending article acceptance. It will be made public upon publication. The dataset DOI is: `https://doi.org/10.5281/zenodo.15396375`.

Chapter 5

Synthesis and Outlook



This thesis focuses on characterizing the interplay between hydrology, terrestrial–aquatic connectivity, and the carbon cycle in freshwater ecosystems in high-latitude tundra lowlands during summer. Through three complementary studies, I investigate how greenhouse gas emissions, carbon composition, and lateral transport interact to shape freshwater carbon across Arctic Lowland Tundra Ecosystems. Specifically, I quantify greenhouse gas emissions from freshwater ecosystems and their role in offsetting the terrestrial carbon sink in the Indigirka Lowlands. I then examine how dissolved greenhouse gas supersaturation relates to DOM and composition. Finally, I assess lateral carbon fluxes and the influence of late-summer rainfall on terrestrial–aquatic connectivity in a coastal catchment in the Hudson Bay Lowlands. Together, these studies show that freshwater carbon fluxes in tundra lowlands emerge from the interaction between hydrological connectivity, carbon composition, and ecosystem-specific processing.

Summer greenhouse gas emissions from freshwaters in the Indigirka Lowlands

The Indigirka Lowlands has a high surface area covered by lakes, ponds, and fluvial systems (Grosse et al., 2013; Muster et al., 2017). We found that in the summer the sampled freshwater ecosystems were supersaturated with CO_2 and CH_4, while N_2O varied between being marginally over- or undersaturated. The data indicate that ponds exhibited the highest CO_2 and CH_4 concentrations, followed by fluvial systems, while lakes showed the lowest concentrations. This pattern aligns with the idea that smaller, more isolated systems experience greater connectivity with organic-rich tundra soils and have higher rates of biological decomposition (Wauthy et al., 2018; Wik et al., 2016; Obernosterer and Benner, 2004; Cory and Kling, 2018). When upscaling derived fluxes and integrating them into the vertical landscape greenhouse gas exchange, we found that N_2O emissions were negligible relative to CO_2 and CH_4 in terms of CO_2 equivalents. Flooding in 2017 provided a unique opportunity to assess the impact of hydrological changes on GHG emissions. Elevated emissions during this period suggest that episodic hydrological events can temporarily override local-scale emission controls, leading to increased CO_2 and CH_4 release. Integrating CO_2-C and diffusive CH_4-C emissions into the total C landscape exchange offset the terrestrial C sink by ~9 to ~13 %. This underscores the importance of accounting for hydrological variability and climate-driven changes in permafrost landscapes when estimating carbon budgets.

Dissolved gas concentrations were measured using the syringe headspace equilibration technique, providing point samples, with fluxes calculated based on parameterized or literature-based gas transfer velocities (k). While one could argue that flux chambers might provide a more direct measurement, their use was simply not feasible due to the remoteness of the field site. More importantly, having reliable data from an understudied region, even with methodological limitations, is far preferable to having no data at all (Metcalfe et al., 2018). Furthermore, flux chambers come with their own set of caveats, and no method is without its trade-offs (Kutzbach et al., 2007; Vachon et al., 2010). Using point samples and approximations remains valid as long as the data is handled correctly, that means being transparent about its limitations, placing it in the appropriate context, and applying robust statistical methods. A key aspect of scientific integrity is not eliminating uncertainty (an impossible task) but rather quantifying and representing it honestly. While some might argue that uncertainty undermines findings, I believe the real risk lies in ignoring it.

In addition to dissolved greenhouse gas concentrations, greenhouse gas emissions are also influenced by the physical processes regulating air–water gas exchange, such as water column mixing and stratification (Jansen et al., 2020). These processes depend on freshwater ecosystem-specific limnological characteristics, including water depth, morphology and surface area, together with climatic drivers such as temperature and wind. Investigating how these physical, biogeochemical, and limnological controls interact remains an important step towards understanding how dissolved greenhouse gas concentrations translate into atmospheric emissions across Arctic freshwater ecosystem types.

Relationships between DOM and greenhouse gas supersaturation

The findings of Chapter 3 demonstrate that relationships between DOM characteristics and dissolved CO_2, CH_4, and N_2O differ among lakes, ponds, and fluvial systems in the Indigirka tundra lowlands during summer. Rather than exhibiting a single, consistent set of DOM–greenhouse gas relationships, each freshwater ecosystem type displayed distinct associations between dissolved greenhouse gases and both DOM quantity and composition. Ponds exhibited the strongest relationships between dissolved CO_2 and CH_4 and DOM quantity, with additional associations with dissolved Fe and pond morphology, indicating that both DOM characteristics and physical ecosystem properties contribute to DOM–greenhouse gas relationships in these shallow systems. Although lakes shared several broad relationships with ponds, different fractions of the DOM pool were associated with dissolved greenhouse gases, suggesting that differences in DOM composition influence which components are most closely associated with dissolved gas concentrations. The distinct DOM–greenhouse gas relationships observed in fluvial systems suggest that the DOM characteristics associated with dissolved greenhouse gases are not conserved across the aquatic continuum, even within a single Arctic landscape.

Unlike dissolved CO_2 and CH_4, dissolved N_2O exhibited one relationship that was conserved across all ecosystem types: a consistent negative association with DOC. In contrast, relationships between dissolved N_2O and optical DOM characteristics differed among ecosystem types, with ponds and lakes exhibiting broadly similar patterns and fluvial systems displaying contrasting relationships. Together, these findings indicate that while DOM quantity exhibits a consistent association with dissolved N_2O, relationships between dissolved N_2O and DOM composition remain ecosystem dependent.

Our inferences are based on observed relationships and supported by previously published findings; however, some methodological limitations remain. Optical absorbance and fluorescence measurements provide direct measurements of the optical properties of DOM. However, the interpretation of derived indices, such as fluorescence and spectral metrics, relies on empirical relationships with DOM composition and characteristics established in previous studies rather than direct measurements of molecular structure or biogeochemical processes (D'Andrilli et al., 2022; Korak and McKay, 2024). Consequently, these indices provide evidence of likely, rather than definitive, DOM characteristics. While widely used, they represent only a snapshot of DOM composition and cannot fully capture the complexity of DOM degradation or the processes governing carbon and nitrogen cycling, as microbial and photochemical transformations are not directly measured (D'Andrilli et al., 2022). Similarly, the small subset of samples analysed using PTR-MS provided complementary information on broad molecular groups within a portion of the DOM pool, rather than a comprehensive characterization of DOM composition. Taken together, and while recognizing the limitations of each approach, these methods allowed DOM composition to be investigated alongside dissolved greenhouse gas concentrations across lakes, ponds, and fluvial systems within the same Arctic lowland study area. This provided new insights into how DOM–greenhouse gas relationships vary among freshwater ecosystem types. Consequently, the relationships identified in this thesis should be

interpreted as associations that generate hypotheses for future investigation rather than direct evidence of the underlying biogeochemical mechanisms.

Late-summer lateral carbon flux in a costal Hudson Bay Lowlands catchment

Recent work by Heffernan et al. (2024) highlights significant research gaps in DOC mobilization, particularly in regions with large permafrost carbon stocks such as the Hudson Bay Lowlands. The persistence of these gaps underscores the need for targeted studies of lateral carbon transport and terrestrial–aquatic connectivity in coastal catchments. Our study addresses this by providing new DOC, POC, and DIC measurements from this underrepresented region, contributing to a more comprehensive understanding of lateral carbon transport in high-latitude lowlands. DOC concentrations remained within a relatively narrow range across the catchment, although changes in DOM optical properties indicate that stability in bulk DOC concentrations did not preclude changes in DOM composition during downstream transport. In contrast, DIC concentrations increased downstream, accompanied by changes in $\delta^{13}\mathrm{C}$-DIC and DOM optical properties. These patterns suggest that processing of the DOC pool contributed to the downstream increase in DIC, while additional DIC inputs from the subsurface likely also contributed. Carbon characteristics differed between landscape types, with greater differences between soil pore water and surface water observed for several parameters in the headwater peatland than in the coastal sandy heathland, highlighting the influence of landscape and hydrological conditions on terrestrial–freshwater carbon transport. Late-summer rainfall further influenced carbon transport by increasing DOC concentrations and aromaticity in surface waters while reducing DIC concentrations, whereas DOM composition within soil pore waters remained relatively stable. These findings indicate that landscape heterogeneity and hydrological variability contribute to spatial and temporal variation in dissolved carbon transport within this coastal low-relief tundra catchment.

This study primarily relied on discrete measurements of dissolved carbon concentrations, isotopic composition, and DOM optical properties, which provided valuable insights into spatial and hydrological patterns. However, the observed temporal and spatial variability suggests that higher-frequency monitoring using in situ sensors could substantially improve our understanding of dissolved carbon dynamics and lateral carbon transport (Shogren et al., 2020b). Efforts were made to deploy continuous DOC and optical property sensors in surface waters and a CO_2 sensor in the riparian zone; however, logistical and technical constraints limited the duration and completeness of these deployments. Future field campaigns with sustained, high-resolution monitoring would enable characterization of diel variability, hydrological event responses, and carbon transformation processes that remain difficult to resolve using discrete sampling alone.

Comparison of the two Arctic lowland study regions

This thesis combines observations from two different Arctic lowland landscapes, providing a broad geographical perspective on freshwater carbon cycling. The Indigirka Lowlands, Chapters 2–3, comprise a mosaic of peat-forming polygonal wetlands, Yedoma uplands, and river floodplains, whereas the study in the Hudson Bay Lowlands, Chapter 4, was conducted in the northernmost coastal portion of the Lowlands, where a low-relief coastal landscape transitions from headwater peatland to coastal sandy heath. Although the two study regions can be compared conceptually, direct comparison between the studies conducted in each region is inherently limited because they addressed different research questions and focused on different aspects of freshwater carbon cycling. Furthermore, field campaigns were conducted in different years and at different stages of the growing season, introducing additional variability related to seasonal and interannual changes in hydrological and biogeochemical conditions.

Nevertheless, some broad comparisons can be made. DOC concentrations in freshwater systems ranged from 1.2 mg C L^{-1} to 46.7 mg C L^{-1} in the Indigirka Lowlands, whereas mean surface water DOC concentrations in the Hudson Bay Lowlands were 8.5 ± 2.2 mg C L^{-1}. These observations likely reflect a combination of contrasting landscape characteristics, vegetation, and hydrological settings, together with differences in sampling year and the stage of the growing season. The Kytalyk study was conducted within an organic-rich polygonal tundra landscape characterized by peat-forming wetlands, Yedoma uplands, and river floodplains, whereas the Churchill ponds occur within a coastal catchment comprising headwater peatland and coastal sandy heath landscapes, resulting in different potential sources and pathways of dissolved organic carbon to surface waters.

In addition, the studies at the two sites highlight the importance of episodic hydrological events in shaping freshwater carbon cycling. Although the hydrological events differed, both flooding in the Indigirka Lowlands and a late-summer rainfall event in the Hudson Bay Lowlands both altered carbon dynamics within freshwater systems. In the Indigirka Lowlands, flooding increased inland water extent and contributed to higher greenhouse gas emissions from freshwater ecosystems across the study area (Chapter 2). In the Hudson Bay Lowlands, a late-summer rainfall event increased hydrological connectivity, enhancing DOM and DIC export, facilitating potential CO_2 and CH_4 evasion, and reducing in-stream residence times (Chapter 4).

Emergent insights from integrating vertical, lateral, and biogeochemical perspectives

When considered individually, Chapters 2–4 quantify emissions, characterize carbon quality, and assess lateral transport; when considered together, they demonstrate that freshwater greenhouse gas emissions in tundra lowlands are an emergent property of hydrological connectivity, carbon quality, and ecosystem-specific processing.

Taken together, the studies in this thesis provide an integrated view of carbon transfer from terrestrial to aquatic systems and its subsequent transformation, transport, and loss within three common freshwater ecosystem types in tundra lowlands: ponds, lakes, and

fluvial networks. Results from the catchment-scale study (Chapter 4) demonstrate that landscape type and soil characteristics exert strong control over hydrological connectivity, determining how terrestrial carbon enters freshwater systems and the degree to which soil and surface waters are coupled. This finding directly reinforces the Chapter 1 framework that permafrost-constrained hydrology and shallow active-layer flow paths promote strong lateral transport and tight terrestrial–aquatic connectivity in high-latitude tundra lowlands (Hinkel and Nelson, 2003; Frey and McClelland, 2009; McGuire et al., 2009).

This terrestrial–aquatic connectivity is critical because Chapter 3 shows that the properties and composition of organic carbon entering freshwater ecosystems are related to dissolved greenhouse gas concentrations, while these relationships are further modulated by freshwater ecosystem type. Differences in connectivity and carbon inputs are reflected in contrasting DOM–greenhouse gas relationships and ultimately contributing to the different possible fates of laterally transported carbon, including greenhouse gas emissions, downstream transport, and burial within freshwater ecosystems. As anticipated in Chapter 1, which emphasized the role of freshwater ecosystems as sites of carbon transformation rather than passive conduits (McGuire et al., 2009; Battin et al., 2023), results from Chapters 2 and 3 show that differences in emissions among freshwater ecosystem types arise not only from variation in dissolved gas concentrations, but also from freshwater ecosystem–specific physical, biogeochemical, and limnological contexts within which carbon processing and gas exchange occur.

The finding that freshwater CO_2 and CH_4 emissions offset the terrestrial carbon sink by approximately 9 % to 13 % (Chapter 2) therefore cannot be interpreted as a static landscape attribute. Instead, it emerges from the interaction between the distribution of freshwater ecosystem types, hydrological connectivity, and the quality of laterally supplied carbon. This synthesis highlights that upscaling freshwater emissions without accounting for DOM characteristics and system-specific processing environments risks introducing substantial bias into regional carbon budget estimates, a concern already raised in Chapter 1 in the context of poorly constrained Arctic freshwater contributions.

Consistent with the expectations outlined in Chapter 1 that Arctic warming and intensification of the hydrological cycle will alter terrestrial–aquatic connectivity (e.g., Bring et al. (2016); Arp et al. (2020); Beel et al. (2021)), Chapters 2 and 4 demonstrate that episodic hydrological events can substantially influence freshwater carbon cycling. In the Indigirka Lowlands, flooding was associated with increased freshwater greenhouse gas emissions due to an expansion of inland water surface area (Chapter 2), whereas a late-summer rainfall event in the Hudson Bay Lowlands increased hydrological connectivity and enhanced lateral carbon transport (Chapter 4). Although this thesis examined the aforementioned aspects of freshwater carbon cycling in response to flooding and rainfall within the scope of the respective studies, these episodic hydrological events are also likely to influence additional components of freshwater carbon cycling that warrant further investigation.

While this thesis focused on freshwater greenhouse gas emissions and lateral carbon transport, carbon burial within freshwater sediments represents another important fate of carbon in freshwater ecosystems that was beyond the scope of this work (Aufdenkampe et al., 2011; Lundin et al., 2015; Battin et al., 2023). Integrating atmospheric emissions,

downstream transport, and sediment burial would provide a more complete understanding of carbon cycling across Arctic lowland freshwater ecosystems.

Overall, this synthesis traces a coherent pathway of carbon from terrestrial sources through hydrologically mediated transfer, freshwater ecosystems, and ultimately to the atmosphere. In doing so, it directly addresses the key uncertainties outlined in Chapter 1 regarding (i) the role of freshwater greenhouse gas emissions in the context of the terrestrial sink, (ii) the relationships between DOM composition and dissolved greenhouse gas concentrations across different freshwater ecosystem types, and (iii) the sensitivity of tundra lowland lateral carbon export to changes in hydrological connectivity and event-driven dynamics.

Future considerations in Arctic freshwater carbon and nitrogen research

Statistical rigor

The integration of upscaled freshwater greenhouse gas emissions into the terrestrial carbon budget, biogeochemical relationships between DOM and dissolved greenhouse gases, and laterally structured catchment data not only shaped the scientific conclusions of this thesis, but also revealed recurring statistical challenges that warrant explicit reflection.

Across the Chapters 2–4, the structure of the data repeatedly highlighted limitations in commonly applied statistical approaches in Arctic biogeochemistry. In Chapter 2, greenhouse gas concentrations were characterised by repeated measurements at uneven intervals within a nested spatial framework. This required careful consideration of how observations could be grouped and summarised for upscaling, and how representative values could be derived without inflating apparent sample sizes. Particular attention was therefore paid to how uncertainty associated with spatial heterogeneity, temporal variability, and aggregation choices was propagated into landscape-scale flux estimates.

Similarly, Chapter 3 demonstrated that commonly used DOM optical indices and molecular descriptors contain substantial overlapping information and shared variance. This limits the interpretability of simple bivariate relationships between individual DOM metrics and dissolved greenhouse gas concentrations. Multivariate and rank-based approaches were therefore necessary to distinguish meaningful biogeochemical patterns from correlations arising from interrelated predictors.

In Chapter 4, the nested structure of the sampling design, with repeated depth profiles along transects embedded within contrasting landscape units, further underscored the importance of accounting for spatial dependence and hierarchical variability when interpreting lateral carbon fluxes. Treating observations as independent would have risked misrepresenting catchment-scale patterns in DOC and DIC dynamics.

Together, these experiences reinforce a broader concern in Arctic freshwater research: that statistical methods are often selected based on precedent rather than on the structure and limitations of the data itself, thereby perpetuating the very uncertainty and poor

constraint that Chapter 1 identifies as a central challenge in quantifying Arctic freshwater carbon fluxes.

This concern is reflected in the frequent misuse of parametric tests on data that violate underlying assumptions, despite clear evidence that this can lead to unreliable conclusions (Zuur et al., 2009). Likewise, hierarchical data structures are often analysed using simple statistical tests, when mixed-effects models provide more appropriate frameworks for accounting for nested variability and repeated measures (Bolker et al., 2009). In addition, inadequate treatment of interrelated predictors remains common in biogeochemical studies, increasing the risk of misleading interpretations (Dormann et al., 2013).

If concerns are raised about overcomplicating statistical approaches, it is important to recognise that overly simplistic methods often produce misleading conclusions (Stephens et al., 2005). A pluralistic and data-driven approach to statistical inference is therefore necessary in environmental sciences to ensure robustness and reproducibility. The broader issue of statistical misuse has been widely documented, with Ioannidis (2005) famously arguing that "most published research findings are false" in part due to inappropriate statistical applications.

In Arctic biogeochemistry, where environmental variability, small sample sizes, nested spatial structures, and irregularly spaced repeated measurements are common, a careful and justified choice of statistical methods is not merely good practice but a fundamental requirement for reducing uncertainty and improving constraint on Arctic freshwater carbon budgets in a rapidly changing climate.

High-frequency and long-term monitoring with sensors

Advancing sensor technology is making high-frequency data collection increasingly feasible, even in remote Arctic environments. Continuous monitoring allows for real-time tracking of hydrologic and biogeochemical fluxes, revealing critical temporal patterns and the impact of episodic events such as extreme rainfall, which are becoming more frequent and intense due to climate change (Shogren et al., 2020b).

Across Chapters 2–4, this thesis relied primarily on discrete sampling campaigns, which provided valuable spatial coverage but limited insight into short-term variability, diel cycles, and rapid event-driven responses. In Chapter 2, point measurements of dissolved greenhouse gases were necessarily aggregated to derive representative flux estimates for upscaling, despite likely variability at sub-daily and event scales. In Chapter 3, DOM composition and associated greenhouse gas relationships were assessed from snapshot samples that could not resolve rapid biogeochemical transformations. Similarly, in Chapter 4, discrete measurements captured spatial patterns in lateral carbon fluxes but were unable to fully characterise transient responses to rainfall and hydrological pulses.

High-frequency sensor deployments would substantially improve the interpretation of these processes by resolving temporal dynamics that are difficult to detect using traditional sampling approaches. Studies have already demonstrated that nighttime CO_2 fluxes in permafrost-peatland lakes can be 2-3 times higher than during the day (Shirokova et al., 2020), underscoring the need for expanded monitoring beyond daylight

hours and across seasons.

Long-term, continuous measurements would also strengthen future upscaling and modelling efforts by providing more representative estimates of mean fluxes and variability, thereby improving uncertainty quantification. Integrating sensor-based observations with spatial surveys and discrete sampling, as applied in this thesis, offers a promising pathway toward more robust assessments of Arctic freshwater carbon dynamics under ongoing climate change.

The role of remote sensing

Remote sensing is an increasingly valuable tool for understanding Arctic biogeochemistry, yet its full potential remains largely untapped. It has already been used to estimate Arctic river discharge (Feng et al., 2021) and contributes to assessments of terrestrial–aquatic interactions (Campbell et al., 2022). Expanding the spatial coverage of Arctic carbon monitoring is particularly important in remote and inaccessible regions.

For example, while Chapter 2 demonstrated strong contrasts in greenhouse gas emissions among ponds, lakes, and fluvial systems, most regional assessments still rely on static inventories of inland water coverage that do not capture seasonal flooding, pond expansion, drainage, or shifts in hydrological connectivity. High-resolution satellite imagery could be used more systematically to track these dynamics and refine estimates of active emitting surface area.

Similarly, the landscape-dependent patterns in lateral carbon fluxes observed in Chapter 4 highlight the potential for remotely sensed indicators of soil moisture, surface wetness, and inundation extent to improve characterization of terrestrial–aquatic connectivity. Such datasets remain underutilized in Arctic carbon studies, despite their relevance for interpreting spatial variability in DOC and DIC export.

Across Chapters 2–4, this thesis relied on intensive field-based sampling within relatively small study areas, reflecting the logistical constraints of working in Arctic environments. In Chapter 2, satellite imagery was used to quantify inland water surface area for upscaling greenhouse gas emissions, but emission estimates remained dependent on measurements from a limited number of sites. In Chapters 3 and 4, detailed biogeochemical data provided valuable insights into ecosystem-specific processes, yet their spatial representativeness was necessarily constrained by access and sampling effort.

Enhanced use of remote sensing could substantially improve the spatial context of such field observations. For example, the proposed global River Observing System (RIOS) aims to integrate remote sensing with autonomous sensor networks and field surveys to better capture the heterogeneity of fluvial carbon fluxes (Battin et al., 2023). Applying such approaches in the Arctic, where access is challenging, would increase the spatial scope of Arctic biogeochemical research.

However, significant challenges remain in ensuring that remotely derived products accurately represent fine-scale hydrological and biogeochemical processes, particularly in heterogeneous permafrost landscapes. The variability among freshwater ecosystem types observed in Chapter 2, ecosystem-specific DOM–GHG relationships in Chapter 3,

and landscape-dependent lateral fluxes in Chapter 4 illustrate the risk of oversimplification when relying on spatial proxies alone.

Future progress will therefore depend on continued development and validation of remote sensing products against high-quality field measurements. Strengthening these links will improve confidence in spatially explicit assessments of Arctic freshwater carbon dynamics, particularly in regions where sustained ground-based monitoring remains difficult.

Holistic approaches to carbon and nitrogen cycling research

A holistic perspective is essential for understanding terrestrial-aquatic connectivity, especially given increasing evidence that significant biogeochemical transformations occur at the terrestrial-aquatic interface (Wologo et al., 2021). Many studies infer terrestrial carbon exports from DOC concentrations in freshwater, yet this approach fails to capture the complex transformations before carbon reaches freshwater ecosystems.

Across Chapters 2–4, this thesis examined multiple components of the carbon cycle, including greenhouse gas emissions (Chapter 2), DOM composition (Chapter 3), and lateral DOC and DIC transport (Chapter 4). Together, these chapters show that carbon is processed along multiple pathways and in multiple forms as it moves through tundra lowland landscapes. However, each chapter necessarily focused on a subset of these pathways, reflecting the practical constraints of field-based research.

Future research should take when possible a comprehensive approach, considering multiple carbon forms (DOC, DIC, POC, CO_2, CH_4) across the full terrestrial-aquatic continuum (Rasilo et al., 2017). Such approaches would improve understanding of how carbon is partitioned between lateral transport, in-stream processing, and atmospheric exchange.

Just as some carbon forms are often overlooked, nitrogen cycling remains poorly integrated into Arctic biogeochemical studies. While N_2O emissions were quantified in Chapter 2 and shown to be small relative to CO_2 and CH_4, Chapters 3 and 4 primarily focused on carbon dynamics, limiting assessment of how nitrogen availability and transformation influence observed patterns. Yet permafrost thaw is altering nitrogen fluxes, increasing dissolved organic nitrogen to nitrate ratios in fluvial systems, with potential implications for ecosystem productivity and biogeochemical feedbacks (Francis et al., 2023).

To develop a more complete understanding of Arctic biogeochemical cycles, future studies should incorporate nitrogen dynamics alongside carbon fluxes, ensuring that both elements are examined within an integrated framework that captures transformations across terrestrial, riparian, and aquatic environments.

Bridging scales: from process-based studies to regional models

Studies such as those presented in this thesis contribute to detailed, process-level understanding of Arctic freshwater carbon dynamics by combining landscape-scale upscaling of greenhouse gas emissions (Chapter 2), ecosystem-specific biogeochemical charac-

terization (Chapter 3), and catchment-scale assessments of lateral carbon fluxes (Chapter 4). By explicitly linking these complementary approaches and carefully accounting for spatial, temporal, and ecosystem-specific variability, this thesis clarifies how local measurements can be interpreted and constrained for use in larger-scale assessments. Scaling freshwater carbon fluxes requires consistent methodologies, cross-system comparisons, and models that bridge localized process details with large-scale ecosystem shifts (McCallister et al., 2018).

Across Chapters 2–4, this thesis revealed substantial spatial, temporal, and ecosystem-specific variability in greenhouse gas emissions, DOM composition, and lateral carbon fluxes. In Chapter 2, upscaling inland water emissions required explicit assumptions regarding representativeness and uncertainty propagation. In Chapter 3, system-specific DOM–GHG relationships highlighted limitations in applying uniform parameterizations across freshwater types. In Chapter 4, landscape-dependent connectivity and processing further demonstrated that lateral fluxes cannot be readily generalized without accounting for catchment context.

Together, these findings illustrate the challenges of translating fine-scale observations into regional estimates and highlight the risk of oversimplification in large-scale models. Bridging this gap remains one of the central challenges in Arctic carbon monitoring and modelling.

Machine learning and remote sensing offer promising opportunities to address this challenge by identifying patterns in complex, multi-source datasets and improving flux predictions (Oliva and Fritz, 2018). When combined with in-situ sensor networks and targeted field campaigns, these approaches can help constrain spatial and temporal variability and improve parameterization of freshwater processes, refine ecosystem-scale carbon budgets and enhance projections of future biogeochemical changes.

Moving forward, continued methodological development and the integration of emerging observational and analytical technologies will be essential for improving the accuracy, transparency, and scalability of Arctic biogeochemical assessments. Strengthening links between process-based studies and modelling frameworks will be essential for improving the accuracy and scalability of Arctic biogeochemical cycles assessments in a rapidly changing environment.

REFERENCES

Abbott, B. W. (2022). Permafrost climate feedbacks. In *Global Arctic: An Introduction to the Multifaceted Dynamics of the Arctic*, pages 189–209. Springer.

Abbott, B. W., Larouche, J. R., Jones, J. B., Bowden, W. B., and Balser, A. W. (2014). Elevated dissolved organic carbon biodegradability from thawing and collapsing permafrost. *Journal of Geophysical Research: Biogeosciences*, 119(10):2049–2063.

Abnizova, A., Siemens, J., Langer, M., and Boike, J. (2012). Small ponds with major impact: The relevance of ponds and lakes in permafrost landscapes to carbon dioxide emissions. *Global Biogeochemical Cycles*, 26(2).

Ala-Aho, P., Soulsby, C., Pokrovsky, O., Kirpotin, S., Karlsson, J., Serikova, S., Vorobyev, S., Manasypov, R., Loiko, S., and Tetzlaff, D. (2018). Using stable isotopes to assess surface water source dynamics and hydrological connectivity in a high-latitude wetland and permafrost influenced landscape. *Journal of Hydrology*, 556:279–293.

Arp, C., Whitman, M., Kemnitz, R., and Stuefer, S. (2020). Evidence of hydrological intensification and regime change from northern alaskan watershed runoff. *Geophysical Research Letters*, 47(17):e2020GL089186.

Arsenault, J., Talbot, J., Brown, L. E., Holden, J., Martinez-Cruz, K., Sepulveda-Jauregui, A., Swindles, G. T., Wauthy, M., and Lapierre, J. (2022). Biogeochemical distinctiveness of peatland ponds, thermokarst waterbodies, and lakes. *Geophysical Research Letters*, 49(11).

Aufdenkampe, A. K., Mayorga, E., Raymond, P. A., Melack, J. M., Doney, S. C., Alin, S. R., Aalto, R. E., and Yoo, K. (2011). Riverine coupling of biogeochemical cycles between land, oceans, and atmosphere. *Frontiers in Ecology and the Environment*, 9(1):53–60.

Bade, D. L., Carpenter, S. R., Cole, J. J., Hanson, P. C., and Hesslein, R. H. (2004). Controls of δ13c-dic in lakes: Geochemistry, lake metabolism, and morphometry. *Limnology and Oceanography*, 49(4):1160–1172.

Barrett, J. L. (2000). Exploring the natural foundations of religion. *Trends in cognitive sciences*, 4(1):29–34.

Bates, D., Mächler, M., Bolker, B., and Walker, S. (2015). Fitting linear mixed-effects models usinglme4. *Journal of Statistical Software*, 67(1).

Battin, T. J., Lauerwald, R., Bernhardt, E. S., Bertuzzo, E., Gener, L. G., Hall Jr, R. O., Hotchkiss, E. R., Maavara, T., Pavelsky, T. M., Ran, L., et al. (2023). River ecosystem metabolism and carbon biogeochemistry in a changing world. *Nature*, 613(7944):449–459.

Beel, C., Heslop, J., Orwin, J., Pope, M., Schevers, A., Hung, J., Lafrenière, M., and Lamoureux, S. (2021). Emerging dominance of summer rainfall driving high arctic terrestrial-aquatic connectivity. *Nature Communications*, 12(1):1448.

Berggren, M., Gudasz, C., Guillemette, F., Hensgens, G., Ye, L., and Karlsson, J. (2019). Systematic microbial production of optically active dissolved organic matter in subarctic lake water. *Limnology and Oceanography*, 65(5):951–961.

Berner, L. T., Massey, R., Jantz, P., Forbes, B. C., Macias-Fauria, M., Myers-Smith, I., Kumpula, T., Gauthier, G., Andreu-Hayles, L., Gaglioti, B. V., et al. (2020). Summer warming explains

widespread but not uniform greening in the arctic tundra biome. *Nature communications*, 11(1):4621.

Biehler, A., Buffin-Bélanger, T., Baudron, P., and Chaillou, G. (2023). Groundwater discharge contribution to dissolved inorganic carbon and riverine carbon emissions in a subarctic region. *Biogeochemistry*, 165(2):129–150.

Bintanja, R. (2018). The impact of arctic warming on increased rainfall. *Scientific reports*, 8(1):16001.

Bintanja, R. and Andry, O. (2017). Towards a rain-dominated arctic. *Nature Climate Change*, 7(4):263–267.

Biskaborn, B. K., Smith, S. L., Noetzli, J., Matthes, H., Vieira, G., Streletskiy, D. A., Schoeneich, P., Romanovsky, V. E., Lewkowicz, A. G., Abramov, A., et al. (2019). Permafrost is warming at a global scale. *Nature communications*, 10(1):264.

Bjorkman, A. D., Myers-Smith, I. H., Elmendorf, S. C., Normand, S., Rüger, N., Beck, P. S., Blach-Overgaard, A., Blok, D., Cornelissen, J. H. C., Forbes, B. C., et al. (2018). Plant functional trait change across a warming tundra biome. *Nature*, 562(7725):57–62.

Bolker, B. M., Brooks, M. E., Clark, C. J., Geange, S. W., Poulsen, J. R., Stevens, M. H. H., and White, J.-S. S. (2009). Generalized linear mixed models: a practical guide for ecology and evolution. *Trends in ecology & evolution*, 24(3):127–135.

Borges, A. V., Darchambeau, F., Lambert, T., Morana, C., Allen, G. H., Tambwe, E., Toengaho Sembaito, A., Mambo, T., Nlandu Wabakhangazi, J., Descy, J.-P., et al. (2019). Variations in dissolved greenhouse gases (co 2, ch 4, n 2 o) in the congo river network overwhelmingly driven by fluvial-wetland connectivity. *Biogeosciences*, 16(19):3801–3834.

Borges, A. V., Darchambeau, F., Teodoru, C. R., Marwick, T. R., Tamooh, F., Geeraert, N., Omengo, F. O., Guérin, F., Lambert, T., Morana, C., Okuku, E., and Bouillon, S. (2015). Globally significant greenhouse-gas emissions from african inland waters. *Nature Geoscience*, 8(8):637–642.

Breiman, L. (2001). Random forests. *Machine Learning*, 45(1):5–32.

Breton, J., Vallieres, C., and Laurion, I. (2009). Limnological properties of permafrost thaw ponds in northeastern canada. *Canadian Journal of Fisheries and Aquatic Sciences*, 66(10):1635–1648.

Bring, A., Fedorova, I., Dibike, Y., Hinzman, L., Mård, J., Mernild, S., Prowse, T., Semenova, O., Stuefer, S. L., and Woo, M.-K. (2016). Arctic terrestrial hydrology: A synthesis of processes, regional effects, and research challenges. *Journal of Geophysical Research: Biogeosciences*, 121(3):621–649.

Buckley, S., McKay, G., Leresche, F., and Rosario-Ortiz, F. (2024). Inferring the molecular basis for dissolved organic matter photochemical and optical properties. *Environmental science & technology*, 58(21):9040–9050.

Bulygina, O. N., Groisman, P. Y., Razuvaev, V., and Korshunova, N. (2011). Changes in snow cover characteristics over northern eurasia since 1966. *Environmental Research Letters*, 6(4):045204.

Callaghan, T. V., Johansson, M., Brown, R. D., Groisman, P. Y., Labba, N., Radionov, V., Barry, R. G., Bulygina, O. N., Essery, R. L., Frolov, D., et al. (2011). The changing face of arctic snow cover: A synthesis of observed and projected changes. *Ambio*, 40(Suppl 1):17–31.

Campbell, A. D., Fatoyinbo, T., Charles, S. P., Bourgeau-Chavez, L. L., Goes, J., Gomes, H., Halabisky, M., Holmquist, J., Lohrenz, S., Mitchell, C., et al. (2022). A review of carbon monitoring in wet carbon systems using remote sensing. *Environmental Research Letters*, 17(2):025009.

Campeau, A., Bishop, K., Nilsson, M. B., Klemedtsson, L., Laudon, H., Leith, F. I., Öquist, M.,

and Wallin, M. B. (2018). Stable carbon isotopes reveal soil-stream dic linkages in contrasting headwater catchments. *Journal of Geophysical Research: Biogeosciences*, 123(1):149–167.

Chapin III, F. S., Woodwell, G. M., Randerson, J. T., Rastetter, E. B., Lovett, G. M., Baldocchi, D. D., Clark, D. A., Harmon, M. E., Schimel, D. S., Valentini, R., et al. (2006). Reconciling carbon-cycle concepts, terminology, and methods. *Ecosystems*, 9(7):1041–1050.

Coch, C., Juhls, B., Lamoureux, S. F., Lafrenière, M., Fritz, M., Heim, B., and Lantuit, H. (2019a). Characterizing organic matter composition in small low and high arctic catchments using terrestrial colored dissolved organic matter (cdom).

Coch, C., Juhls, B., Lamoureux, S. F., Lafrenière, M. J., Fritz, M., Heim, B., and Lantuit, H. (2019b). Comparisons of dissolved organic matter and its optical characteristics in small low and high arctic catchments. *Biogeosciences*, 16(23):4535–4553.

Cole, J. J. and Caraco, N. F. (1998). Atmospheric exchange of carbon dioxide in a low-wind oligotrophic lake measured by the addition of sf6. *Limnology and Oceanography*, 43(4):647–656.

Cole, J. J., Prairie, Y. T., Caraco, N. F., McDowell, W. H., Tranvik, L. J., Striegl, R. G., Duarte, C. M., Kortelainen, P., Downing, J. A., Middelburg, J. J., and Melack, J. (2007). Plumbing the global carbon cycle: Integrating inland waters into the terrestrial carbon budget. *Ecosystems*, 10(1):172–185.

Conway, T. (2007). Atmospheric carbon dioxide dry air mole fractions from the noaa esrl carbon cycle cooperative global air sampling network, 1968-2006. *ftp://ftp. cmdl. noaa. gov/ccg/co2/flask/event/*.

Cory, R. M. and Kling, G. W. (2018). Interactions between sunlight and microorganisms influence dissolved organic matter degradation along the aquatic continuum. *Limnology and Oceanography Letters*, 3(3):102–116.

Cory, R. M., Miller, M. P., McKnight, D. M., Guerard, J. J., and Miller, P. L. (2010). Effect of instrument-specific response on the analysis of fulvic acid fluorescence spectra. *Limnology and Oceanography: Methods*, 8(2):67–78.

Cory, R. M., Ward, C. P., Crump, B. C., and Kling, G. W. (2014). Sunlight controls water column processing of carbon in arctic fresh waters. *Science*, 345(6199):925–928.

Dasari, S., Garnett, M. H., and Hilton, R. G. (2024). Leakage of old carbon dioxide from a major river system in the canadian arctic. *PNAS nexus*, 3(4):pgae134.

Dean, J. F., Billett, M. F., Baxter, R., Dinsmore, K. J., Lessels, J. S., Street, L. E., Subke, J.-A., Tetzlaff, D., Washbourne, I., and Wookey, P. A. (2016). Biogeochemistry of "pristine" freshwater stream and lake systems in the western canadian arctic. *Biogeochemistry*, 130(3):191–213.

Dean, J. F., Meisel, O. H., Martyn Rosco, M., Marchesini, L. B., Garnett, M. H., Lenderink, H., van Logtestijn, R., Borges, A. V., Bouillon, S., Lambert, T., et al. (2020). East siberian arctic inland waters emit mostly contemporary carbon. *Nature Communications*, 11(1):1627.

Dean, J. F., Middelburg, J. J., Röckmann, T., Aerts, R., Blauw, L. G., Egger, M., Jetten, M. S. M., de Jong, A. E. E., Meisel, O. H., Rasigraf, O., Slomp, C. P., in't Zandt, M. H., and Dolman, A. J. (2018). Methane feedbacks to the global climate system in a warmer world. *Reviews of Geophysics*, 56(1):207–250.

Denfeld, B. A., Frey, K. E., Sobczak, W. V., Mann, P. J., and Holmes, R. M. (2013). Summer co2 evasion from streams and rivers in the kolyma river basin, north-east siberia. *Polar Research*, 32(1):19704.

Denfeld, B. A., Wallin, M. B., Sahlée, E., Sobek, S., Kokic, J., Chmiel, H. E., and Weyhenmeyer, G. A. (2015). Temporal and spatial carbon dioxide concentration patterns in a small boreal lake in relation to ice cover dynamics. *Boreal environment research*, 20(6):679–692.

Dentener, F. (2006). Global maps of atmospheric nitrogen deposition, 1860, 1993, and 2050. *ORNL Distributed Active Archive Center (DAAC) dataset 10.3334/ORNLDAAC/830 (2006)*, page 830.

Doctor, D. H., Kendall, C., Sebestyen, S. D., Shanley, J. B., Ohte, N., and Boyer, E. W. (2007). Carbon isotope fractionation of dissolved inorganic carbon (dic) due to outgassing of carbon dioxide from a headwater stream. *Hydrological Processes*, 22(14):2410–2423.

Dormann, C. F., Elith, J., Bacher, S., Buchmann, C., Carl, G., Carré, G., Marquéz, J. R. G., Gruber, B., Lafourcade, B., Leitão, P. J., et al. (2013). Collinearity: a review of methods to deal with it and a simulation study evaluating their performance. *Ecography*, 36(1):27–46.

Downing, J. A. (2010). Emerging global role of small lakes and ponds: little things mean a lot. *Limnetica*, 29(1):9–24.

Downing, J. A., Cole, J. J., Duarte, C., Middelburg, J. J., Melack, J. M., Prairie, Y. T., Kortelainen, P., Striegl, R. G., McDowell, W. H., and Tranvik, L. J. (2012). Global abundance and size distribution of streams and rivers. *Inland waters*, 2(4):229–236.

Drake, T. W., Raymond, P. A., and Spencer, R. G. (2018). Terrestrial carbon inputs to inland waters: A current synthesis of estimates and uncertainty. *Limnology and Oceanography Letters*, 3(3):132–142.

Drake, T. W., Wickland, K. P., Spencer, R. G. M., McKnight, D. M., and Striegl, R. G. (2015). Ancient low–molecular-weight organic acids in permafrost fuel rapid carbon dioxide production upon thaw. *Proceedings of the National Academy of Sciences*, 112(45):13946–13951.

Dredge, L. and McMartin, I. (2011). *Glacial stratigraphy of northern and central Manitoba*. Geological Survey of Canada.

Dredge, L. A. and Nixon, F. (1992). Glacial and environmental geology of northeastern manitoba.

Duguay, C. R. and Lafleur, P. M. (2003). Determining depth and ice thickness of shallow subarctic lakes using space-borne optical and sar data. *International Journal of Remote Sensing*, 24(3):475–489.

Dupas, R., Lambert, T., and Durand, P. (2024). The influence of nitrogen and iron biogeochemical cycles on the production and export of dissolved organic matter in headwater catchments. In *EGU General Assembly Conference Abstracts*, page 5683.

Duvert, C., Butman, D. E., Marx, A., Ribolzi, O., and Hutley, L. B. (2018). Co2 evasion along streams driven by groundwater inputs and geomorphic controls. *Nature Geoscience*, 11(11):813–818.

Dyke, L. D. and Sladen, W. E. (2010). Permafrost and peatland evolution in the northern hudson bay lowland, manitoba. *ARCTIC*, 63(4).

D'Andrilli, J., Silverman, V., Buckley, S., and Rosario-Ortiz, F. L. (2022). Inferring ecosystem function from dissolved organic matter optical properties: A critical review. *Environmental Science &; Technology*, 56(16):11146–11161.

Efron, B. (1987). Better bootstrap confidence intervals. *Journal of the American Statistical Association*, 82(397):171–185.

Elder, C. D., Xu, X., Walker, J., Schnell, J. L., Hinkel, K. M., Townsend-Small, A., Arp, C. D., Pohlman, J. W., Gaglioti, B. V., and Czimczik, C. I. (2018). Greenhouse gas emissions from diverse arctic alaskan lakes are dominated by young carbon. *Nature Climate Change*, 8(2):166–171.

Emmerton, C. A., St. Louis, V. L., Lehnherr, I., Graydon, J. A., Kirk, J. L., and Rondeau, K. J. (2016). The importance of freshwater systems to the net atmospheric exchange of carbon dioxide and methane with a rapidly changing high arctic watershed. *Biogeosciences*, 13(20):5849–5863.

Euskirchen, E., McGUIRE, A. D., Kicklighter, D. W., Zhuang, Q., Clein, J. S., Dargaville, R., Dye, D., Kimball, J. S., McDonald, K. C., Melillo, J. M., et al. (2006). Importance of recent shifts in soil thermal dynamics on growing season length, productivity, and carbon sequestration in terrestrial high-latitude ecosystems. *Global Change Biology*, 12(4):731–750.

Fellman, J. B., Hood, E., and Spencer, R. G. M. (2010). Fluorescence spectroscopy opens new windows into dissolved organic matter dynamics in freshwater ecosystems: A review. *Limnology and Oceanography*, 55(6):2452–2462.

Feng, D., Gleason, C. J., Lin, P., Yang, X., Pan, M., and Ishitsuka, Y. (2021). Recent changes to arctic river discharge. *Nature communications*, 12(1):6917.

Fouché, J., Lafrenière, M. J., Rutherford, K., and Lamoureux, S. (2017). Seasonal hydrology and permafrost disturbance impacts on dissolved organic matter composition in high arctic headwater catchments. *Arctic Science*, 3(2):378–405.

Francis, A., Ganeshram, R. S., Tuerena, R. E., Spencer, R. G. M., Holmes, R. M., Rogers, J. A., and Mahaffey, C. (2023). Permafrost degradation and nitrogen cycling in arctic rivers: insights from stable nitrogen isotope studies. *Biogeosciences*, 20(2):365–382.

Frey, K. E. and McClelland, J. W. (2009). Impacts of permafrost degradation on arctic river biogeochemistry. *Hydrological Processes: An International Journal*, 23(1):169–182.

Frey, K. E., Sobczak, W. V., Mann, P. J., and Holmes, R. M. (2016). Optical properties and bioavailability of dissolved organic matter along a flow-path continuum from soil pore waters to the kolyma river mainstem, east siberia. *Biogeosciences*, 13(8):2279–2290.

Friedlingstein, P., O'Sullivan, M., Jones, M. W., Andrew, R. M., Gregor, L., Hauck, J., Le Quéré, C., Luijkx, I. T., Olsen, A., Peters, G. P., Peters, W., Pongratz, J., Schwingshackl, C., Sitch, S., Canadell, J. G., Ciais, P., Jackson, R. B., Alin, S. R., Alkama, R., Arneth, A., Arora, V. K., Bates, N. R., Becker, M., Bellouin, N., Bittig, H. C., Bopp, L., Chevallier, F., Chini, L. P., Cronin, M., Evans, W., Falk, S., Feely, R. A., Gasser, T., Gehlen, M., Gkritzalis, T., Gloege, L., Grassi, G., Gruber, N., Gürses, O., Harris, I., Hefner, M., Houghton, R. A., Hurtt, G. C., Iida, Y., Ilyina, T., Jain, A. K., Jersild, A., Kadono, K., Kato, E., Kennedy, D., Klein Goldewijk, K., Knauer, J., Korsbakken, J. I., Landschützer, P., Lefèvre, N., Lindsay, K., Liu, J., Liu, Z., Marland, G., Mayot, N., McGrath, M. J., Metzl, N., Monacci, N. M., Munro, D. R., Nakaoka, S.-I., Niwa, Y., O'Brien, K., Ono, T., Palmer, P. I., Pan, N., Pierrot, D., Pocock, K., Poulter, B., Resplandy, L., Robertson, E., Rödenbeck, C., Rodriguez, C., Rosan, T. M., Schwinger, J., Séférian, R., Shutler, J. D., Skjelvan, I., Steinhoff, T., Sun, Q., Sutton, A. J., Sweeney, C., Takao, S., Tanhua, T., Tans, P. P., Tian, X., Tian, H., Tilbrook, B., Tsujino, H., Tubiello, F., van der Werf, G. R., Walker, A. P., Wanninkhof, R., Whitehead, C., Willstrand Wranne, A., Wright, R., Yuan, W., Yue, C., Yue, X., Zaehle, S., Zeng, J., and Zheng, B. (2022). Global carbon budget 2022. *Earth System Science Data*, 14(11):4811–4900.

Frost, G., Macander, M., Bhatt, U., Berner, L., Bjerke, J., Epstein, H., Forbes, B., Lara, M., Magnússon, R. Í., Montesano, P., et al. (2023). Tundra greenness. *Arctic Report Card 2023*, page 67.

Giesler, R., Lyon, S. W., Mörth, C.-M., Karlsson, J., Karlsson, E., Jantze, E. J., Destouni, G., and Humborg, C. (2014). Catchment-scale dissolved carbon concentrations and export estimates across six subarctic streams in northern sweden. *Biogeosciences*, 11(2):525–537.

Gómez-Gener, L., Hotchkiss, E. R., Laudon, H., and Sponseller, R. A. (2021). Integrating discharge-concentration dynamics across carbon forms in a boreal landscape. *Water Resources Research*, 57(8):e2020WR028806.

Grosse, G., Jones, B. M., and Arp, C. D. (2013). Thermokarst lakes, drainage, and drained basins. *Treatise on geomorphology*, 8:325–353.

Grosse, G., Romanovsky, V., Walter, K., Morgenstern, A., Lantuit, H., and Zimov, S. (2008). Distribution of thermokarst lakes and ponds at three yedoma sites in siberia.

Grunert, B. K., Tzortziou, M., Neale, P., Menendez, A., and Hernes, P. (2021). Dom degradation by light and microbes along the yukon river-coastal ocean continuum. *Scientific Reports*, 11(1):10236.

Guebel, D. V. and Torres, N. V. (2013). *Partial Least-Squares Regression (PLSR)*, page 1646–1648. Springer New York.

Guillemette, F. and del Giorgio, P. A. (2011). Reconstructing the various facets of dissolved organic carbon bioavailability in freshwater ecosystems. *Limnology and Oceanography*, 56(2):734–748.

Guo, L., Ping, C., and Macdonald, R. W. (2007). Mobilization pathways of organic carbon from permafrost to arctic rivers in a changing climate. *Geophysical Research Letters*, 34(13).

Gómez-Gener, L., Hotchkiss, E. R., Laudon, H., and Sponseller, R. A. (2021). Integrating discharge-concentration dynamics across carbon forms in a boreal landscape. *Water Resources Research*, 57(8).

Hansen, A. M., Kraus, T. E. C., Pellerin, B. A., Fleck, J. A., Downing, B. D., and Bergamaschi, B. A. (2016). Optical properties of dissolved organic matter (dom): Effects of biological and photolytic degradation. *Limnology and Oceanography*, 61(3):1015–1032.

Harden, J. W., Koven, C. D., Ping, C.-L., Hugelius, G., David McGuire, A., Camill, P., Jorgenson, T., Kuhry, P., Michaelson, G. J., O'Donnell, J. A., et al. (2012). Field information links permafrost carbon to physical vulnerabilities of thawing. *Geophysical research letters*, 39(15).

Harms, T. K., Edmonds, J. W., Genet, H., Creed, I. F., Aldred, D., Balser, A., and Jones, J. B. (2016). Catchment influence on nitrate and dissolved organic matter in alaskan streams across a latitudinal gradient. *Journal of Geophysical Research: Biogeosciences*, 121(2):350–369.

Harms, T. K., Rocher-Ros, G., and Godsey, S. E. (2020). Emission of greenhouse gases from water tracks draining arctic hillslopes. *Journal of Geophysical Research: Biogeosciences*, 125(12).

Hassan, M., Talbot, J., Arsenault, J., Martinez-Cruz, K., Sepulveda-Jauregui, A., Hoyos-Santillan, J., and Lapierre, J. (2023). Linking dissolved organic matter to co2 and ch4 concentrations in canadian and chilean peatland pools. *Global Biogeochemical Cycles*, 37(4).

He, W., Chen, M., Schlautman, M. A., and Hur, J. (2016). Dynamic exchanges between dom and pom pools in coastal and inland aquatic ecosystems: A review. *Science of the Total Environment*, 551:415–428.

Heffernan, L., Kothawala, D. N., and Tranvik, L. J. (2024). Review article: Terrestrial dissolved organic carbon in northern permafrost. *The Cryosphere*, 18(3):1443–1465.

Helms, J. R., Stubbins, A., Ritchie, J. D., Minor, E. C., Kieber, D. J., and Mopper, K. (2008). Absorption spectral slopes and slope ratios as indicators of molecular weight, source, and photobleaching of chromophoric dissolved organic matter. *Limnology and Oceanography*, 53(3):955–969.

Hensgens, G., Laudon, H., Johnson, M. S., and Berggren, M. (2021). The undetected loss of aged carbon from boreal mineral soils. *Scientific Reports*, 11(1):6202.

Hersbach, H., Bell, B., Berrisford, P., Hirahara, S., Horányi, A., Muñoz-Sabater, J., Nicolas, J., Peubey, C., Radu, R., Schepers, D., Simmons, A., Soci, C., Abdalla, S., Abellan, X., Balsamo, G., Bechtold, P., Biavati, G., Bidlot, J., Bonavita, M., De Chiara, G., Dahlgren, P., Dee, D., Diamantakis, M., Dragani, R., Flemming, J., Forbes, R., Fuentes, M., Geer, A., Haimberger, L., Healy, S., Hogan, R. J., Hólm, E., Janisková, M., Keeley, S., Laloyaux, P., Lopez, P., Lupu, C., Radnoti, G., de Rosnay, P., Rozum, I., Vamborg, F., Villaume, S., and Thépaut, J. (2020). The era5 global reanalysis. *Quarterly Journal of the Royal Meteorological Society*, 146(730):1999–2049.

Hinkel, K. and Nelson, F. (2003). Spatial and temporal patterns of active layer thickness at circumpolar active layer monitoring (calm) sites in northern alaska, 1995–2000. *Journal of Geophysical Research: Atmospheres*, 108(D2).

Hinzman, L. D., Deal, C. J., McGuire, A. D., Mernild, S. H., Polyakov, I. V., and Walsh, J. E. (2013). Trajectory of the arctic as an integrated system. *Ecological Applications*, 23(8):1837–1868.

Holgerson, M. A. (2015). Drivers of carbon dioxide and methane supersaturation in small, temporary ponds. *Biogeochemistry*, 124(1):305–318.

Holgerson, M. A., Farr, E. R., and Raymond, P. A. (2017). Gas transfer velocities in small forested ponds. *Journal of Geophysical Research: Biogeosciences*, 122(5):1011–1021.

Holgerson, M. A. and Raymond, P. A. (2016). Large contribution to inland water co2 and ch4 emissions from very small ponds. *Nature Geoscience*, 9(3):222–226.

Hotchkiss, E., Hall Jr, R., Sponseller, R., Butman, D., Klaminder, J., Laudon, H., Rosvall, M., and Karlsson, J. (2015). Sources of and processes controlling co 2 emissions change with the size of streams and rivers. *Nature Geoscience*, 8(9):696–699.

Høye, T. T., Post, E., Meltofte, H., Schmidt, N. M., and Forchhammer, M. C. (2007). Rapid advancement of spring in the high arctic. *Current Biology*, 17(12):R449–R451.

Hu, M., Chen, D., and Dahlgren, R. A. (2016). Modeling nitrous oxide emission from rivers: a global assessment. *Global Change Biology*, 22(11):3566–3582.

Hugelius, G., Loisel, J., Chadburn, S., Jackson, R. B., Jones, M., MacDonald, G., Marushchak, M., Olefeldt, D., Packalen, M., Siewert, M. B., Treat, C., Turetsky, M., Voigt, C., and Yu, Z. (2020). Large stocks of peatland carbon and nitrogen are vulnerable to permafrost thaw. *Proceedings of the National Academy of Sciences*, 117(34):20438–20446.

Hugelius, G., Strauss, J., Zubrzycki, S., Harden, J. W., Schuur, E. A., Ping, C.-L., Schirrmeister, L., Grosse, G., Michaelson, G. J., Koven, C. D., et al. (2014). Estimated stocks of circumpolar permafrost carbon with quantified uncertainty ranges and identified data gaps. *Biogeosciences*, 11(23):6573–6593.

Huguet, A., Vacher, L., Relexans, S., Saubusse, S., Froidefond, J., and Parlanti, E. (2009). Properties of fluorescent dissolved organic matter in the gironde estuary. *Organic Geochemistry*, 40(6):706–719.

Hutchins, R. H. S., Aukes, P., Schiff, S. L., Dittmar, T., Prairie, Y. T., and del Giorgio, P. A. (2017). The optical, chemical, and molecular dissolved organic matter succession along a boreal soil-stream-river continuum. *Journal of Geophysical Research: Biogeosciences*, 122(11):2892–2908.

Ioannidis, J. P. (2005). Why most published research findings are false. *PLoS medicine*, 2(8):e124.

Iwahana, G., Takano, S., Petrov, R. E., Tei, S., Shingubara, R., Maximov, T. C., Fedorov, A. N., Desyatkin, A. R., Nikolaev, A. N., Desyatkin, R. V., and Sugimoto, A. (2014). Geocryological characteristics of the upper permafrost in a tundra-forest transition of the indigirka river valley, russia. *Polar Science*, 8(2):96–113.

Jähne, B., Heinz, G., and Dietrich, W. (1987). Measurement of the diffusion coefficients of sparingly soluble gases in water. *Journal of Geophysical Research: Oceans*, 92(C10):10767–10776.

Jansen, J., Thornton, B. F., Cortés, A., Snöälv, J., Wik, M., MacIntyre, S., and Crill, P. M. (2020). Drivers of diffusive ch 4 emissions from shallow subarctic lakes on daily to multi-year timescales. *Biogeosciences*, 17(7):1911–1932.

Johnston, S. E., Striegl, R. G., Bogard, M. J., Dornblaser, M. M., Butman, D. E., Kellerman, A. M., Wickland, K. P., Podgorski, D. C., and Spencer, R. G. M. (2020). Hydrologic connectivity deter-

mines dissolved organic matter biogeochemistry in northern high-latitude lakes. *Limnology and Oceanography*, 65(8):1764–1780.

Jonasson, S., Michelsen, A., and Schmidt, I. K. (1999). Coupling of nutrient cycling and carbon dynamics in the arctic, integration of soil microbial and plant processes. *Applied Soil Ecology*, 11(2-3):135–146.

Jones, B. M. and Arp, C. D. (2015). Observing a catastrophic thermokarst lake drainage in northern alaska. *Permafrost and Periglacial Processes*, 26(2):119–128.

Judd, K. E. and Kling, G. W. (2002). Production and export of dissolved c in arctic tundra mesocosms: the roles of vegetation and water flow. *Biogeochemistry*, 60(3):213–234.

Kane, D. L., Hinzman, L. D., and Zarling, J. P. (1991). Thermal response of the active layer to climatic warming in a permafrost environment. *Cold Regions Science and Technology*, 19(2):111–122.

Karavanova, E. (2013). Dissolved organic matter: Fractional composition and sorbability by the soil solid phase (review of literature). *Eurasian Soil Science*, 46(8):833–844.

Karlsson, J., Giesler, R., Persson, J., and Lundin, E. (2013). High emission of carbon dioxide and methane during ice thaw in high latitude lakes. *Geophysical Research Letters*, 40(6):1123–1127.

Karlsson, J., Serikova, S., Vorobyev, S. N., Rocher-Ros, G., Denfeld, B., and Pokrovsky, O. S. (2021). Carbon emission from western siberian inland waters. *Nature Communications*, 12(1).

Kellerman, A. M., Dittmar, T., Kothawala, D. N., and Tranvik, L. J. (2014). Chemodiversity of dissolved organic matter in lakes driven by climate and hydrology. *Nature Communications*, 5(1).

Kellerman, A. M., Guillemette, F., Podgorski, D. C., Aiken, G. R., Butler, K. D., and Spencer, R. G. M. (2018). Unifying concepts linking dissolved organic matter composition to persistence in aquatic ecosystems. *Environmental Science &; Technology*, 52(5):2538–2548.

Kellerman, A. M., Kothawala, D. N., Dittmar, T., and Tranvik, L. J. (2015). Persistence of dissolved organic matter in lakes related to its molecular characteristics. *Nature Geoscience*, 8(6):454–457.

Kelley, A., Hirst, C., Ebert, C., Axler, Z., Ledman, J., Opfergelt, S., and Schuur, E. (2026). Permafrost thaw exposes old dissolved organic carbon to photo-and biodegradation. *Environmental Research: Ecology*, 5(1):015003.

Kling, G. W., Kipphut, G. W., and Miller, M. C. (1991). Arctic lakes and streams as gas conduits to the atmosphere: Implications for tundra carbon budgets. *Science*, 251(4991):298–301.

Kling, G. W., Kipphut, G. W., Miller, M. M., and O'Brien, W. J. (2000). Integration of lakes and streams in a landscape perspective: the importance of material processing on spatial patterns and temporal coherence. *Freshwater Biology*, 43(3):477–497.

Knoblauch, C., Spott, O., Evgrafova, S., Kutzbach, L., and Pfeiffer, E. (2015). Regulation of methane production, oxidation, and emission by vascular plants and bryophytes in ponds of the northeast siberian polygonal tundra. *Journal of Geophysical Research: Biogeosciences*, 120(12):2525–2541.

Knutson, J. K., Clayer, F., Dörsch, P., Westermann, S., and de Wit, H. A. (2025). Water chemistry and greenhouse gas concentrations in waterbodies of a thawing permafrost peatland complex in northern norway. *Biogeosciences*, 22(15):3899–3914.

Koehler, B., Landelius, T., Weyhenmeyer, G. A., Machida, N., and Tranvik, L. J. (2014). Sunlight-induced carbon dioxide emissions from inland waters. *Global Biogeochemical Cycles*, 28(7):696–711.

Kolstad, E., Michelsen, A., and Ambus, P. L. (2021). Nitrous oxide surface fluxes in a low arctic heath: Effects of experimental warming along a natural snowmelt gradient. *Soil Biology and Biochemistry*, 160:108346.

Korak, J. A. and McKay, G. (2024). Meta-analysis of optical surrogates for the characterization of dissolved organic matter. *Environmental Science & Technology*, 58(17):7380.

Kortelainen, P., Larmola, T., Rantakari, M., Juutinen, S., Alm, J., and Martikainen, P. J. (2020). Lakes as nitrous oxide sources in the boreal landscape. *Global Change Biology*, 26(3):1432–1445.

Kortelainen, P., Rantakari, M., Huttunen, J. T., Mattsson, T., Alm, J., Juutinen, S., Larmola, T., Silvola, J., and Martikainen, P. J. (2006). Sediment respiration and lake trophic state are important predictors of large co2 evasion from small boreal lakes. *Global Change Biology*, 12(8):1554–1567.

Kothawala, D. N., Stedmon, C. A., Müller, R. A., Weyhenmeyer, G. A., Köhler, S. J., and Tranvik, L. J. (2014). Controls of dissolved organic matter quality: evidence from a large-scale boreal lake survey. *Global Change Biology*, 20(4):1101–1114.

Kothawala, D. N., Von Wachenfeldt, E., Koehler, B., and Tranvik, L. J. (2012). Selective loss and preservation of lake water dissolved organic matter fluorescence during long-term dark incubations. *Science of the Total Environment*, 433:238–246.

Krickov, I. V., Serikova, S., Pokrovsky, O. S., Vorobyev, S. N., Lim, A. G., Siewert, M. B., and Karlsson, J. (2021). Sizable carbon emission from the floodplain of ob river. *Ecological Indicators*, 131:108164.

Kuhn, M., Lundin, E. J., Giesler, R., Johansson, M., and Karlsson, J. (2018). Emissions from thaw ponds largely offset the carbon sink of northern permafrost wetlands. *Scientific Reports*, 8(1):9535.

Kuhn, M. A., Thompson, L. M., Winder, J. C., Braga, L. P. P., Tanentzap, A. J., Bastviken, D., and Olefeldt, D. (2021). Opposing effects of climate and permafrost thaw on ch4 and co2 emissions from northern lakes. *AGU Advances*, 2(4).

Kurek, M. R., Garcia-Tigreros, F., Wickland, K. P., Frey, K. E., Dornblaser, M. M., Striegl, R. G., Niles, S. F., McKenna, A. M., Aukes, P. J. K., Kyzivat, E. D., Wang, C., Pavelsky, T. M., Smith, L. C., Schiff, S. L., Butman, D., and Spencer, R. G. M. (2022). Hydrologic and landscape controls on dissolved organic matter composition across western north american arctic lakes. *Global Biogeochemical Cycles*, 37(1).

Kutzbach, L., Schneider, J., Sachs, T., Giebels, M., Nykänen, H., Shurpali, N., Martikainen, P., Alm, J., and Wilmking, M. (2007). Co 2 flux determination by closed-chamber methods can be seriously biased by inappropriate application of linear regression. *Biogeosciences*, 4(6):1005–1025.

Kuznetsova, A., Brockhoff, P. B., and Christensen, R. H. (2017). lmertest package: tests in linear mixed effects models. *Journal of statistical software*, 82:1–26.

Lambert, T., Bouillon, S., Darchambeau, F., Massicotte, P., and Borges, A. V. (2016). Shift in the chemical composition of dissolved organic matter in the congo river network. *Biogeosciences*, 13(18):5405–5420.

Lapierre, J.-F. and del Giorgio, P. A. (2014). Partial coupling and differential regulation of biologically and photochemically labile dissolved organic carbon across boreal aquatic networks. *Biogeosciences*, 11(20):5969–5985.

Lauerwald, R., Regnier, P., Figueiredo, V., Enrich-Prast, A., Bastviken, D., Lehner, B., Maavara,

T., and Raymond, P. (2019). Natural lakes are a minor global source of n2o to the atmosphere. *Global Biogeochemical Cycles*, 33(12):1564–1581.

Laurion, I., Massicotte, P., Mazoyer, F., Negandhi, K., and Mladenov, N. (2021). Weak mineralization despite strong processing of dissolved organic matter in eastern arctic tundra ponds. *Limnology and Oceanography*, 66(S1).

Laurion, I., Vincent, W. F., MacIntyre, S., Retamal, L., Dupont, C., Francus, P., and Pienitz, R. (2010). Variability in greenhouse gas emissions from permafrost thaw ponds. *Limnology and Oceanography*, 55(1):115–133.

Lawrence, D. M., Slater, A. G., and Swenson, S. C. (2012). Simulation of present-day and future permafrost and seasonally frozen ground conditions in ccsm4. *Journal of Climate*, 25(7):2207–2225.

Leith, F. I., Dinsmore, K. J., Wallin, M. B., Billett, M. F., Heal, K. V., Laudon, H., Öquist, M. G., and Bishop, K. (2015). Carbon dioxide transport across the hillslope–riparian–stream continuum in a boreal headwater catchment. *Biogeosciences*, 12(6):1881–1892.

Lenth, R. (2023). emmeans: Estimated marginal means, aka least-squares means_. *R package version 1.8. 5*.

Liljedahl, A. K., Boike, J., Daanen, R. P., Fedorov, A. N., Frost, G. V., Grosse, G., Hinzman, L. D., Iijma, Y., Jorgenson, J. C., Matveyeva, N., Necsoiu, M., Raynolds, M. K., Romanovsky, V. E., Schulla, J., Tape, K. D., Walker, D. A., Wilson, C. J., Yabuki, H., and Zona, D. (2016). Pan-arctic ice-wedge degradation in warming permafrost and its influence on tundra hydrology. *Nature Geoscience*, 9(4):312–318.

Linke, S., Lehner, B., Ouellet Dallaire, C., Ariwi, J., Grill, G., Anand, M., Beames, P., Burchard-Levine, V., Maxwell, S., Moidu, H., et al. (2019). Global hydro-environmental sub-basin and river reach characteristics at high spatial resolution. *Scientific data*, 6(1):283.

Liu, S., Kuhn, C., Amatulli, G., Aho, K., Butman, D. E., Allen, G. H., Lin, P., Pan, M., Yamazaki, D., Brinkerhoff, C., Gleason, C., Xia, X., and Raymond, P. A. (2022). The importance of hydrology in routing terrestrial carbon to the atmosphere via global streams and rivers. *Proceedings of the National Academy of Sciences*, 119(11).

Liu, Z., Kimball, J. S., Ballantyne, A., Watts, J. D., Natali, S. M., Rogers, B. M., Yi, Y., Klene, A. E., Moghaddam, M., Du, J., and Zona, D. (2023). Widespread deepening of the active layer in northern permafrost regions from 2003 to 2020. *Environmental Research Letters*, 19(1):014020.

Loidi, J., Navarro-Sánchez, G., and Vynokurov, D. (2022). Climatic definitions of the world's terrestrial biomes. *Vegetation Classification and Survey*, 3:231–271.

Lundin, E. J., Giesler, R., Persson, A., Thompson, M. S., and Karlsson, J. (2013). Integrating carbon emissions from lakes and streams in a subarctic catchment. *Journal of Geophysical Research: Biogeosciences*, 118(3):1200–1207.

Lundin, E. J., Klaminder, J., Bastviken, D., Olid, C., Hansson, S., and Karlsson, J. (2015). Large difference in carbon emission–burial balances between boreal and arctic lakes. *Scientific Reports*, 5(1):14248.

Lupon, A., Denfeld, B. A., Laudon, H., Leach, J., Karlsson, J., and Sponseller, R. A. (2019). Groundwater inflows control patterns and sources of greenhouse gas emissions from streams. *Limnology and Oceanography*, 64(4):1545–1557.

Lynch, L. M., Sutfin, N. A., Fegel, T. S., Boot, C. M., Covino, T. P., and Wallenstein, M. D. (2019). River channel connectivity shifts metabolite composition and dissolved organic matter chemistry. *Nature communications*, 10(1):459.

MacDonald, E. N., Tank, S. E., Kokelj, S. V., Froese, D. G., and Hutchins, R. H. S. (2021). Permafrost-derived dissolved organic matter composition varies across permafrost end-members in the western canadian arctic. *Environmental Research Letters*, 16(2):024036.

Macrae, M. L., Brown, L. C., Duguay, C. R., Parrott, J. A., and Petrone, R. M. (2014). Observed and projected climate change in the churchill region of the hudson bay lowlands and implications for pond sustainability. *Arctic, Antarctic, and Alpine Research*, 46(1):272–285.

Magnússon, R. Í., Groten, F., Bartholomeus, H., van Huissteden, K., and Heijmans, M. M. P. D. (2023). Tundra browning in the indigirka lowlands (north-eastern siberia) explained by drought, floods and small-scale vegetation shifts. *Journal of Geophysical Research: Biogeosciences*, 128(7).

Magnússon, R. Í., Limpens, J., van Huissteden, J., Kleijn, D., Maximov, T. C., Rotbarth, R., Sass-Klaassen, U., and Heijmans, M. M. P. D. (2020). Rapid vegetation succession and coupled permafrost dynamics in arctic thaw ponds in the siberian lowland tundra. *Journal of Geophysical Research: Biogeosciences*, 125(7).

Martikainen, P. J., Nykänen, H., Crill, P., and Silvola, J. (1993). Effect of a lowered water table on nitrous oxide fluxes from northern peatlands. *Nature*, 366(6450):51–53.

Martyn Rosco, M., Dean, J. F., Borges, A. V., Meisel, O. H., van Logtestijn, R., Hensgens, G., Karsanaev, S., Maximov, T., Weedon, J. T., Aerts, R., et al. (2025). The importance of inland water co2, ch4, and n2o for summertime greenhouse gas exchange with the atmosphere in arctic tundra lowlands. *Journal of Geophysical Research: Biogeosciences*, 130(6):e2024JG008334.

Materić, D., Ludewig, E., Xu, K., Röckmann, T., and Holzinger, R. (2018). Brief communication: Analysis of organic matter in surface snow by ptr-ms – implications for dry deposition dynamics in the alps.

Materić, D., Peacock, M., Kent, M., Cook, S., Gauci, V., Röckmann, T., and Holzinger, R. (2017). Characterisation of the semi-volatile component of dissolved organic matter by thermal desorption – proton transfer reaction – mass spectrometry. *Scientific Reports*, 7(1).

McCallister, S. L., Ishikawa, N. F., and Kothawala, D. N. (2018). Biogeochemical tools for characterizing organic carbon in inland aquatic ecosystems. *Limnology and Oceanography Letters*, 3(6):444–457.

McClain, M. E., Boyer, E. W., Dent, C. L., Gergel, S. E., Grimm, N. B., Groffman, P. M., Hart, S. C., Harvey, J. W., Johnston, C. A., Mayorga, E., et al. (2003). Biogeochemical hot spots and hot moments at the interface of terrestrial and aquatic ecosystems. *Ecosystems*, pages 301–312.

McCrystall, M. R., Stroeve, J., Serreze, M., Forbes, B. C., and Screen, J. A. (2021). New climate models reveal faster and larger increases in arctic precipitation than previously projected. *Nature Communications*, 12(1).

McGuire, A. D., Anderson, L. G., Christensen, T. R., Dallimore, S., Guo, L., Hayes, D. J., Heimann, M., Lorenson, T. D., Macdonald, R. W., and Roulet, N. (2009). Sensitivity of the carbon cycle in the arctic to climate change. *Ecological monographs*, 79(4):523–555.

McGuire, A. D., Lawrence, D. M., Koven, C., Clein, J. S., Burke, E., Chen, G., Jafarov, E., MacDougall, A. H., Marchenko, S., Nicolsky, D., et al. (2018). Dependence of the evolution of carbon dynamics in the northern permafrost region on the trajectory of climate change. *Proceedings of the National Academy of Sciences*, 115(15):3882–3887.

McKnight, D. M., Boyer, E. W., Westerhoff, P. K., Doran, P. T., Kulbe, T., and Andersen, D. T. (2001). Spectrofluorometric characterization of dissolved organic matter for indication of precursor organic material and aromaticity. *Limnology and Oceanography*, 46(1):38–48.

Meisel, O. H., Rijkers, R., Dean, J. F., in 't Zandt, M. H., van Huissteden, J., Maximov, T. C., Karsanaev, S. V., Belelli Marchesini, L., Goovaerts, A., Wacker, L., Reichart, G.-J., Bouillon, S., Welte, C. U., Jetten, M. S. M., Vonk, J. E., and Dolman, H. (2023). Geochemical, sedimentological and microbial diversity in two thermokarst lakes of far eastern siberia. *Biogeochemistry*, 165(3):239–263.

Meredith, M., Sommerkorn, M., Cassotta, S., Derksen, C., Ekaykin, A., Hollowed, A., Kofinas, G., Mackintosh, A., Melbourne-Thomas, J., Muelbert, M., et al. (2019). Polar regions. chapter 3, ipcc special report on the ocean and cryosphere in a changing climate.

Metcalfe, D. B., Hermans, T. D. G., Ahlstrand, J., Becker, M., Berggren, M., Björk, R. G., Björkman, M. P., Blok, D., Chaudhary, N., Chisholm, C., Classen, A. T., Hasselquist, N. J., Jonsson, M., Kristensen, J. A., Kumordzi, B. B., Lee, H., Mayor, J. R., Prevéy, J., Pantazatou, K., Rousk, J., Sponseller, R. A., Sundqvist, M. K., Tang, J., Uddling, J., Wallin, G., Zhang, W., Ahlström, A., Tenenbaum, D. E., and Abdi, A. M. (2018). Patchy field sampling biases understanding of climate change impacts across the arctic. *Nature Ecology &; Evolution*, 2(9):1443–1448.

Molot, L. A., Hudson, J. J., Dillon, P. J., and Miller, S. A. (2005). Effect of ph on photo-oxidation of dissolved organic carbon by hydroxyl radicals in a coloured, softwater stream. *Aquatic Sciences*, 67(2):189–195.

Morozumi, T., Shingubara, R., Murase, J., Nagai, S., Kobayashi, H., Takano, S., Tei, S., Fan, R., Maximov, T. C., and Sugimoto, A. (2019). Usability of water surface reflectance for the determination of riverine dissolved methane during extreme flooding in northeastern siberia. *Polar Science*, 21:186–194.

Mörsdorf, M. A., Baggesen, N. S., Yoccoz, N. G., Michelsen, A., Elberling, B., Ambus, P. L., and Cooper, E. J. (2020). Corrigendum to mörsdorf et al. (2019) "deepened winter snow significantly influences the availability and forms of nitrogen taken up by plants in high arctic tundra" [soil biology &; biochemistry 135 222–234]. *Soil Biology and Biochemistry*, 142:107654.

Mundy, C. J., Gosselin, M., Starr, M., and Michelc, C. (2009). Riverine export and the effects of circulation on dissolved organic carbon in the hudson bay system, canada. *Limnology and Oceanography*, 55(1):315–323.

Murphy, K. R., Stedmon, C. A., Graeber, D., and Bro, R. (2013). Fluorescence spectroscopy and multi-way techniques. parafac. *Analytical Methods*, 5(23):6557.

Murphy, K. R., Stedmon, C. A., Wenig, P., and Bro, R. (2014). Openfluor–an online spectral library of auto-fluorescence by organic compounds in the environment. *Analytical methods*, 6(3):658–661.

Muster, S., Langer, M., Heim, B., Westermann, S., and Boike, J. (2012). Subpixel heterogeneity of ice-wedge polygonal tundra: a multi-scale analysis of land cover and evapotranspiration in the lena river delta, siberia. *Tellus B: Chemical and Physical Meteorology*, 64(1):17301.

Muster, S., Roth, K., Langer, M., Lange, S., Cresto Aleina, F., Bartsch, A., Morgenstern, A., Grosse, G., Jones, B., Sannel, A. B. K., et al. (2017). Perl: A circum-arctic permafrost region pond and lake database. *Earth System Science Data*, 9(1):317–348.

Myers-Smith, I. H., Forbes, B. C., Wilmking, M., Hallinger, M., Lantz, T., Blok, D., Tape, K. D., Macias-Fauria, M., Sass-Klaassen, U., Lévesque, E., et al. (2011). Shrub expansion in tundra ecosystems: dynamics, impacts and research priorities. *Environmental Research Letters*, 6(4):045509.

Myers-Smith, I. H., Kerby, J. T., Phoenix, G. K., Bjerke, J. W., Epstein, H. E., Assmann, J. J., John, C., Andreu-Hayles, L., Angers-Blondin, S., Beck, P. S. A., Berner, L. T., Bhatt, U. S., Bjorkman, A. D., Blok, D., Bryn, A., Christiansen, C. T., Cornelissen, J. H. C., Cunliffe, A. M., Elmendorf,

S. C., Forbes, B. C., Goetz, S. J., Hollister, R. D., de Jong, R., Loranty, M. M., Macias-Fauria, M., Maseyk, K., Normand, S., Olofsson, J., Parker, T. C., Parmentier, F.-J. W., Post, E., Schaepman-Strub, G., Stordal, F., Sullivan, P. F., Thomas, H. J. D., Tømmervik, H., Treharne, R., Tweedie, C. E., Walker, D. A., Wilmking, M., and Wipf, S. (2020). Complexity revealed in the greening of the arctic. *Nature Climate Change*, 10(2):106–117.

Neilson, B. T., Cardenas, M. B., O'Connor, M. T., Rasmussen, M. T., King, T. V., and Kling, G. W. (2018). Groundwater flow and exchange across the land surface explain carbon export patterns in continuous permafrost watersheds. *Geophysical Research Letters*, 45(15):7596–7605.

Neubauer, S. C. and Megonigal, J. P. (2015). Moving beyond global warming potentials to quantify the climatic role of ecosystems. *Ecosystems*, 18(6):1000–1013.

Nitzbon, J., Westermann, S., Langer, M., Martin, L. C., Strauss, J., Laboor, S., and Boike, J. (2020). Fast response of cold ice-rich permafrost in northeast siberia to a warming climate. *Nature communications*, 11(1):2201.

Obernosterer, I. and Benner, R. (2004). Competition between biological and photochemical processes in the mineralization of dissolved organic carbon. *Limnology and Oceanography*, 49(1):117–124.

Obu, J., Westermann, S., Bartsch, A., Berdnikov, N., Christiansen, H. H., Dashtseren, A., Delaloye, R., Elberling, B., Etzelmüller, B., Kholodov, A., et al. (2019). Northern hemisphere permafrost map based on ttop modelling for 2000–2016 at 1 km2 scale. *Earth-Science Reviews*, 193:299–316.

O'Connor, M. T., Cardenas, M. B., Neilson, B. T., Nicholaides, K. D., and Kling, G. W. (2019). Active layer groundwater flow: The interrelated effects of stratigraphy, thaw, and topography. *Water Resources Research*, 55(8):6555–6576.

Ohno, T. (2002). Fluorescence inner-filtering correction for determining the humification index of dissolved organic matter. *Environmental Science &; Technology*, 36(4):742–746.

Oksanen, J., Blanchet, F. G., Kindt, R., Legendre, P., Minchin, P. R., O'hara, R., Simpson, G. L., Solymos, P., Stevens, M. H. H., Wagner, H., et al. (2013). Package 'vegan'. *Community ecology package, version*, 2(9):1–295.

Oliva, M. and Fritz, M. (2018). Permafrost degradation on a warmer earth: Challenges and perspectives. *Current Opinion in Environmental Science &; Health*, 5:14–18.

Overland, J., Hanna, E., Hanssen-Bauer, I., Kim, S., Walsh, J., Wang, M., Bhatt, U., Thoman, R., and Ballinger, T. (2019). Surface air temperature. *Arctic report card*, 5.

Pan, Q., Zhuo, X., He, C., Zhang, Y., and Shi, Q. (2020). Validation and evaluation of high-resolution orbitrap mass spectrometry on molecular characterization of dissolved organic matter. *ACS Omega*, 5(10):5372–5379.

Papale, D., Reichstein, M., Canfora, E., Aubinet, M., Bernhofer, C., Longdoz, B., Kutsch, W., Rambal, S., Valentini, R., Vesala, T., et al. (2006). Towards a more harmonized processing of eddy covariance co. *Algorithms*, 3:961–992.

Parlanti, E., Wörz, K., Geoffroy, L., and Lamotte, M. (2000). Dissolved organic matter fluorescence spectroscopy as a tool to estimate biological activity in a coastal zone submitted to anthropogenic inputs. *Organic Geochemistry*, 31(12):1765–1781.

Peacock, M., Materić, D., Kothawala, D. N., Holzinger, R., and Futter, M. N. (2018). Understanding dissolved organic matter reactivity and composition in lakes and streams using proton-transfer-reaction mass spectrometry (ptr-ms). *Environmental Science &; Technology Letters*, 5(12):739–744.

Pearson, R. G., Phillips, S. J., Loranty, M. M., Beck, P. S., Damoulas, T., Knight, S. J., and Goetz, S. J. (2013). Shifts in arctic vegetation and associated feedbacks under climate change. *Nature climate change*, 3(7):673–677.

Pedregosa, F., Varoquaux, G., Gramfort, A., Michel, V., Thirion, B., Grisel, O., Blondel, M., Prettenhofer, P., Weiss, R., Dubourg, V., et al. (2011). Scikit-learn: Machine learning in python. *the Journal of machine Learning research*, 12:2825–2830.

Peeters, F., Encinas Fernandez, J., and Hofmann, H. (2019). Sediment fluxes rather than oxic methanogenesis explain diffusive ch4 emissions from lakes and reservoirs. *Scientific Reports*, 9(1):243.

Peter Kershaw, G. and McCulloch, J. (2007). Midwinter snowpack variation across the arctic treeline, churchill, manitoba, canada. *Arctic, Antarctic, and Alpine Research*, 39(1):9–15.

Prėskienis, V., Fortier, D., Douglas, P. M., Rautio, M., and Laurion, I. (2024). Permafrost degradation and soil erosion as drivers of greenhouse gas emissions from tundra ponds. *Environmental Research Letters*, 19(1):014072.

Prėskienis, V., Laurion, I., Bouchard, F., Douglas, P. M., Billett, M. F., Fortier, D., and Xu, X. (2021). Seasonal patterns in greenhouse gas emissions from lakes and ponds in a high arctic polygonal landscape. *Limnology and Oceanography*, 66:S117–S141.

Prokushkin, A. S., Kawahigashi, M., and Tokareva, I. V. (2009). Global warming and dissolved organic carbon release from permafrost soils. In *Permafrost soils*, pages 237–250. Springer.

Prowse, T., Bring, A., Mård, J., Carmack, E., Holland, M., Instanes, A., Vihma, T., and Wrona, F. (2015). Arctic freshwater synthesis: Summary of key emerging issues. *Journal of Geophysical Research: Biogeosciences*, 120(10):1887–1893.

Quick, A. M., Reeder, W. J., Farrell, T. B., Tonina, D., Feris, K. P., and Benner, S. G. (2019). Nitrous oxide from streams and rivers: A review of primary biogeochemical pathways and environmental variables. *Earth-Science Reviews*, 191:224–262.

Ramage, J., Jungsberg, L., Meyer, A., and Gartler, S. (2022). 'no longer solid': perceived impacts of permafrost thaw in three arctic communities. *Polar Geography*, 45(3):226–239.

Ramage, J., Jungsberg, L., Wang, S., Westermann, S., Lantuit, H., and Heleniak, T. (2021). Population living on permafrost in the arctic. *Population and Environment*, 43(1):22–38.

Rantakari, M. and Kortelainen, P. (2005). Interannual variation and climatic regulation of the co2 emission from large boreal lakes. *Global Change Biology*, 11(8):1368–1380.

Rantanen, M., Karpechko, A. Y., Lipponen, A., Nordling, K., Hyvärinen, O., Ruosteenoja, K., Vihma, T., and Laaksonen, A. (2022). The arctic has warmed nearly four times faster than the globe since 1979. *Communications earth & environment*, 3(1):168.

Rasilo, T., Hutchins, R. H., Ruiz-González, C., and Del Giorgio, P. A. (2017). Transport and transformation of soil-derived co2, ch4 and doc sustain co2 supersaturation in small boreal streams. *Science of the Total Environment*, 579:902–912.

Rawlins, M. A., Steele, M., Holland, M. M., Adam, J. C., Cherry, J. E., Francis, J. A., Groisman, P. Y., Hinzman, L. D., Huntington, T. G., Kane, D. L., et al. (2010). Analysis of the arctic system for freshwater cycle intensification: Observations and expectations. *Journal of Climate*, 23(21):5715–5737.

Raymond, P. A., Hartmann, J., Lauerwald, R., Sobek, S., McDonald, C., Hoover, M., Butman, D., Striegl, R., Mayorga, E., Humborg, C., et al. (2013). Global carbon dioxide emissions from inland waters. *Nature*, 503(7476):355–359.

Raymond, P. A., McClelland, J. W., Holmes, R. M., Zhulidov, A. V., Mull, K., Peterson, B. J., Striegl, R. G., Aiken, G. R., and Gurtovaya, T. Y. (2007). Flux and age of dissolved organic carbon exported to the arctic ocean: A carbon isotopic study of the five largest arctic rivers. *Global Biogeochemical Cycles*, 21(4).

Raymond, P. A. and Spencer, R. G. (2015). riverine dom. *Biogeochemistry of marine dissolved organic matter*, 2.

Raymond, P. A., Zappa, C. J., Butman, D., Bott, T. L., Potter, J., Mulholland, P., Laursen, A. E., McDowell, W. H., and Newbold, D. (2012). Scaling the gas transfer velocity and hydraulic geometry in streams and small rivers. *Limnology and Oceanography: Fluids and Environments*, 2(1):41–53.

Raynolds, M. K., Walker, D. A., Balser, A., Bay, C., Campbell, M., Cherosov, M. M., Daniëls, F. J., Eidesen, P. B., Ermokhina, K. A., Frost, G. V., et al. (2019). A raster version of the circumpolar arctic vegetation map (cavm). *Remote Sensing of Environment*, 232:111297.

Rennert, K. J., Roe, G., Putkonen, J., and Bitz, C. M. (2009). Soil thermal and ecological impacts of rain on snow events in the circumpolar arctic. *Journal of Climate*, 22(9):2302–2315.

Repo, E., Huttunen, J., Naumov, A., Chichulin, A., Lapshina, E., Bleuten, W., and Martikainen, P. (2007). Release of co2 and ch4 from small wetland lakes in western siberia. *Tellus B: Chemical and Physical Meteorology*, 59(5):788–796.

Rey, S. J. and Anselin, L. (2009). Pysal: A python library of spatial analytical methods. In *Handbook of applied spatial analysis: Software tools, methods and applications*, pages 175–193. Springer.

Rocher-Ros, G., Giesler, R., Lundin, E., Salimi, S., Jonsson, A., and Karlsson, J. (2017). Large lakes dominate co2evasion from lakes in an arctic catchment. *Geophysical Research Letters*, 44(24).

Rodionow, A., Flessa, H., Kazansky, O., and Guggenberger, G. (2006). Organic matter composition and potential trace gas production of permafrost soils in the forest tundra in northern siberia. *Geoderma*, 135:49–62.

Roiha, T., Laurion, I., and Rautio, M. (2015). Carbon dynamics in highly heterotrophic subarctic thaw ponds. *Biogeosciences*, 12(23):7223–7237.

Rosentreter, J. A., Borges, A. V., Deemer, B. R., Holgerson, M. A., Liu, S., Song, C., Melack, J., Raymond, P. A., Duarte, C. M., Allen, G. H., et al. (2021). Half of global methane emissions come from highly variable aquatic ecosystem sources. *Nature Geoscience*, 14(4):225–230.

Rossum, V. (2009). Python 3 reference manual. *(No Title)*.

Rusydi, A. F. (2018). Correlation between conductivity and total dissolved solid in various type of water: A review. In *IOP conference series: earth and environmental science*, volume 118, page 012019. IOP publishing.

Schaefer, K., Lantuit, H., Romanovsky, V. E., Schuur, E. A., and Witt, R. (2014). The impact of the permafrost carbon feedback on global climate. *Environmental Research Letters*, 9(8):085003.

Schirrmeister, L., Kunitsky, V., Grosse, G., Wetterich, S., Meyer, H., Schwamborn, G., Babiy, O., Derevyagin, A., and Siegert, C. (2011). Sedimentary characteristics and origin of the late pleistocene ice complex on north-east siberian arctic coastal lowlands and islands–a review. *Quaternary international*, 241(1-2):3–25.

Schuur, E. A., Bockheim, J., Canadell, J. G., Euskirchen, E., Field, C. B., Goryachkin, S. V., Hagemann, S., Kuhry, P., Lafleur, P. M., Lee, H., et al. (2008). Vulnerability of permafrost carbon to climate change: Implications for the global carbon cycle. *BioScience*, 58(8):701–714.

Schuur, E. A., McGuire, A. D., Schädel, C., Grosse, G., Harden, J. W., Hayes, D. J., Hugelius, G., Koven, C. D., Kuhry, P., Lawrence, D. M., et al. (2015). Climate change and the permafrost carbon feedback. *Nature*, 520(7546):171–179.

Schuur, E. A., Vogel, J. G., Crummer, K. G., Lee, H., Sickman, J. O., and Osterkamp, T. (2009). The effect of permafrost thaw on old carbon release and net carbon exchange from tundra. *Nature*, 459(7246):556–559.

Schwab, M. S., Hilton, R. G., Raymond, P. A., Haghipour, N., Amos, E., Tank, S. E., Holmes, R. M., Tipper, E. T., and Eglinton, T. I. (2020). An abrupt aging of dissolved organic carbon in large arctic rivers. *Geophysical Research Letters*, 47(23).

Seabold, S., Perktold, J., et al. (2010). Statsmodels: econometric and statistical modeling with python. *SciPy*, 7(1):92–96.

Sepulveda-Jauregui, A., Walter Anthony, K., Martinez-Cruz, K., Greene, S., and Thalasso, F. (2015). Methane and carbon dioxide emissions from 40 lakes along a north–south latitudinal transect in alaska. *Biogeosciences*, 12(11):3197–3223.

Serikova, S., Pokrovsky, O., Ala-Aho, P., Kazantsev, V., Kirpotin, S., Kopysov, S., Krickov, I., Laudon, H., Manasypov, R., Shirokova, L., et al. (2018). High riverine co2 emissions at the permafrost boundary of western siberia. *Nature Geoscience*, 11(11):825–829.

Serikova, S., Pokrovsky, O., Laudon, H., Krickov, I., Lim, A., Manasypov, R., and Karlsson, J. (2019). High carbon emissions from thermokarst lakes of western siberia. *Nature Communications*, 10(1):1552.

Serreze, M. C. and Barry, R. G. (2011). Processes and impacts of arctic amplification: A research synthesis. *Global and planetary change*, 77(1-2):85–96.

Shahgedanova, M. (2003). *The physical geography of northern Eurasia*, volume 3. Oxford University Press.

Shirokova, L., Payandi-Rolland, D., Lim, A., Manasypov, R., Allen, J., Rols, J.-L., Bénézeth, P., Karlsson, J., and Pokrovsky, O. (2020). Diel cycles of carbon, nutrient and metal in humic lakes of permafrost peatlands. *Science of The Total Environment*, 737:139671.

Shogren, A. J., Zarnetske, J. P., Abbott, B. W., Grose, A. L., Rec, A. F., Nipko, J., Song, C., O'Donnell, J. A., and Bowden, W. B. (2024). Hydrology controls dissolved organic carbon and nitrogen export and post-storm recovery in two arctic headwaters. *Journal of Geophysical Research: Biogeosciences*, 129(2).

Shogren, A. J., Zarnetske, J. P., Abbott, B. W., Iannucci, F., and Bowden, W. B. (2020a). We cannot shrug off the shoulder seasons: Addressing knowledge and data gaps in an arctic headwater. *Environmental Research Letters*, 15(10):104027.

Shogren, A. J., Zarnetske, J. P., Abbott, B. W., Iannucci, F., Medvedeff, A., Cairns, S., Duda, M. J., and Bowden, W. B. (2020b). Arctic concentration–discharge relationships for dissolved organic carbon and nitrate vary with landscape and season. *Limnology and Oceanography*, 66(S1).

Siewert, M. B., Hanisch, J., Weiss, N., Kuhry, P., Maximov, T. C., and Hugelius, G. (2015). Comparing carbon storage of siberian tundra and taiga permafrost ecosystems at very high spatial resolution. *Journal of Geophysical Research: Biogeosciences*, 120(10):1973–1994.

Smith, S. L., O'Neill, H. B., Isaksen, K., Noetzli, J., and Romanovsky, V. E. (2022). The changing thermal state of permafrost. *Nature Reviews Earth & Environment*, 3(1):10–23.

Soued, C., del Giorgio, P. A., and Maranger, R. (2015). Nitrous oxide sinks and emissions in boreal aquatic networks in québec. *Nature Geoscience*, 9(2):116–120.

Speetjens, N. J., Tanski, G., Martin, V., Wagner, J., Richter, A., Hugelius, G., Boucher, C., Lodi, R., Knoblauch, C., Koch, B. P., Wünsch, U., Lantuit, H., and Vonk, J. E. (2022). Dissolved organic matter characterization in soils and streams in a small coastal low-arctic catchment. *Biogeosciences*, 19(12):3073–3097.

Spencer, R. G. M., Aiken, G. R., Butler, K. D., Dornblaser, M. M., Striegl, R. G., and Hernes, P. J. (2009). Utilizing chromophoric dissolved organic matter measurements to derive export and reactivity of dissolved organic carbon exported to the arctic ocean: A case study of the yukon river, alaska. *Geophysical Research Letters*, 36(6).

Spencer, R. G. M., Butler, K. D., and Aiken, G. R. (2012). Dissolved organic carbon and chromophoric dissolved organic matter properties of rivers in the usa. *Journal of Geophysical Research: Biogeosciences*, 117(G3).

Stackpoole, S. M., Butman, D. E., Clow, D. W., Verdin, K. L., Gaglioti, B. V., Genet, H., and Striegl, R. G. (2017). Inland waters and their role in the carbon cycle of alaska. *Ecological Applications*, 27(5):1403–1420.

Stedmon, C. A., Markager, S., and Bro, R. (2003). Tracing dissolved organic matter in aquatic environments using a new approach to fluorescence spectroscopy. *Marine Chemistry*, 82(3–4):239–254.

Stephens, P. A., Buskirk, S. W., Hayward, G. D., and Martinez Del Rio, C. (2005). Information theory and hypothesis testing: a call for pluralism. *Journal of Applied Ecology*, 42(1):4–12.

Street, L. E., Dean, J. F., Billett, M. F., Baxter, R., Dinsmore, K. J., Lessels, J. S., Subke, J., Tetzlaff, D., and Wookey, P. A. (2016). Redox dynamics in the active layer of an arctic headwater catchment; examining the potential for transfer of dissolved methane from soils to stream water. *Journal of Geophysical Research: Biogeosciences*, 121(11):2776–2792.

Striegl, R. G., Aiken, G. R., Dornblaser, M. M., Raymond, P. A., and Wickland, K. P. (2005). A decrease in discharge-normalized doc export by the yukon river during summer through autumn. *Geophysical research letters*, 32(21).

Stubbins, A., Lapierre, J.-F., Berggren, M., Prairie, Y. T., Dittmar, T., and del Giorgio, P. A. (2014). What's in an eem? molecular signatures associated with dissolved organic fluorescence in boreal canada. *Environmental Science &; Technology*, 48(18):10598–10606.

Tank, S. E., Fellman, J. B., Hood, E., and Kritzberg, E. S. (2018). Beyond respiration: Controls on lateral carbon fluxes across the terrestrial-aquatic interface. *Limnology and Oceanography Letters*, 3(3):76–88.

Tank, S. E., Lesack, L. F., Gareis, J. A., Osburn, C. L., and Hesslein, R. H. (2011). Multiple tracers demonstrate distinct sources of dissolved organic matter to lakes of the mackenzie delta, western canadian arctic. *Limnology and Oceanography*, 56(4):1297–1309.

Tank, S. E., Vonk, J. E., Walvoord, M. A., McClelland, J. W., Laurion, I., and Abbott, B. W. (2020). Landscape matters: Predicting the biogeochemical effects of permafrost thaw on aquatic networks with a state factor approach. *Permafrost and Periglacial Processes*, 31(3):358–370.

Tarnocai, C. (2009). Arctic permafrost soils. In *Permafrost soils*, pages 3–16. Springer.

Team, R. C. et al. (2016). R: A language and environment for statistical computing. r foundation for statistical computing, vienna, austria. *http://www. R-project. org/*.

Tei, S., Morozumi, T., Nagai, S., Takano, S., Sugimoto, A., Shingubara, R., Fan, R., Fedorov, A., Gavrilyeva, T., Tananaev, N., et al. (2020). An extreme flood caused by a heavy snowfall over the indigirka river basin in northeastern siberia. *Hydrological Processes*, 34(3):522–537.

Thackeray, C. W., Derksen, C., Fletcher, C. G., and Hall, A. (2019). Snow and climate: Feedbacks, drivers, and indices of change. *Current Climate Change Reports*, 5(4):322–333.

Treat, C. C., Virkkala, A.-M., Burke, E., Bruhwiler, L., Chatterjee, A., Fisher, J. B., Hashemi, J., Parmentier, F.-J. W., Rogers, B. M., Westermann, S., et al. (2024). Permafrost carbon: Progress on understanding stocks and fluxes across northern terrestrial ecosystems. *Journal of Geophysical Research: Biogeosciences*, 129(3):e2023JG007638.

Trouet, V. and Van Oldenborgh, G. J. (2013). Knmi climate explorer: a web-based research tool for high-resolution paleoclimatology. *Tree-Ring Research*, 69(1):3–13.

Turetsky, M. R., Abbott, B. W., Jones, M. C., Anthony, K. W., Olefeldt, D., Schuur, E. A., Grosse, G., Kuhry, P., Hugelius, G., Koven, C., et al. (2020). Carbon release through abrupt permafrost thaw. *Nature Geoscience*, 13(2):138–143.

Vachon, D., Prairie, Y. T., and Cole, J. J. (2010). The relationship between near-surface turbulence and gas transfer velocity in freshwater systems and its implications for floating chamber measurements of gas exchange. *Limnology and Oceanography*, 55(4):1723–1732.

van Everdingen, R. O. (1998). *Multi-Language Glossary of Permafrost and Related Ground-Ice Terms*. The Arctic Institute of North America, University of Calgary, Calgary, Alberta, Canada. Revised edition 2005.

van Huissteden, J., Teshebaeva, K., Cheung, Y., Magnússon, R. Í., Noorbergen, H., Karsanaev, S. V., Maximov, T. C., and Dolman, A. J. (2021). Geomorphology and insar-tracked surface displacements in an ice-rich yedoma landscape. *Frontiers in Earth Science*, 9.

Venkiteswaran, J. J., Schiff, S. L., and Wallin, M. B. (2014). Large carbon dioxide fluxes from headwater boreal and sub-boreal streams. *PLoS ONE*, 9(7):e101756.

Virtanen, P., Gommers, R., Oliphant, T. E., Haberland, M., Reddy, T., Cournapeau, D., Burovski, E., Peterson, P., Weckesser, W., Bright, J., van der Walt, S. J., Brett, M., Wilson, J., Millman, K. J., Mayorov, N., Nelson, A. R. J., Jones, E., Kern, R., Larson, E., Carey, C. J., Polat, I., Feng, Y., Moore, E. W., VanderPlas, J., Laxalde, D., Perktold, J., Cimrman, R., Henriksen, I., Quintero, E. A., Harris, C. R., Archibald, A. M., Ribeiro, A. H., Pedregosa, F., van Mulbregt, P., Vijaykumar, A., Bardelli, A. P., Rothberg, A., Hilboll, A., Kloeckner, A., Scopatz, A., Lee, A., Rokem, A., Woods, C. N., Fulton, C., Masson, C., Häggström, C., Fitzgerald, C., Nicholson, D. A., Hagen, D. R., Pasechnik, D. V., Olivetti, E., Martin, E., Wieser, E., Silva, F., Lenders, F., Wilhelm, F., Young, G., Price, G. A., Ingold, G.-L., Allen, G. E., Lee, G. R., Audren, H., Probst, I., Dietrich, J. P., Silterra, J., Webber, J. T., Slavič, J., Nothman, J., Buchner, J., Kulick, J., Schönberger, J. L., de Miranda Cardoso, J. V., Reimer, J., Harrington, J., Rodríguez, J. L. C., Nunez-Iglesias, J., Kuczynski, J., Tritz, K., Thoma, M., Newville, M., Kümmerer, M., Bolingbroke, M., Tartre, M., Pak, M., Smith, N. J., Nowaczyk, N., Shebanov, N., Pavlyk, O., Brodtkorb, P. A., Lee, P., McGibbon, R. T., Feldbauer, R., Lewis, S., Tygier, S., Sievert, S., Vigna, S., Peterson, S., More, S., Pudlik, T., Oshima, T., Pingel, T. J., Robitaille, T. P., Spura, T., Jones, T. R., Cera, T., Leslie, T., Zito, T., Krauss, T., Upadhyay, U., Halchenko, Y. O., and Vázquez-Baeza, Y. (2020). Scipy 1.0: fundamental algorithms for scientific computing in python. *Nature Methods*, 17(3):261–272.

Vitousek, P. M., Aber, J. D., Howarth, R. W., Likens, G. E., Matson, P. A., Schindler, D. W., Schlesinger, W. H., and Tilman, D. G. (1997). Human alteration of the global nitrogen cycle: sources and consequences. *Ecological applications*, 7(3):737–750.

Voigt, C., Marushchak, M. E., Abbott, B. W., Biasi, C., Elberling, B., Siciliano, S. D., Sonnentag, O., Stewart, K. J., Yang, Y., and Martikainen, P. J. (2020). Nitrous oxide emissions from permafrost-affected soils. *Nature Reviews Earth & Environment*, 1(8):420–434.

Voigt, C., Marushchak, M. E., Lamprecht, R. E., Jackowicz-Korczyński, M., Lindgren, A., Mastepanov, M., Granlund, L., Christensen, T. R., Tahvanainen, T., Martikainen, P. J., and Biasi, C. (2017). Increased nitrous oxide emissions from arctic peatlands after permafrost thaw. *Proceedings of the National Academy of Sciences*, 114(24):6238–6243.

Vonk, J. E., Tank, S. E., Bowden, W. B., Laurion, I., Vincent, W. F., Alekseychik, P., Amyot, M., Billet, M. F., Canário, J., Cory, R. M., Deshpande, B. N., Helbig, M., Jammet, M., Karlsson, J., Larouche, J., MacMillan, G., Rautio, M., Walter Anthony, K. M., and Wickland, K. P. (2015). Reviews and syntheses: Effects of permafrost thaw on arctic aquatic ecosystems. *Biogeosciences*, 12(23):7129–7167.

Vorobyev, S. N., Karlsson, J., Kolesnichenko, Y. Y., Korets, M. A., and Pokrovsky, O. S. (2021). Fluvial carbon dioxide emission from the lena river basin during the spring flood. *Biogeosciences*, 18(17):4919–4936.

Waggoner, D. C., Chen, H., Willoughby, A. S., and Hatcher, P. G. (2015). Formation of black carbon-like and alicyclic aliphatic compounds by hydroxyl radical initiated degradation of lignin. *Organic Geochemistry*, 82:69–76.

Walker, D. A., Raynolds, M. K., Daniëls, F. J., Einarsson, E., Elvebakk, A., Gould, W. A., Katenin, A. E., Kholod, S. S., Markon, C. J., Melnikov, E. S., et al. (2005). The circumpolar arctic vegetation map. *Journal of vegetation science*, 16(3):267–282.

Walker, S. A., Amon, R. M., and Stedmon, C. A. (2013). Variations in high-latitude riverine fluorescent dissolved organic matter: A comparison of large arctic rivers. *Journal of Geophysical Research: Biogeosciences*, 118(4):1689–1702.

Walter, K. M., Zimov, S. A., Chanton, J. P., Verbyla, D., and Chapin, F. S. (2006). Methane bubbling from siberian thaw lakes as a positive feedback to climate warming. *Nature*, 443(7107):71–75.

Walvoord, M. A. and Kurylyk, B. L. (2016). Hydrologic impacts of thawing permafrost—a review. *Vadose Zone Journal*, 15(6):1–20.

Wang, J.-J., Lafrenière, M. J., Lamoureux, S. F., Simpson, A. J., Gélinas, Y., and Simpson, M. J. (2018). Differences in riverine and pond water dissolved organic matter composition and sources in canadian high arctic watersheds affected by active layer detachments. *Environmental Science &; Technology*, 52(3):1062–1071.

Wang, Z., Wu, R., Chen, Z., Huang, G., and Yang, X. (2022). Reasons for east siberia winter snow water equivalent increase in the recent decades. *Remote Sensing*, 15(1):134.

Wanninkhof, R. (2014). Relationship between wind speed and gas exchange over the ocean revisited. *Limnology and Oceanography: Methods*, 12(6):351–362.

Ward, C. P. and Cory, R. M. (2016). Complete and partial photo-oxidation of dissolved organic matter draining permafrost soils. *Environmental Science &; Technology*, 50(7):3545–3553.

Ward, N. D., Bianchi, T. S., Medeiros, P. M., Seidel, M., Richey, J. E., Keil, R. G., and Sawakuchi, H. O. (2017). Where carbon goes when water flows: Carbon cycling across the aquatic continuum. *Frontiers in Marine Science*, 4.

Wauthy, M., Rautio, M., Christoffersen, K. S., Forsström, L., Laurion, I., Mariash, H. L., Peura, S., and Vincent, W. F. (2018). Increasing dominance of terrigenous organic matter in circumpolar freshwaters due to permafrost thaw. *Limnology and Oceanography Letters*, 3(3):186–198.

Webb, J. R., Santos, I. R., Maher, D. T., and Finlay, K. (2019). The importance of aquatic carbon fluxes in net ecosystem carbon budgets: A catchment-scale review. *Ecosystems*, 22(3):508–527.

Weishaar, J. L., Aiken, G. R., Bergamaschi, B. A., Fram, M. S., Fujii, R., and Mopper, K. (2003). Evaluation of specific ultraviolet absorbance as an indicator of the chemical composition and reactivity of dissolved organic carbon. *Environmental science & technology*, 37(20):4702–4708.

Weiss, R. (1974). Carbon dioxide in water and seawater: the solubility of a non-ideal gas. *Marine chemistry*, 2(3):203–215.

Weiss, R. F. and Price, B. (1980). Nitrous oxide solubility in water and seawater. *Marine chemistry*, 8(4):347–359.

Wheeler, K., Levia, D., and Hudson, J. (2017). Tracking senescence-induced patterns in leaf litter leachate using parallel factor analysis (parafac) modeling and self-organizing maps. *Journal of Geophysical Research: Biogeosciences*, 122(9):2233–2250.

Wik, M., Varner, R. K., Anthony, K. W., MacIntyre, S., and Bastviken, D. (2016). Climate-sensitive northern lakes and ponds are critical components of methane release. *Nature Geoscience*, 9(2):99–105.

Williamson, C. E., Dodds, W., Kratz, T. K., and Palmer, M. A. (2008). Lakes and streams as sentinels of environmental change in terrestrial and atmospheric processes. *Frontiers in Ecology and the Environment*, 6(5):247–254.

Wolf, D., Klemann, V., Wünsch, J., and Zhang, F.-p. (2006). A reanalysis and reinterpretation of geodetic and geological evidence of glacial-isostatic adjustment in the churchill region, hudson bay. *Surveys in Geophysics*, 27(1):19–61.

Wolfe, B. B., Light, E. M., Macrae, M. L., Hall, R. I., Eichel, K., Jasechko, S., White, J., Fishback, L., and Edwards, T. W. D. (2011). Divergent hydrological responses to 20th century climate change in shallow tundra ponds, western hudson bay lowlands: Pond hydrological response to warming. *Geophysical Research Letters*, 38(23).

Wologo, E., Shakil, S., Zolkos, S., Textor, S., Ewing, S., Klassen, J., Spencer, R. G. M., Podgorski, D. C., Tank, S. E., Baker, M. A., O'Donnell, J. A., Wickland, K. P., Foks, S. S. W., Zarnetske, J. P., Lee-Cullin, J., Liu, F., Yang, Y., Kortelainen, P., Kolehmainen, J., Dean, J. F., Vonk, J. E., Holmes, R. M., Pinay, G., Powell, M. M., Howe, J., Frei, R. J., Bratsman, S. P., and Abbott, B. W. (2021). Stream dissolved organic matter in permafrost regions shows surprising compositional similarities but negative priming and nutrient effects. *Global Biogeochemical Cycles*, 35(1).

Woo, M.-k. (2011). *Active Layer Dynamics*, page 163–227. Springer Berlin Heidelberg.

Wrona, F. J., Johansson, M., Culp, J. M., Jenkins, A., Mård, J., Myers-Smith, I. H., Prowse, T. D., Vincent, W. F., and Wookey, P. A. (2016). Transitions in arctic ecosystems: Ecological implications of a changing hydrological regime. *Journal of Geophysical Research: Biogeosciences*, 121(3):650–674.

Wu, T., Wang, D., Mu, C., Zhang, W., Zhu, X., Zhao, L., Li, R., Hu, G., Zou, D., Chen, J., et al. (2022). Storage, patterns, and environmental controls of soil organic carbon stocks in the permafrost regions of the northern hemisphere. *Science of the Total Environment*, 828:154464.

Xu, W., Frendrup, L. L., Michelsen, A., Elberling, B., and Ambus, P. L. (2023). Deepened snow in combination with summer warming increases growing season nitrous oxide emissions in dry tundra, but not in wet tundra. *Soil Biology and Biochemistry*, 180:109013.

Yamamoto, S., Alcauskas, J. B., and Crozier, T. E. (1976). Solubility of methane in distilled water and seawater. *Journal of Chemical &; Engineering Data*, 21(1):78–80.

Yvon-Durocher, G., Allen, A. P., Bastviken, D., Conrad, R., Gudasz, C., St-Pierre, A., Thanh-Duc, N., and del Giorgio, P. A. (2014). Methane fluxes show consistent temperature dependence across microbial to ecosystem scales. *Nature*, 507(7493):488–491.

Zakharova, E., Kouraev, A., Kolmakova, M., Mognard, N., Zemtsov, V., and Kirpotin, S. (2009). The modern hydrological regime of the northern part of western siberia fromin situand satellite observations. *International Journal of Environmental Studies*, 66(4):447–463.

Zolkos, S., Tank, S. E., Kokelj, S. V., Striegl, R. G., Shakil, S., Voigt, C., Sonnentag, O., Quinton, W. L., Schuur, E. A. G., Zona, D., Lafleur, P. M., Sullivan, R. C., Ueyama, M., Billesbach, D.,

Cook, D., Humphreys, E. R., and Marsh, P. (2022). Permafrost landscape history shapes fluvial chemistry, ecosystem carbon balance, and potential trajectories of future change. *Global Biogeochemical Cycles*, 36(9).

Zuur, A. F., Ieno, E. N., Walker, N. J., Saveliev, A. A., Smith, G. M., et al. (2009). *Mixed effects models and extensions in ecology with R*, volume 574. Springer.

ACKNOWLEDGEMENTS

Josh, thank you for believing in me almost ten years ago, when I was still an MSc student, and for your guidance throughout everything that has followed. Thank you especially for sticking with me through this project, even though you didn't have to. Thank you for always making time for me, for giving me the independence and trust to develop as a researcher in my own way, and for being open to adapting to ways of working that suited me. A big thank you, too, for always reminding me that science is fun and isn't only done right when taken super serious. Thank you for the many chats about science, life, and everything in between. Thank you for being a great mentor and friend!

James, thank you for coming on as a supervisor halfway through my PhD and providing great and much needed support and advice at a time when I really needed it. Han and Jorien, thank you for hiring me for this position. Thanks to my student Matthias for his field support and for being a great MSc student, and thanks to Joost for his assistance in the field. Thank you to Ron for all his work developing the whole sensor set-up I dreamed up, especially for making the ultrasonic sensors. A massive thank you to Vicente, without you we would have not gotten any material or equipment to Churchill, I hope you are enjoying your well deserved retirement back in Spain. Big thanks to Sheldon for not only being an awesome bear guard during our time in the field but also for all the chats and laughs. Thank you to all the staff at Churchill Northern Studies Centre for making our time there so enjoyable and for all your help with logistics and fieldwork, and to all the other scientist at the station for making our time there so enjoyable.

Geert, thank you for all the fieldwork conversations where we could sit together and wonder what on earth we were doing. I always appreciated that we could ask each other questions, no matter how basic, without ever feeling judged. Thank you for the many conversations about science, life, and everything in between enjoiyng meals with srirachi in Churchill or taste testing olives all around Mallorca. Thank you also to Jeremy, Yousef, Fleur, Jim, Alexa, Tan, Ove, Roland, Kirsi and Dirk for being lovely colleagues.

Nils, we've known each other since our customer service days. Thank you for being such a constant presence in my life since then and throughout my PhD. From our long walks during the pandemic, evenings spent playing Mario Kart or Super Smash Bros., and all the conversations in between, your friendship carried me through more than you know. Thank you for always listening to whatever insane story this PhD had produced that week. To you and Günes, thank you for always making me feel so welcome in your home. Being able to stop by for dinner on my way home from preparing for field season or simply knowing your door was always open means the world to me. I feel incredibly lucky to call you both my friends.

To the Spanish Amsterdam OG's: Isis no se que decrite la verdad, ya sabes lo bien que se me dan las palabras. Thank you for always making time to support me even if it was hoping on a zoom call so I could ask whether my statistical approach made sense,

and for putting up with all my rants. Pero sobre todo por haber crecido juntas estos 10 anios, I'm very grateful that we have kept choosing each other through everything - eres familia (será que el banio de De School era magico). Ernesto, thank you for being my unofficial figure supervisor. I really appreciated all your advice over the years, being able to chat news, politics and just general life thoughts and observations but even more, all the laughs along the way - never forget the oompa loompa de las basuras. Finishing the PhD with our trip through Guatemala and Belize was the perfect way to celebrate, could not imagine laughing while getting pelted with rain on a 2 hour boat ride after having to emergency leave our palace with anyone else. Andrea creo que nadie entiende mejor que tu mis sentimentios y pensamientos acerca de lo que ha sido el doctorado por varias razones, agradezco mucho tenerte como amiga y saber que podemos compartir nuestras experiencas y asegurarnos de que para nosotras son validas. Yago muchas gracias por todas las conversaciones y risas, agradezco mucho las tardes con vosotros en vuestro jardin. Pablo, no podría iamginarme mejor cosa que hacer que trabajar juntos en Zanzibar antes de embarcar en un doctorado! Muchas gracias por la oportunidad pero sobre todo por lo divertido que fue hacerlo juntos! Y por todos los otros momentos como navidades y noche viejas juntos, y por seguir haciendo tiempo para vernos cuando estas por Amsterdam, lo agradezco mucho. A todos vosotros, gracias por ser una parte tan importante de mi vida.

Egon, thank you for being such a genuinely kind and thoughtful person, you have a remarkable ability to make the people around you feel calmer and happier. Whether it was going out dancing, festivals in Poland or Portugal, talking through whatever life had thrown our way, our anxieties, or my frustrations with statistics in academia because I knew you would get it, or simply being there when I needed a friend or a place to crash—even helping me move four times in less than two months—I always knew I could count on you. I hope you know you can always count on me. Dani, thank you for being the wholesome and fun friend that you are, the way you move through life and who you are is very inspring to me. From nights and days out dancing to boardgames to many conversations in between, I feel very seen and understood by you and I'm very grateful to have you in my life. Geoffrey, thank you for all the conversations about academia and for reminding me that the PhD struggles aren't unique to my field, and for all the times spent dancing to happy music and eating noodles all over Amsterdam. Eugenia, I'm really glad we've became friends. Even though we've only known each other for a relatively short time, it certainly doesn't feel that way and I can't wait for many more adventures together. Nora, Alfredo, Jemima and Lydia thank you for contributing to making so many great memories in Amsterdam.

To my dear acting friends: Nehmi, Andrea, Heather, Susie, thank you for making the acting journey even more enjoyable through all our chats and laughs and helping it be such a healing experience. Beyond that thank you for being such a wonderful group of friends, I love our outings to the cinema and shows, dinners and knowing you're a call away if a chat is needed. I feel very lucky to have met you all.

Betty and Amber, thank you for being such an important parts of my life since our bachelor days in Dundee. Despite the distance, you've remained two of my closest friends. Betty, all the way from doing crazy activites like jumping through sprinklers during Easter

holidays in first year to recently my PhD times. Also thank you for asking me every year since first year when this PhD was finally going to be finished - I'm very happy to finally be able to say that it is! Thank you Amber not only for your friendship but all our fun trips together too, out backpacking trip in 2016 remains one of my favourite travels and I'm very grateful that you are always up for adventures, even if it means going to a festival in Poland with no music you like. I will never forget you saying you are disliked in the short term but loved in the long term, I was a bit scared of you when we met but love you dearly over 10 years later and can't imagine that changing. And thank you for introducing Joe to me! Joe - very grateful for our chats starting from that first random night in the Stratford flat to New Years eves in Amsterdam and sticking togehter through friendship break ups and all the other ups and downs of life. Iain and Steve, thank you both for your friendship over all these years. No matter how much time passes, it always feels easy to pick up where we left off, and I'm very grateful to have you both in my life.

To all of my wonderful cat-sitting clients, thank you for trusting me with your homes and your cats. During the ups and downs of my PhD, your confidence and gratitude in me reminded me that I and my work are valued and appreciated. Those moments of trust and appreciation meant more than any of you probably realize. Especially to Youngae, thank you for always making time to listen and for never making me feel like I was too much. From sharing beautiful photos of your travels to bonding over cheap veggie boxes, your kindness brought so much warmth throughout my PhD and to my life. I will always be grateful for your and Tito's friendship.

Lucia, thank you for being such an important friend for so many years. We might be complete opposites in many ways, but somehow our friendship has persisted and I have no doubt it will continue doing so.

To my father, thank you for always supporting my academic projects and making time for me whenever I needed help. You were, for example, instrumental in getting my sensors to work while I was in Churchill (see what I did there). Whether it was phone calls during fieldwork to get electrical advice and simply have someone to talk through fieldwork with, or explaining how to attach a toilet seat in my flat, you taught me that with patience, persistence, and logic, one can always find a solution. To my mother, thank you for always picking up the phone and listening to whatever was going on that day, no matter whether I was excited, frustrated, or completely overwhelmed. To my sisters, Claudia and Cristina, thank you for always being there for me and for your support and encouragement throughout my PhD. I especially appreciate having sisters who understand the realities of academia. I look forward to many more board- and card game sessions together starting next year.

Finally, Tuna - I know that you can actually secretely read even though you pretend to only be a meshy chaos child. Thank you for being my constant companion and for reminding me to step away from work and the computer more.

